# Jahn–Teller effect in quasi-two-dimensional doped cuprate antiferromagnets and underdoped high-$T_c$ superconductors (Review)

G. G. Sergeeva* and A. A. Soroka

*National Science Center Kharkov Institute of Physics and Technology, ul. Akademicheskaya 1, Kharkov 61108, Ukraine*

(Submitted January 16, 2004)
Fiz. Nizk. Temp. **30**, 887–912 (September 2004)

The theoretical aspects of research on the role of Jahn–Teller interactions in quasi-two-dimensional cuprate antiferromagnets and high-$T_c$ superconductors (HTSCs) are analyzed. An analysis is made of results that permit one to establish a link between the quasi-two-dimensional character of the properties of underdoped cuprate HTSCs in the normal and superconducting states and the Jahn–Teller (JT) nature of the divalent copper ions. It is shown that the combination of these two features leads to the existence of a pseudogap state. In underdoped cuprate HTSCs with JT lattice distortions the quasi-two-dimensionality gives rise to two-dimensional local and quasilocal states of the charge carriers. This is manifested in substantial temperature dependence of the number of components of the localized and delocalized states of the charge carriers and in repeated dynamical reduction of the dimensionality of underdoped cuprate HTSCs as the temperature is lowered. Such a HTSC, with doping concentrations less than optimal, is found in a quasi-two-dimensional state in the greater part of its phase diagram, both in the normal and superconducting states. This means that the superconducting state of underdoped cuprate HTSCs differs from the BCS state and is closer in its properties to the state of a two-dimensional Berezinskii–Kosterlitz–Thouless (BKT) superconductor without off-diagonal long-range order (ODLRO). It is shown that the difference primarily consists in the mechanism of superconductivity. In spite of the fact that a strong JT electron–phonon interaction in underdoped cuprate HTSCs plays a key role and leads to the formation of two-site JT polarons, the attraction between holes and such polarons and the formation of a superfluid two-site JT polaron with an antiferromagnetic core are due to compensation of the Coulomb repulsion by the polaron energy shift. The hypothesis that the superconducting state in overdoped cuprate HTSCs is a consequence of the establishment of ODLRO in the three-dimensional BCS model with nonconserved total number of charge carriers and nonzero quantum fluctuations of the number of charge carriers is discussed.  [DOI: 10.1063/1.1802932]

## 1. INTRODUCTION

It is known that in their search for compounds with high superconducting transition temperatures (HTSCs), Bednorz and Müller[1] proceeded from the assumption that doped cuprate antiferromagnets contained Jahn–Teller (JT) polarons, with their inherent strong interaction with phonons. While Landau's role in the development of polaron concepts is unquestioned, not everyone knows of the part he played in the discovery of the Jahn–Teller effect. The hypothesis of instability of the nuclear configurations of polyatomic systems in the presence of electronic degeneracy was first stated by Landau in 1934 in a discussion with Teller in Copenhagen. Teller told him of a modification of the Born–Oppenheimer approximation in a linear molecule. Landau advised Teller to be careful and to take into account the possible symmetry breaking in the position of the atoms. Teller was able to convince Landau that this did not happen for linear molecules. Teller acknowledges that this was the only time he won an argument with Landau. ''That is why the effect should have Landau's name on it. He foresaw this effect. Jahn and I only did some technical work.'' [2]

For a long time there was no convincing mathematical proof of the Jahn–Teller theorem.[3] Because of this circumstance and the absence of any conclusions in Ref. 3 as to the possibility of observing the JT effect, for a long time the Jahn–Teller theorem remained ''on the shelf.'' Low's book[4] cites the words of Van Vleck, ''a great advantage of the Jahn–Teller effect is that it does not appear when it is not required,'' to which Low adds, ''nor does it appear when one is attempting to observe and measure it.'' To all appearances, one of the first mathematical generalizations of the Jahn–Teller theory for crystals was made by Van Vleck,[5] where estimates of the equilibrium displacements for the most stable configurations of an octahedral complex were obtained. These estimates made it possible to determine the Jahn–Teller splitting of the orbital energy levels. Only in 1950 was it first conjectured[6] that the dynamic Jahn–Teller effect could be observed by studying the anisotropy of the $g$ factor for divalent copper ions in systems with octahedral symmetry, and already in 1952 such measurements were carried out on $Cu^{2+}$ in $ZnSiF_6 \cdot 6H_2O{:}Cu^{2+}$ at low temperatures:[7] $g_\parallel \approx 2.4$; $g_\perp \approx 2.08$. This was the first observation of the Jahn–Teller effect.

 

It was only in the 1960s that the development of electron paramagnetic resonance technique and the unusual structure of the spectra observed in compounds of divalent copper and rare-earth atoms with a twofold degenerate orbital state of the electrons led to the first convincing evidence of unusual JT dynamics. At the same time, it was shown that vibronic mixing of two electronic states that are close in energy (pseudodegenerate) leads to the dynamic Jahn–Teller effect.[8,9] The consequences of vibronic mixing of pseudodegenerate states are called the pseudo-JT effect.

The first theoretical attempt to link low-temperature superconductivity with the pseudo-JT effect was undertaken in 1961 by Nesbet,[10] who calculated the corrections to the Born–Oppenheimer approximation for a rather strong electron–phonon interaction. As was shown in Ref. 10, in the ground state, taking into account the vibronic mixing of two pseudodegenerate electronic states leads to modified electronic states with minimal energy, which differ qualitatively from the Fermi distribution of a normal metal.

In the search for high-temperature superconductivity, Bednorz and Müller's guiding idea was inspired by the Jahn–Teller polaron model.[11] Based on their experience in studying JT ions in perovskite insulators, they conjectured that the JT polaron model could be applied to the metallic phase of transition metal oxides, e.g., Ba–La–Cu oxides.[12] It was later shown[13] that it is only in the case when the energy of JT stabilization is comparable to the half the bandwidth that one can expect a substantial manifestation of the JT effect. This condition separates the existence regions of localized and delocalized states of the charge carriers. Although its satisfaction is extremely rare, it does hold in manganites and in cuprate HTSCs, where it leads to the existence of JT polarons. Manganites, compounds with colossal magnetoresistance which contain trivalent manganese ions, were discovered in 1950 by the Dutch scientists Jonker and Van Santen. Even though the JT character of divalent copper and trivalent manganese ions was already well known by the end of the 1960s, the first convincing experimental evidence of a manifestation of the JT effect and of the existence of JT polarons in HTSC cuprates[14] and in manganites[15] was obtained only in 1998, with the observation of an oxygen isotope effect in their dynamic phase separation temperature. The great generality of the properties of different weakly doped perovskite oxides (nickelates, manganites, and HTSC cuprates) should be noted; it is a manifestation of the JT effect and of the existence of localized (one-site) and delocalized (two-site) JT polarons.[16,17]

In spite of the theoretical[18–20] and experimental[13,14] evidence of a linkage between high-temperature superconductivity and the JT effect, there was still no generally accepted model consistent with all of the observed properties of the cuprates. The main difficulty with the JT mechanism of superconductivity is that the energy of the JT splitting of the degenerate $d$ states of copper ($\sim 1$ eV) is an order of magnitude greater than the pairing energy ($\sim 0.1$ eV).

In this review we analyze the results of experimental and theoretical research on the quasi-two-dimensional doped cuprate antiferromagnets and underdoped cuprate HTSCs with twofold degenerate (or nearly degenerate) electronic states of divalent copper JT ions, according to which some of the properties of such compounds in the pseudogap and superconducting states can be considered to be manifestations of the JT effect.

### 1.1. Jahn–Teller theorem

The Jahn–Teller theorem states that any complex (except for a linear chain) with degenerate values of the electronic energy levels is unstable against any lattice deformation that lifts the degeneracy of the levels in first order. The JT effect thus leads to the existence of more than one equilibrium position of the complex with equal energy, i.e., the purely electronic degeneracy gives way to a more complicated vibrational (vibronic) degeneracy of the whole complex. This means that the electronic and nuclear Hamiltonians cannot be considered independently for systems with degenerate electronic levels. The eigenfunctions of the combined electronic–nuclear Hamiltonian are called vibronic wave functions.

Electronic degeneracies remain stable only in those systems for which deformations that lift the degeneracy of the electronic levels are not allowed, and two such exceptions to the JT theorem exist: for a Kramers doublet caused by the symmetry of the system with respect to a change in sign of the time, symmetry that cannot be broken by any displacements of the nuclei, and for linear molecules, in which twofold degenerate displacements of the ions are odd irreducible representations, and the degeneracy is lifted in second order of perturbation theory.[21]

For proof of their theorem, Jahn and Teller used perturbation theory, which gives a perfectly satisfactory description of the majority of real systems.[3] However, thirty five years later Teller acknowledged[2] that its proof had been obtained by a ''very inelegant method.'' The theorem of Jahn and Teller has great generality and does not rely on the approach of Ref. 3. Only in 1959 did Clinton and Rice propose an alternative approach to the JT theorem with the use of the Gell-Mann–Feynman theorem,[22] and a year later Kanamori introduced the concept of pseudospin for mathematical description of systems with twofold degenerate electronic states.[23]

According to the Gell-Mann–Feynman theorem, the generalized force acting on a nucleus upon a change in its coordinate $Q_k$ is equal to $F_k = -\langle i|\partial V/\partial Q_i|i\rangle$, where $|i\rangle$ is an electronic state, $V(q,Q)$ is the potential, and $q$ are the electron coordinates. If $F_k \neq 0$ for some configuration of the nuclei, then that configuration is unstable, and a spontaneous deformation occurs such that $F_k = 0$. The theorem of Jahn and Teller says that if $|i\rangle$ is a degenerate state with $Q_k = 0$, then there always exists a mode $Q_k$ for which the matrix element is nonzero and, consequently, $F_k \neq 0$ (see Ref. 24). However, despite the physical generality of this approach, it is difficult to use in practice, and a more applicable approach for real systems is the ''quasimolecular'' approximation, in which one chooses as the collective coordinates $Q_k$ the true normal coordinates of the nuclei of the ''molecular'' octahedral or tetragonal complexes, and the electrons of each complex are divided into ''active'' and ''passive'' groups.

In the harmonic approximation the Hamiltonian of the nuclei of a ''molecular'' complex has the form

$$H_n=\frac{1}{2}\sum_k (P_k^2/\mu_k+\mu_k\omega_k^2Q_k^2), \tag{1}$$

where $P_k$ is the momentum operator, $\mu_k$ is the effective mass, and $\omega_k$ is the frequency of the $k$th normal mode $Q_k$. The active group consists of the small number of electrons with degenerate orbitals which actively take part in the JT effect. The ''passive'' electrons are formed by the filled shells, and the possibility of their transition to excited states can be neglected. In compounds with transition metal ions the active group can include all or part of the $d$ electrons, while the remaining electrons of the $s$ and $p$ orbitals and the bound electrons of the ligands make up the ''passive'' group. Here the ''active'' electrons move in a potential $V(q,Q)$ that can be represented in the form of a series in $Q_k$:

$$V(q,Q)=V_0(q)+\left(\sum_k \partial V/\partial Q_k\right)Q_k+\ldots, \tag{2}$$

as a result of which the Hamiltonian $H_e$ of the active electrons contains terms of first order in the normal coordinates $Q_k$:

$$H_e=H_s+\sum_k (\partial V/\partial Q_k)Q_k. \tag{3}$$

Here $H_s$ is the Hamiltonian of the active electrons at $Q_k=0$, with energy eigenvalues $\overline{E}$.

In the absence of the JT effect (i.e., in the absence of degeneracy of the electronic levels) the Born–Oppenheimer approximation is valid for the eigenfunctions of the electronic–nuclear Hamiltonian:

$$\Psi=\psi_n(q,Q)\varphi(n,Q), \tag{4}$$

where $\psi_n(q,Q)$ and $\varphi(n,Q)$ are the electronic and nuclear wave functions. In Eq. (4) the functions $\psi_n(q,Q)$ are solutions of the Schrödinger equation for the electrons at a fixed position of the nuclei, and the functions $\varphi(n,Q)$ are solutions of the Schrödinger equation for nuclei in which the electron energy $E_n(Q)$ has been added to the internuclear potential. In the one-electron approximation Eqs. (1)–(4) give a complete description of the adiabatic variation of the many-electron wave function, but they cannot describe transitions from one electronic state to another due to motion of the nuclei. With the JT effect taken into account, the motion of the nuclei always causes mixing of the electronic states, the electron wave function depends substantially on the coordinates of the nuclei, and the adiabatic approximation (4) with the last term in (2) taken into account should be replaced by the more general relation[25]

$$\Psi_m=\sum a_{mn}\psi_n(q,Q)\varphi(n,Q), \tag{5}$$

where $a_{mn}$ are matrix elements. The wave function (5) is called the vibronic (combined electronic–vibrational) wave function. As was shown in Ref. 25, the accuracy of Eq. (5) is the same as that of the Born–Oppenheimer approximation (4) in the absence of degeneracy (it is of the order of the electron-to-nuclear mass ratio $\sim m/M$).

Thus degeneracy of the electronic levels in (3) leads to a dynamic ''vibronic'' degeneracy of states with the vibronic wave function (5) and is accompanied by conversion of the independent Hamiltonians of the nuclei (1) and of the active electrons ($H_s$) to a combined electronic–nuclear Hamiltonian

$$H_{ij}=E\delta_{ij}+(1/2)\sum_k [(P_k^2/\mu_k+\mu_k\omega_k^2Q_k^2)\delta_{ij} + h_{ij}(k)Q_k], \tag{6}$$

where the matrix elements $h_{ij}(k)=\langle i|\partial V/\partial Q_i|j\rangle$ are proportional to the strength of the interaction of the electrons with the lattice. Equation (6) is the basic first-order Hamiltonian for the JT effect in systems with twofold degenerate electronic states (a need to consider higher-order terms arises in systems with threefold degenerate states[24]). The expression in square brackets determines the potential energy surface of the nuclei of a ''molecular'' complex in the space of normal coordinates $Q_k$. The last term in (6) says that the minimum of the potential energy is shifted relative to the coordinate $Q_k=0$, and the consequent lowering of the symmetry of the Hamiltonian leads to a number of observable manifestations of the JT effect, which are considered in Sec. 2. For example, the term $h_{ij}(k)Q_k$ with a nondiagonal matrix $h_{ij}(k)$ leads to mixing of the electronic states as a result of nuclear motion. If after averaging over time the average displacement remains finite, then the lowering of the symmetry leads to an observable static JT effect. On the other hand, in the case when the average displacement over the characteristic time of the experiment is equal to zero, the dynamic JT effect is realized, the value of which is determined by the balance between the last two terms in (6).

Vibronic mixing of two nondegenerate electronic states that are close in energy, $E_1\sim E_2$, separated by a gap $\Delta E$ ($E_1>\Delta E=E_1-E_2$),[8,9] leads to a dynamic JT effect, the consequences of which are called the pseudo-JT effect. The pseudo-JT effect differs substantially from the JT effect in that the nearly degenerate electronic states mixed by the vibronic mode can belong to different irreducible representations of the problem. For example, in systems with a center of inversion the mixed electronic states can have opposite parity, which leads to the development of a dipole instability.[26] For studying the pseudo-JT effect it is important to identify the group of close electronic terms in the spectrum of the electronic states of the complex. For octahedral and tetragonal complexes this problem was solved in Refs. 26 and 27, and a general theorem was stated by Bersuker:[28]

*For any configuration of the nuclei of an arbitrary polyatomic system there exist bonding stationary states of the electronic density distribution (in the ground or an excited state) for which the amplitudes of the displacements of the nuclear configuration under consideration do not exceed the amplitude of the stationary states.*

This means that such a configuration need not correspond to a minimum point of the adiabatic potential but can correspond to some point of its basin. In systems with a rather large number of JT ions they cannot be regarded as independent ions, and that leads to cooperative effects. For example, ordering of the local distortions of dipole-unstable unit cells with a pseudo-JT effect in systems with a center of inversion leads to a ferroelectric phase transition, which can be considered a cooperative pseudo-JT effect.[26]

### 1.2. Low-temperature superconductivity and the JT effect

The Bardeen–Cooper–Schrieffer (BCS) theory of low-temperature superconductivity, as was noted in Refs. 29 and 30, takes the electron–phonon interaction into account in the adiabatic approximation but does not consider the correction to the Born–Oppenheimer approximation which arises even in the nondegenerate case if the electron–phonon coupling is strong enough. Usually these corrections are small, of the order of the ratio of the electron-to-nuclear mass ratio, but when degenerate or nearly degenerate low-lying electronic states with delocalized wave functions are taken into account, the interaction of the electrons with phonons can be considered as a dynamic JT effect with a combined electronic–nuclear Hamiltonian (6). For example, it has been shown[8,9] that the vibronic mixing of two close-lying but nondegenerate electronic states $E_1 \sim E_2$ separated by a gap $\Delta E = E_1 - E_2$, leads to a dynamic JT effect, i.e., the pseudo-JT effect.

Among the first papers discussing the consequences of the pseudo-JT effect are those of Nesbet,[30] in which the corrections to the Born–Oppenheimer approximation in the case of a rather strong electron–phonon coupling were found. In this case the ''active'' group of electrons consists of a small number of electrons with nearly degenerate orbitals, and the electronic wave function depends substantially on the coordinates of the nucleus, so that the adiabatic approximation (4) with the second term in (2) taken into account should be replaced by a combined electronic–vibrational wave function (5). The electronic wave functions $\psi_n(q,Q)$ depend on the normal coordinates $Q_k$ of the nuclei, and the motion of the nuclei causes a transition of the electrons from ground-state orbitals to excited orbitals described by the Born–Oppenheimer approximation:

$$\psi_n(q,Q) = \Phi_0 + \sum_{Q_k, i, \alpha} \Phi_i^{\alpha} (i s_{\alpha i} Q_k),$$

$$s_{\alpha i} = i(F_i^{\alpha})_k / (\varepsilon_{\alpha} - \varepsilon_i); \quad F_i^{\alpha} = \langle \alpha | \partial V / \partial Q_k | i \rangle, \tag{7}$$

where $\Phi_0$ is the Hartree–Fock many-electron wave function of the ground state, $\Phi_i^{\alpha}$ is the Slater determinant obtained from $\Phi_0$ with the orbital $\phi_i$ that is occupied in the ground state replaced by the excited orbital $\phi_{\alpha}$; $\varepsilon_i$ and $\varepsilon_{\alpha}$ are the energies of these states. As was mentioned above (Sec. 1), in the one-electron approximation equations (1)–(4) give a complete description of the adiabatic variation of the many-electron wave function, but they cannot describe transitions from one electronic state to another in response to the motion of the nuclei.

In Ref. 30 an expression was obtained for the matrix element of the transition of an electron from an occupied orbital $\phi_i$ to an unoccupied orbital $\phi_{\alpha}$ with the absorption of a phonon with energy $\varepsilon_{\alpha} - \varepsilon_i = \hbar \omega_k$. Processes of absorption or emission of a phonon occur between nondegenerate but nearly degenerate Born–Oppenheimer states, such that the transition probability is proportional to

$$\lim_{\delta_i \to 0} \frac{\delta_i}{(\varepsilon_{\alpha} - \varepsilon_i)^2 + \delta_i^2} = \pi \delta(\varepsilon_{\alpha} - \varepsilon_i), \tag{8}$$

which leads to modification of the stationary states on different sides of the Fermi surface. Here $\delta_i \sim (s/v)\varepsilon_i$, where $s$ is the velocity of longitudinal acoustic waves and $v$ is the velocity of electrons on the Fermi surface. Taking (8) and the finiteness of $\delta_i$ into account, we find that the correction $\varepsilon'(\sigma_i) = \mu(\sigma_i) - \varepsilon(\sigma_i)$ to the Hartree–Fock energy for a single-electron state is of opposite sign on different sides of the Fermi level and has a value of the order of magnitude

$$\varepsilon'(\sigma_F^{\pm}) \approx \mp (s/v)\varepsilon_F, \quad s/v \cong \sqrt{\frac{mZ}{3M}}, \tag{9}$$

where $m$ is the mass of an electron, $M$ is the mass of the ion, $Z$ is the charge of the ion, and $\mu(\sigma_i)$ is the electron chemical potential function. As is seen from (9), there always exists a state whose energy is not shifted, and if the value of $\varepsilon'(\sigma_F)$ is large enough, then $\mu(\sigma_i)$ can have a maximum on the inside of the Fermi surface and a minimum on the outside. The existence of such a sequence of maximum and minimum of the electron chemical potential, as was noted by Frolich,[31] means the presence of a qualitative change in the ground state state of the electron system and can be a sign of a superconducting state.

Thus the nuclear motion causes a transition of the electrons from the ground-state orbitals to unoccupied excited orbitals. As was shown in Ref. 30, the distribution of modified electronic states (7) is qualitatively different from the Fermi distribution for a normal metal. Now two independent stationary states can exist below the critical temperature. The electrical and thermal conductivities of states with higher energy are the same as for a metal, while the current states with lower excitation energy are nondissipative.

Nesbet's papers[30] were published at the time of the triumph of the BCS theory and did not attract much interest. Now, forty years later, however, one can say that Nesbet had predicted the pseudogap state (the dynamic analog of charge ordering) observed in doped cuprate antiferromagnets in which the Fermi surface consists of electron and hole parts that nearly coincide upon a translation by a wave vector of the antiferromagnetic cell (dispersion relations with nesting[32]). For example, in underdoped cuprate HTSCs upon transition to the pseudogap state a maximum is observed in the density of states near the Fermi level for $\varepsilon < \varepsilon_F$ and a minimum for $\varepsilon \sim \varepsilon_F$. The pseudogap state is a state with a pseudogap and two types of excitations (with light and heavy charge carriers[13]), which precedes the transition of underdoped cuprate HTSCs to the superconducting state.

Some remarks critical of Ref. 30 were made in Ref. 33, but we cannot agree with them. For one thing, in Ref. 33 the electron and nuclear Hamiltonians were considered independently, but, on account of the motion of the nuclei, in systems with nearly degenerate low-lying electronic states and with a strong electron–phonon coupling there is a transition from the independent Hamiltonians of the nuclei and ''active'' electrons to a combined electronic–nuclear Hamiltonian (6). Just as in the JT effect, the value of the dynamic pseudoeffect in systems with strong electron–phonon coupling and nearly degenerate low-lying electronic states is determined by the balance between the last two terms in (6). Secondly, the conclusion that the interaction of the electron and phonon subsystems leads to a substantial phonon contribution to the energy correction to the Hamiltonian was reached in Ref. 33 in the form of the Frolich theory.[31] How-

ever, it is known[34,35] that a correct description of the phonon spectrum cannot be given in the framework of the Frolich theory.

### 1.3. High-temperature superconductors and the Jahn–Teller effect (history)

That it was Bednorz and Müller who discovered high-temperature superconductivity was no accident. In 1983, when their collaboration began on the basis of a common interest in the study of superconductivity in complex oxides, Müller had twenty years of successful experience working with JT compounds.[36,37] At the same time, oxide compounds with relatively high critical temperatures (around 13 K), such as $Li_{1+x}Ti_{2-x}O_4$ and $BaPb_{1-x}Bi_xO_3$ were already known. According to BCS theory, such intermediate-valence oxides with a low carrier density ($n=4\times10^{21}$ cm$^{-3}$) should have a large electron–phonon coupling constant. Further attempts to raise $T_c$ in the perovskite $BaPb_{1-x}Bi_xO_3$ by increasing the density of states $n(\varepsilon_F)$ (by changing the Pb:Bi ratio) were unsuccessful because of the metal–insulator transition that occurs in these compounds.

The goal of Bednorz and Müller was to search for oxides such that high critical temperatures $T_c$ could be reached by increasing $n(\varepsilon_F)$ and the electron–phonon coupling. Hopes for an increase in the electron–phonon coupling rested on the polaron contribution, which had been predicted by Chakraverty[38] (see also Ref. 39 and works cited therein). That paper proposed a qualitative phase diagram for the polaron contributions in coordinates of the coupling constant $\lambda=n(E_F)V$ versus $T$. Chakraverty's diagram had three phases: a metallic phase below $\lambda_m$, an insulating polaron phase above $\lambda_d$, and a region of intermediate values $\lambda_m<\lambda<\lambda_d$ in the vicinity of the metal–insulator transition in which high-temperature superconductivity could exist.

The guiding idea in the creation of the general concepts of high-temperature superconductivity was inspired by the JT polaron model in the form proposed by Hock *et al.*[40] for a linear-chain model for narrow-band intermetallides. In the linear-chain model in the case of small JT distortion with energy $E_{JT}$ less than the bandwidth of the metal one observes only a small perturbation of the states of the conduction electrons. With increasing $E_{JT}$ there is an increasing tendency toward localization, and at $E_{JT}$ equal in magnitude to the bandwidth the formation of polarons is assumed. In the opinion of Bednorz and Müller this model could correspond well to Chakraverty's diagrams. Based on their experience in studying isolated JT ions in insulating perovskites, Bednorz and Müller assumed that the JT polaron model[40] could be applied to oxides provided that they were conductors. Oxides containing transition metal ions with a partially filled $e_g$ orbital, such as $Ni^{3+}$, $Fe^{4+}$, or $Cu^{2+}$, manifested a strong JT effect and were considered as possible candidates for new superconductors.

Based on Chakraverty's idea[38] of a possible polaron mechanism of superconductivity and on the possibility in principle for JT polarons to exist in transition metal oxides, Bednorz and Müller began their search for high-temperature superconductivity at the end of 1983, with the La–Ni–O system.[11] The compound $LaNiO_3$ is a metallic conductor with a transfer energy $t$ of the $e_g$ Jahn–Teller electrons greater than the JT stabilization energy ($t>E_{JT}$) and, hence, the JT distortion of the oxygen octahedron surrounding the $Ni^{3+}$ is strongly suppressed. To decrease the width of the metallic band of the Ni ions to a value comparable to the energy $E_{JT}$ of the $Ni^{3+}$ ion, the trivalent Ni was partially substituted by trivalent Al. Here it turned out that increasing the Al concentration radically alters the metallic characteristics of pure $LaNiO_3$, initially increasing the resistivity and then ultimately, at a high enough degree of substitution, leads to semiconductor behavior with a transition to localization at low temperatures. Another way of decreasing the width of the metallic band of Ni was to introduce internal stresses in the $LaNiO_3$ lattice through the substitution of the La ions by Y ions, which have a smaller radius. The behavior of the resistivity was altered in the same way as in the previous case, but neither method led to the desired result.

In 1985 the experimental situation in Bednorz and Müller's laboratory improved, and a new idea had come up of using copper as the transition metal in oxides, which had led to a substantial progress in their studies. In the new series of compounds the partial substitution of the JT ion $Ni^{3+}$ by the non-JT ion $Cu^{3+}$ increased the resistivity, but the metallic character of the solid solution was preserved to 4 K, which indicated the possibility of superconductivity. The turning point for Bednorz and Müller in their discovery of high-temperature superconductivity came at the end of 1985 when they learned of the paper by the French researchers Michel *et al.*,[12] who had studied the oxide of Ba–La–Cu with the Perovskite structure, which has metallic conductivity in the temperature range 100–300 °C. The Michel group was interested in the catalytic properties of oxigen-deficient compounds at high tempertures. It turned out that the oxide of Ba–La–Cu, which contains Cu in two different valence states, $Cu^{3+}$ and the JT state $Cu^{2+}$, and which meets all the criteria of the basic idea of the search for HTSC. They immediately synthesized this oxide from a series of solid solutions in which the Ba:Cu ratio was varied as a means of continuously varying the intermediate valence of the copper.

Measurements of the resistivity of the new compounds in mid-1986 showed that in the high-temperature region the behavior of the temperature dependence for the oxides was no different from the dependences measured previously, but on cooling they observed the characteristic behavior for metals, a fall giving way to a rise, which indicates a localization transition. The resistivity grew as the temperature approached the 30 K region, and then it began to level off and unexpectedly fell to 50% at 11 K. Repeated measurements showed excellent reproducibility of the results. By varying the composition of the compound and the techniques for heat-treatment of the samples, within two weeks' time they had shifted the start of the resistivity drop to 35 K, considerably higher than the critical temperature of $Nb_3Ge$ superconductors.

X-ray diffraction analysis of the samples revealed the presence of at least two different phases in them. The main phase could be identified as having a perovskite structure of the $K_2NiF_4$ type, whereas the diffraction lines of the second phase were similar to an oxygen-deficient perovskite with a three-dimensional network of coupled octahedra. As an electron microscope analysis showed, in both structures the La

was partially substituted by Ba. However, the matter of whether these compounds are substances in which the variable valence of the copper leads to superconductivity remained an open question. Despite the impossibility of making magnetic measurements at that time, Bednorz and Müller, recognizing the great importance of their result, published a paper entitled "Possible high-temperature superconductivity in the system Ba–La–Cu–O." [1]

Systematic measurement of the lattice parameters and electrical properties of the samples upon variation of their composition showed that $La_2CuO_4$ containing Ba is the phase responsible for the superconducting transition. The highest values of $T_c$ were obtained for a Ba concentration corresponding to the maximum distortion of the orthorhombic lattice (before its transition to the trigonal lattice), but after the perovskite phase begins to dominate, the superconducting transition is suppressed, and the samples display only metallic properties.

In September 1986, after the necessary experimental equipment had been assembled, magnetic measurements were carried out and the presence of the Meissner–Oksenfel'd effect in the new class of substances was demonstrated. In the samples that exhibited a drop in resistance a transition was observed from paramagnetism to diamagnetism at low temperatures, indicating the presence of currents of a superconducting nature. An x-ray analysis in combination with resistance and magnetic susceptibility measurements made it possible to conclude that the compound $La_2CuO_4$ with a Ba admixture is in a superconducting state at $T \leqslant 35$ K.

## 2. JAHN–TELLER EFFECT IN SYSTEMS WITH TWOFOLD DEGENERATE AND NEARLY DEGENERATE ELECTRONIC STATES

### 2.1. Static, dynamic, and cooperative Jahn–Teller effects

The JT copper ion $Cu^{2+}$ has one hole in the $d$ shell ($d^9$ configuration). In the copper–oxygen octahedron $Cu^{2+}O_6^{2-}$ the $e_g$ orbital of the $Cu^{2+}$ ion forms $\sigma$ states, which are especially sensitive to the position of the nuclei of the oxygen atoms and can lead to a strong JT effect. In the general case the number of normal coordinates $Q_k$ of the nuclei of the "molecular" octahedron $Cu^{2+}O_6^{2-}$ (with the symmetry group $O_h$) is equal to 15 (Ref. 5). As we are interested in the splitting of the electronic levels, we should take into account in the combined electronic–nuclear Hamiltonian (6) the collective modes $Q_2$ and $Q_3$ (with symmetry $\varepsilon_g(v)$ and $\varepsilon_g(u)$; Fig. 1a,b)

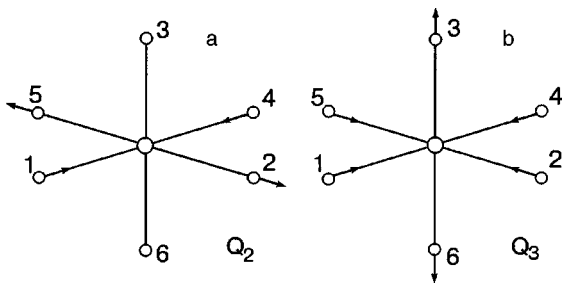


FIG. 1. Collective normal modes $Q_2$ (a) and $Q_3$ (b) of a "molecular" octahedron $Cu^{2+}O_6^{2-}$.

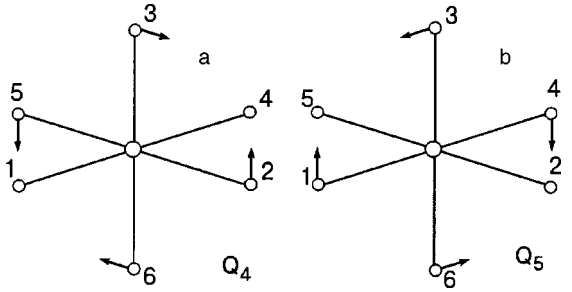


FIG. 2. Collective normal modes $Q_4$ (a) and $Q_5$ (b) of a "molecular" octahedron $Cu^{2+}O_6^{2-}$.

$$Q_2=(x_1-x_4-y_2+y_5)/2,$$
$$Q_3=(2z_3-2z_6-x_1+x_4-y_2+y_5)/2\sqrt{3}. \quad (10)$$

For the dynamic effect we should take into account in (6) the collective modes $Q_4$ and $Q_5$ (with symmetry $\tau_{2g}(\xi)$ and $\tau_{2g}(\eta)$; Fig. 2a,b):

$$Q_4=(z_2-z_5+y_3-y_6)/2$$
$$Q_5=(x_3-x_5+z_1-z_4)/2. \quad (11)$$

In the polar coordinates $(\rho,\theta)$ the modes $Q_2=\rho\sin\theta$ and $Q_3=\rho\cos\theta$, and the quasielastic potential $V(\rho,\theta)$ to a first approximation in the coordinates $(V,Q_2,Q_3)$ is a double-valued surface (Fig. 3) and is independent of the angle $\theta$:

$$V(\rho,\theta)=\pm A\rho+\frac{1}{2}\mu\omega^2\rho^2. \quad (12)$$

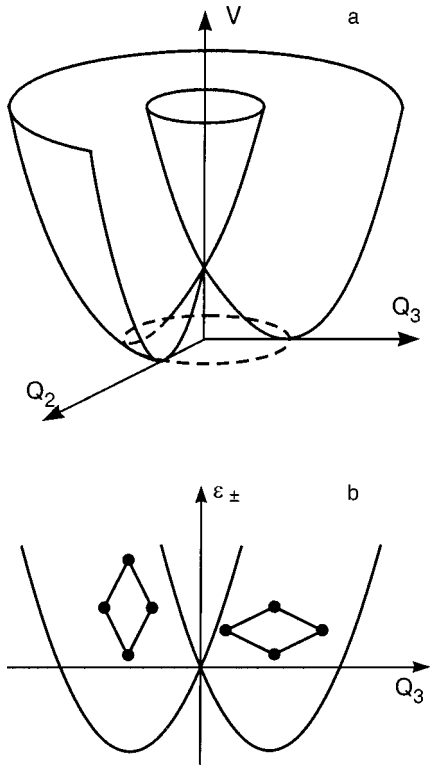


FIG. 3. Potential surface $V(\rho,\theta)$ with a minimum in the $(Q_2,Q_3)$ plane (the "Mexican hat") along which the nucleus moves (a); the section of the surface $V(\rho,\theta)$ by the plane $(V,Q_3)$ and the Jahn–Teller distortion of the positions of the oxygen ion corresponding to the minima of the potential (b).

Here $A$ is a quantity proportional to the interaction of the charge carriers with the lattice, the oscillations of which occur with an effective mass $\mu$ and a frequency $\omega$. The value of $A$ is positive for a hole of the $e_g$ orbital of the $Cu^{2+}$ ion. The surface $V(\rho,\theta)$ along which the nucleus moves (the ''Mexican hat'' shown in Fig. 3a) is a potential surface formed by revolution of the parabola (12) about the $\rho=0$ axis. The minimum with energy $\delta E=-A^2/2\mu\omega^2$, which is called the stabilization energy, lies in the $(Q_2,Q_3)$ plane on a circle of radius $\rho_0=|A|/\mu\omega^2$. The electron wave functions for states on the lower and upper branches of $V(\rho,\theta)$ has the form

$$\psi_-=\psi_u\sin\theta/2+\psi_v\cos\theta/2$$

$$\psi_+=\psi_u\cos\theta/2-\psi_v\sin\theta/2. \tag{13}$$

The dependence of the wave function on $\theta/2$ attests to the twofold degeneracy of $\psi$, and the requirement of single-valuedness of the total wave function leads to a twofold degeneracy of the nuclear wave functions. Figure 3b shows the JT distortions of the positions of the four mobile oxygen ions around the $Cu^{2+}$ ion in the copper–oxygen plane, these distortions corresponding to the minima of the potential $V(\rho,\theta)$ in the $(V,Q_3)$ plane.

Equations (13) for the electron wave function remain valid when the anharmonic terms of a Hamiltonian with cubic symmetry are taken into account, but now with a threefold symmetry with three potential wells along the directions $x$, $y$, $z$. If the state of the system is frozen in one of the three potential wells, this leads to a static JT effect, which was first observed in a study of the anisotropy of the $g$ factor for divalent copper ions in systems with octahedral symmetry at low temperatures.[7] With increasing temperature the thermal excitations lead to transitions through the potential barrier, i.e., the time-averaged symmetry of the environment of the ion will become cubic. This averaging effect gives rise to the dynamic JT effect. Thus an increase in temperature leads to a transition from the static to the dynamic JT effect.

The dynamic JT effect is a manifestation of the difference of the vibronic energy levels in systems with twofold degenerate electronic states from the vibrational levels in systems with nondegenerate states. The vibronic energy levels with doubly degenerate electronic states (13), which interact with doubly degenerate vibrational modes $\varphi_\pm=f_\pm\exp(ij\theta)$ with $j=(2n+1)/2$, satisfy the Schrödinger equation

$$(T_\varepsilon+V)\Psi=E\Psi, \tag{14}$$

where $\Psi=\psi_+\varphi_++\psi_-\varphi_-$ is a single-valued vibronic wave function, and $V(\rho,\theta)$ is given by Eq. (12). In the general case the kinetic energy operator is

$$T_\varepsilon=-\frac{\hbar}{2\mu}\left[\frac{\partial^2}{\partial\rho^2}+\frac{1}{\rho}\frac{\partial}{\partial\rho}+\frac{1}{\rho^2}\frac{\partial^2}{\partial\theta^2}\right]. \tag{15}$$

Relations (14) and (15) lead to two complicated equations for determining the functions $f_+$ and $f_-$. Only in the simple case when the vibronic wave function is equal to either $\psi_+\varphi_+$ or to $\psi_-\varphi_-$ can one obtain a one-dimensional Schrödinger equation that is a good approximation for the vibrational modes $\varphi_+$ or $\varphi_-$ (Refs. 41–43). Such estimates are useful for understanding the manifestations of the dynamic JT effect but, unfortunately, do not permit one to make a quantitative estimate of the energy levels for predicting the possibilities of experimental observation of the dynamic JT effect. Such observations may include a change in the optical absorption bands (Sec. 3).

However, at low temperatures the JT complex can be frozen in one of the potential wells. For example, let the electron wave function $\psi_-$ (13) be frozen with $\theta=0$, and $\psi_-=\psi_v$. The spectrum of the spin resonance for the static JT effect expected at 0 K was first calculated by Bersuker.[44] However, the zero-point vibrations make $\sin^2\theta/2>0$, and in the average $\psi_-$ acquires a nonzero part $\psi_u$. Such a change in the wave function $\psi_-$ has been observed in the hyperfine structure of the spin resonance.[45] Thus thermal excitations as the temperature is increased lead to a transition from the static to the dynamic JT effect, which is often observed in studies of the spin resonance on impurities or defects and is more-convincing evidence of a manifestation of the JT effect. The temperature of such a transition is registered as the temperature of the transition from the anisotropic spin resonance spectrum observed at low temperatures to an isotropic one at high temperatures.

In concentrated systems the individual JT ions cannot be treated as independent. The interaction between local JT distortions makes the latter cooperative and leads to phase transitions called the cooperative JT effect. In substances with high concentrations of JT ions the local distortions are converted into vibrations that propagate over the whole crystal and transport the interaction between JT ions. Just as for an individual ion, the crystal can be found in a degenerate electronic state which transforms according to an irreducible representation $\Gamma$ of the space group of the crystal. The JT distortion of the whole crystal, i.e., the cooperative JT effect, occurs if $\Gamma^2$ contains an irreducible representation of such a distortion. As was first shown by Kristofel',[46] this condition in the absence of perturbations (e.g., impurities or excitons) reduces the possible distortions to optical modes with $\kappa=0$. It was noted[46] that the selection rule $\kappa=0$ is valid if the JT stabilization energy $E_{JT}$ is less than the electron bandwidth $W$, which is determined by the quantity $2t$, where the matrix element $t$ for the transition of an electron from site to site depends on the interaction between ions. For example, if the electron undergoes a transition to a degenerate state in a band with $W<E_{JT}$, then it turns out to be localized at some site and, moving through the crystal, carries a lattice distortion with it. In this case the selection rule is no longer determined by the space group of the symmetry but by the point group, and the cooperative JT effect can be treated in a quasimolecular model in which the true normal coordinates of the nuclei of ''molecular'' octahedral or tetrahedral complexes are chosen as the collective coordinates $Q_k$, and the electrons of each complex are divided into ''active'' and ''passive'' groups. Examples of such degenerate states are the one-site JT polarons in a one-dimensional chain of JT sites with a transition matrix element $t$ (Ref. 40) or $V_k$ centers in alkali metals.[47]

Among the large number of structural transitions, those that occur on account of the collective JT effect are unique in that the microscopic nature of the transition is known exactly.[48,49] For example, the microscopic nature of the ferroelectric phase transition in noncentrosymmetric crystals

has been established: it is due to the cooperative JT effect,[46,50] in which vibronic mixing of only the even electron states occurs. In systems with a center of inversion the nearly degenerate electron states to be mixed by the vibronic oscillations can have opposite parity; this initially leads to the cooperative pseudo-JT effect and the destruction of the centrosymmetry of the system and only then to the development of a dipole instability and the cooperative JT effect.[26]

### 2.2. Jahn–Teller effect in magnetic compounds of transition metals

There is a large class of magnetic insulators in which the JT effect plays an important role and determines the structural and magnetic properties.[48,49] Here the exchange interaction, which is important for the magnetism, influences the properties of the lattice, inducing structural transitions. Such substances include doped cuprate antiferromagnets in which both spin degeneracy and orbital degeneracy exist simultaneously. Among the compounds with the perovskite structure the most interesting properties are found in $KCuF_3$ and $LaMnO_3$ and also in the ''two-dimensional perovskites'' ($K_2CuF_4$).[51] Interestingly, they are characterized by a quasi-one-dimensional or quasi-two-dimensional nature of the magnetic properties while retaining a nearly cubic lattice and also by the appearance of ferromagnetic ordering in antiferromagnets.

It is known that the main mechanism of the exchange interaction in compounds of transition metals is the Kramers–Anderson superexchange, wherein it is not the atomic-wave $d$ orbitals of the ions that overlap but their superpositions with the wave functions of the ligands (fluorine or oxygen ions).[52] However, even when the orbital degeneracy is taken into account the exchange mechanism controls the lifting of the degeneracy, and the most favorable situation from an energy standpoint is ferromagnetic ordering with respect to the spins of the ions and antiferromagnetic ordering with respect to the spins of the orbital electrons. For example, it turns out that for correct description of the orbital and magnetic ordering in $KCuF_3$ it is sufficient to take into account only the exchange interaction. If the orbital structure is known, then one can obtain an effective spin Hamiltonian. Such an analysis has been done[51] for the two-dimensional perovskite $K_2CuF_4$, and it showed that the structure obtained for it previously,[53] with compressed octahedra, is inconsistent with the ferromagnetism that is observed in $K_2CuF_4$. In Ref. 51 a theoretical analysis was done for elongated octahedra alternating along the $x$ and $y$ axis, and the results were later confirmed experimentally. This allows us to say that in all cases, without exception, the JT ion $Cu^{2+}$ in an octahedral environment causes a distensive deformation that stabilizes the hole orbital $d_{x^2-y^2}$.

In real magnetic compounds of transition metals the exchange, JT, and quadrupole mechanisms act jointly. In doped cuprate antiferromagnets both the exchange[54,55] and Jahn–Teller[40] mechanisms separately give rise to polarons. For example, the tunneling of charge along a one-dimensional chain of JT sites leads to a JT polaron (see Sec. 6). As was shown by Anderson,[55] in a two-band model of doped cuprate antiferromagnets virtual processes of transition of a hole (with probability $t_0$) from a doubly degenerate

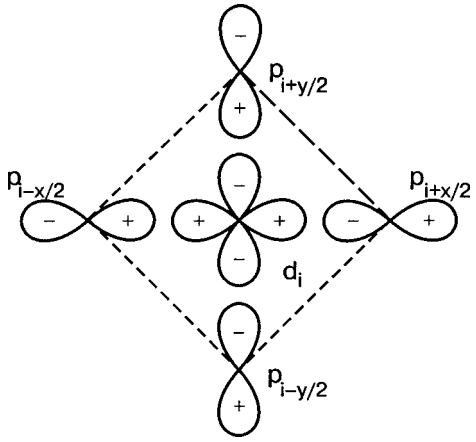


FIG. 4. Zhang–Rice polaron: $d_i$ are the orbital of the copper ion at the $i$th site of the copper–oxygen plane; $p$ are the orbitals of the four oxygen ions closest to the copper ion.

$d$ orbital of the $Cu^{2+}$ copper ion to a $p$ orbital of the oxygen ion leads to a superexchange $J$ with an antiferromagnetic coupling between holes of adjacent copper ions:

$$H_S = J\sum_{i,j} \mathbf{S}_i \cdot \mathbf{S}_j, \quad J = \frac{4t_0^4}{\varepsilon_p^2}\left(\frac{1}{U} + \frac{1}{2\varepsilon_p}\right), \tag{16}$$

where $\mathbf{S}_i$ is the spin operator of a $Cu^{2+}$ hole, $i,j$ are sites of two nearest-neighbor copper ions, $U$ is the Coulomb repulsion at the Cu site, and $\varepsilon_p$ is the energy of a hole on the $p$ orbital of oxygen. The energy of the symmetric state $\varphi_{i\sigma}$ of four holes on the oxygen ions surrounding the $Cu^{2+}$ ion (Fig. 4) is much lower than that of the antisymmetric state, and together with the $d$ orbital of copper either a singlet or triplet spin state is formed. Here $\varphi_{i\sigma}$ is a set of Wannier functions for an individual quasiparticle with spin $\sigma$. As was shown in Ref. 54, the energy $E_-$ of the singlet state

$$\Psi_i^- = \frac{1}{\sqrt{2}}(\varphi_{i\uparrow} d_{i\downarrow} - \varphi_{\downarrow} d_{i\uparrow}) \tag{17}$$

is much lower than that of the triplet state, and one can therefore neglect transitions from the singlet to the triplet state. The singlet state (17) is called a Zhang–Rice polaron. As may be seen from (17), its spin is equal to zero, and the mobility of the polaron is limited to the process $\Psi_i^- d_{j\sigma} \rightarrow \Psi_j^- d_{i\sigma}$, i.e., the motion of a Zhang–Rice polaron from site $i$ to site $j$ is possible only if a hole moves simultaneously in the counter direction from site $j$ to site $i$. Thus in Ref. 54 an effective one-band Hamiltonian for Zhang–Rice singlet states was obtained in which it can be assumed that both the magnetic interactions and the transition matrix elements in it are nonzero only for nearest-neighbor pairs.

### 2.3. Jahn–Teller polarons

When the JT character of the $Cu^{2+}$ ion in the doped cuprate antiferromagnetic insulators and metals (the spin of the $Cu^{2+}$ ion is equal to 1/2) is taken into account, it leads not only to a superexchange $J$ with antiferromagnetic coupling between holes of adjacent copper ions[54,55] but also to twofold degeneracy of the wave functions of the oxygen ions, i.e., to a JT distortion of the positions corresponding to

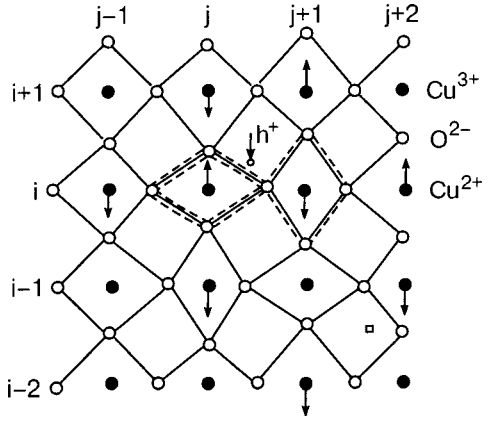


FIG. 5. Transition of a hole $h_{\downarrow}^{+}$ from the molecular orbital $\phi_i$ of a one-site Zhang–Rice polaron (the cluster $m_{ij}$ bounded by the inner dashed line) to an orbital $\phi_\alpha$ of a two-site JT polaron (the two-site cluster $m_{ij}+m_{i,j+1}$ bounded by the outer dashed line).

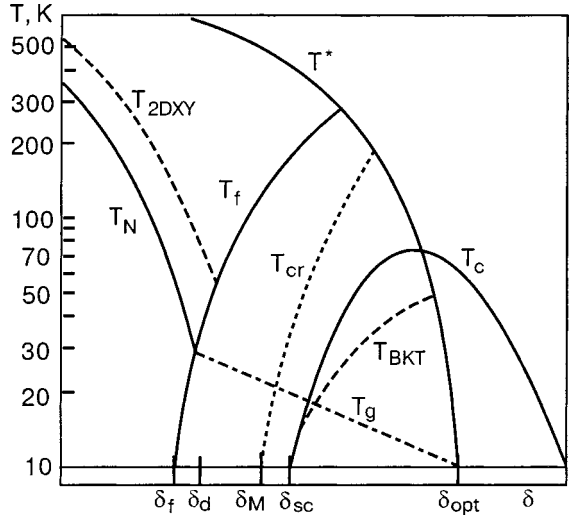


FIG. 6. State diagram of a doped cuprate antiferromagnet on the plane of temperature and dopant concentration $\delta$: $T_N$ is the Néel temperature, $T_f$ is the temperature of ordering of the hole spins at $\delta > \delta_f$; $T_{cr}$ is the temperature of the Mott metal–insulator transition at $\delta = \delta_M$; $\delta_d$ is the concentration at which the antiferromagnet undergoes a transition to the insulator phase; $T_c$ is the temperature of the transition to the superconducting state for $\delta > \delta_{sc}$; $\delta_{\rm opt}$ is the optimal dopant concentration; $T_{2DXY}$ is the temperature of 2D$XY$ magnetic ordering; $T^*$ is the temperature of the transition to the pseudogap state; $T_{BKT}$ is the temperature of the Berezinskii–Kosterlitz–Thouless (BKT) transition; $T_g$ is the temperature of the transition to the cluster spin-glass state at $T \leqslant T_g$.

minima of the potential $V(\rho,\theta)$ for the oxygen ions of the Zhang–Rice polaron (see Fig. 3b). The concept of ''Jahn–Teller polaron'' was introduced in 1983[40] for a charge tunneling along a one-dimensional chain of JT sites with a matrix element $t$ of the transition of the charge between nearest-neighbor sites:

$$\left[ ih\partial/\partial t - \sum_m \left\{ -\hbar^2/2M\partial^2/\partial x_m^2 + \frac{1}{2}M\omega_0^2 x_m^2 \right\} + Ax_n \right] a_n + t(a_{n+1}+a_{n-1}) = 0, \tag{18}$$

where $x$ is the coordinate of the nucleus, $A$ is the coupling constant between the charge and nuclear states, $\omega_0$ is the vibrational frequency of the corresponding collective mode, $a_{n+1} = a_n + \partial a_n/\partial n + (1/2)\partial^2 a_n/\partial n^2$. It is known that for one-dimensional or two-dimensional charge motion, even small distortions of the positions of the oxygen ions lead to a bound state of the charge,[56] i.e., a polaron. Since both mechanisms, exchange and JT, act jointly in doped cuprate antiferromagnets and lead to the formation of a polaron bound to a one-site cluster $Cu^{2+}+4O^{2-}$, such bound states of a charge carrier will be called JT polarons.

The size of the lattice region with which the JT polaron is bound determines its radius, which depends on the ratio of the transition matrix element $t$ to the value of the JT stabilization energy $A^2/2M\omega_0^2 = E_{JT}$. For $2t \gg A^2/2M\omega_0^2$ one can speak of a ''large'' polaron with radius $R_p \approx a(4t/M\omega_0^2)$ and for $2t \ll A^2/2M\omega_0^2$ of a small (one-site) JT polaron with radius $R_p \approx a$, where $a$ is the lattice constant.[13] The value of $2t$ determines the bandwidth $W$, and for $W \ll E_{JT}$ a localization of the charge on a small polaron occurs, while for $W \gg E_{JT}$ one can speak of charge motion, i.e., of delocalization of the state of the charge carrier in a region with the size of a large polaron, $R_p \gg a$. When the condition $E_{JT} \approx t$ is met, a transition from the localized (one-site) polaron to a delocalized polaron begins. For $E_{JT} = t$ the radius of the JT polaron $R_p \approx 2a$, and one can speak of a two-site JT polaron with antiferromagnetic ordering of the spins of the $Cu^{2+}$ ions (i.e., with an antiferromagnetic core), nonzero spin, and radius $R_p \approx 2a$ (Fig. 5). Although the condition $E_{JT} = t$ holds extremely rarely, it does hold[13] in the region of the Mott insulator–metal transition[57] with increasing doping in manganites and cuprate antiferromagnets.

Let us consider the joint effect of the exchange and JT mechanisms, a combination that is characteristic for magnetic compounds of transition metals and their oxides, for the particular example of a doped cuprate antiferromagnet. Figure 6 shows the state diagram of a doped cuprate antiferromagnet on the plane of temperature–dopant concentration $\delta$. At small concentrations $\delta_f < \delta < \delta_d$ in an antiferromagnet the spins of the copper ions and free holes order independently: the first at $T_N(\delta)$, and the hole spins at $T \leqslant T_f(\delta)$. Here $\delta_f$ is the minimum concentration at which ordering of the hole spins begins, and $\delta_d$ is the concentration at which the transition from antiferromagnet to antiferromagnetic insulator occurs, i.e., $T_N(\delta_d) = \min T_N(\delta)$. With increasing concentration $\delta_d < \delta < \delta_M$ the doped antiferromagnet undergoes a transition to an insulating state with localization of the charge on a one-site polaron of radius $R_p \approx a$ and with ordering of the hole spins at $T \leqslant T_f(\delta)$ ($\delta_M$ is the dopant concentration at which the Mott insulator–metal transition occurs). The charge carrier for $\delta_M < \delta < \delta_{\rm opt}$ is a two-dimensional delocalized two-site JT polaron with an antiferromagnetic core and with a size $R_p \approx 2a$ ($\delta_{\rm opt}$ is the optimal dopant concentration, corresponding to the maximum transition temperature $T_{c,\max}$). The transition of a doped cuprate antiferromagnet to the superconducting state at a transition temperature $T_c(\delta)$ occurs in the concentration region $\delta_{\rm sc} < \delta < \delta_{\rm opt}$, where $\delta_{sc} \geqslant \delta_M$. Further growth of the dopant concentration $\delta_{\rm opt} < \delta$ leads to a transition of the charge carrier to a three-dimensional delocalized state—a large polaron of size $R_p \gg a$. As is seen from the state diagram, Bednorz and Müller's search for high-$T_c$ superconductivity turned out to

be successful because they chose the idea of strong electron–phonon interactions inherent to compounds with JT ions (the LSCO sample) in the region of dopant concentrations $\delta_M < \delta < \delta_{\text{opt}}$, close to the Mott insulator–metal transition.

## 3. SPECTROSCOPY OF UNDERDOPED CUPRATE HTSCs

### 3.1. Identification of light and heavy charge carriers and the normal state of underdoped cuprate HTSCs

Optical spectroscopy of underdoped cuprate HTSCs has turned out to be very informative and is a widely used tool for studying their properties. There are three reasons for this. The first relates to the hole character of the charge carriers in them, which has led to the observation of optical response at the superconducting transition in the case of absorption;[58] this response has no analog in low-temperature superconductors. The second reason is that optical spectroscopy is known to be one of the most informative methods for studying magnetically ordered crystals, including antiferromagnets.[59] The third and final reason relates to the fact that theoretical studies of the optical properties of systems with a polaron character of the charge carriers were begun by Holstein in 1959,[60] and key results had been obtained by the end of the 1960s (see the works cited in Ref. 61). It is therefore unsurprising that by 1990 the optical spectra had been studied for the insulating and metallic phases of doped cuprate antiferromagnets (see the review[62]) over the frequency range from the far-infrared to the ultraviolet.

In the insulating phase the absorption of light in the infrared frequency region $\omega < 1.5-2$ eV is very weak. In the normal state of cuprate superconductors the optical conductivity $\sigma(\omega)$ in the region of the intraband transitions $0 < \hbar\omega < 1$ eV depends on temperature and frequency and consists of a narrow Drude-like peak with maximum at $\omega = 0$ and a broad, almost frequency-independent band in the region $0.2 < \hbar\omega < 1$ eV (mid-IR). The height of the Drude peak increases with increasing dopant concentration and attests to the existence of light charge carriers—holes. Here it has been established that the concentration of charge carriers determined through integration of $\sigma(\omega)$ in the region of the intraband transitions grows faster than the density of charge carriers introduced by doping of the material. A qualitative explanation for the results of these of these first optical measurements was proposed in Ref. 63: the structure of the mid-IR band of optical conductivity $\sigma(\omega)$ attests to the photoinduced excitation of a small localized polaron in a delocalized state with an excitation energy of the order of the energy of a Franck–Condon displacement. Later[64] it was established that at the boundary of the Drude peak in the frequency region $\omega \sim 0.15$ eV a polaron component appears which is sensitive to the temperature $T^*$ of transition to the pseudogap state, a circumstance that attests to the existence of a delocalized state of the polaron.

One of the the first convincing pieces of evidence of a connection between the superconducting transition temperature and the mid-IR band in the absorption spectra with $\hbar\omega < 1$ eV was obtained for $La_{2-x}Sr_xCuO_{4+\delta}$ (Refs. 65 and 66). It was found that the oscillator strength of the mid-IR band and the superconducting transition temperature $T_c$ have the same dependence on the Sr concentration. Figure 7 show the oscillator strength of the mid-IR band and $T_c$ as functions of

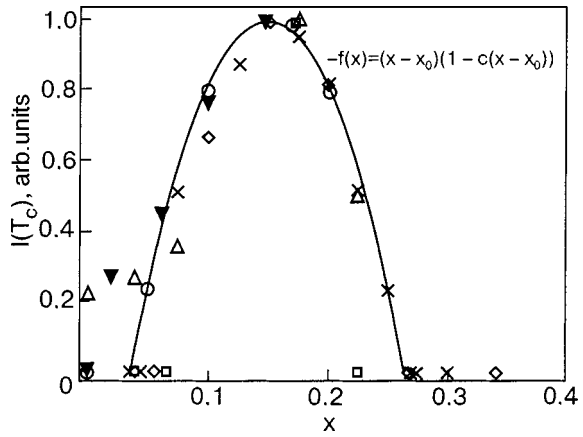


FIG. 7. Dependence of the normalized absorption intensity in the mid-IR region $I$ and of $T_c$ on the Sr concentration $x$ in the compounds $La_{2-x}Sr_xCuO_3$ and $La_{2-x}Sr_xNiO_4$, normalized to the corresponding maximum values.[67] For $La_{2-x}Sr_xCuO_4$: $I$ for a polycrystalline sample (△), for a single crystal (▼); $T_c$ for a polycrystal (□,×) and a single crystal (◇); the symbol (○) shows $I$ of a single crystal for $La_{2-x}Sr_xNiO_4$.

the Sr concentration for $La_{2-x}Sr_xCuO_{4+\delta}$ and $La_{2-x}Sr_xNiO_{4+\delta}$ from Ref. 67 (normalized to their respective maximum values). Figure 8 shows a comparison of the results of the calculation[67] with the measurements[68] of the optical conductivity $\sigma(\omega)$ for $La_{1.9}Sr_{0.1}CuO_{4+\delta}$ with $T_c = 18$ K (large dots); the line shows the results of the calculation of Ref. 67 in the model of photoinduced excitation of a small polaron,[61] the dashed curve shows the polaron contribution, and the dotted curve shows the Drude contribution to $\sigma(\omega)$. As is seen in the figure, the position of the maximum of $\sigma(\omega)$ and the dependence in the frequency region $\hbar\omega \leqslant 0.2$ eV are in satisfactory agreement with the results of the measurements.

The high level of early research[62,65–68] on the optical conductivity of underdoped cuprate HTSCs is noteworthy: they still remain valuable ten years later. For example, Müller noted the surprising agreement of the results of a calculation of the mass renormalization of the heavy charge carrier (polaron) in Ref. 67 with the results of measurements of the temperature dependence of the magnetic susceptibility of $La_{2-x}Sr_xCuO_{4+\delta}$ with $^{16}O$ replaced by the isotope $^{18}O$ (Ref. 69). In that case, as an analysis of the measurements showed, the charge carrier becomes heavier, so that the ratio

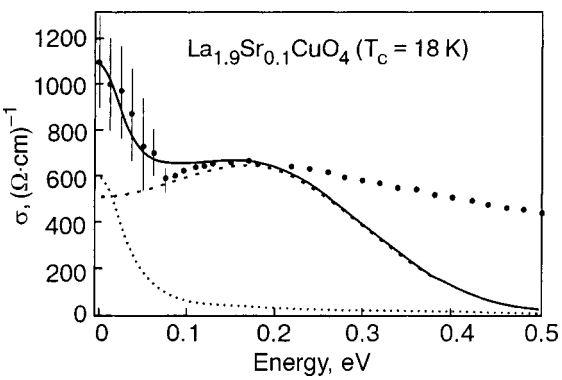


FIG. 8. Comparison of the results of a calculation of the dependence of the optical conductivity $\sigma(\omega)$ with the results of the measurements of Refs. 67 and 68.

of the its mass change $\Delta m_{ab}$ to the bare mass is $\Delta m_{ab}/m_{ab} \approx 9\%$. Approximation of the ratio $(m_{ab} + \Delta m_{ab})/m_{ab} \approx \exp(g^2)$ gives an estimate of $g^2 \approx 2.8$, which agrees with calculations of the heavy carriers (polarons) and vibrational frequency of their phonon ''coat.'' [67]

In spite of the fact that holes and polarons in the metallic state of doped cuprate oxide compounds had been identified in the absorption spectra of the mid-IR band with $\hbar\omega < 1$ eV,[62,63,67–70] complete agreement as to the character of the carriers in underdoped cuprate HTSCs was not achieved for quite some time. Convincing evidence of the existence of two types of carriers in the major part of the phase diagram of such compounds would be found later, in Refs. 67, 69, 71, and 72. The reason for this was primarily the problem of describing the properties of systems in which delocalized (hole) states coexist with localized states (polarons). As Goodenough noted forty years ago,[73] the description of the properties of transition metal compounds inevitably leads to the assumption that such a coexistence occurs. The problem of describing these properties consists in the absence of a sufficiently general definition of the concept of ''localized state,'' and the various models make use of different concrete model representations. In spite of the many-year history of this problem, which was published in the early 1930s by Wilson[74] and Shubin and Vonsovskii[75] and also by Mott,[57,76] there is still no generally accepted description of the localized states.[1)]

### 3.2. Spectroscopy of Jahn–Teller distortions in the copper–oxygen plane

The unusual character of the superconducting transition in underdoped cuprate HTSCs consists in the appearance of a pseudogap in the spectrum of electronic excitations at a temperature $T^* > T_c$ (Refs. 78–81), whereas the phase coherence and global superconductivity are established at $T_c$. The non-Fermi character of the states in a HTSC was predicted over ten years ago in phenomenological models.[82,83] It was shown in the model of Ref. 82 that including transport processes involving a small but nonzero total momentum leads to the appearance of a spin pseudogap (dip of the density of states at $E_F$) and two maxima to the left and right of $E_F$. In the model of a marginal Fermi liquid[83] it is predicted that quantum fluctuations exist at $\delta \sim \delta_c$, where $\delta_c$ is the critical value of the dopant concentration $\delta_c \approx \delta_{\text{opt}}$, at which $T_c \approx T_{c,\max}$. In spite of the fact that by 1990 the predictions of Refs. 82 and 83 had already been confirmed in angle-resolved photoemission experiments,[78] the nature of the pseudogap state remains unclear to this day: Is it only the result of a crossover controlled by fluctuations of the order parameter, or is it a new state whose symmetry is spontaneously broken at $T^*$ (See Refs. 84–88.)

Later, neutron measurements[81,89,90] showed that a splitting of the peak of inelastic scattering on spin fluctuations occurs in underdoped cuprate HTSCs at $T \geqslant T_c$. Those measurements yield unique information: they enable one to determine without the use of any assumptions or models not only the energy and wave vector of the JT distortions in the $CuO_2$ plane but also their size in real space ($\sim 8 \times 20$ Å).[89,90] These distortions are observed along the [X,0,0] and [0,Y,0] axes. A shortcoming of the measurements at $T > T_c$ (Refs. 81 and 90) is their small temperature interval, which is only a few degrees above $T_c$ in the case of optimal doping.

Optical spectroscopy methods are free from this shortcoming. For example, studies of the absorption spectra in the visible frequency region for the metallic phase of $YBa_2Cu_3O_{6+x}$ were done by Eremenko *et al.*:[91–94] for $T < T^*$ they established that an absorption band $A+J$ appears at $\hbar\omega \approx 2.2$ eV, and they identified it as being an electron–two-magnon band.[91,92] Even in the absence of this band at higher temperatures, on cooling below $T^*$ it appears in the metallic phase of the film. In the antiferromagnetic phase the band is noticeably enhanced on cooling below the Néel temperature, and in the superconducting state the $A+J$ band becomes independent of temperature. In Refs. 93 and 94 the structure of the $A+J$ band in the temperature range from 170 to 20 K, a region which includes both the temperature of the transition to the pseudogap state, 130 K $> T^* >$ 120 K, and the superconducting transition temperature $T_c = 88$ K for a $YBa_2Cu_3O_{6+0.85}$ sample. The results of the measurements showed that on passage through $T^*$ the electron–two-magnon band $A+J$ rises in the form a doublet band with maxima at $E_1 = 2.145$ eV and $E_2 = 2.28$ eV. Here the dispersion of each of the doublets coincides with the dispersion of the band for the low-temperature antiferromagnetic phase. These observations attest to the compatibility of short-range antiferromagnetic order with the superconducting state and suggest that the charge carrier in the pseudogap state is simultaneously the carrier of the antiferromagnetic properties of the copper–oxygen plane.

The inelastic neutron scattering data,[89,90] the electron spin resonance results,[95] and the results of measurements of the pair distribution function and the x-ray absorption fine structure (EXAFS)[96,97] show evidence that dynamic, nonlocal instabilities that are close to Jahn–Teller exist in the time interval $10^{-12}$–$10^{-15}$ s. This is just the time interval that is important for the formation of pairs and stripe structures in the pseudogap state. Based on the results of Refs. 96 and 97, the authors of Ref. 98 proposed a three-component model of the pseudogap state at $T^* \geqslant T$ (see also Ref. 99 and Sec. 4.1), in which, instead of holes and JT polarons, the third component is a two-site JT pair with a nonzero wave vector. Their pairing energy $\sim E_{JT}$ agrees with the value of the pseudogap: $kT^* \sim \Delta_p = E_{JT}$ (Ref. 100).

### 3.3. Observation of circular dichroism in the pseudogap state with preservation of translational invariance

One of the few theoretical models of the mechanism of high-temperature superconductivity, in the framework of which an experimental test was proposed for ascertaining the nature of the pseudogap state and the concentration dependence of the superconducting transition temperature $T^*(\delta)$, belongs to Varma.[83,85,101] In Refs. 85 and 101 the hypothesis that the ground states of HTSCs at $T \geqslant T_c$ are of an unusual character was discussed: for $T^*(\delta) \geqslant T \geqslant T_c(\delta)$—the pseudogap state for dopant concentrations $\delta_d \leqslant \delta \leqslant \delta_{\text{opt}}$; at doping close to optimal—states of a marginal Fermi liquid; for $T > T_F(\delta)$ with dopant concentration $\delta \geqslant \delta_{\text{opt}}$—the normal state of an ordinary Fermi liquid. In Refs. 85 and 101 it was proposed that the superconducting state of an overdoped

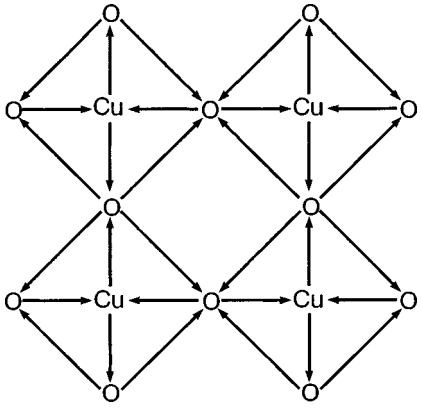


FIG. 9. Model of a system of closed local currents in the copper–oxygen plane of an underdoped cuprate HTSC, proposed in Ref. 101.

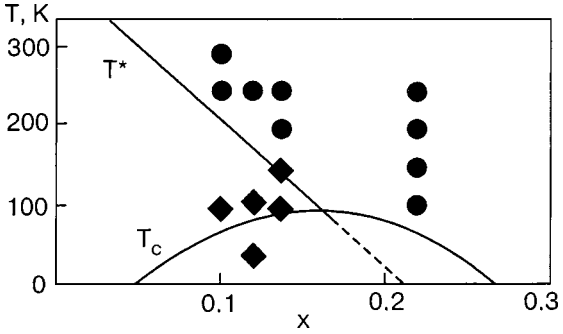


FIG. 10. Results of measurements of the intensity of the photoemission spectrum on thin films of $Bi_2Sr_2CaCu_2O_{8-x}$ (Ref. 103); circular dichroism is observed (♦), circular dichroism is not observed (●).

cuprate HTSC differs from the usual state by the character of the fluctuations: they are scale-invariant quantum fluctuations caused by the existence of a quantum critical point at $\delta \sim \delta_{\text{opt}}$. In Ref. 101 it was conjectured that at $\delta \sim \delta_{\text{opt}}$ each $CuO_4$ square of the copper–oxygen plane consists of four closed local currents, two of which are directed clockwise and the other two counterclockwise (Fig. 9). In such a system of closed local currents there exists a certain parameter—the phase, which distinguishes the direction of motion of the charge in each local ring. In the opinion of the authors of Ref. 102, such a structure of the local currents at $T \geqslant T_c$ should inevitably lead to breaking of the time-reversal symmetry, whereupon a spontaneous ordering without a change of translational symmetry will occur in the subsystem of the local currents.

The experiment proposed by Varma[101,102] consists in making measurements of the intensity of the photoemission spectra (ARPES) with right and left circular polarization of the light and in analysis of the relative difference of the reflection spectra obtained (i.e., circular dichroism); this was recently implemented.[103] Measurements were made on thin (1000–2000 Å) films of $Bi_2Sr_2CaCu_2O_{8-\delta}$. Preliminary measurements made in the temperature interval 100–300 K by x-ray spectroscopy confirmed the absence of changes in translational symmetry. To get an unambiguous result, magnetic circular dichroism resulting from the geometry of the experiment was ruled out.[104] This was done by making the measurements in a special geometry for which the three vectors **q**, **n**, and **p** lie in a mirror plane $m$ of the sample, perpendicular to its surface. Here **q** is the polarization vector of the incident light, **n** is the normal to the surface of the sample, and **p** is the wave vector of the final state. In this case it was established that dichroism is not observed in states with unbroken time-reversal symmetry (in overdoped samples).[103]

For an underdoped sample with $T_c = 85$ K and $T^* \approx 200$ K in this same geometry nonzero circular dichroism is observed in the region of the pseudogap state for $T < T^*(\delta)$ and, as can be seen in Fig. 10, it persists in the superconducting state. This is a very unexpected and important result—it uniquely determines the region of the time-reversal symmetry breaking: $\delta \leqslant \delta_{\text{opt}}$ and $T^*(\delta) \geqslant T \geqslant 0$. It should be noted, however, that the cause of the circular dichroism was not established unambiguously in that paper. First, the possibility of photoinduced dichroism inherent to doped magnets was not ruled out (see, e.g., Ref. 17 and works cited therein). Second, the observed dichroism might be due to nonuniformity of the copper–oxygen planes, which is inherent to underdoped HTSCs at $T < T^*(\delta)$ (see Sec. 4.1 and also Refs. 105 and 106 and the works cited there). As was noted in Ref. 102: these experiments, if they are right, together with the existence of a quantum critical point and properties of marginal Fermi level near optimal doping suggest that the essence of a realistic microscopic theory in cuprates can be found.

## 4. COOPERATIVE PSEUDO-JAHN–TELLER EFFECT IN UNDERDOPED CUPRATE HTSCs

### 4.1. Delocalized and localized states of JT charge carriers

The importance of this problem for underdoped cuprate HTSCs is attested to by the symposium on delocalized and localized states in HTSCs, held in the year 2000. In his opening remarks, Müller mentioned the paper by Gor'kov[107] in which it was shown to be possible in principle for multisite complexes of localized states of the charge carriers (i.e., stripes) to form. The existence of localized states of the charge carriers inevitably follows from the quasi-two-dimensional character of the motion of the charge carrier in underdoped cuprate HTSCs.[56] For doped antiferromagnetic insulators and underdoped cuprate HTSCs at $k_B T > t_c^2(T)/t_{ab}$ the incoherent transport of charge along the $c$ axis occurs as a result of thermal fluctuations ($t_c$ and $t_{ab}$ are the probability of charge tunneling along the $c$ axis and in the CuO plane). With decreasing temperature the thermal fluctuations limit the tunneling of the charge along the $c$ axis, and the density of charge carriers in the plane increases. This leads to a long-range unscreened Coulomb interaction, characteristic for a two-dimensional doped Mott insulator, as a result of which the motion of charge along the $c$ axis is controlled by the cooperative motion of the charges in the plane.[108,109] Here the tunneling probability $t_c$ depends exponentially on temperature. As the temperature is lowered, thermal fluctuations are no longer sufficient for transport of charge along the $c$ axis, and so there exists a temperature $\tilde{T}$ at which

$$k_B \tilde{T} = t_c^2(\tilde{T})/t_{ab} \tag{19}$$

and a dynamical reduction of the dimensionality of the charge motion from three-dimensional to two-dimensional occurs. The two-dimensional character of the charge motion for $T \leqslant \tilde{T}$ leads to a substantial change in the character of the states of hole quasiparticles interacting with JT phonon modes and also to the appearance of quasilocal and local hole states independently of the interaction potential.[56]

It should be noted that for the superconductivity of metals with a narrow band the importance of taking two components of the charge carriers into account simultaneously—a fast component (of delocalized band holes) and a slow component (localized charge carriers)—was first considered in 1985.[110] For underdoped cuprate HTSCs one of the first papers in which the coexistence of two different times scales was discussed is Ref. 18. In the Gor'kov–Sokol model[107] the JT effect leads to localized states:

$$H=\sum_{p,\sigma} \varepsilon(\mathbf{p}) a^{+}_{p,\sigma} a_{p,\sigma} + \varepsilon_l \sum_i a^{+}_{il} a_{il} + H_{GS},$$

$$H_{GS} = g \sum_{i,l} Q_{il} a^{+}_{il} a_{il} + \sum_i \frac{M\omega_0^2}{2} \left( \sum_i Q^2_{il} \right) + \sum_{i,j} W_{i,j} n_{fi} n_{fj}. \quad (20)$$

Here the first term in $H$ is the energy of delocalized holes, the second is the energy of localized charge carriers, i.e., JT polarons, and $H_{GS}$ is the Gor'kov–Sokol Hamiltonian. The first term in $H_{GS}$ is the interaction energy of the JT polarons with the JT mode $Q_{il}$, the second is the vibrational energy of this mode ($M$ and $\omega_0$ are the effective mass and frequency of the JT mode), and the last is the interaction energy between sites $i$ and $j$, with occupation numbers $n_{fi}$ and $n_{fj}$. It is seen from (20) that in the case of attraction, $W_{ij}<0$, the JT polarons will have a tendency to form clusters of a new phase with localized charge carriers. Here the density of carriers in a cluster and in the metal are different, so that the size of the clusters is determined by the condition of electrical neutrality.

The Hamiltonian $H$ does not include processes of $p-d$ hybridization of the $p$ states of the oxygen ions surrounding the $Cu^{2+}$ ion, and the proposed model[107] leads to a second-order phase transition with a critical temperature $T_{\text{crit}}$ determined by the Onsager solution for the phase transition. The temperature $T_{\text{crit}}$ separates a homogeneous "gaseous" phase for $T>T_{\text{crit}}$ and an inhomogeneous gas containing liquid drops for $T<T_{\text{crit}}$. Taking the $p-d$ hybridization processes into account will lead to Anderson superexchange, a finite energy of the local state, a decrease in the critical temperature, and elimination of the first-order phase transition. Taking the combined effects of the Anderson superexchange and the JT mechanism into account leads to the formation of a one-site JT polaron, i.e., a hole localized on a one-site cluster $Cu^{2+}O_4^{2-}$ of the copper–oxygen plane (see Secs. 2.2 and 2.3).

It was no accident that Gor'kov's paper[107] was entitled "Inherent inhomogeneity in two component model for cuprates." In the monoclinic copper oxide CuO, which contains 0.7% $Cu^{3+}$, a stripe structure formed by rhombi $\sim 5$ nm on a side with $Cu^{3+}$ ions at the corners of the rhombi have been observed under an electron microscope at temperatures above the Néel point.[111] In view of the strong anisotropy of the resistivity ($\sim 10^2$), the sample can be considered layered. As was shown in Ref. 112, in a doped layered antiferromagnet the charged impurity leads to the formation of an almost spherical ferromagnetic cluster with a localized hole, i.e., a three-spin polaron[95] (see below). It can be assumed that the inhomogeneity of the pseudogap state of underdoped cuprate HTSCs is a property inherent to layered oxides of transition metals with mixed valence and derives from the unusual character of their normal state. The layered character of these compounds with decreasing temperature leads to a repeated reduction of the dimensionality of the normal and superconducting states (see Sec. 4.2), while the mixed valence of the transition metal ions leads to a multicomponent nature of the delocalized and localized states of the charge carriers. Just as in Ref. 107, in this review we shall mean by a two-component model the coexistence of delocalized and localized states of the charge carriers, regardless of the number of components of each. The repeated reduction of dimensionality of the charge motion in the normal and superconducting states, as will be shown below, leads to a manyfold change in the number of components of the delocalized and localized states of the charge carriers.

For underdoped cuprate HTSCs in a two-component model of the charge carriers (delocalized hole and localized one-site JT polaron) the authors in Ref. 113 considered nearly degenerate states of two molecular orbitals: occupied $\phi_i$ orbitals of the hole on a one-site $Cu^{2+}O_4^{2-}$ cluster and an unoccupied molecular orbital $\phi_\alpha$ of a two-site $Cu^{2+}O_4^{2-} + Cu^{2+}O_4^{2-}$ cluster with a common oxygen ion. Such nearly degenerate states can appear only near the Fermi energy (see Ref. 30 and Sec. 1.2). The dynamic lattice distortions corresponding to two-site JT clusters have been observed on time scales $10^{-13}-10^{-15}$ s in various experiments.[89,90,114,115]

In Ref. 113 it was shown that the vibronic mixing of two nearly degenerate states leads to a dynamic JT effect, one of the consequences of which is the cooperative pseudo-JT effect—the transition to the pseudogap state (see Secs. 1.2 and 1.3). The nearly degenerate electronic states $\psi_n(q,Q)$ depend on the normal coordinates $Q_k$ of the vibrations of the oxygen nuclei, the motion of which causes a transition of the holes from the ground-state orbitals $\phi_i$ to the excited orbitals $\phi_\alpha$ of the two-site cluster $Cu^{2+}O_4^{2-} + Cu^{2+}O_4^{2-}$, which can be described by the Born–Oppenheimer approximation (7). As was shown in Ref. 30, the probability of such a transition upon the absorption of a phonon of energy $\varepsilon_\alpha - \varepsilon_i = \hbar\omega_k$, where $\varepsilon_i$ and $\varepsilon_\alpha$, are the energies of the corresponding states, is determined by expression (8) and leads to modified electronic states with a distribution differing from the Fermi distribution of a normal metal. We assume that after the transition of a hole from the $\phi_i$ orbital to a one-site $m_{ij}$ cluster $Cu^{2} + O_4^{2-}$ the excited orbital $\phi_\alpha$ of the two-site cluster $m_{ij} + m_{i,j+1}$ (Fig. 5) turns out to be occupied. Here the indices $i$ and $j$ are numbers of the row and column of the copper ions, respectively. The state with energy $\varepsilon_\alpha$ can be considered as a quasilocal hole state,[56] i.e., as a delocalized two-site JT polaron with antiparallel spins of two adjacent copper ions; this polaron spends some time on one two-site cluster and then undergoes a transition to another close-lying two-site cluster

with a common oxygen ion. The effective mass of the two-site JT polaron is less than the mass of a one-site JT polaron, their energy levels form a continuous spectrum near $E_F$ and have a small imaginary part, proportional to the number of such states. For $T \leqslant \tilde{T}$ the two-dimensional charge motion in the copper–oxygen plane leads to the situation that upon the absorption of a phonon with energy $\varepsilon_\alpha - \varepsilon_i = \hbar\omega_k$ the two-site JT polaron arises at any nonzero transition probability from the occupied orbital $\phi_i$ to the excited orbital $\phi_\alpha$.[56]

As is seen in Fig. 5, the two-site JT polaron can undergo a transition from the cluster $m_{ij} + m_{i,j+1}$ to another, nearest-neighbor two-site cluster with a common oxygen ion and with two $Cu^{2+}$ JT ions with antiparallel spins and can form a two-site cluster, e.g., $m_{i,j+1} + m_{i+1,j+1}$, $m_{i,j} + m_{i,j-1}$, $m_{ij} + m_{i-1,j}$, etc. However, a two-site JT polaron cannot undergo a transition from a cluster $m_{i,j} + m_{i,j+1}$ to a two-site cluster $m_{i+1,j} + m_{i+1,j-1}$, since only one of the two copper ions in it is $Cu^{2+}$, nor can it make a transition to a two-site cluster $m_{i+1,j} + m_{i,j+1}$, since the latter has no oxygen ion between the two $Cu^{2+}$ ions.

The model proposed in Ref. 113 permits a qualitative explanation of the formation of stripes from three-spin polarons. Let us consider the $Cu^{3+}$ ion of a one-site cluster $Cu^{3+}O_4^{2-}$ (the site $m_{i-1,j+1}$) as a charged impurity surrounded by four $Cu^{2+}$ ions (Fig. 5), which in a layered antiferromagnet leads to the formation of an almost spherical ferromagnetic cluster with a hole localized on it.[112] Here the JT vibrations of the oxygen ions surrounding the $Cu^{3+}$ ion and the $p-d$ hybridization of the orbitals of the oxygen and copper ions initiate a transition $Cu^{3+} \rightarrow Cu_\downarrow^{2+} + h_\uparrow^+$ with total spin equal to zero, which leads to the formation of a local three-spin polaron on a two-site cluster $Cu_\downarrow^{2+}O_4^{2-} + Cu_\downarrow^{2+}O_4^{2-}$ with a common oxygen ion (the localized state of the hole $h_\uparrow^+$ on the two–site cluster $m_{i-1,j+1} + m_{i,j+1}$ with parallel spins of the two copper ions). The region of localization of the hole $h_\uparrow^+$ is determined by the number of nearest-neighbor $Cu_\downarrow^{2+}$ ions to the $Cu_\downarrow^{2+}O_4^{2-} + Cu_\downarrow^{2+}O_4^{2-}$ cluster. This three-spin polaron can be localized at a cluster containing five ferromagnetically ordered $Cu_\downarrow^{2+}$ ions (Fig. 5). Chains of such three-spin polarons on the CuO planes form narrow D stripes with ferromagnetic ordering of the spins of the copper ions in them and distortions of the tetragonal structure, which alternate with U stripes, having almost undistorted octahedral complexes $Cu^{2+}O_6^{2-}$ (Fig. 11).[95,96,114–116] The narrow D stripes are called metallic, since holes can move along them, while along the wide U stripes with antiferromagnetic ordering of the spins of the divalent copper ions are two-site JT polarons.

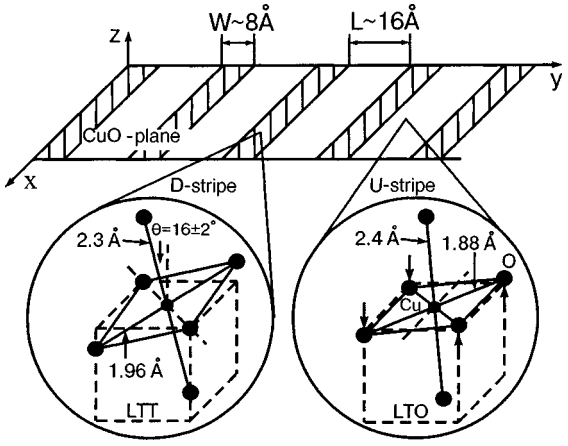


FIG. 11. Stripe structure of the copper–oxygen plane of $La_{2-x}Sr_xCuO_3$ (from Ref. 96). The narrow D stripes are formed by three-spin polarons with a ferromagnetic ordering of the spins of the copper ions in them and with tetragonal distortions of the structure. The wide U stripes consist of almost undistorted $Cu_2O_6$ octahedra.

It was shown in Sec. 1.2 that the vibronic mixing of two nearly degenerate states leads to the pseudo-JT effect, and here the correction to the Hartree–Fock energy for a one-electron state (9) has opposite signs on different sides of $E_F$ and leads to smearing of the Fermi step. In that case the modified electronic states are qualitatively different from the ground state of a normal metal.[30,31,113] The analysis carried out above suggests that for $T \leqslant \tilde{T}$ the strong local correlations characteristic of the two-dimensional doped Mott–Hubbard insulator leads to the cooperative pseudo-JT effect for $T^* \leqslant \tilde{T}$, a consequence of which is a transition to the pseudogap state at $T \leqslant T^*$ with a substantially inhomogeneous state of the copper–oxygen plane. Indeed, it was shown in a recent paper[117] that the transition to the pseudogap state is a manifestation of the finiteness of the phase space in which it is important to take into account the strong local Mott–Hubbard correlations at neighboring sites. In the two-component model of the charge carriers this leads to changes in both the number of JT localized states (the one-site JT polaron and the three-spin JT polaron) and the number of delocalized states (holes in a two-site JT polaron).

### 4.2. Repeated dynamical reduction of the dimensionality of the pseudogap and superconducting states of underdoped cuprate HTSCs

In doped antiferromagnets the dispersion relations for the holes and electrons are characterized by nesting, in which case the Fermi surface consists of electron and hole parts that nearly coincide in certain directions after translation by a wave vector $\mathbf{Q}$ of the antiferromagnetic cell ($\mathbf{Q} = \mathbf{K}/2$, where $\mathbf{K}$ is a reciprocal lattice vector).[32] Taking into account the existence of electrons (light charge carriers from a nesting region of width $Q$) is especially important for a pseudogap state of underdoped cuprate HTSCs when almost all the holes become two-site JT polarons, i.e., heavy charge carriers. With increasing dopant concentration, when there is more than one charge carrier at a given transition metal ion a doped insulator (e.g., $WO_{3-x}$; Ref. 118) undergoes a transition to a metallic state with heavy charge carriers, two-site JT polarons, and with light charge carriers (holes and electrons from the nesting region). Here it becomes possible in principle for a pair consisting of a two-site JT polaron and a light charge carrier to form, both in a doped antiferromagnetic insulator for $\delta_d < \delta < \delta_M$ and also in the metallic state for $\delta_M < \delta < \delta_{\text{opt}}$ (Fig. 6). Here $\delta_{sc}$ is the minimum dopant concentration at which a transition to the superconducting state is observed, and $\delta_{\text{opt}}$ is the optimal dopant concentration of the HTSC.

For underdoped cuprate HTSCs the coexistence of heavy and light charge carriers at $T^* > T > T_c$ has stimulated interest in the study of the possibility of their pairing, but the mechanism of suppression of one-site Coulomb repulsion

has remained unclear.[119] Kudinov[120] first showed that it is possible in principle for the one-site Coulomb repulsion to be suppressed by a polaron energy shift $E_p$ upon the formation of a JT polaron–hole pair. The Kudinov model is easily generalized for the model of two-site JT polarons interacting with light charge carriers if, after a modified Lang–Firsov transformation,[61] one keeps in the Hamiltonian all of the renormalized interactions between charge carriers.[106] We introduce the creation operators for light and heavy charge carriers of the copper–oxygen plane at the oxygen sites $m$ with spin $\sigma$: $a^+_{m\sigma}$ for a hole, $b^+_{m\sigma}=\exp(ix_0p_m)a^+_{m\sigma}$ for a two-site JT polaron, and $d^+_{m\sigma}$ for an electron from the nesting region. In an appendix to Ref. 106 it is proposed that the number of holes is greater than the number of two-site JT polarons, so that $n_{m\sigma}=a^+_{m\sigma}a_{m\sigma}=b^+_{m\sigma}b_{m\sigma}+\Delta n_{m\sigma}$, $\tilde{n}_{m\sigma}=d^+_{m\sigma}d_{m\sigma}$.

A generalization of the Kudinov model[120] for the two-site JT polarons with spin 1/2 in the lowest approximation in the coupling $J$ between the holes and $J_1<J$ between the holes and electrons from the nesting region leads to the Hamiltonian[106]

$$\mathcal{H}=\mathcal{H}_H+V+V_1,$$

$$\mathcal{H}_H=\sum_{m,g,\sigma}[2(-E_p+A_{ph})(n_{m\uparrow}\Delta n_{m\downarrow}+n_{m\downarrow}\Delta n_{m\uparrow}) +2A_{pe}n_{m\uparrow}(\tilde{n}_{m\uparrow}+\tilde{n}_{m\downarrow})], \tag{21a}$$

$$V=J\sum_{m,g,\sigma}(\Lambda a^+_{m\sigma}a_{m+g,\sigma}+\Lambda^{1/2}a^+_{m\sigma}b_{m+g,\sigma}),$$

$$V_1=J_1\sum_{m,g,\sigma}\Lambda^{1/2}b^+_{m\sigma}d_{m+g,\sigma}. \tag{21b}$$

Here $\mathcal{H}_H$ is a Hamiltonian with an attraction of the Hubbard type, and $E_p$ is the polaron energy shift, which is proportional to the JT stabilization energy. In Eq. (21b) the renormalization $\Lambda=\exp(-E_p/h\omega_0)$ was taken into account by a canonical transformation of the interaction $J$ between holes and the $\Lambda^{1/2}$ renormalization of the interactions between light and heavy charge carriers ($\omega_0$ is the JT vibrational frequency of the oxygen ions). It is seen from (21a) that a pair consisting of a two-site JT polaron and a light charge carrier can in principle form at a complex of a two-site JT polaron.

In a two-dimensional superconductor there is no long-range order, and there is no phase coherence in **k** space; therefore, in the BCS model the wave functions of the ground states $\Psi_{ph}(\chi)$ of a two-site JT polaron–hole pair (a boson with charge $2e$ and wave vector equal to zero) and the wave functions $\Psi_{pe}(\chi,Q)$ of local pairs of a two-site JT polaron and an electron from the nesting region (with the wave vector of the pair equal to $Q$) depends on the real function $\chi(k)\neq\text{const}$ (Ref. 106)

$$\Psi_{ph}(\chi)=\prod_k(u_k+e^{i\chi(k)}v_ka^+_{k\uparrow}b^+_{-k\downarrow})|0\rangle \tag{22}$$

$$\Psi_{pe}(\chi,Q)=\prod_k[u'_k+e^{i\chi(k)}v'_kd^+_{k+Q/2,\uparrow}(b^+_{-k+Q/2,\downarrow} +b_{-k+Q/2,\uparrow})]|0\rangle, \tag{23}$$

where the variational parameters $v_k$, $u_k$ and $v'_k$, $u'_k$ are periodic and analytic functions of the wave vector **k**. After going over in Eqs. (21)–(23) to a product over the lattice sites $m$ we have

$$\Psi_{ph}(\chi)=c_1\prod_m\exp\hat{R}_1(m)|0\rangle, \tag{24}$$

$$\Psi_{pe}(\chi,Q)=c_2\prod_m\exp\hat{R}_2(m)|0\rangle, \tag{25}$$

where $c_1$ and $c_2$ are constants. The operators $\exp\hat{R}_1(\mathbf{m})$ and $\exp\hat{R}_2(\mathbf{m})$ acting on the vacuum $|0\rangle$ creates various two-site clusters, one bosonic and two magnetic, with a central oxygen ion at the site $m$. The magnetic clusters to which two-site JT polaron–electron pairs lead are related to local ordering of the spins of the charge carriers and spins of the copper in the CuO plane at $T\leqslant T_f(\delta)$ (Fig. 6). The charge of a two-site JT polaron–electron pair is equal to zero, and the total spin is equal either to zero for antiparallel spins of the polaron and electron or to unity if the spins of the polaron and electron are parallel. The magnetic cluster with spin 1 can be called a vortex-like excitation, while the magnetic two-site cluster with spin zero can be called a two-site antiferromagnetic cluster. Bosonic clusters that appear for $T=T_{cr}(\delta)$ can be called ''superfluid'' two-site JT polarons—a pair of holes move freely from such a polaron to any two-site antiferromagnetic cluster; upon lowering of the the temperature $T<T_{cr}(\delta)$ this leads to zero-dimensional superconducting fluctuations for $\delta_{sc}<\delta<\delta_{opt}$.

The circumstance that the two-site JT polaron is simultaneously a ''heavy'' charge carrier and the carrier of the antiferromagnetic properties of the CuO plane is evidence of the compatibility of the order parameter of the pairing and magnetism, i.e., of $d$-wave symmetry. The formation of local pairs of two-site JT polaron–hole occurs only in the case of compensation of the Coulomb repulsion by a polaron shift $|E_p|>A_{ph}$ at temperatures $T_{cr}(\delta)\sim|-E_p+A_{ph}|$. For $A_{pe}<0$ the temperature $T_f(\delta)$ of formation of a JT polaron–electron pair depends only on the dopant concentration $\delta$. $T_f(\delta)$ can be called the temperature of local ordering of the spins of the charge carriers and the spins of the copper in the CuO plane of a doped antiferromagnet. In the antiferromagnetic state at a low hole concentration $\delta\leqslant\delta_f$ the processes of ordering of the spins of the holes and the copper occur independently—the hole spins order at the temperature $T_f(\delta)$, while the copper spins order at $T_N(\delta)$ (see Fig. 6). With increasing concentration the local ordering of the spins at $T\leqslant T_g(\delta)$ leads to a transition to a three-dimensional cluster spin glass state.[121] For $\delta_d<\delta<\delta_M$ in the pseudogap state of a doped antiferromagnetic insulator the local ordering of the spins of the charge carriers and copper occurs at $T<T_f(\delta)\leqslant T^*(\delta)$ as a result of the formation of the two-site JT polaron–electron pair and the two-site JT polaron–hole pair, which leads to a decrease in the number of charge carriers and the formation of local pairs.

In the metallic state of an underdoped cuprate HTSC for $\delta_{opt}\geqslant\delta\geqslant\delta_M$ and with decreasing temperature $T\leqslant T_{cr}(\delta)$ bosonic clusters with charge $2e$ also form. Upon further decrease in temperature the correlation length $L$ of the bosonic clusters (i.e., the zero-dimensional superconducting fluctua-

tions) increases, so that at a temperature $T<T_{2D}<T_{cr}$ they begin to overlap, and a dimensional crossover from 0D to 2D superconducting fluctuations occurs. This leads to temperature dependence of the coherence length in the CuO plane of the form $\xi_{ab}(T)=\xi_{ab}(T_{BKT})(T/T_{BKT}-1)^{-1/2}$ characteristic for Berezinskii–Kosterlitz–Thouless (BKT) 2D superconductivity with the transition temperature $T_{BKT}$ and a nonzero probability of charge tunneling along the $c$ axis

$$t_c(T)=\frac{\xi_c^2(T_{BKT})}{\xi_{ab}^2(T_{BKT})}\left(\frac{T}{T_{BKT}}-1\right),$$

where $\xi_c$ is the coherence length along the $c$ axis.[109] Upon further decrease in temperature $T\leqslant T_{3D}$ a transition occurs to three-dimensional (3D) fluctuations, and the superconducting transition occurs as two-dimensional with a limited region of 3D superconducting fluctuations with a transition temperature that is determined by the Kac inequality $T_c/E_F \geqslant t_c(T_c)$:[109,122]

$$T_c\geqslant T_{BKT}\frac{\xi_c^2E_F}{\xi_c^2E_F-\xi_{ab}^2T_{BKT}}, \tag{26}$$

where $E_F$ is the Fermi energy. As an analysis of the results of measurements of the resistivity along the $c$ axis have shown,[99] in the Bi-2212 single crystal with $T_c=80$ K, the region of $0D+2D$ superconducting fluctuations $(T_{cr}-T_{3D})\approx 120$ K, and the region of 3D fluctuations $(T_{3D}-T_c)\approx 10$ K. An estimate of the temperature $T_{BKT}\sim 0.7T_c\sim 56$ K agrees with the universal estimate of the region of three-dimensionality of the superconducting state.[123] Here the transition to a 2D superconducting state at $T\leqslant T_{BKT}$ occurs as the temperature is lowered, when $\xi_c(T)$ becomes equal to the distance between CuO planes.

As was shown above, the dynamical reduction of the dimensionality of underdoped cuprate HTSCs with $\delta_{sc}<\delta<\delta_{opt}$ is manifested in changes of their properties and occurs in the pseudogap state as the temperature is lowered to values $T^*$, $T_{cr}$, $T_{2D}$, and $T_{3D}$ and is also observed in the superconducting state at $T_{BKT}$ and $T_g$ (Fig. 6). The reduction of the dimensionality leads to a complex magnetic phase diagram of doped cuprate HTSCs as a function of the concentration $\delta$ and temperature. In doped antiferromagnetic insulators with $\delta_f<\delta<\delta_{sc}$ the reduction of the dimensionality occurs at temperatures $T^*$ and $T_g$, while the line $T_f(\delta)$ separates the existence region of the disordered state of the copper and hole spins and the region of their local ordering (magnetic clusters), which is bounded by four curves: $T_f(\delta)$, $T^*(\delta)$, $T_g(\delta)$, and $T_{3D}(\delta)$. For $T_{cr}(\delta)>T>T_{3D}(\delta)$ the vortexlike excitations coexist with ''bosonic'' clusters in the case of a quasi-two-dimensional character of the superconducting fluctuations and also in the region of the quasi-two-dimensional superconducting state $T_{BKT}\geqslant T\geqslant T_g$.

In the pseudogap state of a cuprate antiferromagnetic insulator at $T\leqslant T^*$ the pair correlations with $d$-wave symmetry of the order parameter are ''built into'' the CuO plane and are a consequence of the strong local correlations which are characteristic for a two-dimensional doped Mott–Hubbard insulator.[77,108,124] The first evidence of strong local correlations and the existence of a dispersion gap, similar to $d$-wave modulation, was obtained in photoemission studies of the insulator $Ca_2CuO_2Cl_2$ (Ref. 125). In the absence of magnetic field the total spins of the individual vortexlike excitations are randomly directed. In the presence of a field the spins order, and the vortexlike excitations are manifested in the Nernst effect,[128,127] and after the magnetic field is switched off they can lead to a weak residual magnetization of the sample in the pseudogap state.[128,129]

Thus for $\delta_{sc}<\delta<\delta_{opt}$ the CuO planes of an underdoped cuprate HTSC are found in a substantially nonuniform state with different local densities of charge carriers and with bosonic and magnetic clusters both in the case of a quasi-two-dimensional character of the superconducting fluctuations $T_{cr}(\delta)>T>T_{3D}(\delta)$ and also in the region of the quasi-two-dimensional superconducting state $T_{BKT}\geqslant T\geqslant T_g$. Direct evidence of local pairing in underdoped cuprate HTSCs with cluster sizes of $\sim 14$ Å was obtained recently in scanning tunneling microscope measurements of the local density of states and the energy of the superconducting gap in the superconductor $Bi_2Sr_2CaCu_2O_{8+x}$ (Ref. 130).

## 5. CONCLUSION

In summarizing the foregoing discussion of the theoretical and experimental results, it should be noted that the authors of this review have attempted to establish the connection between the quasi-two-dimensional character of the properties of underdoped cuprate HTSCs with $\delta<\delta_{opt}$ in the normal and superconducting states and the JT nature of the divalent copper ions. At the present time this question has become particularly topical in connection with high-temperature superconductivity of intercalated films of fullerite $C_{66}$ with a maximum $T_c=146$ K. Loktev *et al.*[131,132] have established that a key role in the mechanisms of superconductivity of such films is played by the strong interactions of degenerate electronic states with intramolecular JT vibrations. In cuprate HTSCs the combination of these two features leads to the existence of a line $T^*(\delta)$ on the state diagram which separates them from the overdoped compounds with $\delta\geqslant\delta_{opt}$. In overdoped cuprate HTSCs it is the three-dimensional character of the interactions that modifies the role of the divalent copper JT ions and, accordingly, the properties of the normal and superconducting states. This is due to different manifestation of the JT character of the divalent copper ions in quasi-two-dimensional and three-dimensional systems.

As was shown in this review, in the underdoped cuprate HTSCs with JT lattice distortions the quasi-two-dimensionality results in the appearance of two-dimensional local and quasilocal states of the charge carriers. This is manifested in the repeated dynamical reduction of the dimensionality of underdoped cuprate HTSCs as the temperature is lowered. On the phase diagram of the states (Fig. 6) it is seen that with decreasing temperature the dynamical reduction of the dimensionality in the normal state occurs at temperatures of $T^*$, $T_{cr}$, $T_{2D}$, and $T_{3D}$ and in the superconducting state at $T_{BKT}$ and $T_g$. In the major part of the diagram, for $\delta_d\leqslant\delta\leqslant\delta_{opt}$, both in the normal and in the superconducting state an underdoped cuprate HTSC is found in a quasi-two-dimensional state. This means that the superconducting state of underdoped cuprate HTSCs differs from the BCS state, and its properties are closer to the state of a two-dimensional Berezinskii–Kosterlitz–Thouless supercon-

ductor without long-range order. The difference lies primarily in the mechanism of superconductivity. Although the strong JT electron–phonon coupling in underdoped cuprate HTSCs plays a key role and leads to the formation of two-site JT polarons, the attraction between the holes and such polarons leads to superconducting fluctuations. This attraction is due to the compensation of the Coulomb repulsion by the polaron energy shift and it causes the formation of a ''superfluid'' two-site JT polaron with an antiferromagnetic core.

In the opinion of the authors the characteristic signs of a BKT nature of the superconductivity of an underdoped cuprate HTSC are as follows:

1. The existence of two-dimensional vortexlike excitations in the normal ($T^*(\delta) > T > T_{3D}(\delta)$) and superconducting ($T_g \leqslant T \leqslant T_{BKT}$) states. It can be conjectured that the circular dichroism observed for underdoped cuprate HTSCs is due namely to the existence of two-dimensional vortexlike excitations and, if that is the case, it should also be observed in low-temperature superconductors with a BKT character of the superconducting transition.

2. The two-dimensional character of the superconducting transition at $T_{BKT}$ from a bounded region of three-dimensional superconducting states at $T_{3D} > T > T_c$ to two dimensional states $T_c > T > T_{BKT}$.

3. The transition to a three-dimensional cluster spin-glass state with decreasing temperature $T \leqslant T_g(\delta)$. It can be assumed that in the antiferromagnetic insulator phase $\delta_f < \delta < \delta_d$ such a glass consists of different three-dimensional clusters—antiferromagnetic and ferromagnetic and form as a result of a three-dimensional analog of dynamic phase separation. With increasing dopant concentration $\delta_{sc} < \delta < \delta_{opt}$ with decreasing temperature at $T = T_g(\delta)$ a transition occurs from the two-dimensional BKT superconductivity to a three-dimensional cluster spin glass state, where the superconductivity is of a percolational character. For optimal doping, as is seen in Fig. 6, one has $T^*(\delta_{opt}) \approx 0$ and $T_g(\delta_{opt} \approx 0)$.

For $\delta \geqslant \delta_{opt}$ it is the three-dimensional character of the interactions that leads to the substantial difference of the normal and superconducting states of overdoped and underdoped cuprate HTSCs. Recent measurements[133] have shown that the superconducting state of overdoped HTSCs with $\delta \geqslant \delta_{opt}$ precedes the coherent metallic state. This permits the assumption that in overdoped cuprate HTSCs, in spite of the coexistence of three-dimensional localized JT and delocalized states of the charge carriers the superconducting state is closer in its properties to the BCS model with long-range order. As was shown in the paper by Kudinov,[77] in the BCS model the establishment of long-range order leads to vanishing of the Fermi feature, and the BCS wave function has the structure of Mott insulator states with Wannier operators $a^+_{\mathbf{m}-\mathbf{g},\sigma}$, all of which decay exponentially with distance from the central site **m**. In spite of the fact that here the state as before is a superposition of states with an even number of charge carriers, because of the exponential decay of the operators $a^+_{\mathbf{m}-\mathbf{g},\sigma}$ the electron density remains localized in the vicinity of site **m**, i.e., the superconducting state in this sense is localized. This means that in the BCS model the establishment of long-range order is due to the localization of the electronic state $a^+_{\mathbf{m}-\mathbf{g},\sigma}$ of the system and leads to nonconservation of the total number of particles. In such a superconductor the rms quantum fluctuations of the total number $N$ of charge carriers in the ground state is nonzero, and in the BCS model they are equal to $\langle \Delta N \rangle_0 = 4\Sigma_{\mathbf{k}} u^2_{\mathbf{k}} v^2_{\mathbf{k}}$. The presence of nonzero quantum fluctuations in the ground state of the superconductor, in the opinion of Kudinov,[77] is equivalent to the realization of the BCS model with ODLRO.

From this standpoint in optimally doped of cuprate HTSCs with $\delta = \delta_{opt}$ the states at $T = 0$ are a consequence of the existence of a quantum critical point, starting with which for $\delta \geqslant \delta_{opt}$ the superconducting state is a consequence of the establishment of an ODLRO state in the BCS model with nonconserved total number of charge carriers and with nonzero quantum fluctuations of the uniform of charge carriers in the ground state. At the present time the nature of the excitations, the exchange of which leads to the formation of Cooper pairs in the BCS model of optimally doped and overdoped cuprate HTSCs remains an open question. Only recently was an experiment proposed with the aim of solving this problem.[134] It is known that the phonon mechanism of pairing in low-temperature superconductors has been identified from reconstruction of the spectral function of the phonons (the Eliashberg function) for measurements of the complex tunneling conductivity. In Ref. 134 it was proposed to use a modification of the method of photoemission spectroscopy for determining the spectral function of pairing in a cuprate HTSC with $\delta \geqslant \delta_{opt}$. The proposed self-consistent method does not make use of model forms of the pairing spectral function. The method is based on the assumptions that in such HTSCs the Migdal theorem holds, the pairing energy is small, and the variables of the pairing spectral function (wave vector and energy) are different. The authors of Ref. 134 hope that the implementation of the proposed experiment will make it possible to give an answer to one of the central question of the problem of high-temperature superconductivity.

*E-mail: gsergeeva@kipt.kharkov.ua

[1)]See Vonsovkii's Translation Editor's Appendix to the Russian version of Mott's book[57] and also the paper by Kudinov.[77]

[1]J. G. Bednorz and K. A. Müller, Z. Phys. B: Condens. Matter **64**, 189 (1986).
[2]E. Teller, *The Jahn-Teller Effect in Molecules and Crystals*, R. Englman (ed.), Wiley-Interscience (1972).
[3]H. A. Jahn and E. Teller, Proc. R. Soc. London, Ser. A **161**, 220 (1937).
[4]W. Low, *Paramagnetic Resonance in Solids*, Suppl. 2 of Solid State Physics Ser., Academic Press, New York and London (1960).
[5]J. H. Van Vleck, J. Chem. Phys. **7**, 72 (1939).
[6]A. Abragam and M. H. L. Pryce, Proc. R. Soc. London, Ser. A **63**, 409 (1950).
[7]A. Bleaney and K. D. Bowers, Proc. R. Soc. London, Ser. A **65**, 667 (1952).
[8]U. Opik and M. H. L. Pryce, Proc. R. Soc. London, Ser. A **238**, 425 (1957).
[9]H. C. Longuet-Higgins, U. Opik, M. H. L. Pryce, and R. A. Sack, Proc. R. Soc. London, Ser. A **244**, 1 (1958).
[10]R. K. Nesbet, Phys. Rev. **126**, 2014 (1962); *ibid.* **128**, 139 (1963).
[11]J. G. Bednorz and K. A. Müller, ''Perovskite-type oxides—the new approach to high—$T_c$ superconductivity,'' Nobel Lecture, Stockholm, Dec. 8, 1987.
[12]C. Michel, L. Er-Rakho, and B. Raveau, Mater. Res. Bull. **20**, 667 (1985).
[13]K. A. Müller, J. Supercond. **12**, 3 (1999).
[14]A. Lanzara *et al., Proceedings of the Second International Conference on*

*Stripes and High-$T_c$ Superconductors, June 2–6, 1998, Rome* (1998).
[15]M. Medarde, P. Lacorre, K. Konder, F. Fauth, and A. Furrer, Phys. Rev. Lett. **80**, 2397 (1998).
[16]V. M. Loktev and Yu. G. Pogorelov, Fiz. Nizk. Temp. **26**, 231 (2000) [Low Temp. Phys. **26**, 171 (2000)].
[17]V. V. Eremenko, S. L. Gnatchenko, I. S. Kachur, V. G. Piryatinskaya, A. M. Ratner, M. B. Kosmina, B. P. Nazarenko, and V. M. Puzikov, J. Phys.: Condens. Matter **15**, 4025 (2003).
[18]L. P. Gorkov and A. V. Sokol, JETP Lett. **46**, 420 (1987).
[19]M. Weger and Englman, Physica A **168**, 324 (1999).
[20]D. Mihailovic and V. V. Kabanov, Phys. Rev. B **63**, 054505 (2001).
[21]R. Renner, Z. Phys. **92**, 172 (1934).
[22]W. L. Clinton and B. Rice, J. Chem. Phys. **30**, 542 (1959).
[23]J. Kanamori, J. Appl. Phys. (Suppl.) **31**, 14S (1960).
[24]M. D. Sturge, Solid State Phys. **20**, 91 (1967).
[25]H. C. Longuet-Higgins, Adv. Spectrosc. **2**, 429 (1961).
[26]I. B. Bersuker, Phys. Lett. **20**, 5891 (1966).
[27]I. B. Bersuker, B. G. Vekhter, G. S. Danil'chuk, L. S. Kremenchugskiĭ, A. A. Muzalevskiĭ, and M. A. Rafalovich, Fiz. Tverd. Tela (Leningrad) **11**, 2452 (1969) [Sov. Phys. Solid State **11**, 1961 (1969)].
[28]I. B. Bersuker and V. Z. Polinger, *Vibronic Interactions in Molecules and Crystals*, Springer, New York (1989), Nauka, Moscow (1983).
[29]J. M. Ziman, Proc. Cambridge Philos. Soc. **51**, 707 (1955).
[30]R. K. Nesbet, Phys. Rev. **126**, 2014 (1962); *ibid.* **128**, 139 (1963).
[31]H. Frolich, Phys. Rev. **79**, 845 (1950).
[32]V. N. Krivoruchko, K. Yu. Medvedeva, and Yu. E. Kuzovlev, J. Supercond. **12**, 155 (1999).
[33]R. Englman, Phys. Rev. **129**, 551 (1963).
[34]E. G. Brovman and Yu. M. Kagan, Zh. Éksp. Teor. Fiz. **52**, 557 (1967) [Sov. Phys. JETP **25**, 365 (1967)]; Usp. Fiz. Nauk **112**, 369 (1974) [Sov. Phys. Usp. **17**, 125 (1975)].
[35]B. T. Geĭlikman, Usp. Fiz. Nauk **115**, 403 (1975) [Sov. Phys. Usp. **18**, 190 (1975)].
[36]U. T. Hochi, K. A. Müller, and P. Wysling, Phys. Lett. **15**, 1 (1965).
[37]O. F. Schirmer, K. A. Müller, and J. Schneider, Phys. Konden. Mater. **3**, 323 (1965).
[38]B. K. Chakraverty, J. Phys. (France) Lett. **40**, L99 (1979); J. Phys. (France) **42**, 1351 (1981).
[39]V. L. Vinetskiĭ, N. I. Kashirina, É. A. Pashitskiĭ, in *Radio Spectroscopy of Solids* [in Russian], A. B. Raĭtsin (ed.), Naukova Dumka, Kiev (1992).
[40]K. H. Hock, H. Nickisch, and H. Thomas, Helv. Phys. Acta **56**, 236 (1983).
[41]J. C. Sloncewski, Phys. Rev. **131**, 1596 (1963).
[42]M. C. M. O'Brien, Proc. R. Soc. London, Ser. A **281**, 323 (1964).
[43]M. C. M. O'Brien, Proc. Phys. Soc. **86**, 847 (1965).
[44]I. B. Bersuker, Zh. Éksp. Teor. Fiz. **44**, 1239 (1963) [Sov. Phys. JETP **17**, 836 (1963)].
[45]J. H. E. Griffiths, J. Owen, and I. M. Ward, Proc. R. Soc. London, Ser. A **219**, 526 (1953).
[46]N. N. Kristofel', Fiz. Tverd. Tela (Leningrad) **6**, 3266 (1964) [Sov. Phys. Solid State **6**, 2613 (1965)].
[47]C. J. Delbecq, B. Smaller, and P. H. Yuster, Phys. Rev. **111**, 1235 (1958).
[48]M. Kharchenko, V. Kut'ko, M. Kobets', and Yu. Kharchenko, Fiz. Sb. Nauk. Tov. im. T. Shevchenka **4**, 80 (2001).
[49]S. S. Gerashenko, O. V. Miloslavskaya, Yu. N. Kharchenko, V. I. Kut'ko, N. M. Nesterenko, L. Masalik, K. Hermanowicz, M. Maczka, and J. Hanuza, Science **20**, 81 (2002).
[50]B. G. Vekhter, Fiz. Tverd. Tela (Leningrad) **15**, 509 (1973) [Sov. Phys. Solid State **15**, 354 (1973)].
[51]D. I. Khomskii and K. I. Kugel, Solid State Commun. **13**, 763 (1973).
[52]P. W. Anderson, Phys. Rev. **115**, 2 (1959).
[53]K. Knox, J. Chem. Phys. **30**, 991 (1959).
[54]F. C. Zhang and T. M. Rice, Phys. Rev. B **37**, 3759 (1988).
[55]P. W. Anderson, in *Frontiers and Borderlines in Many-Particle Physics*, Proceeding of Varrena Summer School, Varrena, Italy (1987).
[56]I. M. Lifshits, Usp. Fiz. Nauk **83**, 617 (1964) [Sov. Phys. Usp. **7**, 549 (1965)].
[57]N. F. Mott, *Metal-Insulator Transitions*, Taylor and Francis, London (1974), Nauka, Moscow (1979).
[58]I. Fugol, G. Saemann-Ischenko, V. Samovarov, Yu. Rybalko, V. Zhuravlev, Y. Strobel, B. Holzapfel, and P. Berberich, Solid State Commun. **80**, 201 (1991).
[59]V. V. Eremenko, N. F. Kharchenko, Yu. G. Litvinenko, and V. M. Naumenko, *Magnetooptics and Spectroscopy of Antiferromagnets* [in Russian], Naukova Dumka, Kiev (1989).
[60]T. Holstein, Ann. Phys. (N.Y.) **8**, 325 (1959).
[61]Yu. Firsov, in *Polarons* [in Russian], Yu. Firsov (ed.), Nauka, Moscow (1985).
[62]T. Timusk and D. V. Tanner, in *Physical Properties of High Temperature Superconductors I*, D. M. Ginsberg (ed.), World Scientific, Singapore (1989).
[63]D. Mihailovic, C. M. Foster, K. Voss, and A. J. Heeger, Phys. Rev. B **42**, 7989 (1990).
[64]D. Mihailovic, T. Mertelj, and K. M. Müller, Phys. Rev. B **57**, 6116 (1998).
[65]J. Orenstein, G. A. Thomas, J. Orenstein, D. H. Rapkine, C. G. Bethea, B. Fevine, B. Batlog, R. J. Cava, D. W. Johnson, Jr., and E. A. Rietman, Phys. Rev. B **36**, 8896 (1987).
[66]S. Etemad, D. E. Aspnes, M. K. Kelly, R. Thompson, J.-M. Tarascon, and G. W. Hull, Phys. Rev. B **37**, 3396 (1988).
[67]X.-X. Bi and P. C. Eklund, Phys. Rev. Lett. **70**, 2625 (1993).
[68]S. Uchida, T. Ido, H. Takagi, T. Arima, Y. Tokura, and S. Tajima, Phys. Rev. B **43**, 7942 (1991).
[69]K. A. Müller, Physica C **341–348**, 11 (2000).
[70]G. A. Thomas, J. Orenstein, D. H. Rapkine, M. Copizzi, A. J. Millis, R. N. Bhatt, L. F. Schneemeyer, and J. V. Waszczak, Phys. Rev. Lett. **61**, 1313 (1988).
[71]K. A. Müller, Guo-meng Zhao, K. Konder, and H. Keller, J. Phys.: Condens. Matter **10**, L291 (1998).
[72]T. Mertelj, J. Demsar, B. Podobnik, I. Poberaj, and D. Mihailovic, Phys. Rev. B **55**, 6061 (1997).
[73]J. B. Goodenough, *Magnetism and the Chemical Bond*, Interscience, New York (1963), Metallurgiya, Moscow (1968).
[74]A. H. Wilson, Proc. R. Soc. London, Ser. A **133**, 458 (1931).
[75]S. P. Shubin and S. V. Vonsovskii, Proc. R. Soc. London, Ser. A **445**, 149 (1934).
[76]N. F. Mott, Proc. Phys. Soc. **47**, 571 (1935).
[77]E. K. Kudinov, Fiz. Tverd. Tela (St. Petersburg) **41**, 3812 (1999) [Phys. Solid State **41**, 1450 (1999)].
[78]C. G. Olson, R. Liu, D. W. Lynch, R. S. List, A. J. Arko, B. W. Veal, Y. C. Chang, P. Z. Jiang, and A. P. Paulikas, Phys. Rev. B **423**, 7942 (1990).
[79]H. Ding, T. Yokoya, J. C. Campuzano, T. Takahashi, M. Randeria, M. R. Norman, T. Mochiku, K. Kadowaki, and J. Giapintzakis, Nature (London) **382**, 51 (1996).
[80]A. G. Loeaser, Z.-X. Shen, D. S. Dessau, D. S. Marshall, C.-H. Park, and P. Fournier, Science **273**, 325 (1996).
[81]P. Dai, H. A. Mook, and F. Dogan, Phys. Rev. Lett. **63**, 1996 (1989).
[82]A. P. Kampf and J. R. Scrieffer, Phys. Rev. B **42**, 7967 (1990).
[83]C. M. Varma, Phys. Rev. Lett. **63**, 1996 (1989).
[84]T. C. Hsu, J. B. Marson, and I. Affleck, Phys. Rev. B **43**, 2866 (1991).
[85]C. M. Varma, Phys. Rev. Lett. **83**, 3538 (1999).
[86]J. L. Tallon and J. W. Loram, Physica C **349**, 53 (2001).
[87]P. A. Lee and X.-G. Wen, Phys. Rev. Lett. **80**, 2193 (1998).
[88]S. V. Borisenko, A. Kordyuk, and S. Legner, cond-mat/0312036.
[89]H. A. Mook and F. Dogan, Nature (London) **401**, 145 (1999).
[90]R. J. McQeenly, Y. Petrov, T. Egami, M. Yethiraj, G. Shirane, and Y. Endoh, Phys. Rev. Lett. **82**, 628 (1999).
[91]V. V. Eremenko, V. N. Samovarov, V. L. Vakula, M. Yu. Libin, and S. A. Uyutnov, Fiz. Nizk. Temp. **26**, 1091 (2000) [Low Temp. Phys. **26**, 809 (2000)].
[92]V. V. Eremenko, V. N. Samovarov, V. L. Svishchev, V. L. Vakula, M. Yu. Libin, and S. A. Uyutnov, Fiz. Nizk. Temp. **26**, 739 (2000) [Low Temp. Phys. **26**, 541 (2000)].
[93]V. V. Eremenko, V. N. Samovarov, V. L. Vakula, M. Yu. Libin, S. A. Uyutnov, and V. M. Rashkovan, Fiz. Nizk. Temp. **27**, 1327 (2001) [Low Temp. Phys. **27**, 981 (2001)].
[94]V. N. Samovarov, V. L. Vakula, M. Yu. Libin, S. A. Uyutnov, and G. G. Sergeeva, Fiz. Nizk. Temp. **28**, 934 (2002) [Low Temp. Phys. **28**, 674 (2002)].
[95]B. I. Kochelaev, Phys. Rev. Lett. **79**, 4279 (1997).
[96]A. Bianconi, N. L. Saini, A. Lanzara, M. Missori, T. Rossetti, H. Oyanagi, H. Yamaguchi, K. Oka, and T. Ito, Phys. Rev. Lett. **76**, 3412 (1996).
[97]E. Bozin, S. Billingt, G. H. Kwei, and H. Takagi, Phys. Rev. B **59**, 4445 (1997).
[98]D. Mihailovic and V. V. Kabanov, Phys. Rev. B **63**, 054505 (2001).
[99]G. G. Sergeeva and V. L. Vakula, cond-mat/0207052.
[100]J. Demsar, B. Podobnik, V. V. Kabanov, Th. Wolf, and D. Mihailovic, Phys. Rev. Lett. **82**, 4918 (1999).
[101]C. M. Varma, Phys. Rev. B **61**, R3804 (2000).
[102]M. E. Simon and C. M. Varma, Phys. Rev. Lett. **89**, 2470003 (2002).
[103]A. Kaminski, S. Rosenkranz, H. M. Fretwell, J. C. Campusano, Z. Li, H.

Raffy, W. G. Cullen, H. You, C. G. Olson, C. M. Varma, and H. Hochst, Nature (London) **416**, 610 (2002); cond-mat/0204106.
[104]D. Venus, Phys. Rev. B **48**, 6144 (1993).
[105]B. G. Lazarev, Ya. D. Starodubov, M. B. Lazareva, L. A. Chirkina, V. A. Okovit, and G. G. Sergeeva, Vopr. At. Nauki Tekh., No. 5, 55 (2003).
[106]G. G. Sergeeva, Fiz. Nizk. Temp. **29**, 1181 (2003) [Low Temp. Phys. **29**, 895 (2003)].
[107]L. P. Gorkov, J. Supercond. **14**, 365 (2001).
[108]F. G. Pikus and A. L. Efros, Phys. Rev. B **51**, 16871 (1995).
[109]G. G. Sergeeva, V. Yu. Gonchar, and A. V. Voitsenya, Fiz. Nizk. Temp. **27**, 634 (2001) [Low Temp. Phys. **27**, 468 (2001)].
[110]S. P. Ionov, Izv. Akad. Nauk SSSR, Ser. Fiz. **49**, 90 (1985).
[111]X. G. Zheng, C. N. Xu, and Y. Tomokiyo, Phys. Rev. Lett. **85**, 5170 (2000).
[112]E. I. Nagaev, Phys. Rev. B **60**, 455 (1999).
[113]G. G. Sergeeva and A. A. Soroka, cond-mat/0311177.
[114]B. I. Kochelaev, J. Supercond. **12**, 53 (1999).
[115]A. Bianconi, in *High-$T_c$ Superconductivity: Ten Years after the Discovery*, ASI Series: Applied Sciences, E. Kaldis, E. Liarocapis, and K. A. Müller (eds.) (1997), Vol. 343, p. 383.
[116]G. G. Sergeeva and V. L. Vakula, **48**, 869 (2003); cond-mat/0301037.
[117]T. D. Stanesku and P. Phillips, Phys. Rev. Lett. **91**, 017002 (2003).
[118]E. Salje and B. Gutter, Philos. Mag. B **50**, 607 (1984).
[119]A. F. Barabanov, L. A. Maksimov, and A. V. Mikheenkov, JETP Lett. **47**, 328 (2001).
[120]E. K. Kudinov, Fiz. Tverd. Tela (St. Petersburg) **44**, 667 (2002) [Phys. Solid State **44**, 692 (2002)].
[121]C. H. Niedermayer, C. Bernhard, T. Blasius, A. Golnik, A. Moodenbaugh, and J. I. Budnik, Phys. Rev. Lett. **80**, 3843 (1998).
[122]E. I. Kats, Zh. Éksp. Teor. Fiz. **56**, 1675 (1969) [Sov. Phys. JETP **29**, 897 (1969)].
[123]G. G. Sergeeva, Fiz. Nizk. Temp. **27**, 845 (2001) [Low Temp. Phys. **27**, 624 (2001)].
[124]R. Resta and S. Sorella, cond-mat/9808151.
[125]F. Ronning, C. Kim, D. L. Feng, D. S. Marshall, A. G. Loeser, L. L. Miller, J. N. Eckstein, I. Bosovic, and Z.-X. Shen, Science **282**, 2067 (1998).
[126]Y. Wang, Z. A. Xu, T. Kakeshita, S. Uchida, S. Ono, Y. Ando, and N. P. Ong, Phys. Rev. B **64**, 224519 (2001).
[127]J. R. Kirtley, Physica C **368**, 55 (2002).
[128]M. S. M. Minhaj, J. Obien, D.-C. Long, J. T. Chen, and L. E. Wenger, J. Supercond. **7**, 715 (1994).
[129]B. G. Lazarev, Ya. D. Starodubov, M. B. Lazareva, L. A. Chirkina, G. G. Sergeeva, and V. S. Okovit, Czech. J. Phys. **46**, Suppl. S3, 1245 (1996).
[130]Z. Wang, J. R. Engelbrecht, S. Wang, H. Ding, and S. H. Pan, Phys. Rev. B **65**, 064509 (2002).
[131]V. M. Loktev and É. A. Pashitskiĭ, Fiz. Nizk. Temp. **28**, 421 (2002) [Low Temp. Phys. **28**, 295 (2002)].
[132]V. M. Loktev, É. A. Pashitskiĭ, R. Shekhter, and M. Jonson, Fiz. Nizk. Temp. **28**, 1150 (2002) [Low Temp. Phys. **28**, 821 (2002)].
[133]A. Kaminski, S. Rozenkranz, H. M. Fretwell, Z. Z. Li, H. Raffy, M. Randeria, M. R. Norman, and J. C. Campuzano, Phys. Rev. Lett. **90**, 237001 (2003).
[134]A. Vekhter and C. M. Varma, Phys. Rev. Lett. **90**, 237003 (2003).

Translated by Steve Torsveit

## QUANTUM LIQUIDS AND QUANTUM CRYSTALS

# Heat capacity of cylindrically confined helium: theoretical predictions versus experimental data

K. A. Chalyy*

*Faculty of Physics, Taras Shevchenko National University of Kiev, Acad. Glushkov Pr. 6, Kiev 03022, Ukraine*

(Submitted November 25, 2003; revised February 19, 2004)
Fiz. Nizk. Temp. **30**, 913–919 (September 2004)

Different systems which could exhibit size-dependent second-order phase transitions have been studied experimentally during the last quarter century. The validity of the proposed theoretical results is verified by comparing high-resolution experimental data with an analytical evaluation of the heat capacity of confined $^4$He. It is shown that the theoretical approach to the problem of the finite-size effect gives results that reasonably match the experimental data over a wide range of system sizes, from tens of nanometers up to a few micrometers for the cylindrical type of confinement geometry. The dependences of the shift of transition temperature on the cylinder size and boundary conditions are analyzed. The agreement of the results with finite-size scaling theory is confirmed. © *2004 American Institute of Physics.*
[DOI: 10.1063/1.1802933]

### 1. INTRODUCTION: CONFINED HELIUM EXPERIMENTS

The physical properties of a liquid system are strongly dependent on its size. Spatial limitation of a liquid matter system can cause significant changes in its properties. Analysis of such microscopic systems and their thermodynamic, static properties as well as measurement of the optical and transport properties has become a key task in various fields. The behavior of condensed and soft matter systems at small length scales is becoming a topic of technological importance[1] in view of modern achievements in micro- and nanofabrication techniques.[2]

Most of the recent advances toward better understanding of the effect of spatial limitation and finite-size-induced phenomena could not be realized without the basic research results of confined helium experiments.

Among the pioneering investigations in this field was an experimental study by Chen and Gasparini,[3] which was conducted about quarter century ago. Chen and Gasparini measured the specific heat of $^4$He near the superfluid transition for films from about 10 Å to 56 Å thick and for samples confined to a *cylindrical geometry* of 200 to 2000 Å in diameter.

Comparatively recently, the most reliable data[1,4,5] on cylindrically confined helium have became available from the Stanford research group lead by J. A. Lipa. It was pointed out in Ref. 4 that the common confining geometries are planes and cylinders, allowing the study of crossover from bulk three-dimensional behavior to two- and one-dimensional behavior, respectively.

By approaching the transition very closely, it becomes possible to use well-defined geometries amenable to detailed theoretical analysis. When the correlation length $\xi$ is on the order of the average distance to the walls, the sharp peak in the specific heat of bulk helium is predicted to be rounded and shifted to a lower temperature. However, in the region where the confinement effects are strong, there does not appear to be a detailed theoretical prediction of the shape of the heat capacity curve that is directly applicable to cylindrical geometry.[6]

In Ref. 6 Coleman and Lipa reported the results of heat capacity measurements as a function of temperature near the $\lambda$ point of $^4$He confined in 8-$\mu$m diameter cylinders that have exceptionally uniform diameters and smooth surfaces. Later in Ref. 1 the results of a more specific analysis of the 8-$\mu$m data were presented and the new data of an experimental study of a 0.26-$\mu$m cylinder were discussed. In contrast to the much earlier results[3] with smaller holes, they found good agreement with scaling-law exponents derived by renormalization methods.

For comparably large systems the size-dependent shift of the critical temperature is extremely small, which makes it difficult to detect due to the smearing effect of Earth's gravity. Most of the experiments on the effects of confinement on helium in planar and cylindrical geometries to date have been restricted to the submicron (or nano) regime.[3,7,8] However, Lipa *et al.*[1] stressed that by using high-resolution thermometry techniques[9] it has become possible to explore the region extending up to about 100 $\mu$m under microgravity conditions. This circumstance provides sufficient background to consider the comparably big systems as ''finite-size'' ones. This development has dramatically increased the range over which length scaling can be tested and has eased the problem of uncontrolled surface effects.

Experimental studies in finite-size liquids are quite difficult to conduct due to the fact that blurring effect of the Earth's gravity often causes phenomena very similar to the finite-size effect. This creates a high demand for a theory that fits the existing experimental results and which could be used

 

for explicit calculations of the properties in a wide range of sizes and for different types of system geometries. At present, for the case of cylindrical geometry, the primary source of predictions is from Monte Carlo studies (see, for example, Ref. 10).

In this paper we present a comparative study of experimental data and theoretical approaches to the finite-size effect in the liquid helium heat capacity in the close vicinity of the λ-transition temperature $T_\lambda$. Actual analytical calculations are conducted without taking the gravity effect into account. Consequently, it could be applicable for reliable comparison with the results of microgravity experiments in Earth orbit or with a number of Earth-based measurements of the $^4$He heat capacity in cylindrical confinement. In such Earth-based measurements the characteristic size of the system is supposed to be small enough to allow one to neglect the influence of gravity on the precision of new transition temperature detection.

## 2. HELIUM-IN-CYLINRICAL-CONFINMENT HEAT CAPACITY: THEORETICAL PREDICTIONS

A system can be considered as finite-sized near a critical point or a phase transition point if its characteristic linear size $Z$ becomes comparable with the correlation length $\zeta$ of the order parameter fluctuation. As is well known from the fluctuation (scaling) theory of phase transitions (see, e.g., Refs. 11–13), the correlation length is expressed by

$$\zeta = \zeta_0 \tau^{-\nu}, \tag{1}$$

where the amplitude of the correlation length in classical liquids can reach the value $\zeta_0 \approx 1-10$ nm, and $\tau = |T-T_c|/T_c$ is the temperature variable. Nowadays, it has become possible to approach the critical point of classical liquids with respect to the temperature variable to within ''distances'' like $|T-T_c|_{\min} \approx 10^{-2}-10^{-3}$ K for $T_c \approx 10^2$ K, or, using dimensionless values, $\tau_{\min} = |T-T_c|/T_c \approx 10^{-5}$. As the critical exponent of the correlation length is equal to $\nu \approx 0.6705$ (Ref. 14) for the space dimensionality $d=3$, the maximum values of the correlation length in classical liquids can approach such values as $\zeta \approx 1-10\ \text{nm} \times (10^{-5})^{-0.67} \approx 10^3-10^4$ nm.

Spatial insufficiency on an even bigger scale can be realized for quantum liquids, where, because of the very small values of the critical temperature, the correlation length becomes two orders of magnitude larger; i.e., for instance, in liquid helium $\tau \approx 10^{-8}$ and $\zeta/\zeta_0 \approx 10^{5.4}$. So, classical liquid systems that have linear size $Z$ up to a micrometer (for quantum liquids, even to tens of micrometers) could be considered as finite-sized near the critical point (or λ point). The physical properties of finite-size systems preserve their singular behavior only for the directions in which the system still has semi-infinite size. However, taking into account the limited temperature resolution of even extremely precise modern experiments,[4,7] it should be noted that over the limit of a system's smallest confining size of about a few hundreds micrometers the finite-size effect seems to be almost impossible to detect even under conditions of microgravitation. In the case of Earth-based experiments due to the gravity effect that limit will not exceed ten micrometers.[15]

Using high-resolution thermometers[9] it has become possible to determine the exact location of the λ-transition temperature with a precision of $\pm 5$ nK.[6] Since the useful resolution of measurements at the lambda point on Earth is limited in principle by the pressure dependence of the transition temperature (gravity effect), it is important to be sure that the observed rounding of the specific heat is in fact produced by finite-size effects. In spite of that, it has been suggested[6] that gravity does not play a major role in the actual Earth-based experiments with the typical confined size less than 10 $\mu$m. This statement is supported by the fundamental studies of Ahlers (see, for example, Ref. 16) and could be explained in terms of direct calculations of temperature variation due to the gravity effect. In order to proceed, we have to consider the limiting value of the cylinder length $L$ over which the results of a study of the finite-size effect become independent of further increase of $L$. It was found[17,18] that there is no need to take the actual $L \to \infty$ limit, because it turns out that for $L = 5D$ and larger ($D$ is the diameter of a pore), the finite-size effect due to the finite value of $L$ becomes insignificant. The vertical variation of transition temperature $\delta T_\lambda$ over height $L$ of the sample due to the hydrostatic pressure induced by Earth's gravity is determined[19] by the expression $\delta T_\lambda = \gamma L$ with $\gamma = 1.273$ $\mu$K/cm. Thus, for cylinder of radius $D = 8$ $\mu$m[1,6] even the enhanced limit of $L = 80$ $\mu$m corresponds to a maximum variation $\delta T_\lambda \approx 10^{-8}$ K between the bottom and top of the chamber. It is assumed[20] that data are unaffected by gravity if $|T-T_\lambda| \geqslant 10\delta T_\lambda$. In all cases to be discussed below this condition is satisfied. This makes it possible to neglect the gravity effect and simultaneously conduct a reliable study of the finite-size effect in some range of confining sizes. The corresponding theoretical predictions could be suitable for comparison with actual Earth-based measurements.[3,5,6] Furthermore, the same theoretical approach is applicable for comparative study of the results of the microgravity Confined Helium Experiment (CHEX)[1] conducted aboard the space shuttle and, hopefully, future experiments[17,20] which are scheduled to be carried out on the Low Temperature Microgravity Physics Facility (LTMPF) aboard the International Space Station.

The major interest in the statistical physics approach to finite-size phase transitions is to find the pair correlation function $G_2$ of the order parameter fluctuations and the associated correlation length $\zeta$. Here we consider a cylindrical sample with diameter $D$ and length $L \gg D$ and study the region where the value of the correlation length $\zeta$ becomes comparable to or even larger than $D$ but still smaller than $L$. The correlation length could be defined[21] as $\zeta = (M_2)^{1/2}$ in terms of the pair correlation function $G_2$ of the order parameter fluctuations for the reduced geometry of cylindrical form, where $M_2$ denotes the normalized second moment of $G_2$ (for details see Ref. 22). The pair correlation function associated with the order parameter fluctuations was deduced by applying the Helmholtz operator. We have derived $G_2$ from the corresponding differential equation with Dirichlet boundary conditions on the inner wall surface of a cylinder and the condition of $G_2$ decay at long distances, i.e., zero value of $G_2$ on the top and bottom ends of the cylinder. In particular, this type of boundary condition seems to represent

the boundary conditions of the real confined helium experiments more appropriately.[23,24] As follows from the discussion in Ref. 22, anomalous growth of the correlation length might occur at some new temperature $T_c^*$ which is lower than the bulk $T_c$ and accordingly is located in the region of negative $\tau$. For such a case the behavior of the correlation length might obey a scaling law akin to (1), namely

$$\zeta^* = \zeta_0 \tau^{*-\nu}, \tag{2}$$

where $\tau^* = (T - T_c^*)/T_c^*$ is the new temperature variable for a spatially limited system. It should be noted that the defining condition (2) used above means physically that upon the achievement of the new critical temperature $T_c^*$ of a spatially limited liquid in a sample of cylindrical geometry there might exist anomalous growth of the longitudinal component of the correlation length $\zeta^*$ along the cylinder axis as is described by

$$\zeta^* = \zeta_0 \left[ \tau + \left( \frac{\psi_1}{K} \right)^{1/\nu} (\tau + 1) \right]^{-\nu}, \tag{3}$$

where $\zeta_0$ is the amplitude of correlation length, $K = r/\zeta_0$ is the geometrical factor, $r$ is the cylinder radius, $\tau = (T - T_c)/T_c$ is the temperature variable, $\nu$ is the critical exponent of the correlation length, and the quantity $\psi_1$ is determined by the expression $J_0(\psi_1) = eA$ for the case of the constant boundary condition $G_2 = A$ on the cylinder wall surface. Here $J_0$ is the zero-order Bessel function, and $e$ is a transcendental constant equal to 2.7182. In the case of the zero boundary condition $A = 0$, the value of the parameter $\psi_1$ is equal to the first zero of the zero-order Bessel function, $\mu_1 = 2.4048$. Here the boundary effect to the pair correlation function $G_2$ is translated to the boundary condition for the corresponding differential equation.[22]

In order to verify the validity of the theoretical results proposed here and in Refs. 22 and 25 before, it is important to have the possibility of comparing the results with high-resolution experimental data. Since most of the data[1,3,5,6] available to date are derived from the study of the heat capacity of confined $^4$He, it is necessary to obtain an analytical expression for this property particularly. Such a calculation could be conducted on a background of the formulas for the temperature dependence of the correlation length and well-known scaling relations for the heat capacity. While the correlation length $\zeta$ is proportional to $\tau^{-\nu}$, the analogous formula for the temperature dependence of the heat capacity $C$ reads $C \sim \tau^{-\alpha}$, where $\alpha$ is the heat capacity critical exponent, which assumed positive. Combining the two,[26] one can get a scaling relation between the heat capacity and the correlation length:

$$C - \zeta^{\alpha/\nu}. \tag{4}$$

The hyperscaling relation $\alpha = 2 - 3\nu$ (Ref. 27) with $\nu = 0.6705$ yields $\alpha/\nu = -0.0172$. In fact, near the lambda point a small negative value of $\alpha \approx -0.026$ was observed in early experiments.[28] Later, in the most precise microgravity experiment in Earth orbit,[29] it was confirmed to be $\alpha = -0.01285$. However, it is known that near the liquid–gas critical point the exponent $\alpha$ appears to be positive and close to 0.1.[30]

TABLE I. Transition temperature shift: Experimental data versus correspondent theoretical calculation for helium confined in cylindrical samples of different diameters.

| Diameter $D$ of the cylinder | Shift $\Delta\tau_E$, Experiment | Shift $\Delta\tau_T$, Theory | Point No./[Ref.] |
|---|---|---|---|
| 300 Å | $4.0 \cdot 10^{-3}$ | $3.6 \cdot 10^{-3}$ | *C1*/[3] |
| 800 Å | $6.5 \cdot 10^{-4}$ | $8.3 \cdot 10^{-4}$ | *C2*/[3] |
| 1000 Å | $4.3 \cdot 10^{-4}$ | $5.9 \cdot 10^{-4}$ | *C3*/[3] |
| 2000 Å | $1.2 \cdot 10^{-4}$ | $2.1 \cdot 10^{-4}$ | *C4*/[3] |
| 0.26 μm | $1.53 \cdot 10^{-4}$ | $1.44 \cdot 10^{-4}$ | *C5*/[1,5] |
| 8 μm | $1.20 \cdot 10^{-6}$ | $0.87 \cdot 10^{-6}$ | *C6*/[6] |
| 8.17 μm | $1.24 \cdot 10^{-6}$ | $0.85 \cdot 10^{-6}$ | *C7*/[1,5] |

Using the general formula (4) it became possible to obtain a formula for the heat capacity in a particular type of confining geometry by assuming $\zeta = \zeta^*$. The correlation length $\zeta^*$ expressed by Eq. (3) is directly associated with the cylindrical geometry and corresponds to the case of zero boundary condition for the pair correlation function $G_2$ on the inner surface of the confining system. That is why the new expressions for the heat capacity also will retain special parameters, which are related to the particular form of the system. This makes possible an easy comparison with the data of the corresponding experiments. For the case of cylindrical geometry it reads

$$C_{\text{cyl}} \propto \left[ \tau + \left( 2 \frac{\mu_1}{K_{\text{cyl}}} \right)^{1/\nu} (\tau + 1) \right]^{-\alpha}. \tag{5}$$

This equation (5) shows that the heat capacity in the cylindrical geometry remains finite at the bulk $T_\lambda$ ($\tau = 0$) and grows up to its limit at some point below $T_\lambda$ in the region of negative $\tau$.

To carry out further comparison with experimental data, here in Eq. (5) the geometrical factor was redefined: $K_{\text{cyl}} = D/\zeta_0$, with $D$ being the cylinder diameter. The amplitude of the correlation length $\zeta_0$ for helium is equal to 0.36 nm below the transition temperature and to 0.143 nm above it.[31] The parameter $\mu_1 = 2.4048$ is the first zero of the cylindrical Bessel function.[32] The critical exponent $\nu$ is taken to be equal to 0.6705 (Ref. 14), and $\alpha = -0.01285$.[29]

Using Eq. (5) it is possible to evaluate the shift $\Delta\tau$ of the transition temperature from the location of the heat capacity maximum. The corresponding new transition temperature $T_c^*(K)$ is determined by the expression

$$T_c^*(K) = T_c [1 + (2\mu_1 / K_{\text{cyl}})^{1/\nu}]^{-1}. \tag{6}$$

In Table I the experimental data from Refs. 1, 3, 5, 6 for confined helium are combined with the results calculated from Eq. (5) for the same values of the system's sizes. Here, in Table I the quantity $\Delta\tau_E = (T_\lambda - T_m)/T_m$ represents the shifts of the helium heat capacity maximum $T_m$ from its bulk value $T_\lambda$ observed experimentally in respect that $T_\lambda > T_m$, and $\Delta\tau_T$ is the shift calculated according to the proposed theoretical approach from the expression:

$$\Delta\tau_T = (2\mu_1 \zeta_0 / D)^{1/\nu}. \tag{7}$$

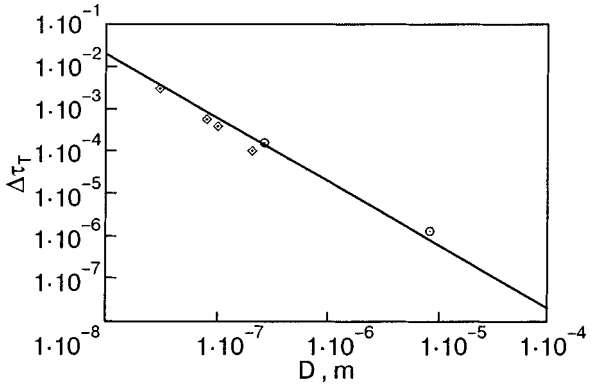


FIG. 1. The dependence of the shift of the transition temperature $\Delta\tau_T$ on the cylindrical pore diameter $D$ in log–log scale [according to Eq. (7)]—solid line. The slope of the plot corresponds to $\nu=0.6705$. ◇ represents the experimental data of Chen and Gasparini.[3] ⊙ represents the experimental data of Lipa *et al.*[5]

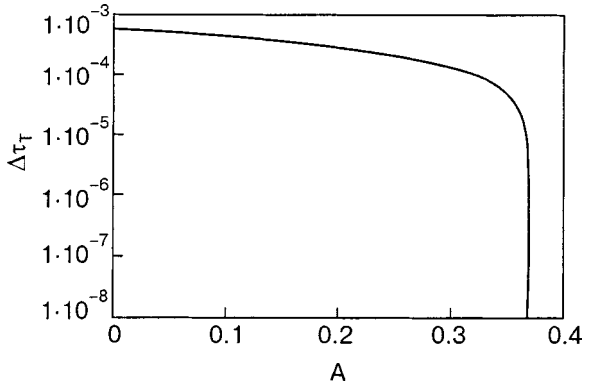


FIG. 2. The dependence of the shift of the transition temperature $\Delta\tau_T$ on the boundary constant $A$ for the sample in a cylindrical pore of diameter 1000 Å in semilog scale [according to Eq. (8)].

### 3. DISCUSSION

In Fig. 1 the dependence of the shift of the transition temperature $\Delta\tau_T$ on the cylindrical pore diameter $D$, which varies from 10 nm up to 10 $\mu$m, is presented in log–log scale for the case of the zero boundary condition. It shows that the value of $\Delta\tau_T$ is decreasing with increasing cylinder diameter. The slope of the plot in Fig. 1 is $1/\nu\approx1.49$, in agreement with the finite-size scaling theory predictions:[13,33] $\Delta\tau = aH^{-1/\nu}$, where $a$ is a constant depending on the geometry. In the case considered above, the linear size of the system $H$ is treated as the cylinder diameter $D$, and consequently the expression for the scaling coefficient $a$ reads: $a=(2\mu_1\zeta_0)^{1/\nu}$.

In Table I the point set $\Delta\tau_E$ $C1-C4$ is taken from the graph presented in the pioneering paper of Ref. 3. At that time, cylindrical pores with diameters 300, 800, 1000, and 2000 Å were investigated. Since it was difficult to determine $\Delta\tau_E$ precisely from that graph in the paper[3] (tabulated data were not included there), the accuracy of these data is limited. A comparison shows that the theoretical values $\Delta\tau_T$ systematically overestimate the shift of the new transition temperature by 30% on average, except $C1$, with a better match. It should be noted that points $C1-C4$ were taken in experiments conducted about twenty-five years ago, but their results are still cited in the related modern papers (see, for example, Ref. 6). However, some remarks[5] concerning the low accuracy and rough agreement with scaling of these early results have to be considered. Values $\Delta\tau_T$ are calculated for the case of zero boundary condition for the pair correlation function $G_2$ that provides the maximum possible value of the shift $\Delta\tau$ for a particular size of the system. However, in a real experiment, depending on the specific features of the surface interaction, the value of the boundary constant could be nonzero—as is also expected to be the case for the binary-mixture experiments—which lead to a decrease of the shift of the new transition temperature. This could be one of the possible reasons for this deviation $\Delta\tau_E$ with $\Delta\tau_T$.

Judicious consideration of the boundary condition is important. As we deal with a liquid in a reduced geometry of cylindrical form, here we introduce the boundary condition to the pair correlation function $G_2$ on the inner surface of the cylinder in the form $G_2=A$. Here $A$ is a certain constant, the exact value of which depends on particular problem. This expression applies to the limiting case of a completely hydrophobic inner cylinder surface for $A=0$ (i.e., the zero boundary condition of the first type sometimes referred as the ''homogeneous condition'') and a hydrophilic one for $A=1$. In practice the situation with intermediate values of $A$ could arise, indicating a partial wetting for which the numerical value in the function varies from 0 to 1. In the general case of constant boundary condition $G_2=A$ on the cylinder surface the shifts $\Delta\tau_T$ will depend on $A$ as

$$J_0(D\Delta\tau_T^{\nu}/2\zeta_0)=eA. \tag{8}$$

For example, for the helium sample in a cylindrical chamber of diameter 1000 Å (this value corresponds to the point $C3$ in Table I) in the case of the constant boundary condition, the dependence of the shift of the transition temperature $\Delta\tau_T$ on the boundary constant $A$ is illustrated by Fig. 2. As can be seen from Fig. 2, while the boundary constant $A$ is decreasing in value the shift $\Delta\tau_T$ grows and reaches its maximum at $A=0$. Since $A$ characterizes the border of the system, this behavior of the shift of the transition temperature may be explained as being due to a competition between the surface interaction near the walls and finite-size effects.

Concerning point $C6$ for an 8-$\mu$m cylinder,[6] the theoretical value $\Delta\tau_T$ appears to be about 30% smaller than the results of that high-precision modern experiment. Reference points $C5$ and $C7$ are taken from the most recent results now available from measurements of the heat capacity of 8.17 $\mu$m and 0.26 $\mu$m cylindrically confined helium.[1,5] This set of the points shows better agreement between the theoretical calculations and experimental data in terms of the shift of transition temperature, especially for the 0.26 $\mu$m diameter pore. It was noticed[5] that the results of the new measurement for 8.17 $\mu$m cylinders do not compare well with previous observations[6] in the region near the heat capacity peak. In contrast, the results for 0.26 $\mu$m Anopore cylinders are in good agreement with Monte Carlo predictions.[10,18]

The heat capacity of $^4$He confined in an 8-$\mu$m diameter cylindrical sample versus reduced temperature on a logarithmic scale is presented in Fig. 3. This data set, calculated

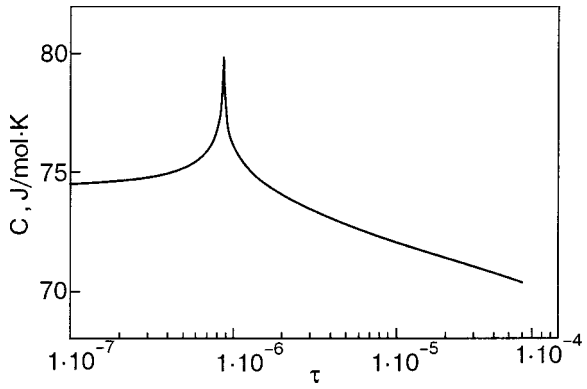


FIG. 3. The dependence of the confined helium heat capacity $C$ on the reduced temperature $\tau$ for the 8-$\mu$m diameter cylindrical sample in semilog scale [according to Eq. (5)].

from Eq. (5), obviously corresponds to the region of negative values of reduced temperature $\tau \leqslant 0$, where $T < T_\lambda$.

## 4. CONCLUSIONS

Finally, it should be noted that over the range of temperature variable from $10^{-2}$, with nanokelvin accuracy, up to the new transition temperature of the confined system, the correlation length, calculated from Eq. (3) in the same way at the heat capacity but with the corresponding critical exponent $\nu$, demonstrates growth at a rate of about $10^5$ times. Consequently, the correlation length reaches a value of the order of tens of micrometers, which in most of the cases considered cases is much greater than the diameter of the cylinder. In fact, the same set of formulas gave good agreement with the experimental results for cylindrical geometry in terms of the shift of the transition temperature and also of the rate of heat capacity growth near the new transition temperature. We believe that other static and dynamical physical properties of finite-size systems, which could be represented near the criticality in terms of scaling relations with a correlation length, could be described in the framework of this study. At this point, the current theoretical approach gave results that are reasonably matched to confined $^4$He heat capacity experimental data over a wide range of system sizes, from tens of nanometers up to about ten micrometers for the cylindrical type of geometry.

In further development of this study we are going to present the results[25] of the heat capacity calculations in the cases of planar and barlike geometry and confirm their consistency with a number of available experimental results[1,7,8,34–36] and Monte Carlo simulations.[10,18]

The results of the complex experimental, numerical and theoretical research on confined systems are considered to be essential for fundamental studies. However, it could be even more important for providing authentic and explicit information on the static and dynamic properties of liquid matter on the micro- and nano-scales to scientists and engineers for practical applications in the field of technical problem-solving and the development of the novel technologies.

K. Ch. would like to express heartiest gratitude to deceased Prof. K. Hamano of Japan and to thank Prof. L. Bulavin at Kiev National University, Prof. A. Chalyi at National Medical University, Ukraine, and Profs. K. Kubota and T. Yamamoto at Gunma University, Japan for numerous helpful discussions and enlightening comments in the course of this research.

*E-mail: kirchal@univ.kiev.ua

[1] J. A. Lipa, M. Coleman, D. R. Swanson, J. A. Nissen, Z. K. Geng, and K. Kim, Physica B **280**, 50 (2000).
[2] G. Fasol, Science **280**, 545 (1998).
[3] Tar-pin Chen and F. M. Gasparini, Phys. Rev. Lett. **40**, 331 (1978).
[4] J. A. Lipa, D. R. Swanson, J. A. Nissen, Z. K. Geng, P. R. Williamson, D. A. Stricker, T. C. P. Chui, U. E. Israelsson, and M. Larson, Phys. Rev. Lett. **84**, 4894 (2000).
[5] J. A. Lipa, M. Coleman, and D. A. Stricker, J. Low Temp. Phys. **124**, 443 (2001).
[6] M. Coleman and J. A. Lipa, Phys. Rev. Lett. **74**, 286 (1995).
[7] S. Mehta and F. M. Gasparini, Phys. Rev. Lett. **78**, 2596 (1997).
[8] S. Mehta, M. O. Kimball, and F. M. Gasparini, J. Low Temp. Phys. **114**, 467 (1999).
[9] X. Qin, J. A. Nissen, D. R. Swanson, P. P. Williamson, D. A. Stricker, J. A. Lipa, T. C. P. Chui, and U. E. Israelsson, Cryogenics **36**, 781 (1996).
[10] N. Schultka and E. Manousakis, Phys. Rev. Lett. **75**, 2710 (1995).
[11] A. Z. Patashinskii and V. L. Pokrovskii, *The Fluctuation Theory of Phase Transitions*, Pergamon Press, Oxford, (1979).
[12] M. E. Fisher, in *Critical Phenomena, Proceedings of the International School of Physics, "Enrico Fermi,"* Course 51, M. S. Green (ed.), Academic Press, New York (1971).
[13] M. E. Fisher, Rev. Mod. Phys. **46**, 597 (1974).
[14] L. S. Goldner and G. Ahlers, Phys. Rev. B **45**, 13129 (1992).
[15] G. Ahlers, J. Low Temp. Phys. **113**, 835 (1998).
[16] G. Ahlers, J. Low Temp. Phys. **115**, 143 (1999).
[17] K. Nho and E. Manousakis, Phys. Rev. B **64**, 144513 (2001).
[18] N. Schultka and E. Manousakis, J. Low Temp. Phys. **111**, 783 (1998).
[19] G. Ahlers, Phys. Rev. **171**, 275 (1968).
[20] P. B. Weichman, A. W. Harter, and D. L. Goodstein, Rev. Mod. Phys. **73**, 1 (2001).
[21] J. L. Lebowitz and J. L. Percus, Phys. Rev. **122**, 1675 (1961).
[22] K. A. Chalyi, K. Hamano, and A. V. Chalyi, J. Mol. Liq. **92**, 153 (2001).
[23] V. Dohm, Phys. Scr. **49**, 46 (1993).
[24] P. Sutterand and V. Dohm, Physica B (Amsterdam) **194–196**, 613 (1994).
[25] K. A. Chalyy, Doctor Thesis, Gunma Univ., Japan (2001).
[26] S. Bhattacharyya and J. K. Bhattacharjee, Phys. Rev. B **58**, 15146 (1998).
[27] M. E. Fisher, Rep. Prog. Phys. **30**, 615 (1967).
[28] K. H. Mueller, G. Ahlers, and F. Pobell, Phys. Rev. B **14**, 2096 (1976).
[29] J. A. Lipa, D. R. Swanson, J. A. Nissen, T. C. P. Chui, and U. E. Israelsson, Phys. Rev. Lett. **76**, 944 (1996).
[30] J. A. Lipa, M. J. Buckingham, and C. Edwards, Phys. Rev. Lett. **25**, 1086 (1970).
[31] A. Singsaas and G. Ahlers, Phys. Rev. B **30**, 5103 (1984).
[32] I. S. Gradshteyn and I. M. Ryzhik, *Tables of Integrals, Series, and Products*, Academic Press, New York (1980), Nauka, Moscow (1971).
[33] K. Binder, Annu. Rev. Phys. Chem. **43**, 33 (1992).
[34] M. O. Kimball, S. Mehta, and F. M. Gasparini, J. Low Temp. Phys. **121**, 29 (2000).
[35] S. Mehta, M. O. Kimball, and F. M. Gasparini, J. Low Temp. Phys. **113**, 435 (1998).
[36] J. A. Nissen, T. C. P. Chui, and J. A. Lipa, J. Low Temp. Phys. **92**, 353 (1993).

This article was published in English in the original Russian journal. Reproduced here with stylistic changes by AIP.

# Classification of the equilibrium states of a superfluid liquid with *d* pairing

A. P. Ivashin,* M. Y. Kovalevsky, and N. N. Chekanova

*National Science Center Kharkov Institute of Physics and Technology, ul. Akademicheskaya 1, Kharkov 61108, Ukraine*

(Submitted January 30, 2004)
Fiz. Nizk. Temp. **30**, 920–927 (September 2004)

A classification of the equilibrium states of a quantum liquid with *d* pairing is given on the basis of the concept of quasi-averages. The order-parameter operator is represented in terms of Fermi operators. It is shown that the set of such equilibrium states can be classified in terms of the quantum number corresponding to the projection of the orbital angular momentum of a Cooper pair on the anisotropy direction. The explicit form of the three admissible generators of the unbroken symmetry is found and the corresponding equilibrium values of the order parameter are obtained. A generalization to possible nonuniform equilibrium structures is carried out, and the corresponding form of the order parameter of such structures is found. © *2004 American Institute of Physics.* [DOI: 10.1063/1.1802951]

## 1. INTRODUCTION

It is known that the classification of equilibrium states of condensed media on the basis of the Ginzburg–Landau phenomenological approach requires knowledge of the form of the free energy as a function of the order parameter and depends substantially on the form of the model under consideration. Another group-theoretical approach is based on representation of the unbroken symmetry of the degenerate equilibrium state as subgroups of the symmetry of the normal phase. Essential to this approach are the corresponding transformation properties of the order parameter under the symmetry transformations of the Hamiltonian. This treatment is free from any model assumptions about the form of the free energy. A classification of the uniform states in the framework of these two approaches has been carried out for superfluid $^3$He,[1–3] which is described by a tensor order parameter. The question of the possible nonuniform superfluid equilibrium states of $^3$He is studied in Ref. 4. Another important example of a degenerate condensed medium is a superfluid liquid in a state of *d* pairing, which is also characterized by a tensor order parameter.[5] Such a state describes the nuclear matter of neutron stars.[6–9] By virtue of the strong spin–orbit coupling there is $^3P_2$ pairing of the neutrons ($l=1$, $S=1$; $J=2$). This type of pairing is possible for $^3$He with $l=2$ (Ref. 20) and for a number of high-temperature superconductors.[11–13] The order parameter describing the state with $J=2$ is a symmetric and traceless tensor. A classification of possible states for this type of pairing was done in Refs. 5 and 14 using a phenomenological approach. In the present paper we propose a microscopic approach to the classification of uniform equilibrium states, based on the concept of quasi-averages.[4,15–18] The admissible symmetry properties of the equilibrium state of a quantum liquid and the order-parameter structures corresponding to them are found from the conditions of unbroken and space symmetry at nonzero values of the order parameter.

## 2. GENERAL PROPERTIES OF THE ORDER PARAMETER AND THE SYMMETRY OF THE EQUILIBRIUM STATE

A theoretical principle of the statistical physics of condensed media with spontaneous symmetry breaking is the concept of Bogolyubov quasi-averages,[15] which generalizes the Gibbs distribution to degenerate condensed media. According to Ref. 15, the quasi-average of a physical quantity in a state of statistical equilibrium with broken symmetry is defined by the formula

$$\langle \hat{a}(x)\rangle \equiv \lim_{\nu\to 0}\ \lim_{V\to\infty} \mathrm{Tr}\ \hat{w}_\nu \hat{a}(x),$$

$$\hat{w}_\nu \equiv \exp(\Omega_\nu - Y_a \hat{\gamma}_a - \nu \hat{F}). \tag{1}$$

Here $\hat{\gamma}_a$ are additive integrals of the motion ($\hat{\mathcal{H}}$ is the Hamiltonian, $\hat{\mathcal{P}}_k$ is the momentum operator, $\hat{N}$ is the particle number operator, $\hat{S}_\alpha$ is the spin operator) and $Y_a \equiv Y_0, Y_k, Y_4, Y_\alpha$ are the thermodynamic forces corresponding to them. For our later convenience we shall assume that in the equilibrium state there are no macroscopic fluxes in the laboratory reference frame, i.e., $Y_k=0$ and the internal magnetic field is equal to zero. The thermodynamic potential $\Omega_\nu$ is determined by the normalization condition $\mathrm{Tr}\,\hat{w}_\nu=1$. The operator $\hat{F}$ has the symmetry of the condensed phase to be investigated and is a linear functional of the order parameter operator $\hat{\Delta}_a(x)$:

$$\hat{F} \equiv \int d^3x (f_a(x,t)\hat{\Delta}_a(x) + \text{h.c.}). \tag{2}$$

The index $a$ characterizes the tensor dimension of the order parameter parameter. In particular, with the use of a scalar order parameter $\hat{\Delta}(x) \equiv (i/2)\hat{\psi}^+(x)\sigma_2\hat{\psi}(x)$ one can describe a superfluid Fermi liquid with singlet pairing,[4] a vector order parameter $\hat{\Delta}_\alpha(x) \equiv \hat{\psi}^+(x)\sigma_\alpha\hat{\psi}(x)$ describes magnetic systems with spontaneous breaking of the symmetry with respect to rotations in spin space, while a tensor form of the order parameter is present in liquid crystals[19] and quantum liquids with triplet pairing.[4] The quantity $f_a(x,t)$ included in

 

the operator $\hat{F}$ is a function of the coordinates conjugate to the order parameter operator, specifying its equilibrium values in the sense of quasi-averages: $\Delta_a(x,t)=\langle\hat{\Delta}_a(x)\rangle$. The structure of the functions $f_a(x,t)$ is determined by the symmetry properties of the quantum-liquid states under investigation. In the framework of the microscopic theory, this makes it possible to introduce additional thermodynamic parameters in the Gibbs distribution.

A description of condensed media with spontaneously broken symmetry relies heavily on the representation of the order parameter. Let us formulate the transformation properties of the order parameter operators. The condition of translational invariance has the form

$$i[\hat{\mathcal{P}}_k,\hat{\Delta}_a(x)]=-\nabla_k\Delta_a(x). \tag{3}$$

The generator of the group of phase transformations is the particle number operator $\hat{N}$. The order parameter operator $\hat{\Delta}_a(x)$ transforms according to the relations

$$[\hat{N},\hat{\Delta}_a(x)]=-g_a\hat{\Delta}_a(x). \tag{4}$$

The constants $g_a$ depend on the tensor dimension of the order parameter operator.

Under transformations related to the internal symmetry group with generators $\hat{S}_\alpha$ ($\alpha=x,y,z$), the operators $\hat{\Delta}_a(x)$ transform according to the representations of this group:

$$i[\hat{S}_\alpha,\hat{\Delta}_a(x)]=-g_{\alpha ab}\hat{\Delta}_b(x) \tag{5}$$

or in compact notation

$$i[\hat{S}_\alpha,\hat{\Delta}(x)]=-\hat{g}_\alpha\hat{\Delta}(x),$$

where $(\hat{g}_\alpha)_{\mathrm{ab}}\equiv g_{\alpha ab}$ are some constants. The generators of the internal symmetry group $\hat{S}_\alpha$ satisfy the relations

$$i[\hat{S}_\alpha,\hat{S}_\beta]=-\varepsilon_{\alpha\beta\gamma}\hat{S}_\gamma, \tag{6}$$

where the antisymmetric tensor $\varepsilon_{\alpha\beta\gamma}$ has the sense of structure constants. Using the Jacobi identity for the operators $\hat{T}$ and $\hat{\Delta}(x)$, from formulas (5) and (6) one can obtain the relation

$$[\hat{g}_\alpha,\hat{g}_\beta]=-\varepsilon_{\alpha\beta\gamma}\hat{g}_\gamma. \tag{7}$$

Under transformations related to the group of space rotations with generators $\hat{\mathcal{L}}_i$ ($i=1,2,3$), the order parameter operators $\hat{\Delta}(x)$ at the point $x=0$ transform according to the representations of that group:

$$i[\hat{\mathcal{L}}_i,\hat{\Delta}_a(0)]=-g_{iab}\hat{\Delta}_b(0).$$

Hence, noting that $[\hat{\mathcal{L}}_i,\hat{\mathcal{L}}_j]=i\varepsilon_{ijk}\hat{\mathcal{L}}_{k,as}$, we obtain relations analogous to (7):

$$[\hat{g}_i,\hat{g}_j]=-\varepsilon_{ijk}\hat{g}_k. \tag{8}$$

since $\hat{\Delta}_a(x)=\exp(-i\hat{\mathcal{P}}x)\hat{\Delta}_a(0)\exp(i\hat{\mathcal{P}}x)$, by virtue of (3) we find

$$i[\hat{\mathcal{L}}_i,\hat{\Delta}_a(x)]=-g_{iab}\hat{\Delta}_b(x)-\varepsilon_{ijk}x_k\nabla_j\hat{\Delta}_a(x). \tag{9}$$

It is known from the phenomenological theory that for adequate description of the thermodynamics of nonequilibrium processes in condensed media with broken symmetry, generally speaking, it is necessary to introduce new thermodynamic parameters unrelated to the conservation laws but deriving from the physical nature of the thermodynamic phase. In the case of normal condensed media the thermodynamic parameters are determined solely by the densities of additive integrals of the motion. The theory of many-particle systems, which describes the equilibrium properties of a normal Fermi liquid, is based on the Gibbs statistical operator

$$\hat{w}=\exp(\Omega-Y_0\hat{\mathcal{H}}-Y_4\hat{N}). \tag{10}$$

The set of thermodynamic forces $Y_a$ includes $Y_0^{-1}\equiv T$ (the temperature) and $Y_4/Y_0\equiv\mu$ (the chemical potential). The additive integrals of the motion which appear in the Gibbs distribution lead to a certain symmetry of the equilibrium state. The symmetry properties of the equilibrium statistical operator (10) have the form

$$[\hat{w},\hat{\mathcal{P}}_k]=0,\ [\hat{w},\hat{\mathcal{H}}]=0,\ [\hat{w},\hat{N}]=0,$$

$$[\hat{w},\hat{S}_\alpha]=0,\ [\hat{w},\hat{\mathcal{L}}_k]=0 \tag{11}$$

and reflect the phase and space–time translational invariance. The conditions of symmetry with respect to rotations in spin space and configuration space mean that the weak dipole and spin–orbit couplings are neglected in the characterization of the equilibrium state. The total symmetry group of the normal equilibrium state of a Fermi liquid has the form

$$G=[SO(3)]_S\times[SO(3)]_{\mathcal{L}}\times[U(1)]_\varphi\times[T(3)]\times[T(1)].$$

Here $[SO(3)]_S$ and $[SO(3)]_{\mathcal{L}}$ are the symmetry groups relative to rotations in spin space and configuration space, $[T(3)]$ and $[T(1)]$ are the translation groups in space and time, and $[U(1)]_\varphi$ is the phase symmetry group. Each element of the group is a unitary operator $U\equiv\exp(i\hat{G}g)$ ($g$ are real and continuous transformation parameters) that leaves the Gibbs distribution invariant:

$$U\hat{w}U^+=\hat{w}.$$

The operators $\hat{\mathcal{P}}_k$, $\hat{N}$, $\hat{S}_\alpha$, $\hat{\mathcal{L}}_k$, and $\hat{\mathcal{H}}$ are generators of these transformations. An average of the form $\mathrm{Tr}[\hat{w},\hat{G}]\hat{b}(x)$ goes to zero at an arbitrary quasilocal operator $\hat{b}(x)$ for $\hat{G}\in(\hat{\mathcal{P}}_k,\hat{N},\hat{S}_\alpha,\hat{\mathcal{L}}_k)$. In particular, this is valid for operators $\hat{b}(x)\equiv\hat{\Delta}_a(x)$ having the physical meaning of order parameter operators and being noncommutative with the integrals of the motion, $\hat{G}$. Since the averages $\mathrm{Tr}\,\hat{w}[\hat{G},\hat{\Delta}_a(x)]$ by virtue of relations (3), (4), (5), and (9) are linear and homogeneous in the order parameter $\hat{\Delta}_a(x)$, which implies that the order parameter vanishes in the normal state.

We shall show how to formulate the symmetry properties of the equilibrium state and to introduce additional thermodynamic parameters for degenerate condensed media. We consider translationally invariant subgroups of the unbroken symmetry $\mathcal{H}$ of the total symmetry group $G$. Translational invariance means that the equilibrium statistical operator satisfies the symmetry relation

$$[\hat{w},\hat{\mathcal{P}}_k]=0. \tag{12}$$

To analyze the translationally invariant subgroups of the unbroken symmetry of the equilibrium states, we start, in accordance with Ref. 17, from the relation

$$[\hat{w},\hat{T}]=0, \tag{13}$$

where the generator of the unbroken symmetry $\hat{T}$ is a linear combination of integrals of the motion:

$$\hat{T}=a_i\hat{\mathcal{L}}_i+b_\alpha\hat{S}_\alpha+c\hat{N}\equiv\hat{T}(\xi) \tag{14}$$

with real parameters $(a_i,b_\alpha,c\equiv\xi)$. Unitary transformations form a continuous subgroup of unbroken symmetry $U(\xi)U(\xi')=U(\xi''(\xi,\xi'))$ of the equilibrium state. From the equations

$$i\mathrm{Tr}[\hat{w},\hat{T}(\xi)]\hat{\Delta}_a(x)=0,\ \ i\mathrm{Tr}[\hat{w},\hat{\mathcal{P}}_k]\hat{\Delta}_a(x)=0,$$

taking the algebraic relations (3)–(5) and (9) and definition (14) into account, we obtain the equation

$$a_i g_{iab}\Delta_b+b_\alpha g_{\alpha ab}\Delta_b+igc\Delta_a=0. \tag{15}$$

In accordance with (14) we have

$$T_{ab}\Delta_b=0,\ \ T_{ab}\equiv a_i g_{iab}+b_\alpha g_{\alpha ab}+igc\,\delta_{ab}. \tag{16}$$

The condition $\Delta_a\neq 0$ for a nontrivial solution of the system of linear equations (16) leads to the relation

$$\det|T_{ab}(\xi)|=0, \tag{17}$$

which imposes restrictions on the admissible values of the parameters $\xi$ related to the generator of the unbroken symmetry.

Let us now consider the equilibrium states that do not have the property of translational invariance (12). In a superfluid condensed medium different physical possibilities for breaking of this invariance of the equilibrium state can in principle exist. This can happen because of the breaking of phase invariance (the superfluid momentum is nonzero) or symmetry with respect to rotations in configuration (spin) space when the vector of the cholesteric (magnetic) helix is nonzero. We assume that the spatial symmetry of equilibrium states of this kind can be specified by the relation

$$[\hat{w},\hat{P}_k]=0,\ \ \hat{P}_k=\hat{\mathcal{P}}_k-p_k\hat{N}-q_{k\alpha}\hat{S}_\alpha-t_{kj}\hat{\mathcal{L}}_j\equiv\hat{P}_k(\eta), \tag{18}$$

where $\eta\equiv p_k,q_{k\alpha},t_{kj}$ are some real parameters of the generator of space symmetry $\hat{P}_k(\eta)$. The generator of the unbroken symmetry of such states will include the momentum operator:

$$\hat{T}\equiv a_1\hat{\mathcal{L}}_i+b_\alpha\hat{S}_\alpha+c\hat{N}+d_i\hat{\mathcal{P}}_i,a_i,b_\alpha,c,d_i\equiv\xi. \tag{19}$$

The relations

$$i\mathrm{Tr}[\hat{w},\hat{T}(\xi)]\hat{\Delta}_a(x)=0,$$

$$i\mathrm{Tr}[\hat{w},\hat{P}_k(\eta)]\hat{\Delta}_a(x)=0 \tag{20}$$

in accordance with (18) and (19) lead to coupling of the parameters $\xi$ and $\eta$ which appear in the definition of the generators of the unbroken and space symmetry. These relations must be supplemented by two more conditions on the parameters of the unbroken and space symmetry, which follow from the Jacobi identity for the operators $\hat{w},\hat{T},\hat{P}_k$ and $\hat{w},P_i,\hat{P}_k$:

$$\mathrm{Tr}[\hat{w},[\hat{T}(\xi),\hat{P}_k(\eta)]]\hat{\Delta}_a=0,$$

$$\mathrm{Tr}[\hat{w},[\hat{P}_i(\eta),\hat{P}_k(\eta)]]\hat{\Delta}_a=0. \tag{21}$$

We note that $\hat{P}_k(\eta)$ is not a translation operator in the usual meaning of the word, since, generally speaking, its spatial components do not commute with each other: $[\hat{P}_k,\hat{P}_i]\neq 0$.

Let us apply the proposed approach to the study of the equilibrium properties of a quantum liquid with $d$ pairing. The order parameter operator of the $d$ pairing, $\hat{\Delta}_{ik}(x)$ is defined in terms of the creation and annihilation operators of a Fermi particle at the point $x$:

$$\hat{\Delta}_{ik}(x)\equiv\nabla_i\hat{\psi}(x)\sigma_2\nabla_k\hat{\psi}(x)+\nabla_k\hat{\psi}(x)\sigma_2\nabla_i\hat{\psi}(x)$$
$$-\frac{2}{3}\delta_{ik}\nabla_j\hat{\psi}(x)\sigma_2\nabla_j\hat{\psi}(x), \tag{22}$$

where $\sigma_2$ is a Pauli matrix. This operator is symmetric with respect to the indices $i$ and $k$ and has the property $\hat{\Delta}_{ii}=0$. An analogous form of the order parameter was considered in a classification of the equilibrium states in liquid crystals,[19] where the order parameter is represented in the form of an Hermitian, symmetric, and traceless tensor. The operators for the particle number $\hat{N}$, momentum $\hat{\mathcal{P}}_k$, spin $\hat{S}_\alpha$, and orbital angular momentum $\hat{\mathcal{L}}_k$ have the form

$$\hat{N}=\int d^3x\hat{n}(x),\quad \hat{S}_i=\int d^3x\hat{s}_i(x),$$

$$\hat{\mathcal{P}}_i=\int d^3x\,\hat{\pi}_i(x),\quad \hat{\mathcal{L}}_i=\int d^3x\hat{l}_i(x), \tag{23}$$

where the corresponding densities of integrals of the motion, $\hat{n}(x)$, $\hat{s}_i(x)$, $\hat{\pi}_i(x)$, and $\hat{l}_i(x)$ are given in terms of the creation $\hat{\psi}^+(x)$ and annihilation $\overline{\hat{\psi}}(x)$ operators by the expressions

$$\hat{n}(x)=\hat{\psi}^+_\sigma(x)\hat{\psi}_\sigma(x),$$

$$\hat{s}_\alpha(x)=\hat{\psi}^+_\sigma(x)(s_\alpha)_{\sigma,\sigma'}\hat{\psi}_{\sigma'}(x),$$

$$\hat{\pi}_i(x)=-\frac{i}{2}[\hat{\psi}^-_\sigma(x)\nabla_i\hat{\psi}_\sigma(x)-\nabla_i\hat{\psi}^+_\sigma(x)\hat{\psi}_\sigma(x)],$$

$$\hat{l}_i(x)=\varepsilon_{ikl}x_k\hat{\pi}_l(x). \tag{24}$$

Using explicit expressions for the integrals of the motion and the order parameter in terms of the field operators (22)–(24), we obtain the operator algebra:

$$[\hat{N},\hat{\Delta}_{ik}(x)]=-2\hat{\Delta}_{ik}(x),[\hat{S}_\alpha,\hat{\Delta}_{ik}(x)]=0,$$

$$i[\hat{\mathcal{P}}_l,\hat{\Delta}_{ik}(x)]=-\nabla_l\hat{\Delta}_{ik}(x),$$

$$i[\hat{\mathcal{L}}_l,\hat{\Delta}_{ik}(x)]=-\varepsilon_{lij}\hat{\Delta}_{jk}(x)-\varepsilon_{lkj}\hat{\Delta}_{ij}(x)$$
$$-\varepsilon_{luv}x_u\nabla_v\hat{\Delta}_{ik}(x). \tag{25}$$

The average value of the order parameter $\Delta_{ik}(x,\hat{\rho})=\mathrm{Tr}\,\hat{\rho}\hat{\Delta}_{ik}(x)$, where $\hat{\rho}$ is an arbitrary statistical operator, has the properties $\Delta_{ik}(x,\hat{\rho})=\Delta_{ki}(x,\hat{\rho})$, $\Delta_{ii}(x,\hat{\rho})=0$ and therefore contains ten independent quantities. We choose the parametrization of $\Delta_{ik}$ in the form

$$\Delta_{ik}(x,\hat{\rho})\equiv Q_{ik}(x,\hat{\rho})+i\underline{Q}_{ik}(x,\hat{\rho}),$$

$$Q_{ik}\equiv A\left[n_in_k-\frac{1}{3}\delta_{ik}\right]+B\left[m_im_k-\frac{1}{3}\delta_{ik}\right],$$

$$Q_{ik}=C\left(n_in_k-\frac{1}{3}\delta_{ik}\right)+D\left(m_im_k-\frac{1}{3}\delta_{ik}\right)$$
$$+E(m_in_k+m_kn_i)+F(n_il_k+n_kl_i)+G(l_im_k+l_km_i). \quad (26)$$

Here $A,B,\ldots,G$ are the moduli of the order parameter, **m**, **n**, and **l** are the anisotropy axes, which are mutually orthogonal unit vectors: $\mathbf{n}^2=\mathbf{m}^2=\mathbf{l}^2=1$, $\mathbf{n}\cdot\mathbf{m}=0$, $\mathbf{m}\cdot\mathbf{l}=0$, $\mathbf{n}\cdot\mathbf{l}=0$. The form of the order parameter (22), (26) and the operator algebra (25) together with (20) and (21) enable one to analyze the equilibrium states of a quantum liquid with *d* pairing.

### 3. TRANSLATIONALLY INVARIANT EQUILIBRIUM STATES OF A SUPERFLUID LIQUID WITH *d* PAIRING

We consider the translationally invariant equilibrium states of the superfluid component and establish the possible equilibrium structures of the order parameter. In analyzing the translationally invariant subgroups of the unbroken symmetry of the equilibrium states we proceed from relations (12) and (13). According to Eq. (13),

$$\mathrm{Tr}[\hat{w},\hat{T}]\hat{\Delta}_{ik}(x)=0$$

or, with (14) and (25) taken into account,

$$a_m(\varepsilon_{mij}\Delta_{jk}+\varepsilon_{mkj}\Delta_{ij})+2ic\Delta_{ik}=0.$$

As a result, we arrive at a system of linear and homogeneous equations

$$F^{ik}_{jl}\Delta_{jl}=0, \quad (27)$$

where $a_l(\varepsilon_{lij}\delta_{kl}+\varepsilon_{lkj}\delta_{il})+2ic\,\delta_{kl}\delta_{ji}\equiv F^{ik}_{jl}$.

Going over in formula (27) from the double to a single summation in which the summation indices run over the values $\alpha,\beta$: $11\equiv1$; $12\equiv2;\ldots33\equiv9$, we obtain the equation

$$F^{\beta}_{\alpha}\Delta_{\alpha}=0,\ \det|F^{\beta}_{\alpha}|=0. \quad (28)$$

The relation $\det|F^{\beta}_{\alpha}|=0$ is the existence condition for a nontrivial solution of the system of linear homogeneous equations (28). The three solutions of the equation $\det|F^{\beta}_{\alpha}|=0$ have the form

$$c=0,\ c=\pm\frac{1}{2}a, c=\pm a.$$

Consequently, the generators of the unbroken symmetry of the equilibrium state of the superfluid liquid with *d* pairing can be written in the form

$$T=\frac{a_i}{a}\hat{\mathcal{L}}_i-\frac{m}{2}\hat{N}.$$

Here $m\equiv2c/a$ is a quantum number that takes on values $0,\pm1,\pm2$. Using definition (26), we obtain from (27) an equation determining the explicit form of the order parameter in equilibrium:

$$\frac{a_i}{a}(\varepsilon_{iuj}Q_{jv}+\varepsilon_{ivj}Q_{ju})-mQ_{uv}=0,$$
$$\frac{a_i}{a}(\varepsilon_{iuj}Q_{jv}+\varepsilon_{ivj}Q_{ju})+mQ_{uv}=0. \quad (29)$$

In solving this system of equations we resolve the vector **a** with respect to the indicated set of basis vectors: $\mathbf{q}\equiv\mathbf{a}/a=\alpha\mathbf{n}+\beta\mathbf{m}+\gamma\mathbf{l}$. The values of $\alpha$, $\beta$, and $\gamma$ are related by the equation $\alpha^2+\beta^2+\gamma^2=1$. We set $m=0$ in (29) and consider the following cases:

1. $\alpha\neq0$, $\beta\neq0$, $\gamma\neq0$. In this case the amplitudes of the order parameter $A=0$ and $B=0$ and, consequently, $\Delta_{uv}=iQ_{uv}$:

$$\Delta_{uv}=\frac{iE}{\alpha\beta}\left(q_uq_v-\frac{1}{3}\delta_{uv}\right). \quad (30)$$

2. $\gamma=0$, $\beta\neq0$, $\alpha\neq0$ (and the equivalent cases $\beta=0$, $\alpha\neq0$, $\gamma\neq0$ and $\alpha=0$, $\beta\neq0$, $\gamma\neq0$). Here again we have $A=0$, $B=0$, and $\Delta_{uv}=iQ_{uv}$:

$$\Delta_{uv}=\frac{i\widetilde{C}}{\alpha^2}\left(q_uq_v-\frac{1}{3}\delta_{uv}\right). \quad (31)$$

3. $\alpha\neq0$, $\beta=\gamma=0$ (and the equivalent cases $\beta\neq0$, $\alpha=\gamma=0$ and $\gamma\neq0$, $\beta=\alpha=0$). Here $A\neq0$, $C\neq0$, i.e., the real and imaginary parts of the order parameter are nonzero: $\Delta_{uv}=Q_{uv}+iQ_{uv}$:

$$\Delta_{uv}=(A+iC)\left(q_uq_v-\frac{1}{3}\delta_{uv}\right). \quad (32)$$

In all three cases we obtained a structure of the order parameter similar to a uniaxial liquid crystal with a complex amplitude.

For $m\neq0$ the solution of equations (29) has the form

$$\Delta_{uv}=A\left(n_un_v-\frac{1}{3}\delta_{uv}\right)+B\left(m_um_v-\frac{1}{3}\delta_{uv}\right)+i[E(m_vn_u$$
$$+m_un_v)+F(l_vn_u+l_un_v)+G(l_vm_u+l_um_v)], \quad (33)$$

where $E=(\gamma/m)(B-A)$, $G=-(\alpha/m)B$, $F=(\beta/m)A$.

Similarly, let us consider all the possible values of the coefficients $\alpha$, $\beta$, and $\gamma$ for the $m=0$ case.

1. $\alpha\neq0$, $\beta\neq0$, $\gamma\neq0$. In this case the amplitudes of the order parameter $A=0$ and $B=0$ and, hence, $\Delta_{uv}=0$ (there is no nontrivial solution).

2. $\gamma=0$, $\beta\neq0$, $\alpha\neq0$ (and the equivalent cases $\beta=0$, $\alpha\neq0$, $\gamma\neq0$ and $\alpha=0$, $\beta\neq0$, $\gamma\neq0$). Here we have $A\neq0$, $B\neq0$. For such values of the parameters there exists only the solution for $m=\pm1$:

$$\Delta_{uv}=A(n_un_v-m_um_v)\pm\frac{iA}{\sqrt{2}}(l_v(n_u+m_u)+l_u(n_v+m_v)), \quad (34)$$

and here $\beta^2=\alpha^2=1/2$.

3. $\gamma=0$, $\beta=0$, $\alpha=1$ (and the equivalent cases $\beta=0$, $\alpha=0$, $\gamma=1$ and $\alpha=0$, $\gamma=0$, $\beta=1$). A solution exists only for $m=\pm2$:

$$\Delta_{uv}=A(m_um_v-l_ul_v)\mp iA(l_vm_u+l_um_v). \quad (35)$$

In order to compare the results obtained with the results of Refs. 5 and 14, we introduce the average

$$\Delta\equiv k_i\Delta_{ij}k_j, \quad (36)$$

where the unit vector **k** is given by

$$\mathbf{k}\equiv \sin\theta\sin\varphi\mathbf{m}+\cos\theta\mathbf{n}+\sin\theta\cos\varphi\mathbf{l}. \quad (37)$$

For solutions (31), (32), and (33) at $m=0$ we find, in accordance with (36) and (37),

$$\Delta_1^{(0)}=\pm i\sqrt{\frac{3}{2}}\left[(\beta k_y+\alpha k_2+\gamma k_2)^2-\frac{1}{3}\right],$$

$$\Delta_2^{(0)}=\pm i\sqrt{\frac{3}{2}}\left[(\beta k_y+\alpha k_z)^2-\frac{1}{3}\right],$$

$$\Delta_3^{(0)}=(A+iC)\left(k_z^2-\frac{1}{3}\right), \quad (38)$$

where $A^2+C^2=3/2$. These solutions correspond to the ''real'' state obtained in Ref. 5.

Solution (34) for $m=\pm 1$ leads, by virtue of (36) and (37), to the relation

$$\Delta^{(1)}=A(k_x+k_y)(\pm i\sqrt{2}k_z+k_y-k_x), \quad (39)$$

where $A^2=1/4$.

Finally, for solution (35) ($m=\pm 2$) we obtain

$$\Delta^{(2)}=A(k_x\pm ik_y)^2,$$

where $A^2=1/4$. This solution corresponds exactly to the ''axial'' case of Ref. 5.

Comparing the expressions obtained for the order parameter with the results of Refs. 5 and 14, we see that there is no equivalence in the solutions for the ''cyclic'' state (39). The reason is that, in contrast to the approach of Ref. 20, here we are considering only the spontaneous breaking of a continuous symmetry and are not taking into account a breaking of discrete symmetry. Therefore, the solutions (39) and the ''cyclic'' state of Ref. 14 are of different origins. Analysis of the equilibrium states of superfluid systems with allowance for the possibility of discrete symmetry breaking requires a separate treatment.

## 4. INHOMOGENEOUS EQUILIBRIUM STATES OF THE SUPERFLUID PHASES OF A QUANTUM LIQUID WITH *d* PAIRING

For classification of the inhomogeneous states we first consider the subgroups of the space symmetry, the generator of which consists of two operators. Let

$$[\hat{w},\hat{P}_k]=0,$$

$$\hat{P}_k\equiv\hat{\mathcal{P}}_k-p_k\hat{N}. \quad (40)$$

According to (40) and the algebra (25), we obtain the following equation for the order parameter:

$$\nabla_i\Delta_{qk}(x)=2ip_i\Delta_{qk}(x), \quad (41)$$

the solution of which has the form

$$\Delta_{qk}(x)=\exp(2i\varphi(x))\underline{\Delta}_{qk}(0),\quad \varphi(x)=\varphi+\mathbf{px}, \quad (42)$$

where $\underline{\Delta}_{qk}(0)$ is the homogeneous part of the order parameter, which is independent of the coordinates. By virtue of the explicit form of the generator of the unbroken symmetry (19) and Eq. (41), the following equation is valid:

$$a_k(\varepsilon_{kil}\underline{\Delta}_{ql}+\varepsilon_{kql}\underline{\Delta}_{li}+\varepsilon_{kuv}x_u\nabla_v\Delta_{qi})+2i\underline{c}\underline{\Delta}_{qi}=0,$$

where $\underline{c}\equiv c+\mathbf{p}\cdot\mathbf{d}$. The requirement that the term linear in the coordinate in this equation be zero implies the following relation for the equilibrium structure of the order parameter:

$$a_k(\varepsilon_{kil}\underline{\Delta}_{ql}+\varepsilon_{kql}\underline{\Delta}_{li})+2i\underline{c}\underline{\Delta}_{qi}=0,\ \mathbf{a}\times\mathbf{p}=0.$$

We see that the classification procedure set forth above is valid for the homogeneous part of the order parameter $\underline{\Delta}_{qk}(0)$ (42).

Let us now investigate the space symmetry, which is determined by the relation

$$[\hat{w},\hat{P}_k]=0,\ \hat{P}_k\equiv\hat{\mathcal{P}}_k-t_{kj}\hat{\mathcal{L}}_j. \quad (43)$$

The condition of space symmetry (43) and the algebra (25) lead to the system of equations

$$\nabla_i\Delta_{qk}(x)=t_{ij}(\varepsilon_{jkl}\Delta_{ql}(x)+\varepsilon_{jql}\Delta_{lk}(x)+\varepsilon_{juv}x_u\nabla_u\Delta_{qk}(x)),$$

$$t_{ij}\varepsilon_{juv}\nabla_v\Delta_{qk}(x)=0, \quad (44)$$

from which we obtain a condition on the admissible structure of the parameter $t_{ij}$:

$$t_{ij}\varepsilon_{juv}t_{v\lambda}(\varepsilon_{\lambda kl}\Delta_{ql}(x)+\varepsilon_{\lambda ql}\Delta_{lk}(x))=0. \quad (45)$$

The value of $t_{kj}$ will be sought in the form $t_{kj}=t\delta_{kj}+t_i\varepsilon_{ikj}+t_{kj}^2$, where $t_{kj}^2$ is a symmetric and traceless tensor. We substitute this expression into (45) and take into account that this relation is valid for any values of the indices. By convolving it with the tensor $(\delta_{ki}\delta_{lu}-\delta_{ku}\delta_{li})$, we obtain equations of coupling to the parameters of the matrix $t_{kj}$:

$$6t^2-t_n^2-t_{i\lambda}^s t_{i\lambda}^s=0. \quad (46)$$

By convolving relation (46) with the tensor $\varepsilon_{klu}$, we arrive at the equation

$$t_j(t\delta_{ij}+t_{ij}^s)=0. \quad (47)$$

A consequence of Eqs. (46) and (47) is that $t_j=0$. We now turn to the Jacobi identity for the operators $\hat{w}$, $\hat{P}_i$, $\hat{P}_k$. In accordance with the explicit form of (43) we find the conditions on the structure of the matrix elements $t_{ij}$:

$$t_{ii}t_{kl}^2-t_{ik}t_{kl}t_{li}=0,\quad t_{ik}t_{ki}-t_{ii}t_{kk}=0. \quad (48)$$

It is not hard to find the explicit form of the matrix $t_{ij}$ satisfying Eqs. (46)–(48):

$$t_{ik}=tl_il_k. \quad (49)$$

The spatially nonuniform part of the order parameter can be found from Eq. (44) with (49) taken into account. The solution has the form

$$\Delta_{qi}(x)=a_{qv}(\mathbf{l}\psi(x))a_{ik}(\mathbf{l}\psi(x))\underline{\Delta}_{vk}(0), \quad (50)$$

where $a_{ik}(\mathbf{l}\psi(x))$ is an orthogonal matrix of rotation in configuration space around the axis $\mathbf{l}$ by an angle $\psi(x)=\psi-t\mathbf{l}\cdot\mathbf{x}$. This solution describes a helicoidal structure. The quantity $2\pi t^{-1}$ determines the pitch of the helicoid, the direction of which is specified by the unit vector $\mathbf{l}$.

The condition of unbroken symmetry (13), (19) with (43), (50) taken into account leads to the equation

$$\underline{a}_k(\varepsilon_{kil}\Delta_{ql}+\varepsilon_{kql}\Delta_{li}+\varepsilon_{kuv}x_u\nabla_v\Delta_{qi})+2ic\Delta_{qi}=0, \quad (51)$$

where $\underline{a}_i \equiv a_i + t l_i \mathbf{l}\cdot\mathbf{d}$. Hence we obtain the relation $\underline{\mathbf{a}}\times\mathbf{l}=0$, which restricts the structure of the order parameter and which arises from the requirement that there be no term linear in the coordinate in Eq. (51) and the equation for the uniform part of the order parameter

$$\underline{a}_k(\varepsilon_{kil}\underline{\Delta}_{ql}+\varepsilon_{kql}\underline{\Delta}_{li})+2ic\underline{\Delta}_{qi}=0.$$

The general structure of the space symmetry operator according to (40) and (43) has the form

$$\hat{P}_k \equiv \hat{\mathcal{P}}_k - p_k\hat{N} - t l_j l_k \hat{\mathcal{L}}_j . \tag{52}$$

The condition of space symmetry of the equilibrium state of the Fermi liquid under consideration must be supplemented with the condition that the symmetry of the equilibrium state (13) be unbroken, where the generator $\hat{T}$ is defined by Eq. (19). In accordance with these symmetry conditions we write the relations

$$i\mathrm{Tr}[\hat{w},\hat{T}]\hat{\Delta}_{qk}(x)=0,\ \ i\mathrm{Tr}[\hat{w},\hat{P}_i]\hat{\Delta}_{qk}(x)=0.$$

Hence we obtain equations establishing the equilibrium structure of the order parameter and find the restrictions on the parameters $a_i$, $b_\alpha$, $c$, $d_i$ of the generator $\hat{T}$ and on the parameters $p_k$, $t$, $l_k$ of the space symmetry operator $\hat{P}_k$:

$$\begin{aligned}&\underline{a}_i(\varepsilon_{ikl}\Delta_{ql}(x)+\varepsilon_{iql}\Delta_{lk}(x)+\varepsilon_{iuv}x_u\nabla_v\Delta_{qk}(x))\\&\qquad+2i\underline{c}\Delta_{qk}(x)=0,\\&\nabla_i\Delta_{qk}(x)=2ip_i\Delta_{qk}(x)+tl_il_j[\varepsilon_{jkm}\Delta_{qm}(x)+\varepsilon_{jqm}\Delta_{mk}(x)\\&\qquad+\varepsilon_{juv}x_u\nabla_v\Delta_{qk}(x)].\end{aligned}\tag{53}$$

The parameters $\underline{a}_i$, $\underline{c}$ are related to the quantities $a_i$, $c$ by the relations

$$\underline{a}_j \equiv a_i + t l_i \mathbf{l}\cdot\mathbf{d}, \underline{c} \equiv c + \mathbf{p}\cdot\mathbf{d}.$$

The requirement that there be no terms linear in the coordinates in Eqs. (53) leads to the relations

$$\begin{aligned}&l_j\varepsilon_{juv}[2ip_v\Delta_{qk}(x)+tl_vl_r(\varepsilon_{rkm}\Delta_{qm}(x)+\varepsilon_{rqm}\Delta_{mk}(x))]=0,\\&\underline{a}_j\varepsilon_{juv}[2ip_v\Delta_{qk}(x)+tl_vl_m(\varepsilon_{mkn}\Delta_{qn}(x)+\varepsilon_{mqn}\Delta_{nk}(x))]=0,\end{aligned}\tag{54}$$

which permit relating the direction of the vectors $\mathbf{p}$ and $\mathbf{l}$ relative to each other and to the vector $\underline{\mathbf{a}}$. Equations (53) and (54) are the basis for analysis of the classification of the equilibrium states of superfluid phases of a quantum liquid with $d$ pairing with the space symmetry generator (52). The solution of this equation in (53) has the form

$$\Delta_{qi}(x)=e^{2i\varphi(x)}a_{qv}(\mathbf{l}\psi(x))a_{ik}(\mathbf{l}\psi(x))\underline{\Delta}_{vk}(0).\tag{55}$$

Relation (54) holds if the vectors $\mathbf{p}$, $\mathbf{l}$, and $\underline{\mathbf{a}}$ are collinear. In this case the first equation of (53) permits one to reduce the equation for the uniform part of the order parameter $\underline{\Delta}_{vk}(0)$ to the form

$$\underline{a}_i(\varepsilon_{ikl}\underline{\Delta}_{ql}(0)+\varepsilon_{iql}\underline{\Delta}_{lk}(0))+2i\underline{c}\underline{\Delta}_{qk}(0)=0.$$

Let us study the condition of stationarity of the superfluid states of a quantum liquid with $d$ pairing. The time dependence in $\Delta=\Delta(x,t)$ is due to the fact that the introduction of a source $F$ breaks the invariance of the equilibrium statistical operator $\hat{w}$ with respect to translations in time, i.e., $[\hat{w},\hat{\mathcal{H}}]\neq 0$. The equilibrium statistical operator satisfies the Neumann condition, as a consequence of which

$$\exp(-i\hat{\mathcal{H}})\hat{w}(t)\exp(i\hat{\mathcal{H}}\tau)=\hat{w}(t+\tau).$$

The equilibrium Gibbs statistical operator obeys the relation

$$[\hat{w},\hat{H}]=0,\ \ \hat{H}=\hat{\mathcal{H}}+p_0\hat{N},\ \ p_0=Y_4/Y_0.$$

Taken together with the stationarity condition, the Neumann condition permits determination of the time dependence of equilibrium averages. In particular, for the order parameter we have

$$\mathrm{Tr}\ \hat{w}(t)\hat{\Delta}_{qk}(x)=\mathrm{Tr}\ \hat{w}(0)\exp(i\hat{N}p_0t)\hat{\Delta}_{qk}(x)\exp(-i\hat{N}p_0t),$$

from which we get

$$\Delta_{qk}(x,t)=\exp(2ip_0t)\mathrm{Tr}\ \hat{w}(0)\hat{\Delta}_{qk}(x).\tag{56}$$

Relations (55) and (56) determine the space–time dependence of the order parameter in the equilibrium state.

## CONCLUSION

The classification of equilibrium states of a quantum liquid with $d$ pairing has been generalized to nonuniform equilibrium states on the basis of the concept of quasi-averages. The admissible conditions of the unbroken and space symmetries has been found. The possibility of liquid-crystal ordering in such quantum liquids has been shown.

This study was supported by the Russian Foundation for Basic Research (Grant N 03-02-17695) and by INTAS (Grant N 00-00577).

*E-mail: ivashin@kipt.kharkov.ua

[1] G. Barton and M. Moore, J. Phys. C **7**, 4220 (1974).
[2] H. W. Capel, *Proceedings of the 5th International Symposium on Selected Topics in Statistical Mechanics*, Dubna, Aug. 22–24, 1989; publ. World Scientific, Singapore (1990), p. 73.
[3] D. Vollhardt and P. Wölfle, *The Superfluid Phases of Helium 3*, Taylor and Francis, London–New York (1990).
[4] M. Yu. Kovalevsky, S. V. Peletminsky, and N. N. Chekanova, Fiz. Nizk. Temp. **28**, 327 (2002) [Low Temp. Phys. **28**, 227 (2002)].
[5] N. D. Mermin, Collected articles ''Superfluidity of helium-3'' [in Russian], (1977), p. 110.
[6] D. Pines and A. Alpar, Nature (London) **316**, 27 (1985).
[7] M. Baldo, J. Cugnon, A. Lejeune, and U. Lombardo, Nucl. Phys. A **536**, 349 (1992).
[8] V. C. Schaab, F. Weber, M. Weigel, and N. Glendenning, Nucl. Phys. A **605**, 531 (1996).
[9] O. Elgaroy, L. Engvik, M. Hjorth-Jensen, and E. Osnes, Nucl. Phys. A **607**, 425 (1996).
[10] N. D. Mermin and C. Stare, Phys. Rev. Lett. **30**, 1135 (1973).
[11] D. J. Van Harlingen, Rev. Mod. Phys. **67**, 515 (1995).
[12] C. C. Tsuei and J. R. Kirtley, Rev. Mod. Phys. **72**, 969 (2000).
[13] H. Won and K. Maki, Phys. Rev. B **49**, 1397 (1994).
[14] T. L. Ho and S. S. Yip, Phys. Rev. Lett. **82**, 247 (1999).
[15] N. Bogolyubov, Proc. Steklov Institute of Mathematics **2**, 3 (1988).
[16] N. N. Bogolyubov Jr., M. Yu. Kovalevskiĭ, A. M. Kurbatov, S. V. Peletminskiĭ, and A. N. Tarasov, Usp. Fiz. Nauk **159**, 585 (1989) [Sov. Phys. Usp. **32**, 1041 (1989)].
[17] V. P. Mineev, Sov. Sci. Rev., Sect. A **2**, 173 (1980).
[18] M. Yu. Kovalevskiĭ and A. A. Rozhkov, Teor. Mat. Fiz. **113**, 313 (1997).
[19] M. Yu. Kovalevskiĭ and N. N. Chekanova, Vestnik Kharkovskogo Universiteta, No. 541, ser. fizicheskaya ''Yadra, chastitsy, polya,'' issue 4(16), 59 (2001).
[20] C. Bruder and D. Vollhardt, Phys. Rev. B **34**, 131 (1986)

Translated by Steve Torstveit

# Unified equation of state of $^3$He–$^4$He liquid mixtures over the whole concentration range at temperatures of 2.25–4.2 K and pressures up to 10 MPa

R. M. Sibileva,* L. V. Karnatsevich, and M. A. Khazhmuradov

*National Science Center Kharkov Institute of Physics and Technology, ul. Akademicheskaya 1, Kharkov 61108, Ukraine*

A. V. Meriuz

*National Technical University Kharkov Polytechnic Institute, ul. Frunze 21, Kharkov 61102, Ukraine*

(Submitted February 10, 2004; revised March 11, 2004)
Fiz. Nizk. Temp. **30**, 928–931 (September 2004)

A unified empirical equation of state for $^3$He–$^4$He mixtures is found in analytical form on the basis of the existing experimental $P-V-T$ data for pure $^3$He, $^4$He, and their mixtures in the homogeneous liquid phase in the temperature interval 2.25–4.2 K and pressure interval 0–10 MPa. An algorithm for calculating the fitting coefficients of an approximating expression for $P(V,T,c)$ is constructed. The average absolute error for the determination of $P$ is $\pm 0.015$ MPa. © *2004 American Institute of Physics.* [DOI: 10.1063/1.1802952]

## 1. INTRODUCTION

Detailed data tables for the thermodynamic characteristics of $^3$He–$^4$He mixtures over a wide range of temperatures and pressures are needed for designing dilution refrigerators utilizing $^3$He in $^4$He, which are widely used in modern cryogenic technique. Because of the nonideality of $^3$He–$^4$He mixtures in the liquid and dense fluid phases the required $P-V-T$ relations cannot be obtained by starting from the corresponding data for pure isotopes.

The molar volumes of $^3$He–$^4$He liquid mixtures at pressures up to 10 MPa in the temperature interval 1.5–4.2 K have been determined experimentally at the Laboratory of Molecular Physics and Cryogenic Technique at the Kharkov Institute of Science and Technology.[1] Mixtures with $^3$He concentrations of 35.2, 50.7, and 65.1% were studied, and also pure $^3$He and $^4$He. The most convenient way of using experimental data in practice is undoubtedly to compose an empirical equation of state of the mixtures in analytical form, with the concentration $c$ of the mixture as one of the variables, i.e., $P=P(T,V,c)$, where $P$ is the pressure, $T$ is the temperature, and $V$ is the molar volume.

In our previous paper[2] we used the experimental results of Ref. 1 and the $P-V-T$ data on the vapor-saturation line[3,4] and on the start-of-solidification line of the mixtures[5] to find an empirical equation of state in analytical form for equimolar liquid mixtures in the pressure interval 1.5–4.2 K and pressure interval 0–10 MPa. The quality of approximation corresponded to the error in the experimental determination of $V$ as a function of $P$ and $T$ and on average equaled 0.5%.

In a continuation of that study we now address the problem of using the whole body of experimental data[1] obtained in our laboratory for $^3$He–$^4$He and also the $P-V-T$ relations for mixtures in the liquid phase along the vapor-saturation and start-of-solidification lines. We obtain an approximating expression for the dependence of $P$ on $T$, $V$, and $c$ and calculate the adjustable parameters in that expression.

## 2. CHOICE OF THE ANALYTICAL FORM OF THE APPROXIMATING EXPRESSION AND CALCULATION OF THE FITTING PARAMETERS

A preliminary processing of the experimental data showed that $P(T,V,c)$ depends on the concentration $c$ of the mixture in a practically linear manner. The approximating expression for the pressure $P$ was written in the form

$$P(T,V,c)=B_0(T,V)+cB_1(T,V). \tag{1}$$

The form of the functions $B_0(T,V)$ and $B_1(T,V)$ is analogous to the approximating expression for $P(T,V)$ proposed in Ref. 2 for an equimolar mixture:

$$B_0(T,V)=\sum_{i=1}^{4} A_{0i}V^{-(i+2)},$$

$$A_{0i}=10^{2i+5}\sum_{j=1}^{6} c_{ij}T^{j-1}. \tag{2}$$

This analytical form is close to the expression proposed by McCarty[6] for the equation of state of $^4$He.

Analogously, the function $B_1(T,V)$ has the form

$$B_1(T,V)=\sum_{i=1}^{4} A_{1i}V^{-(i+2)},$$

$$A_{1i}=10^{2i+5}\sum_{j=1}^{6} n_{ij}T^{j-1}. \tag{3}$$

Thus

$$B_0(T,V)=\sum_{i=1}^{4}\left(10^{2i+5}\sum_{j=1}^{6} c_{ij}T^{j-1}\right)V^{-(i+2)},$$

$$B_1(T,V)=\sum_{i=1}^{4}\left(10^{2i+5}\sum_{j=1}^{6} n_{ij}T^{j-1}\right)V^{-(i+2)}. \tag{4}$$

Here $c_{ij}$ and $n_{ij}$ are adjustable parameters of the equation.

 

TABLE I. Parameters of Eqs. (4).

| | | |
|---|---|---|
| $c_{11}= 9.53559061$ | $c_{35}= 3.85148500\cdot10^{-2}$ | $n_{23}= 5.11269804$ |
| $c_{12}=-13.2837482$ | $c_{36}=-1.87902454\cdot10^{-3}$ | $n_{24}= -1.27382166$ |
| $c_{13}= 7.23976856$ | $c_{41}= -0.123917328$ | $n_{25}= 0.150496848$ |
| $c_{14}= -1.92799611$ | $c_{42}= 0.168634693$ | $n_{26}=-6.59496588\cdot10^{-3}$ |
| $c_{15}= 0.250564135$ | $c_{43}=-8.95642269\cdot10^{-2}$ | $n_{31}= -1.62714175$ |
| $c_{16}=-1.26835869\cdot10^{-2}$ | $c_{44}= 2.30987071\cdot10^{-2}$ | $n_{32}= 2.13974692$ |
| $c_{21}= -6.75953671$ | $c_{45}=-2.87784257\cdot10^{-3}$ | $n_{33}= -1.07972036$ |
| $c_{22}= 9.34047336$ | $c_{46}= 1.37471442\cdot10^{-4}$ | $n_{34}= 0.258172437$ |
| $c_{23}= -5.04816635$ | $n_{11}= -10.8758290$ | $n_{35}=-2.85479771\cdot10^{-2}$ |
| $c_{24}= 1.33062079$ | $n_{12}= 14.8347513$ | $n_{36}=1.10646565\cdot10^{-3}$ |
| $c_{25}= -0.170645120$ | $n_{13}= -7.86620292$ | $n_{41}= 0.118185237$ |
| $c_{26}= 8.48645096\cdot10^{-3}$ | $n_{14}= 2.01945197$ | $n_{42}= -0.151559652$ |
| $c_{31}= 1.58960358$ | $n_{15}= -0.249344254$ | $n_{43}=7.36931680\cdot10^{-2}$ |
| $c_{32}= -2.17938087$ | $n_{16}= 1.17224544\cdot10^{-2}$ | $n_{44}=-1.66072555\cdot10^{-2}$ |
| $c_{33}= 1.16781118$ | $n_{21}= 7.343956573$ | $n_{45}= 1.64601906\cdot10^{-3}$ |
| $c_{34}= -0.3045562759$ | $n_{22}= -9.85275702$ | $n_{46}=-4.87523739\cdot10^{-5}$ |

Thus, the approximating expression for the pressure $P$ contains 48 terms. This number of terms in the equation is dictated by the fact that Eq. (1) is an expansion of the pressure $P$ in three parameters: temperature, molar volume, and mixture concentration. The expansion of the pressure in powers of $V$ for an isotherm consists of four terms; the addition of another term of the expansion has practically no effect on the accuracy of the approximation, but doing without the fourth term leads to a degradation of the accuracy of the approximation by a factor of 2–4. The expansion with respect to $T$ has 6 terms; the optimality of this number of terms was also investigated. The equation for $P$ for an equimolar mixture in our previous study[2] also contained precisely 24 terms. The introduction of concentration dependence doubles the number of terms of the expansion.

The data file used for calculating the 48 adjustable parameters included the results of Ref. 1 (around 1000 experimental points for three mixtures and for pure $^3$He and $^4$He) and the data of Refs. 3–5 for the $P-V-T$ relations for mixtures and the pure substances along the saturated-vapor and start-of-solidification lines. The isotherms $T=1.5$, 1.75, 2.00 K were not included in the data file, since $^4$He is superfluid at those temperatures.

The results of the calculation of the fitting of the adjustable parameters of Eq. (4) are listed in Table I.

The average absolute deviation between all the experimental and calculated values of the pressure $P$ for the mixtures and pure $^3$He and $^4$He is $\pm0.015$ MPa for the isotherms with $T=2.5-4.2$ and $\pm0.02$ MPa for the $T=2.25$ K isotherm.

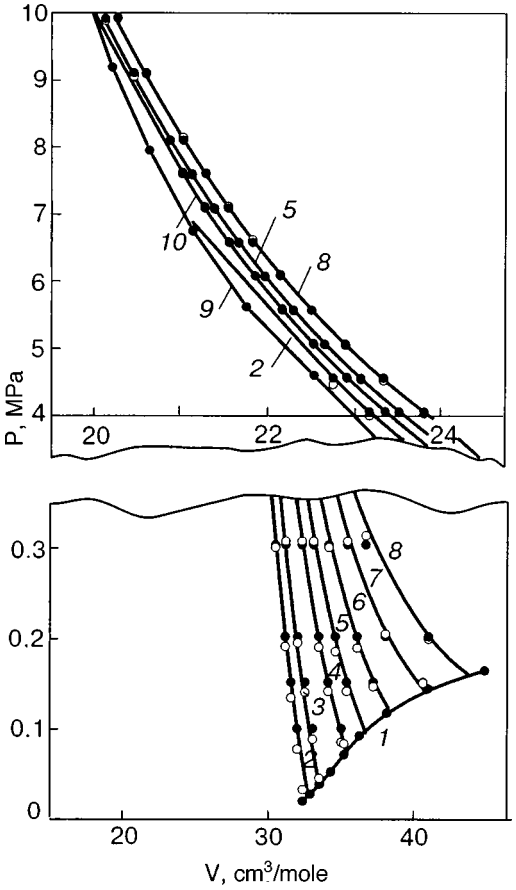


FIG. 1. Comparison of the experimental and calculated $P-V$ relations for an equimolar mixture along the following isotherms: vapor-pressure line (*1*), $T=2.25$ (*2*), 2.75 (*3*), 3.00 (*10*), 3.25 (*4*), 3.50 (*5*), 3.75 (*6*), 4.00 (*7*), 4.20 (*8*), start-of-solidification line (*9*); ●— experimental data,[1,3–5] ○— values calculated according to the equation of state for an equimolar mixture.[2]

To illustrate the quality of the approximation, we show in Fig. 1 the isotherms $P(V)$ for an equimolar mixture, calculated according to the unified equation (1) of the present paper, the points calculated according to the approximating expression for for this mixture from our previous paper,[2] and

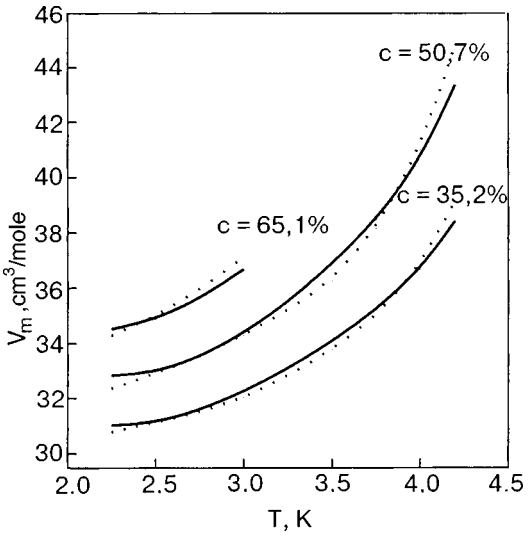


FIG. 2. Temperature dependence of the molar volume on the saturation line for mixtures with $c=35.2$, 50.7, and 65.1% $^3$He. The solid curves are calculated, the dotted curves experimental.

the experimental data[1] for this mixture. It may be seen that the average deviation between the two calculations and the experiment is $\pm 0.015$ MPa.

Figure 2 shows the molar volume on the saturation line as a function of temperature for three mixtures, as calculated according to Eq. (1) of the present paper, and the experimental data of Refs. 3 and 4. The average deviation of the theory and experiment is less than 1%, a quite acceptable result.

## CONCLUSION

Thus we have constructed a rather faithful unified equation of state for $^3$He–$^4$He mixtures in the region of the homogeneous liquid state. The approximating expression obtained is convenient to use in practice for mixtures of any concentration and for pure $^3$He and $^4$He.

In addition, the expressions obtained can be used in calculations of various thermodynamic quantities for mixtures of helium isotopes in the liquid phase.

*E-mail: rsibileva@mail.ru

[1] I. V. Bogoyavlenskii and S. I. Yurchenko, Fiz. Nizk. Temp. **2**, 1379 (1976) [Sov. J. Low Temp. Phys. **2**, 672 (1976)].
[2] L. V. Karnatsevich, R. M. Sibileva, M. A. Khazhmuradov, I. N. Shapoval, and A. V. Meriuts, Fiz. Nizk. Temp. **28**, 338 (2002) [Low Temp. Phys. **28**, 235 (2002)].
[3] E. C. Kerr, *Proceedings of the Fifth International Conference on Low-Temperature Physics and Chemistry LT-5*, Madison (1958).
[4] B. N. Esel'son, V. G. Ivantsov, P. S. Novikov, and R. I. Shcherbachenko, Ukr. Fiz. Zh. (Russ. Ed.) **14**, 1837 (1969).
[5] R. C. Pandorf, E. M. Ifft, and D. O. Edwards, Phys. Rev. **163**, 175 (1967).
[6] D. McCarty, J. Phys. Chem. Ref. Data **2**, 923 (1973).

Translated by Steve Torstveit

## LOW-TEMPERATURE MAGNETISM

# Features of the low-temperature magnetic-field-induced order–order transitions in alloys of the system $Fe_{a-x}Mn_xAs$ with $a \leqslant 1.6$

S. K. Asadov, V. I. Val'kov,* E. A. Zavadskii, V. I. Kamenev, and B. M. Todris

*A. A. Galkin Donetsk Physicotechnical Institute, ul. R. Lyuksemburg 72, Donetsk 83114, Ukraine*
(Submitted September 3, 2003; revised March 2, 2004)
Fiz. Nizk. Temp. **30**, 932–937 (September 2004)

Spontaneous and magnetic-field-induced first-order transitions of the order–order type in $Fe_{0.5}Mn_{1.1}As$ and $Fe_{0.55}Mn_{1.04}As$ single crystals with the $C38$ lattice (symmetry space group $P4/nmm$) are investigated at hydrostatic pressures up to 7 kbar in the temperature range from 4.2 to 300 K. The temperature and field dependences of the magnetization at different values of the pressure are measured in static and pulsed magnetic fields. It is established on the basis of the results that the first-order transitions from a low-magnetic to a high-magnetic phase induced by magnetic field pulses at low temperatures are irreversible, but with a finite existence time of the high-magnetic phase. A qualitative explanation of the observed effect is proposed on the basis of the theory of magnetostrictive blocking of the formation of new-phase nuclei at first-order phase transitions. © *2004 American Institute of Physics.*
[DOI: 10.1063/1.1802953]

### INTRODUCTION

Alloys of the $Fe_{a-x}Mn_xAs$ system near the stoichiometric composition ($a=2.0$) have the $C38$ tetragonal crystal lattice (space group $P4/nmm$) in which the magnetically active ions can occupy inequivalent crystallographic positions I or II with a tetrahedral or octahedral environment of the As ions, respectively. The magnetic moments of the ions in different positions can differ substantially even for ions of the same species. For example, in the two-component alloys $Fe_2As$ and $Mn_2As$ their values in units of Bohr magnetons are $1.0\mu_B$ and $1.5\mu_B$ for Fe(I) and Fe(II), and $3.7\mu_B$ and $3.5\mu_B$ for Mn(I) and Mn(II). In the three-component alloy Fe–Mn–As the iron and manganese ions occupy positions I and II, respectively, and their magnetic moments are equal to $0.2\mu_B$ for Fe(I) and $3.6\mu_B$ for Mn(II).[1]

Experimental studies of the $Fe_{a-x}Mn_xAs$ system have been carried out mainly for alloys of the stoichiometric composition ($a=2$) and compounds with a small deviation from stoichiometry, in the range $1.95 \leqslant a \leqslant 2.35$. At present there are no data on the values of the magnetic moments of the atoms in positions I and II. It is known only that for $x \geqslant 1$ the Mn atoms are distributed over both the I and II positions, while the Fe atoms occupy only position I.[2] Magnetic measurements have shown that with decreasing temperature some $Fe_{a-x}Mn_xAs$ alloys exhibit spontaneous first-order transitions from a high-temperature antiferromagnetically ordered phase to a low-temperature phase with a canted ferrimagnetic structure.[3] Such a structure can be characterized as a state with coexisting ferromagnetic and antiferromagnetic components of the total magnetic moment of the crystallochemical cell. A feature of such a structure is a strong dependence of the saturation magnetization on the magnetic field $H$. The action of hydrostatic and uniaxial pressure on the sample leads to changes in the phase transition temperature: hydrostatic pressure and uniaxial pressure along the tetragonal axis $c$ stabilize the antiferromagnetic phase. Uniaxial pressure along the directions perpendicular to the $c$ axis, on the contrary, increase the temperature range in which the ferromagnetic phase is stable.[4] The imposition of a high magnetic field in the stability region of the antiferromagnetic phase can induce a first-order transition to a ferrimagnetic phase.[5,6]

In this paper we present the results of experimental research on the phase behavior of the alloys $Fe_{0.5}Mn_{1.1}As$ and $Fe_{0.55}Mn_{1.04}As$ with a strong deviation from stoichiometry ($a=1.6$ and 1.59, respectively). At such concentrations of iron and manganese these alloys exhibit substantially different magnetic behavior, and they should accordingly be placed in a new class of iron–manganese arsenides with the $C38$ crystal lattice.

### EXPERIMENTAL TECHNIQUE

The samples used were single crystals mechanically cut from polycrystalline masses obtained by sintering of the three components followed by fusing of the sintered product.[3] The magnetization measurements under pressure were made by the pendulum method at static magnetic field strengths up to 12 kOe. The sample was placed in a miniature suspended beryllium bronze high-pressure container of the piston-in-cylinder type. The pressure at room temperature was produced by a press and fixed by a plunger nut. The pressure medium was benzene. The temperature was varied from 4.2 to 300 K. It is known that the pressure in apparatus of this type decreases as the temperature is lowered. For this reason the initial and intermediate values of the pressure are indicated along the temperature curves obtained under pres-

 

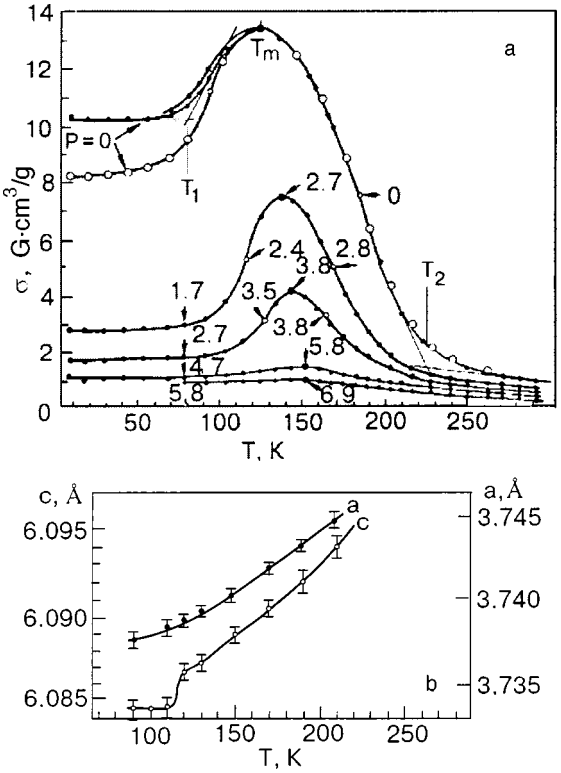


FIG. 1. Temperature dependence of the magnetization $\sigma$ (a) and crystal lattice parameters $a$ and $c$ (b) for $Fe_{0.55}Mn_{1.04}As$. In Fig. 1a: ●— cooling and heating in the presence of field; ○— heating of a sample cooled beforehand at $H=0$. The numbers give the values of the pressure in kbar at the corresponding temperatures.

sure. The pressure values were determined by a Manganin sensor. For measurements in pulsed magnetic fields up to 150 kOe we used an inductive method. A miniature solenoid with the sample inside was placed in a high-pressure container filled with gaseous helium. The helium was compressed to 2 kbar by means of a membrane compressor. A two-step closed-cycle helium expander was used to cool the container. Measurements were made in a range of temperatures from 17 to 300 K. The pressure was held constant. The state of the samples was monitored and x-ray measurements were made on a DRON-3.0 diffractometer with the use of a low-temperature attachment in which the preliminarily misadjusted sample was cooled by liquid nitrogen vapor. The single crystals of both compositions ($Fe_{0.5}Mn_{1.1}As$ and $Fe_{0.55}Mn_{1.04}As$) have a tetragonal crystal lattice.

## RESULTS OF THE MEASUREMENTS

Figure 1a shows the temperature dependence of the magnetization $\sigma$ for the $Fe_{0.55}Mn_{1.04}As$ sample at various pressures $P$. Measurements were made in a static magnetic field of 12 kOe oriented perpendicular to the tetragonal axis $c$ of the crystal. It follows from Fig. 1a that three phase states with different magnetic behavior are realized in the investigated temperature interval at atmospheric pressure.

In the high-temperature region ($T>T_2$) the magnetization is small and grows slowly and continuously as the temperature is lowered. We assume that these temperatures correspond to a paramagnetic state, since the magnetic susceptibility does not exhibit any of the anomalies characteristic of antiferromagnetic order up to 500 K.

Starting at $T_2$ as the temperature is lowered there is a sharp growth in the magnetization, which attests to the onset of magnetic ordering in the sample. The transition to a magnetically ordered state is not accompanied by hysteresis effects and is apparently a second-order phase transition. The growth of the magnetization continues down to a temperature $T_m$, where it gives way to a decrease in the magnetization in the temperature interval from $T_m$ to $T_1$, and then the magnetization stabilizes in value at temperatures below $T_1$. The decrease of the magnetization in the temperature interval from $T_m$ down to $T_1$ is a consequence of a transition of the sample from a magnetically ordered state with high magnetization (the high-magnetic (HM) phase) to a magnetically ordered state with low magnetization (the low-magnetic (LM) phase). The transition HM↔LM is a smeared first-order phase transition. This is evidenced by the presence of a small temperature hysteresis, the sharp change of the crystal lattice parameter $c$ in this temperature interval (Fig. 1b), and other features characteristic of first-order phase transitions at high magnetic field, which will be discussed below. Interestingly, the magnetization of the LM phase at low temperatures depends on the conditions of cooling of the sample. Cooling the sample in a field of 12 kOe leads to a 25% higher value of the magnetization as compared to cooling in the absence of magnetic field. X-ray measurements showed that the sample is crystallographically uniform in the temperature intervals corresponding to the HM and LM phases.

It also follows from Fig. 1a that increasing the pressure leads to a decrease in the temperature region in which the HM phase exists. The magnetization of both phases decreases, and the value of $T_m$ increases slightly. At pressures of the order of 7 kbar one can discern a small anomaly on the $\sigma(T)$ curve at $T=T_m$.

For the $Fe_{0.5}Mn_{1.1}As$ sample the shape of the $\sigma(T)$ curve and the character of its change under pressure are similar to those shown in Fig. 1. However, for this sample the value of $T_1$ is lower, 70 K. This does not permit a comparison of the temperature dependence of its magnetization and lattice parameters, since the measurement of the latter was limited by the boiling temperature of nitrogen. The field curves of the magnetic characteristics, both in static and pulsed magnetic fields, were also similar for the two samples, but more-detailed measurements were made for the $Fe_{0.5}Mn_{1.1}As$ sample. For that reason the data for that sample have been used in Figs. 2–5.

Figure 2 characterizes the process of magnetization of the $Fe_{0.5}Mn_{1.1}As$ single crystal at temperatures corresponding to the HM (130 K) and LM (77 K) phases, for different orientations of the magnetic fields with respect to the tetragonal axis $c$. It follows from the magnetization curves shown that both phases have a spontaneous magnetic moment and that the $c$ axis is an axis of hard magnetization.

Figure 3 shows the magnetization curves of the $Fe_{0.5}Mn_{1.1}As$ crystal in pulsed magnetic fields ($\mathbf{H}\|\mathbf{c}$) at different pressures in the existence region of the LM phase ($T=20$ K). The right- and leftward arrows indicate the directions of increasing and decrease magnetic field strength, respectively. It is found that increasing the field initially leads

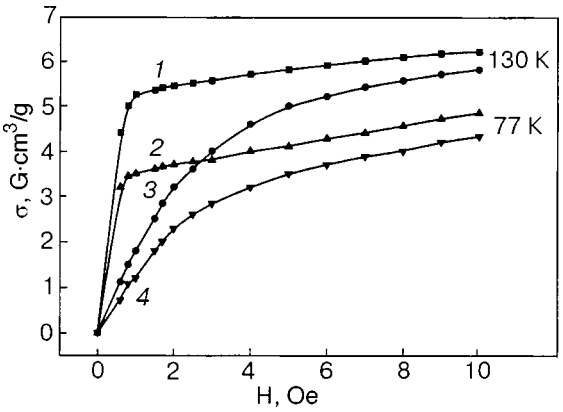


FIG. 2. Magnetization curves for $Fe_{0.5}Mn_{1.1}As$ at different temperatures and orientations of the static field **H** relative to the tetragonal axis *c* of the crystal: $\mathbf{H}\perp\mathbf{c}$ (*1,3*); $\mathbf{H}\|\mathbf{c}$ (*2,4*).

to a monotonic growth in the magnetization. When the field reaches a certain value a relatively sharp increase in magnetization occurs. The formation of a state with high magnetization is induced by the field of the first-order phase transition LM→HM. That the transition of the sample under the influence of magnetic field ($H_{c1}$ is the critical field of this transition) occurs to the HM state is evidenced by the substantial difference of $H_{c1}$ as the temperature approaches the temperature interval of the HM↔LM phase transformation. In the incipient HM phase (in fields $H>H_{c1}$) the monotonic increase of the magnetization with increasing field continues but at a slower rate. When the field is decreased back to zero the magnetization of the induced HM state decreases smoothly, remaining higher than in the initial LM phase at all

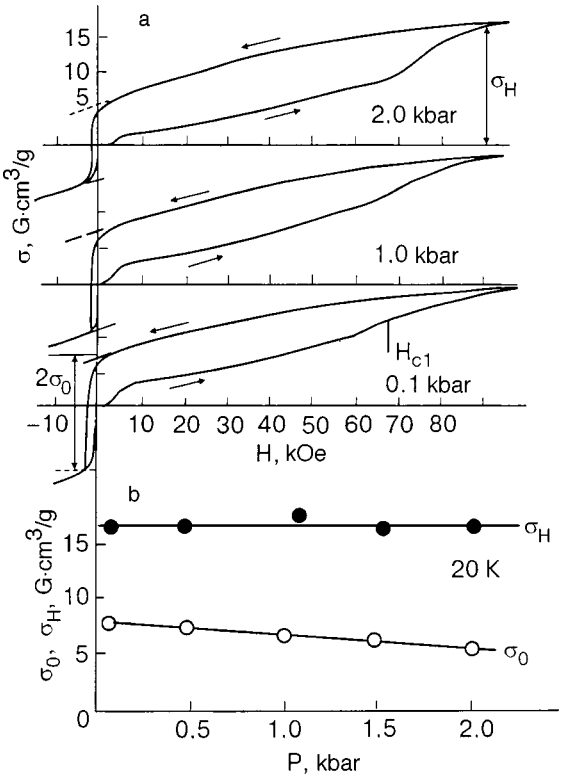


FIG. 3. Magnetization curves $\sigma(H)$ for $Fe_{0.5}Mn_{1.1}As$ at different pressures: the sample temperature was 20 K; the right- and leftward arrows indicate increasing and decreasing field strength, respectively.

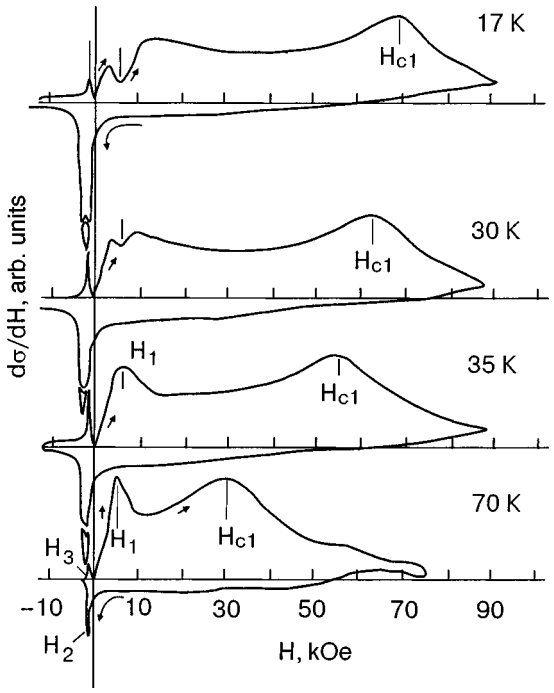


FIG. 4. Curves of $\sigma'(H)$ for $Fe_{0.5}Mn_{1.1}As$ for different temperatures at atmospheric pressure. The vertical lines in the peak regions give the values of the critical field $H_{c1}$ and fields of technical saturation for increasing ($H_1$,$H_3$) and decreasing ($H_2$) amplitude of the damped pulsed field.

values of the field. In the process of magnetization reversal of a sample the HM phase persists upon a change in polarity of the field. Thus the magnetic-field-induced LM→HM phase transition is irreversible. It should be noted that the field-induced HM phase is not long-lived. It persists over the time of action of three half-periods of the field variation, a total of ~1 ms. However, in the repeated action of a pulsed magnetic field on the sample after 5 min (the time required to return the apparatus to the initial state), the shape of the magnetization curves was repeated exactly, i.e., the initial LM state is restored over that time. Pressure has practically no influence on the value of the saturation magnetization of the induced HM phase, $\sigma_H$, and leads only to a decrease of the spontaneous magnetization $\sigma_0$ of that phase (Fig. 3b). This last finding agrees with the data in Fig. 1 showing a decrease in the magnetization of the HM phase under pressure.

Additional information above the character of the magnetization of a sample in the LM phase can be obtained from an analysis of the field dependence of the differential magnetic susceptibility $\sigma'=\partial\sigma/\partial H$, which is presented in Fig. 4.

In the temperature range $T_m>T>35$ K during three half-periods of variation of the pulsed field the $\sigma'(H)$ curves display four peaks. The first peak arising as the field is increased appears in the low-field region and characterizes the process of technical saturation of the sample in the LM state. The second peak, in the high field region, corresponds to the critical field for induction of the HM phase, $H_{c1}$. The third and fourth peaks appear after the field is lowered back down, at every change in sign of the field, and characterize the boundaries of the hysteresis loop of the magnetization reversal of the induced HM phase.

For $T<35$ K the first of the peaks indicated above splits.

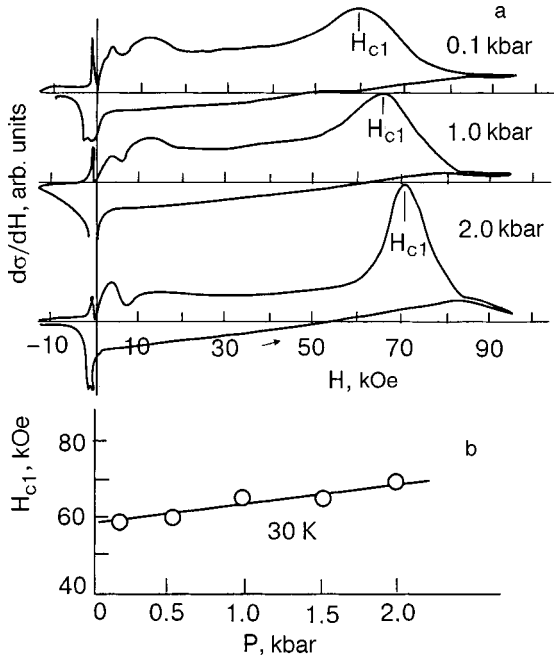


FIG. 5. Curves of $\sigma'(H)$ for $Fe_{0.5}Mn_{1.1}As$ for different pressures at $T=30$ K (a) and the pressure dependence of the critical field for induction of the HM phase, $H_{c1}$ (b).

Its splitting reflects the fine structure of the magnetization curve of the LM phase, which had been smoothed out at high temperatures. It follows from Fig. 5 that applied pressure enhances the contrast of the splitting and increases the value of the critical field $H_{c1}$.

## ANALYSIS AND DISCUSSION OF THE RESULTS

The data obtained on the spontaneous (brought on by a change in temperature) and magnetic-field-induced transitions in the alloys under discussion raises some general questions for magnetically ordered compounds with the $C38$ crystal lattice.

Some of them can be solved by noting the similarity and differences of the magnetic properties of the alloys used in the present study and alloys of the system $Mn_{2-x}Cr_xSb$.[7] The alloys of that system have an analogous $C38$ lattice. They also exhibit spontaneous and magnetic-field-induced first-order transitions from a low-temperature to a high-temperature phase. The spontaneous transitions are accompanied by a change in the lattice parameters and by temperature hysteresis. However, in their case the magnetic-field-induced transitions are reversible. This indicates that the LM phase is the only stable one at low temperatures and it corresponds to a minimum of energy.

In the samples investigated in the present study the field-induced LM→HM transitions are irreversible. In spite of the fact that the lifetime of the induced HM phase is finite, it also must correspond to a minimum of energy. However, while the minimum of the LM phase is absolute, that of the HM state is only a relative minimum, and the state is metastable. Metastable states have previously been found in the system $Fe_{a-x}Mn_xAs$ with $1.95 \leqslant a \leqslant 2.35$ (Refs. 8 and 9) and in a number of alloys based on manganese arsenide[10] which have the hexagonal crystal lattice $B8_1$. The distinguishing feature of these alloys is that after application of a magnetic field they exist for an arbitrarily long time. An explanation of this phenomenon was given in Refs. 11 and 12 on the basis of the concepts of a blocking of the formation of new-phase nuclei at first-order phase transitions in solids when a change in the volume of the sample is involved. The nucleation conditions are made more stringent by the elastic coupling between the nucleus and matrix due to the difference of the specific volumes of the old and new phases. Depending on the ratio of the elastic coupling energy to the energy benefit of the phase change (the energy of the phase transition), different lengths of time will be required for the system to return from the field-induced metastable state to the absolutely stable state. If the elastic coupling energy is substantially larger than the energy difference of the old and new phases, then the nucleation process will be blocked, and the metastable state will persist for an arbitrarily long time. Such a situation is apparently realized in experiments.[8–10]

In the samples investigated in the present study the specific volumes of the HM and LM phases differ insignificantly. Because of this, the nucleation-blocking effect should also be insignificant. Moreover, the smeared character of the transitions themselves is evidence of the presence of lattice inhomogeneities that can serve as nucleation centers and thus facilitate the appearance and growth of nuclei. These two factors lead to the rapid vanishing of the irreversibly induced metastable HM phase. It should be noted that the HM phase is metastable at large distances from the temperature of the phase transformation HM→LM, since the irreversible character of the induced transition LM→HM is preserved all the way to the lowest temperature that could be achieved in the experiments, 17 K (see Fig. 4). In this interval of temperatures a magnetic field alters the ratio of elastic energy to phase transition energy in favor of stabilizing the HM phase, the state with the larger magnetization. Therefore, when the sample is cooled in a magnetic field, this phase is partially preserved, as is attested to by the manner in which the temperature dependence of the magnetization is influenced by whether the sample was cooled in the presence or absence of magnetic field (see Fig. 1).

## CONCLUSION

The explanation proposed above for the features of the induced transitions in several alloys of the $Fe_{a-x}Mn_xAs$ system is based on general principles of the theory of the blocking of nucleation of magnetically ordered phases and does not take into consideration a number of the specific characteristics of the samples of this system. First, as was shown in Ref. 13, magnetically ordered phases here are states in which a spatially uniform (ferromagnetic) component of the total magnetic momentum of the crystallographic cell coexists with a periodic (antiferromagnetic) component. Second, in the samples studied, with a significant deviation from the stoichiometric composition, magnetic phases can have features due to a deficit of magnetic ions in the lattice. The role of nonstoichiometry in the formation of the boundaries of the magnetic phase diagrams in alloys of the system $Fe_{a-x}Mn_xAs$ has never been discussed even on a qualitative level.

It is hoped that the results of our experimental research will stimulate the discussion of the properties of these materials from various points of view.

*E-mail: valkov@dpms.fti.ac.donetsk.ua

[1] S. Yoshii and H. Katsuraki, J. Phys. Soc. Jpn. **22**, 674 (1967).
[2] F. Grandjean and A. Gerard, J. Magn. Magn. Mater. **1**, 64 (1975).
[3] R. Rosenberg, W. Cloud, F. Darnel, and R. Flipper, Phys. Rev. A **25**, 723 (1967).
[4] S. A. Buzhinskiĭ, V. I. Val'kov, and N. A. Romanova, Fiz. Tverd. Tela (Leningrad) **33**, 1936 (1991) [Sov. Phys. Solid State **33**, 1090 (1991)].
[5] V. I. Val'kov, É. A. Zavadskiĭ, V. I. Kamenev, and V. M. Kirbitov, Fiz. Tverd. Tela (Leningrad) **26**, 870 (1984) [Sov. Phys. Solid State **26**, 527 (1984)].
[6] M. Ohashi, Y. Yamaguchi, and T. Kanomata, J. Magn. Magn. Mater. **104–107**, 925 (1992).
[7] V. I. Val'kov, V. I. Kamenev, S. A. Buzhinsky, and N. A. Romanova, Fiz. Nizk. Temp. **28**, 275 (2002) [Low Temp. Phys. **28**, 194 (2002)].
[8] V. I. Val'kov, É. A. Zavadskiĭ, V. M. Kirbitov, I. A. Sibarova, and B. M. Todris, Ukr. Fiz. Zh. (Russ. Ed.) **32**, 1418 (1987).
[9] S. A. Buzhinskiĭ, V. I. Val'kov, É. A. Zavadskiĭ, N. A. Romanova, and E. A. Khapalyuk, Fiz. Tverd. Tela (St. Petersburg) **37**, 1455 (1995) [Phys. Solid State **37**, 788 (1995)].
[10] A. A. Galkin, É. A. Zavadskiĭ, V. M. Smirnov, and V. I. Val'kov, JETP Lett. **20**, 111 (1974).
[11] I. N. Nechiporenko, Fiz. Nizk. Temp. **1**, 1481 (1975) [Sov. J. Low Temp. Phys. **1**, 712 (1975)].
[12] V. G. Bar'yakhtar, I. M. Vitebskiĭ, and D. A. Yablonskiĭ, Fiz. Tverd. Tela (Leningrad) **23**, 1448 (1981) [Sov. Phys. Solid State **23**, 843 (1981)].
[13] T. Goto, J. Magn. Magn. Mater. **51–57**, Pt. 2, 931 (1986).

Translated by Steve Torstveit

# Magnetic and transport properties controlled by structural disorder in $La_{0.7}Ca_{0.3}MnO_3$ films

V. G. Prokhorov,* V. A. Komashko, and G. G. Kaminsky

*Institute of Metal Physics, National Academy of Sciences of Ukraine, Kiev 03142, Ukraine*

V. L. Svetchnikov

*NCHREM, Rotterdamseweg 137, 2628AL, Delft, The Netherlands*

Y. P. Lee and S. Y. Park

*Quantum Photonic Science Research Center and Department of Physics, Hanyang University Seoul 133-791, Korea*

(Submitted December 19, 2003; revised April 1, 2004)
Fiz. Nizk. Temp. **30**, 938–944 (September 2004)

The magnetic properties of an amorphous, a partially disordered, and a lattice-strained crystalline $La_{0.7}Ca_{0.3}MnO_3$ film are investigated. It is shown that the amorphous film exhibits Curie–Weiss-type paramagnetism with the effective magnetic moment of 4.2 $\mu_B$/Mn ion and a small ferromagnetic contribution governed by the formation of quasi-two-dimensional crystalline interfacial inclusions. The crystalline film with randomly oriented nanocrystalline inclusions demonstrates a superposition of ferromagnetic character (in the crystalline matrix) and superparamagnetic character (in the inclusions). The fitted average size of the superparamagnetic particles in the case of a Langevin function is coincident with that of the nanocrystalline clusters revealed in high-resolution electron-microscopy images. An increase in the applied magnetic field leads to a reduction in the average magnetic moment of the superparamagnetic particles, which is due to an enhancement of the ferromagnetic coupling between the individual randomly oriented crystallites. The completely crystalline film undergoes only a ferromagnetic transition with a saturation magnetization at 5 K of 2.73 $\mu_B$/Mn ion.  [DOI: 10.1063/1.1802954]

## 1. INTRODUCTION

The hole-doped perovskite manganites of the general formula $R_{1-x}A_xMnO_3$ (R is a rare-earth cation, A is an alkali or alkaline-earth cation) have attracted considerable attention not only because of their interesting fundamental science, connected with the discovery of colossal magnetoresistance (CMR), but also their potential for device applications.[1,2] It was found recently that the lattice strain (and stress) accumulated owing to the epitaxial growth of a film plays an important role in the formation of the spin- and charge-ordered states in the CMR films.[3–6] The influence of the kind of single-crystalline substrates on the magnetic and electronic properties of manganite films has been quite well investigated.[7,8] It was shown that the presence of grain boundaries in the polycrystalline manganites leads to a large MR effect over a wide temperature range below the Curie temperature ($T_C$), whereas the CMR of the single-crystalline materials is restricted to a narrower temperature range just around $T_C$.[9–11] On the other hand, the influence of structural quench disorder on the magnetic ordering is still poorly understood.

In this paper we report the peculiar results for amorphous (LCM1), strain-free crystalline (with nanocrystalline mosaic-like inclusions) (LCM2), and lattice-strained crystalline (LCM3) $La_{0.7}Ca_{0.3}MnO_3$ films. It is shown that the state of the Mn spins can be controlled by microstructure. We present an unusual type of the randomly oriented nanocrystalline mosaic structure which manifests the magnetic-field-effected superparamagnetic behavior and sheds new light on the nature of magnetic ordering in the CMR materials.

## 2. EXPERIMENTAL TECHNIQUES

All the films were prepared by rf magnetron sputtering using a so-called ''soft'' (or powder) target.[12] The total pressure in chamber was $5\times10^{-2}$ Torr with a gas mixture of Ar and $O_2$ (3:1). The substrate was a $LaAlO_3$ (001) single crystal (LAO) with a lattice parameter $a\simeq0.379$ nm for the pseudocubic symmetry. The substrate temperature during deposition was 20 (LCM1), 400 (LCM2), and 720 °C (LCM3). All the films have a thickness of $d\simeq30$ nm. The $\theta$–$2\theta$ x-ray diffraction (XRD) patterns were obtained using a Rigaku diffractometer with Cu $K_\alpha$ radiation. The lattice parameters evaluated directly from the XRD data were plotted against $\cos^2\theta\sin\theta$. With an extrapolated straight line to $\cos^2\theta\sin\theta=0$, a more precise determination of the lattice parameter was obtained. Cross-section specimens were prepared by the standard techniques using mechanical polishing followed by ion-beam milling under grazing incidence. The high-resolution electron-microscopy (HREM) studies were carried out using a Philips CM300UT-FEG microscope with a field emission gun operated at 300 kV. The point resolution of the microscope was of the order of 0.12 nm. The resis-

 

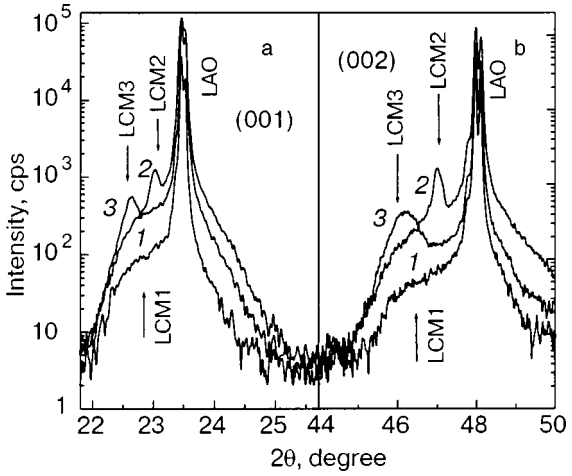


FIG. 1. (001) (a) and (002) (b) XRD peaks for the LCM1 (*1*), LCM2 (*2*), and LCM3 (*3*) films. LAO denotes the substrate.

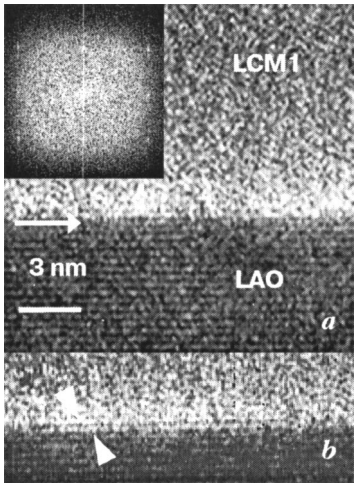


FIG. 2. Cross-sectional HREM image of the LCM1 film near the interface. The inset is the corresponding FFT (a). The same image with a crystalline monolayer on the substrate surface, denoted by the white arrows (b).

tance measurements were performed by using the four-probe method in a temperature range of 4.2–300 K and in a magnetic field up to 5 T. The in-plane field-cooled (FC) and zero-field-cooled (ZFC) magnetization was taken with a Quantum Design SQUID magnetometer in a temperature range of 4.2–300 K.

### 3. MICROSTRUCTURE OF THE FILMS

Figures 1a and 1b present the (001) and the (002) Bragg reflections, respectively, for the LCM1 (*1*), LCM2 (*2*), and LCM3 (*3*) films and for the LAO substrate. The LCM1 film displays only a smooth plateau instead of a real Bragg peak. Therefore, the film deposited at a low temperature is in an amorphous phase. The LCM2 film shows weak Bragg peaks on a background of the same smooth plateau. The out-of-plane lattice parameter for the LCM2 film, $c \simeq 0.3866$ nm, is very close to that for the bulk.[13,14] This suggests that the incipient crystalline phase grows in equilibrium conditions without a significant influence of the substrate and is formed through the amorphous state. The LCM3 film, deposited at a high temperature, displays intense Bragg peaks with a larger out-of-plane lattice parameter, $c \simeq 0.3927$ nm, that is typical for the thin CMR films and explained by the accumulation of an in-plane biaxial compressive strain during the deposition.[7,8,12,15]

Figure 2a is a high-magnification cross-sectional HREM image for the amorphous LCM1 film. It was obtained with an incident beam parallel to a cubic direction of the substrate and to the film/substrate interface. The inset in Fig. 2a displays the fast Fourier transform (FFT) of the HREM image across the interface. It is seen that the FFT produces a bright uniform halo instead of a rectangular pattern of circular spots. Only the slightly luminescent spots corresponding to the crystal lattice of the substrate are barely noticeable. This coincides with the XRD data and confirms an amorphous structure of the LCM1 film. On the other hand, Fig. 2b shows that a trace of a crystalline phase is found on the substrate surface (denoted by white arrows). The analysis of the HREM images reveals that this crystalline phase does not cover the whole substrate surface and does not exceed one or two unit cells in thickness. Figure 3a demonstrates the same HREM image for the LCM2 film. Even though the FFT of LCM2 results in the formation of a rectangular pattern of spots (see inset A in Fig. 3a), they are significantly smeared and include the bright halo that attests to the presence of the amorphous (or crystal-disordered) phase in the film. This sort of off-structural inclusion is represented in Fig. 3b as area A and its FFT as the inset. The wide ring in the FTT indicates that the inclusions consist of randomly oriented nano-scale crystallites. Therefore, in this case we are dealing with a nanocrystalline mosaic microstructure rather than with an amorphous one, which was observed in LCM1. However, inset B in Fig. 3a shows that the matrix of LCM2 shows a perfect cubic crystalline lattice with equal in-plane and out-of-plane lattice parameters, $a \simeq c \simeq 0.387$ nm, and a right angle between the atom rows. It is matched with the XRD

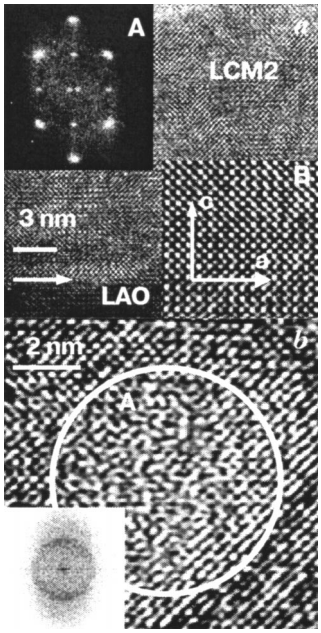


FIG. 3. Cross-sectional HREM image of the LCM2 film near the interface. Inset A is the corresponding FFT. Inset B represents the atomic lattice of the crystalline matrix (a). The HREM image with an off-structural inclusion designated by area A. The inset is the FFT of area A (b).

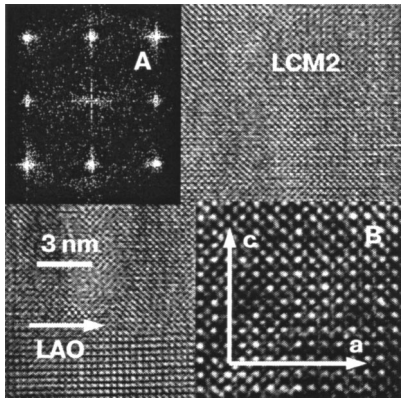


FIG. 4. Cross-sectional HREM image of the LCM3 film near the interface. Inset A is the corresponding FFT. Inset B represents the atomic lattice of the film.

data and prove that the crystal lattice of the LCM2 film is strainless. Figure 4 presents the HREM image for the LCM3 film. In this case the FFT produces a well-defined rectangular pattern of circular spots (see inset A) which indicates the formation of a perfect crystal lattice. However, together with the perpendicular crystal axes, a tetragonal distortion of the lattice ($c/a \simeq 1.026$) is also found in inset B. The estimated in-plane lattice parameter for the LCM3 film, $a \simeq 0.3826$ nm, is smaller than that for the bulk compound, $a \simeq 0.3858$ nm.[14] This difference leads to formation of the aforementioned in-plane biaxial compressive strain, $\varepsilon_{100} = (a_{\text{film}} - a_{\text{bulk}})$, and an out-of-plane uniaxial tensile strain, $\varepsilon_{001} = (c_{\text{film}} - c_{\text{bulk}})/c_{\text{bulk}}$. Calculations show that in this case $\varepsilon \simeq -0.83\%$ and $\varepsilon \simeq 1.79\%$, respectively. To summarize the microstructural measurements, we note that LCM1 is mainly in an amorphous crystal structure, LCM2 contains a complex of the strainless crystalline matrix with nanocrystalline mosaic-type inclusions, and finally LCM3 represents a strained crystal lattice with a slight tetragonal distortion.

## 4. EXPERIMENTAL RESULTS

Figure 5 shows both FC (solid) and ZFC (open) temperature-dependent magnetization curves, $M(T)$, at a magnetic field $H = 100$ Oe for the LCM1 (a), the LCM2 (b), and the LCM3 (c) films. The amorphous LCM1 film demonstrates an M($T$) behavior which is typical for paramagnetic (PM) materials.[16] At the same time, two peculiarities, a minor splitting between the ZFC and FC $M(T)$ curves and a slight decrease in the magnetization near the expected Curie point (denoted by arrow in Fig. 5a), indicate the presence of a ferromagnetic (FM) phase. It is claimed that a small FM contribution is connected with the mentioned ultrathin crystalline layer on the substrate surface (see Fig. 2b). The inset in Fig. 5a displays the $M(H)$ dependence at room temperature, which demonstrates a diamagnetic behavior, introduced by the LAO. The measurements performed reveal that the diamagnetic contribution is about $-3.3\times10^{-3}$ e.m.u./g for all the films prepared. This contribution was first subtracted from the magnetization curves for the analyses. Figure 5b shows that the $M(T)$ dependence for the LCM2 film represents a superposition of two contributions: a well-defined FM transition at $T_C \simeq 260$ K, and a paramagnetic term which is manifested by a rapid increase of the $M(T)$ at $T \to 0$. Taking into account the XRD and HREM data, one can conclude that the FM phase belongs to the crystalline matrix and the PM phase corresponds to the nanocrystalline inclusions. Figure 5c shows that the crystalline LCM3 film undergoes only a FM transition at $T_C \simeq 204$ K, which is lower than that for LCM2 and can be explained by the lattice strains generated in the film.[17] The inset in Fig. 5c presents the hysteresis loop of the magnetization, measured at 5 K, for the LCM3 film. It is seen that the magnetization is saturated at $H_s \simeq 9000$ Oe and that the coercive field is about 500 Oe. An analysis shows that the saturation magnetization does not exceed 2.73 $\mu_B$/Mn, which is a typical value for lattice-strained thin films[16] and is much smaller than that observed for the bulk, 3.5 $\mu_B$/Mn.[17]

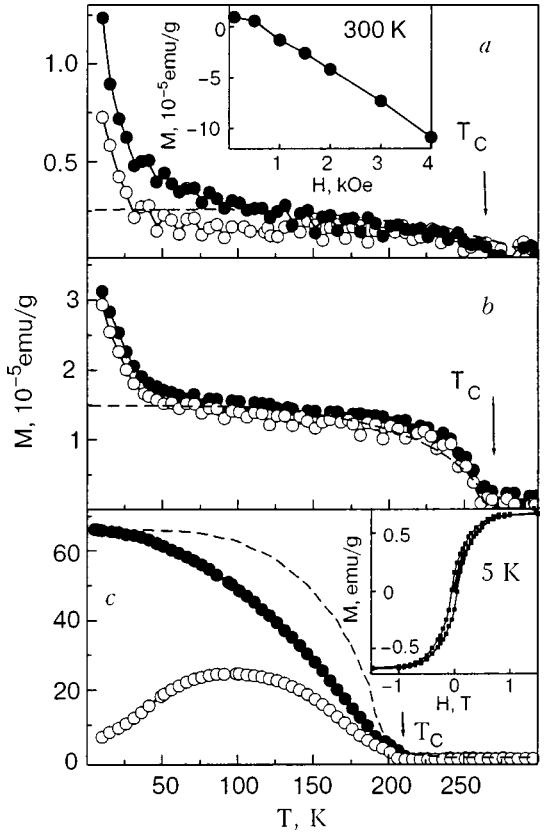


FIG. 5. Field-cooled (solid) and zero-field-cooled (open) magnetization curves for the LCM1 (a), LCM2 (b), and LCM3 (c) films. The inset in (a) displays the field-dependent magnetization at 300 K for LCM1. The inset in (c) shows the hysteresis loop at 5 K for LCM3. The dashed lines are the theoretical curves, based on the mean-field approximation for ferromagnetic materials. The lines are a guide to the eye.

Figure 6 displays the temperature dependence of the resistance, $R(T)$, for the LCM3 film with (solid) and without (open) an applied magnetic field of 5 T. Unfortunately, our setup was limited to $10^7$ $\Omega$, and $R(T)$ could not be measured for LCM1 and LCM2, since their resistances at room temperature are about $10^{12}$ and $10^7$ $\Omega$, respectively. The magnetic field was directed parallel to the film surface and at a right angle to the transport current. The metal–insulator (MI) transition is observed at $T_P \simeq 180$ K, much lower than $T_C$. Inset A in Fig. 6 shows the temperature dependence of the MR for the same film. The MR value is defined by $100\%[R(0) - R(H)]/R(H)$, where $R(0)$ and $R(H)$ are the resistances without and with a magnetic field, respectively. It

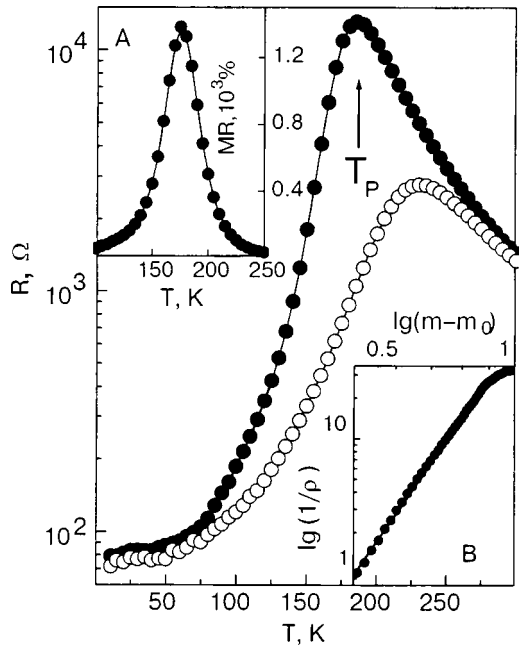


FIG. 6. Temperature dependence of the resistance for LCM3 film without (open) and with (solid) an applied magnetic field of 5 T. The lines are a guide to the eye. Inset A shows the temperature dependence of the MR ratio in an applied magnetic field of 5 T. Inset B displays the $\log(1/\rho)$ versus $\log(m-m_0)$ plot with the slope corresponding to the percolation exponent $t \simeq 5.7$.

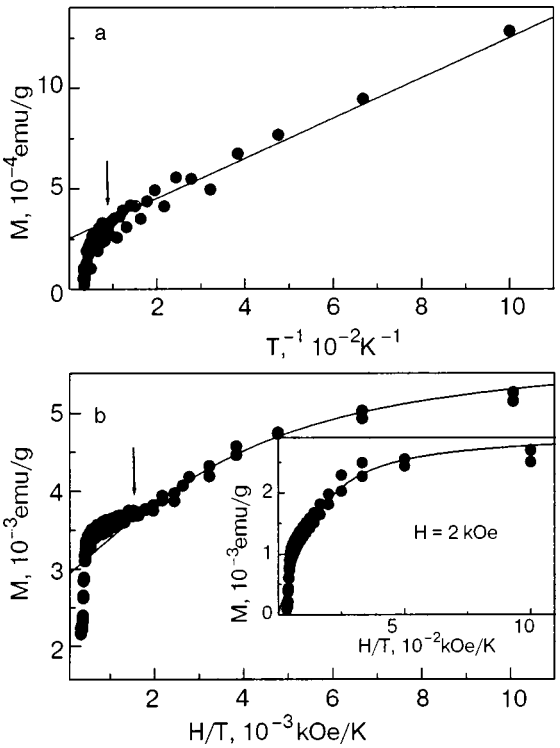


FIG. 7. $M$ versus $T^{-1}$ plot for the LCM1 film at $H=100$ Oe. The solid line represents the CW-type paramagnetic approximation. The arrow indicates the deviation of the experimental curve from the CW-type straight line, reflecting the presence of a FM phase (a). $M$ versus $H/T$ plot for the LCM2 film at $H=100$ Oe. The solid line represents a Langevin function describing the magnetic behavior of superparamagnetic particles. The arrow indicates the presence of a FM phase. The inset is the same plot at $H=2$ kOe (b).

is seen that the $MR(T)$ dependence has a peak-like shape and reaches almost 1500% at the maximum.

## 5. DISCUSSION

As was mentioned above, the amorphous LCM1 film demonstrates mainly paramagnetic $M(T)$ behavior with a trace of FM. Thus, the expression for the total magnetization of LCM1 can be written as $M(T,H)=M^{PM}(T,H)+M^{FM}(T,H)$. The paramagnetic contribution to the magnetization can be written, in the whole temperature range, as[16]

$$M^{PM}(T,H)=\left(\chi_0+\frac{C_{CW}}{T+\theta}\right)H \tag{1}$$

where $\chi_0$ is the temperature-independent susceptibility, and the second term is a Curie–Weiss (CW)-type susceptibility with a constant $C_{CW}$ and a characteristic temperature $\theta$. Figure 7a demonstrates that the experimental data for LCM1 are excellently described by the CW expression with the following fitting parameters: $\chi_0 \simeq 2.5\times10^{-4}$ cm$^3$/g, $C_{CW}\simeq 1.04\times10^{-2}$ cm$^3$/g, and $\theta=3$ K. The effective moment estimated from $C_{CW}$ comes out to be $\mu_{\text{eff}}\simeq 4.2\mu_B$/Mn, which is almost coincident with the theoretical value, $\mu_{\text{eff}}^{\text{theo}}\simeq 4.6\ \mu_B$/Mn, which is obtained from the following expression:

$$\mu_{\text{eff}}^{\text{theo}}=g\sqrt{xS_1(S_1+1)+(1-x)S_2(S_2+1)}. \tag{2}$$

Here $x$ is the Ca concentration, $S_1=3/2$ and $S_2=2$ are the spin values of $Mn^{4+}$ and $Mn^{3+}$ ions, respectively, and $g=2$ is the Lande factor. Therefore, one can conclude that the amorphous LCM1 film is mainly a typical CW-type paramagnet. On the other hand, the magnetization decreases sharply and deviates from a straight line in the range of small values of $T^{-1}$ ($T\geqslant 130$–$150$ K), as denoted by an arrow in Fig. 7a. It is reasonable to suggest that the observed deviation from the CW law is governed by the FM transition of the crystalline interfacial layers. The mean-field theory gives the following temperature dependence of the spontaneous magnetization for a ferromagnet below $T_C$:[16]

$$\frac{M^{FM}}{M_0^{FM}}=\tanh\left[\frac{M^{FM}}{M_0^{FM}}\cdot\frac{T_C}{T}+\frac{\chi_{\text{diff}}H}{M_0^{FM}T}\right], \tag{3}$$

where $M_0^{FM}$ is the spontaneous magnetization at $T\to 0$ and $\chi_{\text{diff}}$ is the differential susceptibility. The dashed lines in Fig. 5a,b,c are the theoretical curves calculated in the mean-field approximation. $\chi_{\text{diff}}=2.19\times10^{-4}$ cm$^3$/g was taken from the magnetization hysteresis loop for LCM3 (see inset in Fig. 5c), which is already in the FM state at a magnetic field of 100 Oe.

Figure 7b shows the $M(T,H)$ versus $H/T$ plot for the LCM2 film, measured at $H=100$ Oe, and the inset presents the same plot at $H=2$ kOe. It is seen that the experimental curves cannot be described by the CW approximation, since they do not demonstrate a linear behavior in the whole temperature range. Such a nonlinearity of the $M(H/T)$ is more typical for superparamagnetic (SPM) particles and can be described by the Langevin function:[16]

$$M^{SPM}(T,H)=M_s^{SPM}\left[\coth\left(\frac{\mu H}{k_BT}\right)-\frac{k_BT}{\mu H}\right], \tag{4}$$

where $M_s^{SPM}$ is the saturation magnetization of the SPM phase and $\mu$ is the average magnetic moment of the SPM particles. The solid lines represent the Langevin functions best fitting the experimental data. These lines correspond to an average magnetic moment of the SPM particles of 3000 $\mu_B$ at $H=100$ Oe and 800 $\mu_B$ at $H=2$ kOe. By taking 3.5 $\mu_B$/Mn atom[18] and assuming a spherical shape of the SPM clusters with a volume of $\pi D^3/6$, where $D$ is the average diameter, we estimate their average diameter to be $D \simeq 5$ nm for 100 Oe and $\simeq 3$ nm for 2 kOe. Analysis of the HREM images (see Fig. 3b) shows that the randomly oriented crystallites in inclusions have a similar size to this estimate for the SPM clusters. Therefore, one can conclude that nanocrystalline clusters play the role of the SPM particles in this film. The observed decrease in the average moment of the SPM particles in an applied magnetic field can be explained by a partial SPM-to-FM transition due to an enhancement of the ferromagnetic coupling between adjacent nanocrystalline clusters. It is provided by the high conductive transparency of boundaries in such a type of nanocrystalline mosaic structure. In this case the arrangement of magnetic moments in the increasing field can lead to a recovery of the double exchange interaction between neighboring crystallites.

As already described, the observed decrease in $T_C$ for the LCM3 film is explained by an influence of the lattice strain which was accumulated in the film during the epitaxial growth. For weaker strains and a cubic symmetry, the Curie point can be expressed, according to Millis model, by[17]

$$T_C(\varepsilon)=T_C(\varepsilon=0)\left(1-\alpha\varepsilon_B-\frac{1}{2}\Delta\varepsilon_{JT}^2\right), \tag{5}$$

where $\varepsilon_B=(2\varepsilon_{100}+\varepsilon_{001})$ is the bulk strain, $\varepsilon_{JT}=\sqrt{2/3}(\varepsilon_{001}-\varepsilon_{100})$ is the Jahn–Teller strain, $\alpha=(1/T_C)(dt_C/d\varepsilon_B)$, and $\Delta=(1/T_C)(d^2T_C/d\varepsilon_{JT}^2)$. The magnitudes of $\alpha$ and $\Delta$ represent the relative weights for symmetry-conserving bulk and symmetry-breaking Jahn–Teller strains, respectively. According to the theoretical model,[17] $\alpha \simeq 10$ for a reasonable electron–phonon coupling ($0.5 \leqslant \lambda \leqslant 1$) in these compounds. Taking into account that the Curie temperature for the strain-free bulk $La_{0.7}Ca_{0.3}MnO_3$ compound is $T_C(\varepsilon=0) \simeq 265$ K[14,19] and using the values obtained for $\varepsilon_{100}$, $\varepsilon_{001}$, and $T_C$ for LCM3, we determined $\Delta$ to be about 950, which is of the same order of magnitude as the prediction of the theoretical model.[17] A possible explanation for this discrepancy is that the lattice mismatch between LCM3 and LAO is so large that the effect of structural disorder becomes dominant over the strain effect and that the role of Jahn–Teller distortion in formation of the ferromagnetic ordering is distinctly decreased. On the other hand, the additional deformation of the crystal lattice can be connected with the so-called ''chemical-pressure'' effect which is provided by the high diffusion rate of oxygen in these materials. Therefore, the modified lattice parameters are caused by both the simple elastic strain and the nonstoichiometry. In any case, the results obtained reflect a strong correlation between crystal lattice distortion and the electronic and magnetic states in CMR materials.

According to percolation theory, the conductivity can expressed as $\sigma \sim (p-p_0)^t$, where $p$ is the concentration of a metallic phase and $p_0$ is its critical value.[20] Taking into account that the value of the spontaneous magnetization is proportional to the concentration of the FM metallic phase and that $p_0=0.395$ for three-dimensional systems,[21] we can express the percolating conductivity for LCM3 by the formula $(1/\rho)\sim(m-m_0)^t$, where $\rho=R(T)/R(T_P)$, $R(T_P)$ is the resistance at the temperature of the MI transition, $m=M(T)/M(0)$, and $m_0=0.395$. Inset B in Fig. 6 exhibits a linear dependence of $\log(1/\rho)$ versus $\log(m-m_0)$, and the slope of the curve corresponds to the exponent $t \simeq 5.7$. This experimental value for $t$ is very close to that ($t \simeq 5.3$) obtained by a numerical calculation for the three-dimensional system, considering the spin effects.[21] Therefore, one can conclude that the MI transition in the LCM3 film has a percolating nature. It is reasonable to suggest that the nonuniformly distributed lattice strains in the film play a key role in blocking the complete transition to the FM phase within a narrow temperature range.

## 6. CONCLUSION

In summary, $La_{0.7}Ca_{0.3}MnO_3$ films were successfully prepared to have three characteristic structures: amorphous, strain-free crystalline (with randomly oriented nanocrystalline mosaic inclusions), and lattice-strained crystalline, and their the magnetic properties were investigated. It was shown that the amorphous film exhibits a Curie–Weiss-type PM behavior with freely moving individual Mn spins and a small FM contribution governed by the quasi-two-dimensional crystalline interfacial phase. The crystalline film with nanocrystalline mosaic inclusions demonstrates a superposition of the FM (corresponding to the crystalline matrix) and the SPM (to the nanocrystalline mosaic inclusions) contributions. The fitted average size of SPM particles using a Langevin function is coincident with that of the nanocrystalline mosaic clusters represented by the HREM images. An increase in the applied magnetic field leads to a reduction in the average magnetic moment of the SPM particles, which is due to an enhancement of the FM coupling between the individual crystallites in the mosaic inclusions and a partial SPM-to-FM transition. The observed suppression of the contribution from the Jahn–Teller distortion to the FM ordering with increasing lattice mismatch between substrate and lattice-strained film manifests a physical limit of the small-strain approach[17] in describing the magnetic properties of manganite films.

This work was supported by the KOSEF through the Quantum Photonic Science Research Center.

*E-mail: pvg@imp.kiev.ua

[1] Y. Tokura and Y. Tomioka, J. Magn. Magn. Mater. **200**, 1 (1999).
[2] A. P. Raminez, J. Phys. C **9**, 8171 (1997).
[3] F. Tsui, M. C. Smoak, T. K. Nath, and C. B. Eom, Appl. Phys. Lett. **76**, 2421 (2000).
[4] R. A. Rao, D. Lavric, T. K. Nath, C. B. Eom, L. Wu, and F. Tsui, Appl. Phys. Lett. **73**, 3294 (1998).
[5] S. Jacob, T. Roch, F. S. Razavi, G. M. Gross, and H.-U. Habermeier, J. Appl. Phys. **91**, 2232 (2002).
[6] A. Biswas, M. Rajeswari, R. C. Srivastava, T. Venkatesan, R. L. Green, Q. Lu, A. L. de Lozanne, and A. J. Millis, Phys. Rev. B **63**, 184424 (2001).

[7] O. I. Lebedev, G. Van Tendeloo, S. Amelinckx, H. L. Ju, and K. M. Krishnan, Philos. Mag. **80**, 673 (2000).
[8] J. R. Sun, C. F. Yeung, K. Zhou, L. Z. Zhou, C. H. Leung, H. K. Wong, and B. G. Shen, Appl. Phys. Lett. **76**, 1164 (2000).
[9] H. Y. Hwang, S.-W. Cheong, N. P. Ong, and B. Batlogg, Phys. Rev. Lett. **77**, 2041 (1996).
[10] A. Gupta, G. Q. Gong, G. Xiao, P. R. Duncombe, P. Lecoeur, P. Trouilloud, Y. Y. Wang, V. P. Dravid, and J. Z. Sun, Phys. Rev. B **54**, R15 629 (1996).
[11] R. Gross, L. Alff, B. Büchner, B. H. Freitag, C. Htsfener, J. Klein, Y. Lu, W. Mader, J. B. Philirr, M. S. R. Rao, P. Reutler, S. Ritter, S. Thienhaus, S. Uhlenbruck, and B. Wiedenhorst, J. Magn. Magn. Mater. **211**, 150 (2000).
[12] V. G. Prokhorov, G. G. Kaminsky, V. A. Komashko, J. S. Park, and Y. P. Lee, J. Appl. Phys. **90**, 1055 (2001).
[13] R. Mahendiran, S. K. Tiwary, A. K. Raychaudhuri, and T. V. Ramakrishnan, Phys. Rev. B **53**, 3348 (1996).
[14] Y. H. Li, K. A. Thomas, P. S. I. P. N. de Silva, L. F. Cohen, A. Goyal, M. Rajeswari, N. D. Mathur, M. G. Blamire, J. E. Evetts, T. Venkatesan, and J. L. MacManus-Driscoll, J. Mater. Res. **13**, 2161 (1998).
[15] V. G. Prokhorov, Y. P. Lee, V. A. Komashko, V. L. Svetchnikov, and J. S. Park, Phys. Status Solidi A **196**, 74 (2003).
[16] B. D. Cullity, *Introduction to Magnetic Materials*, Addison-Wesley, Reading, Mass. (1972).
[17] A. J. Millis, T. Darling, and A. Migliori, J. Appl. Phys. **83**, 1588 (1998).
[18] E. O. Wollan and W. C. Koehler, Phys. Rev. **100**, 545 (1955).
[19] G. L. Liu, J. S. Zhou, and J. B. Goodenough, Phys. Rev. B **64**, 144414 (2001).
[20] E. Dagotto, T. Hotta, and A. Moreo, Phys. Rep. **344**, 1 (2001).
[21] Y. Xiong, S.-Q. Shen, and X. C. Xie, Phys. Rev. B **63**, 140418 (2001).

This article was published in English in the original Russian journal. Reproduced here with stylistic changes by AIP.

# Electronic mechanism of structural phase transitions in manganese arsenide

V. I. Val'kov* and A. V. Golovchan

*A. A. Galkin Donetsk Physicotechnical Institute, ul. R. Lyuksemburg 72, Donetsk 83114, Ukraine*
(Submitted January 26, 2004; revised March 10, 2004)
Fiz. Nizk. Temp. **30**, 945–957 (September 2004)

The spin-fluctuation theory of magnetism is generalized to magnets with complex crystal and magnetic structure. An expression is obtained for the free energy of a system of itinerant $p$ and $d$ electrons, which are described by the Hubbard Hamiltonian with the static displacements of the ion cores, which lead to a change of the lattice symmetry, taken into account. The calculation of the free energy is done using the approximation of uniform local fields. The approach developed is applied to a study of the concrete magnetic and structural order parameters in ferromagnetic MnAs at $T=0$. It is shown that the appearance of structural distortions of the initial nickel arsenide lattice (nonzero structural order parameter) leads to a lowering of the average energy of the band electrons. The competition of the energy of the electrons and of the ion–ion coupling can stabilize these distortions. The interaction of the structural and magnetic order parameters tends to suppress the structural distortions. It is shown that the appearance of magnetization in the system (spontaneous or magnetic-field induced) can lead to restoration of the initial nickel arsenide structure. Such a magnetostructural transition is observed experimentally.  [DOI: 10.1063/1.1802956]

## 1. INTRODUCTION

Interest has grown of late in the electronic structure of manganese arsenide as one of the components of the system (Ga,Mn)As, which is a promising material for spintronics.[1–3] It therefore remains a topical problem to ascertain the interrelation between the structural and magnetostructural phase transitions in manganese arsenide, which have still not been given a microscopic justification. A structural phase transition of the displacive type from the paramagnetic (PM) state to the hexagonal crystal structure $B8_1$ (space group $P6_3/mmc$) in the PM state with the rhombic crystal structure $B31$ (space group $P_{nma}$) is a second-order transition and occurs at $T_t=400$ K. The magnetostructural first-order phase transition from the PM phase $B31$ to the ferromagnetic (FM) phase $B8_1$ occurs at $T_C=313$ K and is accompanied by a large magnetostrictive effect. The phase transition temperature shifts under magnetic field and hydrostatic pressure.

Studies of the phase transitions in manganese arsenide using phenomenological models[4–7] based on symmetry-group analysis have determined the magnetic and structural order parameters and established a number of important experimentally verifiable relations between the symmetry of the crystal lattice and the elastic constants and magnetic states of the system, which determine the $P-T-H$ phase diagram. Naturally, in this and other[8] approaches the mechanism of the structural and magnetostructural transformations cannot be understood, and the magnetic and crystal structural properties are considered without reference to the band structure. Even in Refs. 2, 3 and 9–14, however, in which the itinerant nature of the carriers of the magnetism was taken into account and the band structure of MnAs was calculated from first principles for the crystallographic phases $B8_1$ (PM, FM) and $B31$ (PM), the mechanism of the paramagnetic structural $B8_1(\mathrm{PM})\leftrightarrow B31(\mathrm{PM})$ and magnetostructural $B8_1(FM)\leftrightarrow B31(\mathrm{PM})$ phase transitions was not revealed. For example, in Ref. 13 the focus of attention was on modeling of certain features of the magnetic behavior of MnAs caused by the structural transition $B8_1(\mathrm{PM})\leftrightarrow B31(\mathrm{PM})$. However, the calculations were done in the framework of the spin-fluctuation theory for a single-band Hubbard Hamiltonian with the use of a piecewise linear model approximation for the electron density of states. Because the free energy of the system was constructed without introducing a structural order parameter, it was impossible to explore the possibility that the formation of the $B31$ structure can be justified on the basis of energy considerations.

The goals of the present study are:

1) to calculate the free energy of a system of interacting electrons in a lattice with the fluctuating ferromagnetic and structural order parameters taken into account;

2) to analyze the possibility of a crystal-structural and a magnetostructural phase transition in MnAs as a consequence of a certain dependence of the band energy of $p$ and $d$ electrons on the structural configuration of the Mn and As atoms.

It is advisable first to consider the problem of the phase transition in MnAs from the standpoint of the symmetry-group approach, for which purpose we analyze the results of Refs. 5–7.

## 2. SYMMETRY ANALYSIS OF THE MAGNETIC AND CRYSTALLOGRAPHIC TRANSITIONS IN MnAs

The most consistent phenomenological description of the phase transition in manganese arsenide was given in Refs. 5–7. In those paper the structural and magnetic order parameters were determined and invariants were constructed that describe their interrelationship and their coupling with elastic lattice deformations with respect to the most symmetric nickel arsenide crystal structure (PM, $B8_1$). In Refs. 6 and 7 the magnetic and structural order parameters chosen were the

 

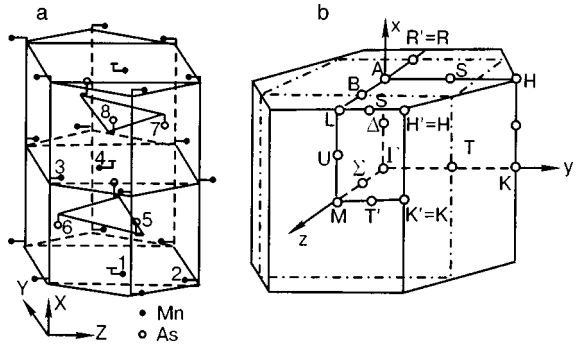


FIG. 1. a—Crystallographic unit cell of MnAs in the rhombic arrangement. b—Brillouin zone of the initial nickel arsenide lattice (solid lines) with the symmetry space group $P6_3/mmc$. As a result of the structural transition $P6_3/mmc-P_{nma}$ the Brillouin zone boundaries are compressed along the $z$ axis. The new boundaries are shown by the dot-and-dash line.

ferromagnetism vector **m** and the component of the irreducible displacement vector of the manganese, $\varphi=g_z/b\sqrt{3}$ from the sets of irreducible magnetic vectors (1) and irreducible displacements of the magnetic ions (2) for the crystal-chemical unit cell of the initial PM phase ($B8_1$) in the rhombic arrangement (Fig. 1a):

$$\begin{aligned} m_1 &= M_1 + M_2 + M_3 + M_4 = m,\\ m_2 &= M_1 - M_2 + M_3 - M_4,\\ m_3 &= M_1 + M_2 - M_3 - M_4,\\ m_4 &= M_1 - M_2 - M_3 + M_4; \end{aligned} \tag{1}$$

$$\begin{aligned} f &= u_1 + u_2 + u_3 + u_4,\\ g &= u_1 - u_2 + u_3 - u_4,\\ c &= u_1 + u_2 - u_3 - u_4,\\ a &= u_1 - u_2 - u_3 + u_4; \end{aligned} \tag{2}$$

$$\begin{aligned} f_1 &= u_5 + u_6 + u_7 + u_8,\\ g_1 &= u_5 - u_6 - u_7 + u_8,\\ c_1 &= u_5 + u_6 - u_7 - u_8,\\ a_1 &= u_5 - u_6 + u_7 - u_8; \end{aligned} \tag{3}$$

$M_i$ is the magnetization of the $i$th magnetic sublattice of the MnAs system, $u_n$ is the displacement vector of the atoms of the $n$th sublattice, $|u_n|=|u_{n'}|$, $n\in 1-4$; $|u_m|=|u_{m'}|$, $m\in 5-8$.

The expression for the total nonequilibrium thermodynamic potential density (TPD) of the system, $\Omega$, according to Ref. 6 does not take into account the energy contributions from the displacements of the arsenic and has the form

$$\Omega=\Omega(m)+\Omega(\varphi)+\Omega(u)+\Omega(m,u) +\Omega(u,\varphi)+\Omega(m,\varphi), \tag{4}$$

where $\Omega(m)$ and $\Omega(\varphi)$ are the TPDs of the magnetic and structurally distorted lattice subsystems; $\Omega(u)$ and $\Omega(m,u)$ are the elastic and magnetoelastic energy densities, $\Omega(\varphi,u)$ and $\Omega(\varphi,m)=\frac{1}{2}\delta m^2\varphi^2$ are the TPDs characterizing the coupling of the structural distortions with the elastic strains $u$ and the magnetization $m$, respectively. Here it is postulated that the coefficients $a_m(T)$ and $a_\varphi(T')$ of the quadratic terms of the expansions of $\Omega(m)$ and $\Omega(\varphi)$ in power series in $m$ and $\varphi$ are linear functions of temperature and can have a change of sign as the temperature decreases. The phase diagrams calculated on the basis of the TPD (4) describe a sequence of structural and magnetostructural transitions $P6_3/mmc(\mathrm{PM})-P_{nma}(\mathrm{PM})-P6_3/mmc(\mathrm{FM})$, but obviously the cause of the sign change of $a_\varphi(T')$ and the physical nature of the coefficient $\delta$ and, hence, the mechanism of these transitions, remain outside the scope of that approach.

Below we consider a model for magnetostructural transitions in manganese arsenide based on unified energy considerations of the electronic band structure responsible for the features of the crystalline, magnetic, and transport properties. Here, unlike Ref. 6, it is taken into account that the real transition $B8_1-B31$ is accompanied by two-component displacements of the manganese and arsenic ions along the $z$ and $x$ axes. These displacements are described by the irreducible displacement vector **g** for manganese and $\mathbf{a}_1$ (2)–(3) for arsenic. Therefore, as a quantitative measure of the distortions of the $B8_1$ lattice one can take the parameters $\varphi=\pm|g_z|/c$, $\varepsilon=\pm|g_x|/a\ll\varphi$ for manganese and $\varphi_1=\pm|a_{1x}|/a$, $\varepsilon_1=\pm|a_{1z}|/c\ll\varphi_1$ for arsenic, constructed from the thermodynamically averaged values of the individual ion displacements $u_n$. Then the mathematical description of the structural transition $B8_1-B31$ consists of calculating the free energy of the system of ions and itinerant electrons as functions of these parameters, $F(\varphi,\varepsilon,\varphi_1,\varepsilon_1)$, and ascertaining the conditions for the formation of a minimum of this function at nonzero values of the arguments. In practical calculations we shall limit ourselves to only the parameters $\varphi$ and $\varphi_1$.

### 3. SYSTEM HAMILTONIAN

Since the results of experimental and theoretical studies of MnAs indicate a local character of the formation of the spin density[9,11] and the participation of $d$ electrons in the formation of the conduction band,[9,10] it is appropriate to use the Hubbard Hamiltonian[15] for description of the magnetic properties of MnAs.

For a magnet with several ions in a unit cell that admits displacement of these ions to a new equilibrium position, the Hubbard Hamiltonian has the form

$$H_e=H_0+H_1, \tag{5}$$

$$H_0=\sum_{i,j}\sum_{\sigma m,m'}\sum_{n,n'} t_{nim,n'jm'}(\varphi,\varphi_1)a^+_{ni,m\sigma}a_{n'j,m'\sigma} =\sum_{k,\sigma}\sum_{n,n'}\sum_{m,m'}\gamma_{nm,n'm'}(k,\varphi,\varphi_1)c^+_{nm,k\sigma}c_{n'm',k\sigma}, \tag{6}$$

$$t_{inm,jn'm'}(\varphi,\varphi_1)=\frac{1}{N_0}\sum_{\mathbf{k}}\gamma_{nm,n'm'}(\mathbf{k},\varphi,\varphi_1) \times\exp\{i\mathbf{k}\cdot(\mathbf{R}_{in}-\mathbf{R}_{jn'})\}, \tag{7}$$

$$a_{ni,m\sigma}=\frac{1}{\sqrt{N_0}}\sum_k c_{nk,m\sigma}\exp(ikR_{ni}), \tag{8}$$

where $a^+_{nm,j\sigma}$ and $a_{nm,j\sigma}$ are, respectively, the Fermi creation and annihilation operators for an electron on the $m$th orbital of the $n$th ion in the $j$th cell, with spin projection $\sigma$ on the

TABLE I. Positions of the atoms in the $B31$ structure.

| No. | Mn position | No. | As position |
|---|---|---|---|
| 1 | $\left(0,0,\frac{c\varphi}{4}\right)$ | 5 | $\left(\frac{a}{4}(1+\varphi_1),\frac{b}{2},\frac{c}{6}\right)$ |
| 2 | $\left(0,\frac{b}{2},\frac{c}{2}-\frac{c\varphi}{4}\right)$ | 6 | $\left(\frac{a}{4}(1-\varphi_1),0,-\frac{c}{3}\right)$ |
| 3 | $\left(\frac{a}{2},\frac{b}{2},\frac{c}{2}+\frac{c\varphi}{4}\right)$ | 7 | $\left(\frac{a}{2}+\frac{a}{4}(1-\varphi_1),0,\frac{c}{3}\right)$ |
| 4 | $\left(\frac{a}{2},0,-\frac{c\varphi}{4}\right)$ | 8 | $\left(\frac{a}{2}+\frac{a}{4}(1+\varphi_1),\frac{b}{2},-\frac{c}{6}\right)$ |

quantization axis $z$, $\Sigma_j = N_0$ is the number of unit cells, with $\Sigma_n = N_L = 8$ atoms per cell (four Mn and four As ions), $R_{ni}$ is the translation vector of the $n$th sublattice in a rhombic arrangement, and the transfer integrals $t_{nim,n'i'm'}(\varphi,\varphi_1)$ are calculated according to Harrison.[16] The positions of the manganese and arsenic atoms in the rhombic cell, with displacements described by the parameters $\varphi$ and $\varphi_1$ taken into account, are listed in Table I. The lattice parameters were defined so that $a \| x$, $b \| y$, $c \| z$ $(c = b\sqrt{3})$ (Fig. 1a).

Expressions (5)–(8) take into account only the average displacements of the ions, described by the parameters $\varphi$ and $\varphi_1$. The coupling of the electrons with the thermal fluctuations of the displacements, $\delta u_{ni}$, is neglected.

The Hamiltonian $H_1$ of the intra-ion interaction of the electrons is written in the form

$$H_1 = -J\sum_j \sum_{n\in M_n} (\mathbf{S}_{nj})^2 + \mathbf{H}\sum_j \sum_{n\in M_n} \mathbf{S}_{nj}$$
$$\equiv -\frac{1}{4}J\sum_{l,j} (\mathbf{M}_{l,j})^2 + g\mathbf{H}\sum_j \mathbf{M}_{1,j}, \tag{9}$$

$$S^{\alpha}_{nj} = \sum_m S^{\alpha}_{nmj}, \tag{10}$$

$$S^{\alpha}_{nmj} = \frac{1}{2}\sum_{\sigma\sigma'} a^{+}_{nm,j\sigma}\tau^{\alpha}_{\sigma\sigma'}a_{nm,j\sigma'}, \tag{11}$$

$$\begin{aligned} M_{1j} &= S_{1j} + S_{2j} + S_{3j} + S_{4j},\\ M_{2j} &= S_{1j} - S_{2j} + S_{3j} - S_{4j},\\ M_{3j} &= S_{1j} + S_{2j} - S_{3j} - S_{4j},\\ M_{4j} &= S_{1j} - S_{2j} - S_{3j} + S_{4j}. \end{aligned} \tag{12}$$

In the expression for the Hamiltonian $H_1$ of the intra-ion interaction of the electrons, which is presented in two equivalent forms, the index $n$ numbers only the magnetic manganese ions $(n \in 1-4)$. The use of the second form, in our view, is more reasonable for compounds containing several magnetic ions in the $j$th crystal-chemical cell. The index $l$ numbers the four configurations of the spin operators in cell $j$, corresponding to the four irreducible magnetic vectors (1), $J$ is the intra-ion exchange integral, $\mathbf{H}$ is the external magnetic field, $\tau_{\sigma\sigma'}$ is the vector of Pauli matrices, $g = -2$ is the $g$ factor of the electron, and $\alpha \in x,y,z$.

The total model Hamiltonian $H$ of the system of itinerant electrons and ions, with the possibility of a change of the structural configuration taken into account, is written in the form

$$H = H_e(\varphi,\varphi_1) + W, \tag{13}$$

$$W = E_l + \frac{1}{2}\sum_{n,i,n',i'} A_{nin'i'}\exp(-|R_{ni}-R_{n'i'}|/\rho_{nn'}), \tag{14}$$

where the interaction energy $W$ of the ion cores contains two contributions: the energy of the Coulomb interaction of point ions immersed in a neutral background (the first term) and the ion–ion repulsion energy due to the overlap of their electron densities (in the Mayer form[17]). Here $R_{ni}$ is the radius vector of ion $ni$, which takes into account the average value of the displacements $u_n$ and the deviations $\delta u_{ni}$ from the averages, $q_n$ is the effective charge of ion $n$, $A_{nin'i'}$ are parameters of the model, and $\rho_{nn'}$ are the ion radii. For concrete calculations it is convenient to write $W$ in the form of an expansion in the deviations of the displacement vectors, $\delta u_{ni}$, and limit consideration to the harmonic approximation:

$$W = W_0(\varphi,\varphi_1) + \frac{1}{2}\sum_{n,i,\alpha,n',i',\alpha'} \frac{\partial^2 W(\varphi,\varphi_1)}{\partial\delta u_{ni\alpha}\partial\delta u_{n'i'\alpha'}} \times \delta u_{ni\alpha}\delta u_{n'i'\alpha'}$$
$$\equiv W_0(\varphi,\varphi_1) + \Delta W(\varphi,\varphi_1,\delta u_{ni\alpha},\delta u_{n'i'\alpha'}), \tag{15}$$

where the first term corresponds to expression (14) for the average values of the displacements $u_n$ and $u_{n'}$, described, as in Eqs. (7) and (8), by configurations $\varphi$ and $\varphi_1$. The second term can be brought to diagonal form by introducing the normal coordinates $Q_l(q)$ of the lattice $(l \in 3N_L)$. This is the main term governing the temperature-dependent part of the free energy of the lattice.

## 4. FREE ENERGY

The free energy of a system with Hamiltonian (13) at constant pressure and volume has the form

$$F = F_i\left(\varphi,\varphi,\frac{1}{\beta}\right) + F_e, \tag{16}$$

$$F_i\left(\varphi,\varphi,\frac{1}{\beta}\right) = W_0(\varphi,\varphi_1) + \Delta W\left(\varphi,\varphi,\frac{1}{\beta}\right), \tag{17}$$

$$\Delta W\left(\varphi,\varphi,\frac{1}{\beta}\right) = -\frac{1}{\beta}\ln\int \exp\{-\beta\Delta W(\varphi,\varphi,Q_l(q), Q_{l'}(q))\}dQ_{l_1}(q)\ldots dQ_{l_{3n}}(q), \tag{18}$$

$$F_e = \Omega + \mu N, \quad N = -\frac{\partial\Omega}{\partial\mu}, \tag{19}$$

$$\Omega = \Omega_0 + \Delta\Omega, \tag{20}$$

$$\exp(-\beta\Omega_0) = \mathrm{Tr}\{\exp(-\beta\tilde{H}_0)\} = \mathrm{Tr}\{\exp[-\beta(H_0-\mu N)]\}, \tag{21}$$

$$\exp(-\Delta\Omega/T) = \left\langle T_\tau \exp\left[-\int_0^\beta H_1(\tau)d\tau\right]\right\rangle_{\overline{H}_0}, \tag{22}$$

where $H_1(\tau)=\exp(\tau\tilde{H}_0)H_1\exp(-\tau\tilde{H}_0)$,

$$\langle A\rangle_{\bar{H}_0}=\mathrm{Tr}\{A\exp[\beta(\Omega_0-\tilde{H}_0)]\} \tag{23}$$

(for any operator $A$), $\mu$ is the chemical potential, $T_\tau$ is the imaginary-time-ordering operator, $\Omega$ is the thermodynamic potential (TP) of the system, and $\beta=1/T$.

The calculation of the free energy $F_e$ of a system of interacting electrons is a complicated many-particle problem. One of the methods used to solve it is based on reducing it to a single-particle problem of the interaction of the electrons with random fields fluctuating in space and time.[18] We shall use this method below to calculate expression (22), which determines the magnetic contribution $\Delta\Omega$ to the total free energy $F$ (for the other approaches to this problem see the review[19]).

Using a Stratonovich–Hubbard transformation,[20,21] we can put expression (22) in the form

$$\exp(-\beta\Delta\Omega)=\int\prod_{q\neq 0}\prod_{l}\frac{d\eta_{l,q}(\tau)}{\pi^3}\frac{d\eta_{l,0}(\tau)}{\pi^{3/2}}\mathrm{e}^{-\beta\psi\{\eta_{lq}\}},$$

$$\psi=\psi_0+\psi_1, \tag{24}$$

$$\psi_0=\beta^{-2}N_0\sum_{q\neq 0}\sum_{l}\sum_{\alpha=+,-,z}\int_0^\beta|\eta^\alpha_{l,q}(\tau)|^2d\tau+\beta^{-2}N_0\times\sum_{l,\alpha}\int_0^\beta\left|\eta^\alpha_{l,0}(\tau)-\frac{gH^\alpha_l}{C}\right|^2d\tau, \tag{25}$$

$$\psi_1=-\beta^{-1}\ln\left\langle T_\tau\exp\left(-\beta\sum_\alpha\tilde{H}^\alpha_1\right)\right\rangle_{\bar{H}_0}=-\beta^{-1}\left\langle T_\tau\exp\left(-\beta\sum_\alpha\tilde{H}^\alpha_1\right)\right\rangle_{\tilde{H}_0,c}, \tag{26}$$

$$\eta_j(\tau)=\sum_{q,\omega}\eta_{q\omega}\mathrm{e}^{-i(qR_j+\omega\tau)},$$

$$\eta_{q\omega}=(N_0\beta)^{-1}\sum_j\int_0^\beta\eta_j(\tau)\mathrm{e}^{-i(qR_j+\omega\tau)}d\tau,$$

where

$$\tilde{H}^\alpha_1=N_0\beta^{-1}C\sum_l\sum_q\int_0^\beta(\eta^{\alpha^+}_{l,q}(\tau))^*M^\alpha_{l,q}(\tau)d\tau,$$

$\alpha=z,+,-;\ q$

is a wave vector belonging to the first Brillouin zone for the $B31$ structure; $C=\sqrt{J/b}$, $\eta_{lq}(\tau)=\Sigma_\omega\eta_{l,q\omega}\mathrm{e}^{-i\omega\tau}$, $\eta^\pm_{l,q}(\tau)=\eta^x_{l,q}(\tau)\pm\eta^y_{l,q}(\tau)$, and $M^\alpha_{l,q}(\tau)$ and $(\eta^{\alpha^-}_{l,q}(\tau))^*$ are the $\alpha$th Fourier component of the operator of the $l$th irreducible magnetic vector (1) and the component of the fluctuating exchange field conjugate to it.

Since in this paper we are considering the low-temperature stabilization of a single FM phase, we shall assume that the main contribution to $\psi_1$ and to the TP is made by the Fourier component $\eta_{1q}(\tau)\equiv\eta_q(\tau)$ of the field $\eta_{1j}$ corresponding to the FM configuration of the spin operators $M_{1j}$. The contributions of the other Fourier components of the fields $\eta_{l\neq 1,j}$, which describe three types of antiferromagnetic (AFM) configurations of the spin operators, will be neglected.

Although there are many methods of calculating the functional $\psi_1$, the majority of them have been developed for rather simple Hamiltonians. In this paper we shall use the uniform local fields approximation—an approach which was proposed in Ref. 22 and developed further in Refs. 23–25, since it is least difficult to generalize to the case of magnets with several magnetic atoms in the unit cell.

When the second-order corrections, which take into account the quadratic fluctuations of the field, $\Sigma_{q\omega\neq 0}X_{q\omega}|\eta_{q\omega}|^2$, are included, the expression for $\psi_1\{\eta,\varphi,\varphi_1\}$ in the uniform local fields approximation for a material with a unit cell whose basis contains four "nonmagnetic" (As) and four "magnetic" (Mn) ions with nonequivalent $p$-$d$ electronic Bloch states has the form

$$\psi_1\{\eta,\varphi,\varphi_1\}=L(\eta,\varphi,\varphi_1)+\beta^{-1}\sum_{(q\omega)\neq 0}X_{q\omega}|\eta_{q\omega}|^2, \tag{27}$$

$$L\{\eta,\varphi,\varphi_1\}=-\beta^{-1}\sum_{S=1}^{32}\sum_{\sigma=\pm 1}\sum_k\ln\{1+\exp[-\beta(E_{S\sigma}\times(k,\varphi,\varphi_1,C\eta/2)-\mu)]\}-\Omega_0, \tag{28}$$

where $E_{S\sigma}(k,\varphi,\varphi_1,C\eta/2)$, the energy spectrum of the band electrons magnetically biased by the random field $\eta$, is determined from the solution of the secular equation

$$\det\begin{vmatrix}\gamma^{\mathrm{Mn-Mn}}_{nm,n'm''}(k,\varphi,\varphi_1)-\sigma C\eta/2-E\delta_{nm,n'm'} & t^{\mathrm{Mn-As}}_{nm,n'm''}\\ t^{\mathrm{As-MN}}_{mn,n'm''} & \gamma^{\mathrm{As-As}}_{mn,n'm''}(k,\varphi,\varphi_1)-E\delta_{nm,n'm'}\end{vmatrix}=0, \tag{29}$$

where the matrices $\gamma^{\mathrm{Mn-Mn}}_{nm,n'm''}(k,\varphi,\varphi_1)$, $\gamma^{\mathrm{As-As}}_{nm,n'm''}(k,\varphi,\varphi_1)$, and $t^{\mathrm{Mn-As}}_{nm,n'm''}(k,\varphi,\varphi_1)$, $t^{\mathrm{As-Mn}}_{nm,n'm''}(k,\varphi,\varphi_1)$ have dimensions of $20\times 20$, $12\times 12$, $12\times 20$, and $20\times 12$, respectively.

The contribution of the quadratic long-wavelength fluctuations of the field can be modeled by a Lindhard function[23] $X_{q\omega}\cong aq^2-ib\omega/q$ or calculated exactly (Appendix A).

After some changes of integration variables $\eta^\alpha_{q\omega}$ and evaluation of the integrals (24) by the method of steepest descent, the final expression for the free energy $F_e\{m,\varphi,\varphi_1\}$ of the electronic system takes the form (Appendix A)

$$F_e\{m,\varphi,\varphi_1\}=-\beta^{-1}\sum_{S,k,\sigma}\ln\left[1+\exp\left\{-\beta\left(E_{S\sigma}\times\left(k,\varphi,\varphi_1,\frac{Jm}{4g}\right)-\mu\right)\right\}\right]+\mu N+\frac{J}{4g^2}\sum_{(q,\omega)\neq 0}|\mathbf{m}_{q\omega}|^2(1+X_{q\omega})+\frac{JN_0}{4g^2}\mathbf{M}^2-\beta^{-1}\sum_{(q,\omega)\neq 0}\sum_{\alpha=x,y,z}\ln m^{\alpha}_{q\omega}, \tag{30}$$

$$m^2=\left(\mathbf{M}+\frac{2g^2}{J}\mathbf{H}\right)^2+\frac{1}{N_0}\sum_{(q,\omega)\neq 0}\mathbf{m}^2_{q\omega}, \tag{31}$$

where the magnetic moment, defined as $\mathbf{M}=-\partial F_e/\partial\mathbf{H}$, coincides with the saddle-point value of the variable $\mathbf{M}$.

## 5. ANALYSIS OF THE MECHANISM OF STRUCTURAL TRANSITIONS IN MnAs

The basic assumptions of the model of structural transitions in MnAs are based on the experimental facts and their obvious consequences, the most important of which are the following:

1) the $B8_1-B31$ transition, described by the parameters $(\varphi,\varphi_1)$, leads to a doubling of the initial $B8_1$ unit cell and to a change in the position of the Brillouin zone boundaries (Fig. 1b);

2) on the new zone boundaries a lifting of the degeneracy of some of the states of the electron energy spectrum can occur (depending on the structure factors of the manganese and arsenic sublattices), and these states can become separated by local gaps.

The basic assumptions of the model are as follows.

—The formation of gaps whose values depend on the parameters $(\varphi,\varphi_1)$, leads to a lowering of the band energy of the electrons. It is assumed that this lowering is especially effective if the Fermi level intersects part of the gaps.

—A competition between the free energy $F_e\{m,\varphi,\varphi_1\}$ and the model interaction energy of the ion cores $F_i(\varphi,\varphi,1/\beta)$ determines the stability region of the $B31$ structure in respect to temperature $(0\leqslant T\leqslant T_t)$.

—The redistribution of electrons over spin subbands as a result of the appearance of a uniform magnetization can cause instability of the $B31$ structure for $T<T_t$ and can lead to a magnetostructural transition from $B31$ (PM) to $B8_1$ (FM).

Since in this paper we are analyzing the possibility in principle of structural and magnetostructural transitions, the analysis below will be done for $T=0$, and questions related to the temperature-induced structural and magnetostructural transitions in this approach will not be considered.

### 5.1. Expression for the free energy at $T=0$

At $T=0$ the free energy per unit cell of the system and the equation for the chemical potential are given by expressions derived with the use of the relation

$$\sum_k=\frac{VN_0}{(2\pi)^3}\int d^3k:$$

$$F\{M,\varphi,\varphi_1\}=\frac{V}{(2\pi)^3}\sum_{S,\sigma}\int d^3kE_{S\sigma}\left(k,\varphi,\varphi_1,\frac{JM}{4g}\right)\times\Theta\left(\mu-E_{S\sigma}\left(k,\varphi,\varphi_1,\frac{JM}{4g}\right)\right)+\frac{J}{4g^2}M^2+\frac{W(\varphi,\varphi_1)}{N_0}+W_1(\varphi,\varphi_1), \tag{32}$$

$$\frac{N}{N_0}=\frac{V}{(2\pi)^3}\sum_{\sigma}\int d^3k\Theta\left(\mu-E_{S\sigma}\left(k,\varphi,\varphi_1,\frac{JM}{4g}\right)\right), \tag{33}$$

Expression (32) can be regarded as the nonequilibrium free energy of the system, which is characterized by two structural order parameters $(\varphi,\varphi_1)$ and one magnetic order parameter $M$, the equilibrium values of which correspond to a minimum of $F\{M,\varphi,\varphi_1\}$, $V$ is the volume of the unit cell of the crystal, $N_0$ is the number of unit cells in the crystal, $\Theta(x)$ is the Heaviside step function, and

$$W_1(\varphi,\varphi_1)=K(\varphi^2+\varphi_1^2), \tag{34}$$

$W_1(\varphi,\varphi_1)$ is the correction to $W(\varphi,\varphi_1)/N_0$ due to the use of the "rough" approximation for the ion–ion repulsion energy, which did not take into account the asphericity of the ionic potential and the fine structure of the indirect ion–ion interaction.

### 5.2. Influence of structural distortions on the free energy

Figure 2 shows contour diagrams of $F\{M,\varphi,\varphi_1\}$ in the coordinates $(\varphi,\varphi_1)$, calculated for two fixed values of the magnetic moment per cell. In all of the calculations the number of electrons per cell was equal to $N/N_0=40$ [Note: $N/N_0=4(n_p+n_d)$, where $n_p=3$ is the number of $p$ electrons of As and $n_d=7$ is the effective number of $d$ electrons of Mn, because of the transition of the $s$ electrons of Mn into the conduction band], and the parameter values used in the calculation are presented in Table II.

As we see from the figures, the minimum of the free energy is attained for $\varphi=\varphi_1=0.2$ for $M=0$ and at $\varphi=\varphi_1=0$ for $M=10\mu_B$.

It follows from these plots that, first, the $B31$ crystal structure corresponds to a minimum of the free energy for a nonmagnetic system. Second, under the influence of the exchange splitting induced by an external magnetic field or a spontaneous magnetization, a magnetostructural transition $B31-B8_1$ can occur. These processes are illustrated more clearly in Fig. 3a, which shows the variation of $F\{M,\varphi,\varphi_1\}$ along the line $\varphi=\varphi_1$ for different values of $M$. The reason for this behavior of the system is explained in Fig. 3b, which gives the dependence of the average energy $E(M,\varphi,\varphi_1)$ of the band electrons (the first term in (32)) along the line $\varphi=\varphi_1$ for different values of the magnetization $M$. From a comparison of curves *4* $(M=0)$ and *5* $(M=10\mu_B)$ it is seen that both are descending functions of the parameter $\varphi=\varphi_1$, although the rate of descent is higher in the case $M=0$. Therefore the sum of curves *4* and *6* can produce a minimum of $F\{M,\varphi,\varphi_1\}$ at $\varphi\neq 0$ (curve *1* in Fig. 3a); the analogous

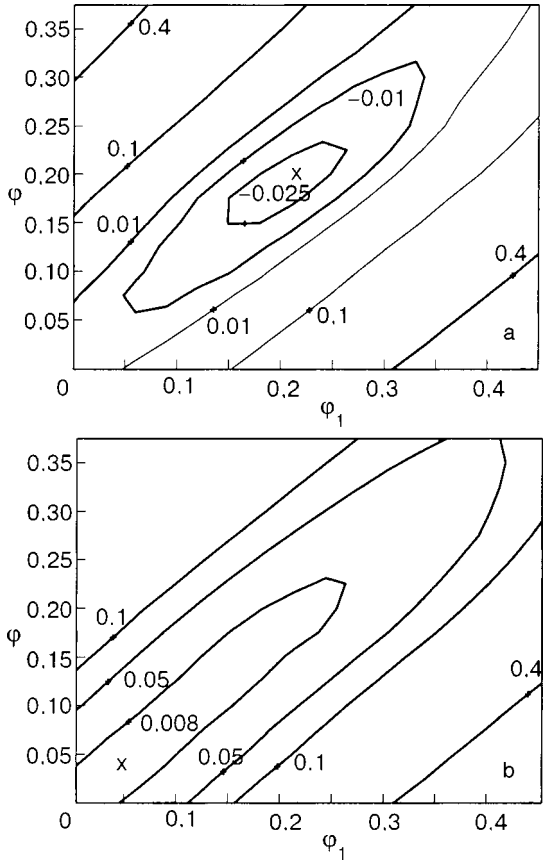


FIG. 2. Dependence of the free energy per unit cell on the value of the structural order parameters $(\varphi,\varphi_1)$ for different values of the magnetic moment of the unit cell, $M$ $[\mu_B]$: 0 (a), 10 (b); ×—position of a minimum.

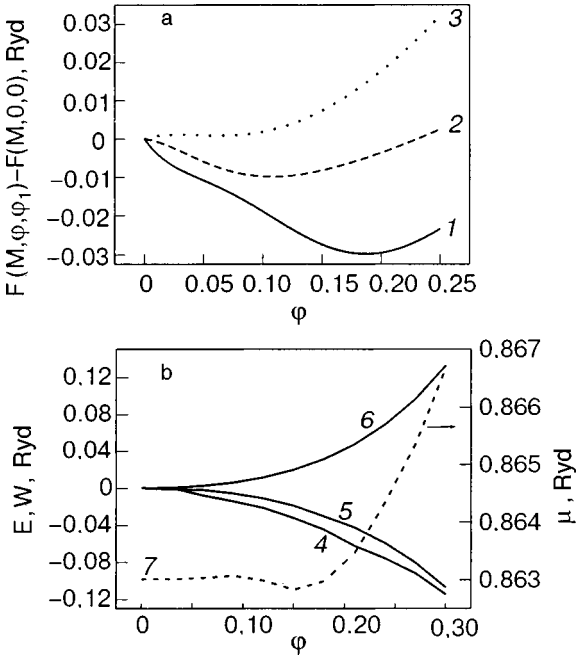


FIG. 3. a—Influence of the magnetic moment $M$ of the unit cell on the stability of the $B31$ structure along the direction $\varphi_1=\varphi$: reduced free energy as a function of the structural order parameters for $M=0$ (*1*), $5\mu_B$ (*2*), $10\mu_B$ (*3*). b—Dependence on the structural order parameters under the condition $\varphi_1=\varphi$ for the different contributions to the free energy: The reduced average energy of the band electrons $E(M,\varphi,\varphi)-E(M,0,0)$ for $M=0$ (*4*) and $10\mu_B$ (*5*); the reduced interaction energy of the ion cores $W(\varphi,\varphi)-W(0,0)$ (*6*); the chemical potential $\mu$ for $M=0$ (*7*).

sum for curves *5* and *6* gives curve *3*, for which the minimum of $F\{M,\varphi,\varphi_1\}$ is reached at $\varphi=\varphi_1=0$.

### 5.3. Influence of distortions on the stabilization of the magnetic state

Let us analyze the behavior of $F\{M,\varphi,\varphi_1\}$ for different values of the structural order parameters $\varphi$ and $\varphi_1$ (Fig. 4).

1. An increase in the degree of distortion (the moduli of $\varphi$ and $\varphi_1$) leads to a decrease in the equilibrium value of the magnetic moment (curves *2,8,9*) or to its complete suppression (curve *3*).

2. The most important influence on the stability of the magnetic order is that of the distortion of the manganese sublattice, $\varphi$ (curves *2,3*).

3. The distortion $\varphi_1$ of the arsenic sublattice has practically no influence on the magnetic state of the system (curves *6,8*). Apparently this is due to the fact that in the model under consideration the magnetism is due to the exchange splitting of the electronic states that are close genetically to the *d* states of manganese and are therefore most sensitive to displacements of the manganese ions.

### 5.4. Influence of structural distortions on the density of states

The character of the variation of the electron density of states $g_\sigma(\varepsilon,\varphi,\varphi_1,M)$ as a result of structural transitions can be traced from the theoretical curves (Fig. 5) calculated for different values of the structural and magnetic order parameters:

$$g_\sigma(\varepsilon,\varphi,\varphi_1,M)=\frac{V}{(2\pi)^3}\sum_S\int d^3k\,\delta \times\left[\varepsilon-E_{S\sigma}\left(\mathbf{k},\varphi,\varphi_1,\frac{JM}{4g}\right)\right], \qquad (35)$$

TABLE II. Parameters used for calculating the contour diagrams.

| Quantity | $K$, Ryd | $A_{\mathrm{As-As}}$, Ryd | $A_{\mathrm{Mn-Mn}}$, Ryd | $A_{\mathrm{Mn-As}}$, Ryd | $q_{\mathrm{Mn}}$, $e$ |
|---|---|---|---|---|---|
| Value | 0.35 | 0.5 | 1.0 | 3.0 | 0.6 |
| Quantity | $\rho_{\mathrm{Mn-As}}$, Å | $\rho_{\mathrm{Mn-Mn}}$, Å | $\rho_{\mathrm{As-As}}$, Å | $q_{\mathrm{As}}$, $e$ | $J$, Ryd |
| Value | 0.8 | 0.86 | 0.69 | 1.0 | 0.02 |
| Quantity | $a(B8_1)$, Å | $c(B8_1)$, Å | $a(B31)$, Å | $b(B31)$, Å | $c(B31)$, Å |
| Value | 3.72 | 5.72 | 5.72 | 3.72 | $b(B31)\sqrt{3}$ |

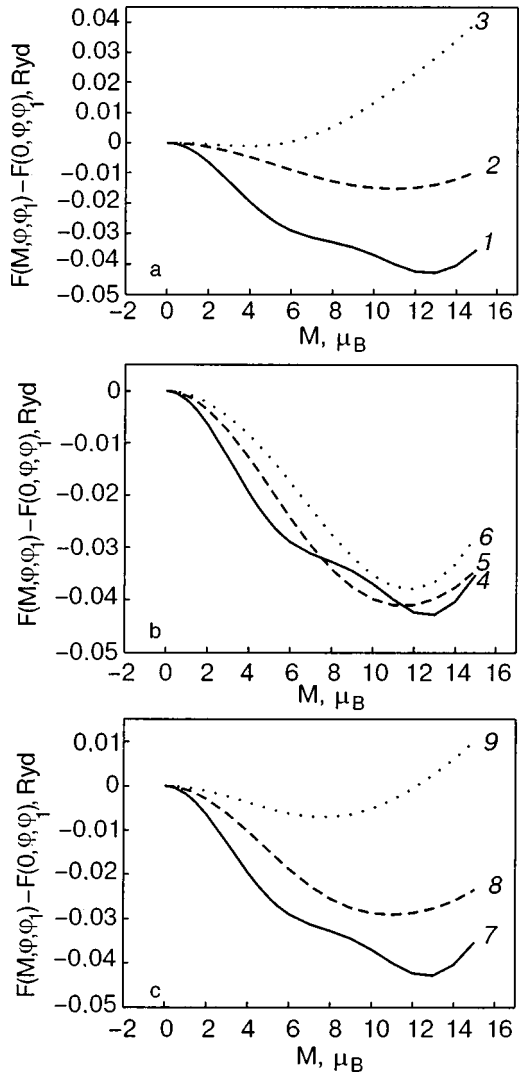


FIG. 4. Influence of the structural order parameter on the stability of the magnetically ordered state: $\varphi=0$, $\varphi_1\equiv 0$ (curves *1,4,7*); $\varphi=0.1$, $\varphi_1=0$ (*2*); $\varphi=0.3$, $\varphi_1=0$ (*3*); $\varphi=0$, $\varphi_1=0.1$ (*5*); $\varphi=0$, $\varphi_1=0.4$ (*6*); $\varphi=0.05$, $\varphi_1=0.05$ (*8*); $\varphi=0.2$, $\varphi_1=0.3$ (*9*).

where the integrals on the right-hand side have been calculated by the method of tetrahedra.[26]

As is seen in Fig. 5c,d, the appearance of structural distortions ($M=0$) leads to splitting of the main peak of $g_\sigma(\varepsilon)$ and a decrease of its value at the Fermi level. These features of the behavior of the density of states are manifested in the magnetic characteristics of MnAs. The main role in this is played by the values of the first and second derivatives of the density of states with respect to energy at the Fermi level:

$$g'=(\partial g_\sigma(\varepsilon,\varphi,\varphi_1,0)/\partial\varepsilon)_{\varepsilon=\varepsilon_F},$$

$$g''=(\partial^2 g_\sigma(\varepsilon,\varphi,\varphi_1,0)/\partial\varepsilon^2)_{\varepsilon=\varepsilon_F}.$$

For $\varphi=\varphi_1=0$ one has $g'>0$, $g''\leqslant 0$, while for $|\varphi|>0$ one has $g'<0$, $g''>0$.

Such a change in sign of the second derivative can give rise to anomalous temperature behavior of the static PM susceptibility $\chi(T)$ in the region of growing structural distortions (Appendix C).

## CONCLUSION

The theoretical part of this article is devoted to a derivation of the free energy of a system of itinerant electrons in a lattice with a basis and a varying structural configuration and gives an idea of the implementation of the spin-fluctuation approach for a specific material, e.g., manganese arsenide. Application of the approach described above to the study of the ground state of this compound permits justification of both the spontaneous lowering of the symmetry of the initial lattice and its restoration under the influence of the exchange field on the basis of energy considerations.

It follows from what we have said that the basic idea of the model is correct. However, the approach used for stabilization of the distorted lattice is essentially phenomenological in nature. For a rigorous description of the ion–ion interaction one should use the modern approach to this problem,[27,28] which allow one to address the problem of taking into account the magnetoelastic interactions in manganese arsenide. The latter are to a large degree responsible for the character of the magnetostructural phase transition.

In the future we hope to employ this conceptual framework to study the magnetostructural properties at finite temperatures.

## APPENDIX A

The uniform local fields approximation is used in the summation of the terms of an infinite series (the right-hand side of expression (26), expanded in a power series in $\tilde{H}_1^\alpha$):

$$\begin{aligned}\psi_1=&-\sum_{p=1}^{\infty}\frac{C^p}{\beta p}\sum_{q_1\ldots q_p}\sum_{\alpha_1\ldots\alpha_p}\sum_{\omega_1\ldots\omega_p}(\eta^{\alpha_1^+}_{\omega_1 q_1})^*\cdots\\ &\times(\eta^{\alpha_p^+}_{\omega_p q_p})^*\int_0^\beta d\tau_1\ldots\int_0^\beta d\tau_p e^{-i(\omega_1\tau_1\ldots\omega_p\tau_p)}\\ &\times\langle T_\tau M^{\alpha_1}_{q_1}(\tau_1)\ldots M^{\alpha_p}_{q_p\alpha_p}(\tau_p)\rangle_{\tilde{H}_0,c}\\ =&-\sum_{p=1}^{\infty}\frac{C^p}{\beta p}\sum_{q_1\ldots q_p}\sum_{\alpha_1\ldots\alpha_p}\sum_{\omega_1\ldots\omega_p}(\eta^{\alpha_1^-}_{\omega_1 q_1})^*\cdots\\ &\times(\eta^{\alpha_p^+}_{\omega_p q_p})^*\times\varphi_{2p}^{\alpha_1\ldots\alpha_p}(q_1\ldots q_p,\omega_1\ldots\omega_p),\end{aligned}\qquad\text{(A1)}$$

where $\langle\ldots\rangle_{\tilde{H}_0,c}$ denotes the sum of all connected diagrams.

The essence of the approximation consists in the fact that the right-hand side of (A1) is approximated by an expression in which the vertex parts $\varphi_{2p}^{\alpha_1\ldots\alpha_p}(q_1\ldots q_p,\omega_1\cdots\omega_p)$ for $p\geqslant 2$ are calculated for $q_i,\omega_i=0$. This allows one to sum the series and obtain an approximate expression for $\psi_1$ in the form of Eqs. (27), (28), and (A1).

An advantage of this approach is the possibility of taking into account the contribution to the free energy from all powers of the $\alpha$ component of the random fields $\eta^{\alpha_p^+}_{\omega_p q_p}$. A shortcoming is the limited description of the fluctuation dynamics that determines the domain of applicability of the approximation, $J/\tilde{W}<1$, where $\tilde{W}$ is the width of the conduction band.[29]

The contribution of long-wavelength fluctuations of the field (the dynamic second-order correction, which takes into

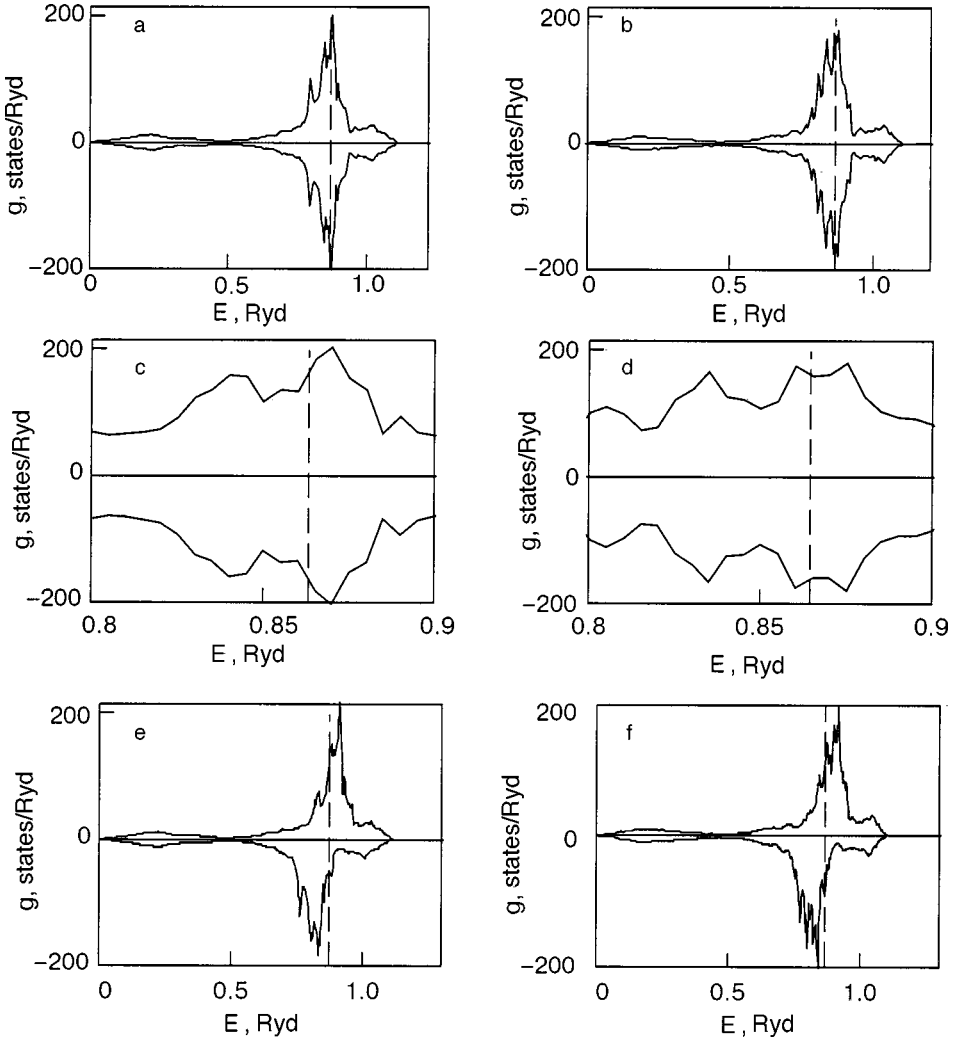


FIG. 5. Influence of the structural and magnetic order parameters on the density of states: initial nonmagnetic structure $B8_1$ (a,c); nonmagnetic structure $B31$ (b,d); magnetic structures $B8_1$ (e) and $B31$ (f). The dashed line denotes the position of the Fermi level. The upper half corresponds to the "spin up" and the lower to the "spin down" subband.

account the quadratic fluctuations of the field) can be calculated exactly by a direct evaluation of the right-hand side of the expression

$$\sum_{q\omega} X_{1,q\omega}|\eta_{1,q\omega}|^2 = -\frac{1}{2}\sum_{\alpha_1,\alpha_2}\left(\int_0^\beta d\tau_1\int_0^\beta d\tau_2 \times\langle T_\tau \tilde{H}_1^{\alpha_1}(\tau_1)\tilde{H}_1^{\alpha_2}(\tau_2)\rangle_{\tilde{H}_0,c} - \frac{\partial^2 L\{\eta\}}{\partial\eta^{\alpha_1}\partial\eta^{\alpha_2}}\right). \quad \text{(A2)}$$

Here $X_{1q\omega}\equiv X_{q\omega}$ is given by the formula

$$X_{q\omega} = J\sum_{S=1}^{N_L}(\chi^0_{SS,00}-\chi^0_{SS,q\omega})P_{SS} - J\sum_{S,S_1=1}^{N_L}(\chi^0_{SS_1,q\omega})P_{SS_1}, \quad \text{(A3)}$$

where $N_L$ is the number of atoms in the basis, $\chi^0_{SS_1,q\omega}$ are the generalized inhomogeneous magnetic susceptibilities,

$$\chi^0_{SS_1,q\omega} = \sum_k \frac{f(E_S(k,\varphi,\varphi_1,0)-\mu)-f(E_{S_1}(k+q,\varphi,\varphi_1,0)-\mu)}{E_S(k,\varphi,\varphi_1,0)-E_{S_1}(k+q,\varphi,\varphi_1,0)-i\omega}, \quad \text{(A4)}$$

and $P_{SS_1}$ are factors that take the hybridization of the subbands into account. Diagonalization of the matrix (29) corresponds to a transition from the operators $a_{nm,k\sigma}$ to their linear combination

$$c_{S,k\sigma} = \sum_{n,m} U_{S,nm}a_{nm,k\sigma},$$

and therefore

$$P_{SS_1} = \left(\sum_{nm} U^*_{S,nm}U_{nm,S_1}\right)\left(\sum_{nm} U^*_{S_1,nm}U_{nm,S}\right).$$

If we introduce the notation

$$\frac{\beta C}{2g}M = \lambda_0^\alpha = \eta_0^\alpha - \frac{gH^\alpha}{C}$$

and make a change from the complex variables $\eta^\alpha_{q\omega}$ to the two real variables

$$\left(\frac{\beta C}{2g}m_{q\omega}^{\alpha}\right)^2=(\lambda_{q\omega}^{\alpha})^2=|\eta_{q\omega}^{\alpha}|^2 \text{ and } \theta_{q\omega}^{\alpha}-\arg\eta_{q\omega}^{\alpha},$$

then the former expression for $\psi\{\eta\}$, which was independent of $\theta_{q\omega}^{\alpha}$,

$$\psi\{\eta,\varphi,\varphi_1\}=-\beta^{-1}\sum_{S,k,\sigma}\ln\{1+\exp[-(E_{S\sigma}(k,\varphi,\varphi_1,C\eta/2)-\mu)\beta]\}+\beta^{-1}\sum_{q\omega\neq 0}(1+X_{q\omega})|\eta_{q\omega}|^2+N_0\beta^{-1}\left|\eta_0-\frac{g\mathbf{H}}{C}\right|^2-\Omega_0 \tag{A5}$$

now becomes

$$\psi\{m,\varphi,\varphi_1\}=-\beta^{-1}\sum_{S,k,\sigma}\ln\left[1+\exp\left\{-\beta\left(E_{S\sigma}\times\left(k,\varphi,\varphi_1,\frac{Jm}{4g}\right)-\mu\right)\right\}\right]+\frac{J}{4g^2}\sum_{(q,\omega)\neq 0}|\mathbf{m}_{q\omega}|^2(1+X_{q\omega})+\frac{JN_0}{4g^2}\mathbf{M}^2-\beta^{-1}\sum_{(q,\omega)\neq 0}\sum_{\alpha=x,y,z}\ln m_{q\omega}^{\alpha}-\Omega_0(\varphi,\varphi_1), \tag{A6}$$

$$m^2=\left(\mathbf{M}+\frac{2g^2}{J}\mathbf{H}\right)^2+\frac{1}{N_0}\sum_{(q,\omega)\neq 0}\mathbf{m}_{q\omega}^2.$$

Then, taking into account that $d\eta_{q\omega}^{\alpha}=\lambda_{q\omega}^{\alpha}d\lambda_{q\omega}^{\alpha}d\theta_{q\omega}^{\alpha}$, $d\eta_0^{\alpha}=d\lambda_0^{\alpha}$, expression (24) can lead to the form

$$\exp[-\beta\Delta\Omega(m,\varphi,\varphi_1)]=\text{const}\cdot\int d\mathbf{M}\int\prod_{(q,\omega)\neq 0}\prod_{\alpha=x,y,z}dm_{q\omega}^{\alpha}\times\exp[-\beta\psi\{m,\varphi,\varphi_1\}-\beta\Omega_0(\varphi,\varphi_1)]. \tag{A7}$$

Let us estimate the integrals with respect to $M^{\alpha}$, $m_{q\omega}^{\alpha}$ in (A7) by the method of steepest descent. The equations determining the saddle points, $\partial\psi/\partial\mathbf{M}=0$ and $\partial\psi/\partial m_{q\omega}^{\alpha}=0$, reduce to the form

$$\mathbf{M}\left(1-\frac{g}{2N_0}\sum_{S,k,\sigma}\sigma f\left(E_{S\sigma}\left(k,\varphi,\varphi_1,\frac{Jm}{4g}\right)-\mu\right)\frac{1}{m}\frac{\partial E_{S\sigma}}{\partial b}\right)=\frac{2g}{N_0}\sum_{S,k,\sigma}\sigma f\left(E_{S\sigma}\left(k,\varphi,\varphi_1,\frac{Jm}{4g}\right)-\mu\right)\frac{\partial E_{S\sigma}}{\partial b}\frac{\mathbf{H}g^2}{Jm}, \tag{A8}$$

$$(m_{q\omega}^{\alpha})^2\left(1+X_{q\omega}-\frac{g}{2N_0}\sum_{S,k,\sigma}\sigma f\left(E_{S\sigma}\left(k,\varphi,\varphi_1,\frac{Jm}{4g}\right)-\mu\right)\times\frac{1}{m}\frac{\partial E_{S\sigma}}{\partial b}\right)=\frac{2g^2}{\beta J}, \tag{A9}$$

where $b=C\eta/2$.

The chemical potential is determined from the equation

$$\frac{N}{N_0}=\sum_{S,\sigma}\int\frac{d^3k}{1+\exp\left\{\beta\left(E_{S\sigma}\left(k,\varphi,\varphi_1,\frac{Jm}{4g}\right)-\mu\right)\right\}}, \tag{A10}$$

where $N/N_0$ is the number of electrons in the Brillouin zone.

When this is taken into account, the free energy is given by the expression

$$F_e\{m,\varphi,\varphi_1\}=\psi\{m,\varphi,\varphi_1\}, \tag{A11}$$

where the saddle-point values $M^{\alpha}$ and $m_{q\omega}^{\alpha}$ are substituted in for $m$.

## APPENDIX B

To calculate the Coulomb interaction energy of point ions immersed in a neutralizing background, we use the Ewald–Fuchs method,[30] the generalization of which to a lattice with a basis has the form

$$E_l=\frac{e^2}{2}\left\{\frac{4\pi}{V}\sum_{l\neq 0}\left(\sum_n q_nS_{ln}\right)\frac{\exp\left(-\frac{g_l^2}{4\eta}\right)}{g_l^2}-2\sqrt{\frac{\eta}{\pi}}\left(\sum_n q_n^2\right)+\sum_{i\approx 0}\sum_{n,n'}q_nq_{n'}\frac{G(|R_{i,nn'}|\sqrt{\eta})}{|R_{i,nn'}|}-\frac{\pi}{\eta V}\left(\sum_n q_n\right)^2\right\}, \tag{B1}$$

where $n=\overline{1.8}$ numbers the positions of the ions in the basis, $q_n$ is the charge of the ion at position $n$, $\mathbf{g}_l$ is the reciprocal lattice vector, $\eta$ is the Ewald parameter, which regulates the convergence of the series ($\eta=\pi^2/2V^{2/3}$), $\mathbf{R}_{i,nn'}=\mathbf{R}_i+\mathbf{r}_n-\mathbf{r}_{n'}$, $\mathbf{R}_i$ is a lattice vector, $\mathbf{r}_n$ is a vector specifying the position of an atom in the basis, $V$ is the unit cell volume, $E_l$ is the unit cell energy, and $S_{ln}$ is the structure factor:

$$S_{ln}=\sum_{n'}q_{n'}\exp[i\mathbf{g}_l\cdot(\mathbf{r}_n-\mathbf{r}_{n'})];G(x)=\frac{2}{\sqrt{\pi}}\int_x^{\infty}e^{-t^2}dt.$$

In Eq. (32) the term $W(\varphi,\varphi_1)=N_0E_l(\mathbf{r}_n(\varphi,\varphi_1))$. In calculating the lattice sums we have used six coordination spheres.

## APPENDIX C

Following Ref. 31, we can write the expression for the inverse paramagnetic susceptibility $\chi^{-1}(T)$ in the form

$$\chi^{-1}(T)=[2g^2(\varepsilon_F)\mu_BN_0]^{-1}\left\{a_1-\alpha+\frac{5}{3}a_3\xi^2+\ldots\right\},$$
$$a_1=2(g^2\mu_B^2N_0)^{-1}\left\{1+\frac{1}{6}(\pi kT)^2\left[\left(\frac{g'}{g}\right)^2-\frac{g''}{g}\right]+\ldots\right\},$$
$$a_3=2\left(\frac{g\mu_B}{2}\right)^2(3!)^{-1}a_1^3\left\{3\left(\frac{g'}{g}\right)^2-\frac{g''}{g}\right\}. \tag{C1}$$

Since the square of the amplitudes of the spin fluctuations $\xi^2$ in an itinerant ferromagnet is proportional to the temperature and it is this quantity that determines the strong

Curie–Weiss temperature dependence of the PM susceptibility, it follows from Eq. (C1) that the change in sign of $g''$ at the Fermi level can lead to a change in sign of $\partial\chi^{-1}(T)/\partial T$. In MnAs in the region of stability of the $B31$ phase this quantity is negative, a result which is seen to agree qualitatively with the behavior of the calculated density of states (C1). In Ref. 13, where a piecewise-linear density of states was used, this effect is attributed to a decrease in the density of states on decreasing temperature (a decrease of the coefficient $a_1$). In the model used in the present study there is a similar decrease of $a_1$, but it is supplemented further by the structural changes of the density of states, which are directly due to the spin-fluctuation mechanism of temperature dependence of the thermodynamic quantities in magnets.

*E-mail: valkov@dpms.fti.ac.donetsk.ua

[1] J. Mira, F. Rivadulla, J. Rivas, A. Fondado, R. Caciuffo, F. Carsughi, T. Guidi, and J. B. Goodenough, cond-mat/0201478.
[2] B. Sanyal, L. Bergqvist, and O. Eriksson, cond-mat/0308524.
[3] A. Debernardi, M. Peressi, and A. Balderaschi, cond-mat/0210235.
[4] C. P. Bean and D. S. Rodbell, Phys. Rev. **126**, 104 (1962).
[5] I. M. Vitebskiĭ, V. I. Kamenev, and D. A. Yablonskiĭ, Fiz. Tverd. Tela (Leningrad) **23**, 215 (1981) [Sov. Phys. Solid State **23**, 121 (1981)].
[6] É. A. Zavadskiĭ, V. I. Kamenev, E. P. Stefanovskiĭ, A. L. Sukstanskiĭ, and D. A. Yablonskiĭ, Preprint DonFTI-91-14 [in Russian], Donetsk (1991).
[7] S. K. Asadov, É. A. Zavadskiĭ, V. I. Kamenev, E. P. Stefanovskiĭ, A. L. Sukstanskiĭ, and B. M. Todris, Fiz. Tverd. Tela (St. Petersburg) **42**, 1649 (2000) [Phys. Solid State **42**, 1696 (2000)].
[8] T. Kato, K. Nagai, and T. Aisaka, J. Phys.: Solid State Phys. **16**, 3183 (1983).
[9] L. M. Sandratskii, R. F. Egorov, and A. A. Berdyshev, Phys. Status Solidi B **103**, 511 (1981).
[10] J. M. Tyler and J. L. Fry, Phys. Rev. B **1**, 4604 (1970).
[11] S. Haneda, N. Kazama, Y. Yamaguchi, and H. Watanabe, J. Phys. Soc. Jpn. **42**, 1201 (1977).
[12] R. Podloucky, J. Magn. Magn. Mater. **43**, 204 (1984).
[13] K. Motizuki and K. Katoh, J. Phys. Soc. Jpn. **53**, 735 (1984).
[14] K. Motizuki, K. Katoh, and A. Yanase, J. Phys. C: Solid State Phys. **19**, 495 (1986).
[15] J. Hubbard, Proc. R. Soc. London, Ser. A **276**, 238 (1963).
[16] W. A. Harrison, *Electronic Structure and the Properties of Solids*, Freeman, San Francisco (1980), Mir, Moscow (1983), Vol. 2.
[17] M. Born and K. Huang, *Dynamical Theory of Crystal Lattices*, Clarendon Press, Oxford (1954), Izd-vo Inostr. Lit., Moscow (1958).
[18] T. Moriya, *Spin Fluctuations in Itinerant Electron Magnetism*, Springer-Verlag, Berlin (1985), Mir, Moscow (1988).
[19] S. Y. Savrasov and G. Kotliar, cond-mat/0308053.
[20] R. L. Stratonovich, Dokl. Akad. Nauk SSSR **105**, 1097 (1957) [Sov. Phys. Dokl. **2**, 416 (1958)].
[21] J. Hubbard, Phys. Rev. Lett. **3**, 77 (1959).
[22] J. A. Hertz and M. A. Klenin, Phys. Rev. B **10**, 1084 (1974).
[23] A. A. Povzner, A. G. Volkov, and P. V. Gel'd, Fiz. Met. Metalloved. **58**, 47 (1984).
[24] A. A. Povzner and A. G. Volkov, Fiz. Met. Metalloved. **66**, 1073 (1988).
[25] A. G. Volkov, A. A. Povzner, V. V. Kryuk, and P. V. Bayankin, Fiz. Tverd. Tela (St. Petersburg) **41**, 1792 (1999) [Phys. Solid State **41**, 1644 (1999)].
[26] P. E. Blochl, O. Jepsen, and O. K. Andersen, Phys. Rev. B **49**, 16223 (1994).
[27] V. V. Nemoshkalenko and V. N. Antonov, *Methods of Computational Physics in Solid State Theory: Band Theory of Metals* [in Russian], Naukova Dumka, Kiev (1985).
[28] T. Huhne, C. Zecha, H. Ebert, P. H. Dederichs, and R. Zeller, Phys. Rev. B **58**, 10236 (1998),
[29] Yu. A. Izyumov, Usp. Fiz. Nauk **165**, 403 (1995),
[30] K. Fuchs, Proc. R. Soc. London, Ser. A **151**, 585 (1935).
[31] M. Shimizu, Rep. Prog. Phys. **44**, 329 (1981).

Translated by Steve Torstveit

# Spectrum of dynamic magnetic susceptibility of a randomized $f-d$ magnet with spin–lattice coupling. I. Shift of the magnetic resonance frequencies

A. B. Beznosov* and E. S. Orel

*B. Verkin Institute for Low Temperature Physics and Engineering, National Academy of Sciences of Ukraine, pr. Lenina 47, Kharkov 61103, Ukraine*

(Submitted January 28, 2003; revised February 19, 2004)
Fiz. Nizk. Temp. **30**, 958–968 (September 2004)

In narrow-band ferromagnetic conductors containing local $f$ and quasilocal $d$ magnetic moments the interatomic spin correlations created by the combined effects of the intra-atomic interactions of the quasilocal electrons and their intersite hops are playing a role in the formation of the magnetic resonance spectra. This role is examined, and the transformation of the spectra of the transverse dynamic magnetic susceptibility under conditions of weak spin–lattice coupling and spatial randomization of the $g$ factors of the quasilocal and local spin subsystems is investigated. A calculation done by the method of two-time retarded Green's functions shows that the interaction of the $d$ and $f$ electrons leads to an effective renormalization of the $g$ factors of both magnetic subsystems, and at zero temperature the spin–lattice coupling lowers the frequency of the inhomogeneous magnetic resonance and causes threshold damping of acoustic and optical magnons. © *2004 American Institute of Physics.*
[DOI: 10.1063/1.1802957]

## 1. INTRODUCTION

Magnetoelastic effects in randomized spin systems have been attracting attention recently in connection with the extensive use of doped many-component magnetically concentrated oxide conductors as magnetic field sensors in modern technique.[1,2] In particular, this interest relates to the manifestation of a colossal magnetoresistive effect in these substances due to the transition of the system to a ferromagnetic state. The interaction of the magnetic and elastic subsystems is of fundamental importance for the physics of these compounds,[3] in which the ferromagnetic order arises due to the so-called double-exchange mechanism,[1,2,4] as it substantially influences the character of the magnetic phases and the mechanisms of the phase transitions in them.[5,6] The changes caused by this interaction in the spectrum of the dynamic magnetic susceptibility are a source of information about the forces acting both within each of the subsystems mentioned and between them, and it is of practical interest as well. The goal of the present study is to investigate the influence of the spin–lattice coupling on the formation of the spectrum of the dynamic magnetic susceptibility of narrow-band magnetic conductors.

The interatomic spin correlations, which shape the collective character of the excitations in magnets, have a substantial influence on the manifestation of features in the spectrum of the magnetic linear response function due to disruptions of the translational symmetry of the system.[7] In the present paper we investigate the spectrum of the dynamic magnetic susceptibility of an $f-d$ magnet[7–9] over a wide frequency range. The spectrum under consideration is shaped by spin correlations that derive from the combined effects of the intra-atomic interactions of the *quasilocal* $d$ electrons (the exchange with the electrons of the *localized* $f$ shells and the Hubbard repulsion) and their intersite hopping, with allowance for spatial randomization of the $g$ factors of the $d$ and $f$ subsystems[9] and a weak spin–lattice coupling. The influence of spatial randomization of the spin subsystem on the spectrum of the dynamic magnetic susceptibility of an $f-d$ magnet was first studied in Ref. 7, and expressions were obtained for the coherent and incoherent components of the susceptibility of a system with randomized $g$ factors of the $d$ electrons. In Ref. 9 we solved an analogous problem for an $f-d$ magnet with anisotropic local exchange and randomization of the $g$ factors for quasilocal and local spins. In Ref. 8 the role of randomization of the interaction Hamiltonian of the system with the external field in the formation of the spectrum of the linear response function of an $f-d$ metal was elucidated. In the present paper we continue those investigations,[7–9] focusing our attention on the problem of spin–lattice coupling.

## 2. MODEL AND METHOD

In this paper we calculate the transverse dynamic magnetic susceptibility of a narrow-band magnetic conductor containing both local and quasilocal magnetic moments[8,10] (for the sake of definiteness below we shall speak of the model of a conducting ferromagnetic compound based on a rare-earth metal). The main elements of the electronic structure of such systems which are responsible for their special properties in the ground state are partially filled magnetically active local levels and a spin-polarized narrow conduction band (the corresponding results of the band calculations for gadolinium may be found in Refs. 11–13). The spectra of excitations that alter the spin of the system are shaped by electronic transitions to vacant states in the bands with spin orientation opposite to the magnetization of the system. Such excitations include spin waves (acoustic and optical modes) and one-electron Stoner transitions.[10,14] The schemes of the

 

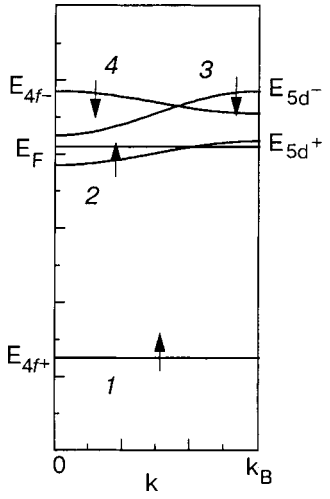


FIG. 1. Scheme of the electron energy spectrum of the model: *1*—partially filled magnetically active $4f$ level ($E_{4f+}$), *2*—partially filled $5d$ band, *3*—band of unfilled $5d$ states, *4*—band of unfilled $4f$ states, $E_F$—the Fermi energy, $E_{d+}$, $E_{d-}$, and $E_{4f-}$—maximum energies in the corresponding bands, $k_B$ is the Brillouin quasimomentum; the arrows represent the spin indices of the electron states.

electron energy spectrum (Fig. 1) and spectrum of elementary excitations (Fig. 2) used in the present paper are analogous to those considered in Refs. 8, 10 and 7, 9, respectively. Also shown in Fig. 2 is the scheme of the relative position of the phonon band and the acoustic magnon band, which is shifted upward by the applied external magnetic field. In the calculations we use the Green's function method,[15] which permits treating the effects in the magnetic and elastic subsystems in a unified approach.[14,16]

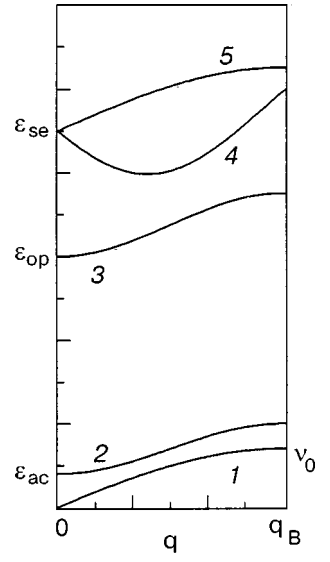


FIG. 2. Scheme of the spectra of the elementary excitations in the model used: *1*—phonon spectrum, *2*—acoustic magnon spectrum, *3*—optical magnon spectrum, *4,5*—lower and upper boundaries of the continuum of single-particle (Stoner) electronic excitations with a spin flip (the figure corresponds to the one-dimensional case with $k_F=0.4k_B$), $\varepsilon_{ac}$ and $\varepsilon_{op}$ are the energies at the corresponding zone centers ($\mathbf{q}=0$), $\varepsilon_{se}$ is the energy of the Stoner excitations at zero quasimomentum transfer (all three bands are shifted upward by an applied external magnetic field), $\nu_0$ is the phonon energy at the Brillouin zone boundary.

## 3. HAMILTONIAN

The Hamiltonian of the system in an external magnetic field $H$ directed along the $z$ coordinate axis has the form

$$\mathcal{H}=\mathcal{H}_e+\mathcal{H}_m+\mathcal{H}_{\rm ph}+\mathcal{H}_{m\rm ph}, \tag{1}$$

where

$$\mathcal{H}_e=-T\sum_{\boldsymbol{\lambda},\boldsymbol{\eta},\sigma} c^+_{\boldsymbol{\lambda}+\boldsymbol{\eta},\sigma}c_{\lambda,\sigma}+\frac{U}{2}\sum_{\boldsymbol{\lambda},\sigma}\hat{n}_{\boldsymbol{\lambda},\sigma}\hat{n}_{\boldsymbol{\lambda},-\sigma}$$

$$-2J\sum_{\boldsymbol{\lambda},\sigma,\sigma'}(\mathbf{S}_{\boldsymbol{\lambda}}\cdot\mathbf{s})_{\sigma,\sigma'}c^+_{\boldsymbol{\lambda},\sigma}c_{\boldsymbol{\lambda},\sigma'} \tag{2}$$

the electron Hamiltonian in the occupation number representation, determines the energies of both single-particle and collective states, in particular, the magnon spectrum;[7,9,14] the term

$$\mathcal{H}_m=-\mu_B H\sum_{\boldsymbol{\lambda}}(g_f S^z_{\boldsymbol{\lambda}}+g_d s^z_{\boldsymbol{\lambda}}) \tag{3}$$

describes the interaction of the spin subsystem with the external magnetic field $H$; the expression

$$\mathcal{H}_{\rm ph}=\sum_{\mathbf{p}} v_{\mathbf{p}}\left(\frac{1}{2}+b^+_{\mathbf{p}}b_{\mathbf{p}}\right) \tag{4}$$

gives the Hamiltonian of the acoustic phonons; and, the term

$$\mathcal{H}_{m\rm ph}=\frac{1}{\sqrt{N}}\sum_{\mathbf{q},\mathbf{p}}\xi_{\mathbf{q},\mathbf{p}}a^+_{\mathbf{q}+\mathbf{p}}a_{\mathbf{q}}(b_{\mathbf{p}}+b^+_{-\mathbf{p}}) \tag{5}$$

describes the coupling of deviations of the spins of the $d$ electrons with the displacements of the sites of the crystal lattice (i.e., the interaction between phonons and magnons in a system of quasilocal spins; see Fig. 3).

The following notation has been used in expressions (2)–(5) (see Refs. 14–16): $T>0$ is the hopping integral of electrons between nearest-neighbor sites $\boldsymbol{\lambda}$ and $\boldsymbol{\eta}$ (no confusion should arise with the notation for temperature, since the problem is actually being considered in the low-temperature limit); $U>0$ is the Hubbard interaction constant; $J>0$ is the intra-atomic $d$–$f$ exchange integral; $g_d$ ($g_f$) is the crystal-averaged value of the $g$ factor for the $d$ and $f$ electrons (see Sec. 4); $\mu_B$ is the Bohr magneton, $c^+$ and $c$ are the electron Fermi operators; $\sigma$ is the spin index (the values of this index are represented by the symbols $\uparrow(\downarrow)$ or $+(-)$; see Fig. 1); $n_{\boldsymbol{\lambda}\sigma}=c^+_{\boldsymbol{\lambda}\sigma}c_{\boldsymbol{\lambda}\sigma}$; $\mathbf{S}_{\boldsymbol{\lambda}}$ is the spin of the $f$ shell, $(2\mathbf{s})_{\sigma\sigma'}$ are Pauli matrices

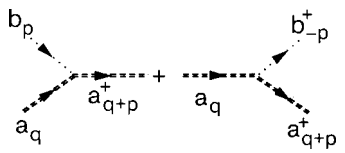


FIG. 3. Minimal magnon–phonon interaction diagram in an isotropic magnet: absorption and emission of a phonon by a magnon; $a^+$ ($a$) and $b^+$ ($b$) are the creation (annihilation) operators for magnons and phonons, respectively. The double magnon line reflects the electronic nature (see Eq. (5)) of the elementary excitation under consideration.

$$a_{\mathbf{q}}^{+}=\frac{1}{\sqrt{N}}\sum_{\mathbf{k}} c_{\mathbf{k}+\mathbf{q},\downarrow}^{+}c_{\mathbf{k},\uparrow},$$

$$a_{\mathbf{q}}=\frac{1}{\sqrt{N}}\sum_{\mathbf{k}} c_{\mathbf{k},\uparrow}^{+}c_{\mathbf{k}+\mathbf{q},\downarrow} \tag{6}$$

are the creation and annihilation operators of spin waves (optical magnons) in a system of quasilocal electrons (see below);[14] $\mathbf{k}$, $\mathbf{q}$, and $\mathbf{p}$ are the quasi-wave vectors; $b_{\mathbf{p}}^{+}$ and $b_{\mathbf{p}}$ are the Bose creation and annihilation operators for phonons; $\nu_{\mathbf{p}}$ is the phonon energy; $\xi_{\mathbf{q},\mathbf{p}}$ are the amplitudes of the weak magnon–phonon interaction; and, $N$ is the number of sites in the crystal. For the sake of definiteness we shall assume that the following conditions hold (see Ref. 16):[1)]

$$\upsilon_{\mathbf{p}}=\upsilon_{-\mathbf{p}},\ \ \xi_{\mathbf{q},\mathbf{p}}=(\xi_{\mathbf{q}+\mathbf{p},-\mathbf{p}})^{*},\ \ \xi_{\mathbf{q},0}=0,\ \ \xi_{0,\mathbf{p}}=0,$$
$$\xi_{\mathbf{q},\mathbf{p}}=\xi\Xi_{\mathbf{q},\mathbf{p}},\ \ 0\leqslant\Xi_{\mathbf{q},\mathbf{p}}\leqslant 1, \tag{7}$$

where the * denotes complex conjugation and where for convenience we have introduced the force constant $\xi$ and the dimensionless normalized amplitude $\Xi_{\mathbf{q},\mathbf{p}}$ of the spin–lattice interaction.

The electron and spin operators of the quasilocal subsystem are related by the Bogolyubov relations[17]

$$s_{\boldsymbol{\lambda}}^{+}=s_{\boldsymbol{\lambda}\uparrow}^{+}s_{\boldsymbol{\lambda}\downarrow},\ \ s_{\boldsymbol{\lambda}}^{-}=s_{\boldsymbol{\lambda}\downarrow}^{+}s_{\boldsymbol{\lambda}\uparrow},$$

$$s_{\boldsymbol{\lambda}}^{z}=\frac{1}{2}(s_{\boldsymbol{\lambda}\uparrow}^{+}s_{\boldsymbol{\lambda}\uparrow}-s_{\boldsymbol{\lambda}\downarrow}^{+}s_{\boldsymbol{\lambda}\downarrow}); \tag{8}$$

the transition to the $\mathbf{k}$ representation is given by the transformations

$$c_{\mathbf{k}\sigma}^{+}=\frac{1}{\sqrt{N}}\sum_{\boldsymbol{\lambda}} c_{\boldsymbol{\lambda},\sigma}^{+}\exp(i\mathbf{k}\cdot\boldsymbol{\lambda}),$$

$$c_{\mathbf{k},\sigma}=\frac{1}{\sqrt{N}}\sum_{\boldsymbol{\lambda}} c_{\boldsymbol{\lambda},\sigma}\exp(-i\mathbf{k}\cdot\boldsymbol{\lambda}). \tag{9}$$

Using relations (8) and (9), it is easy to see that the Fourier transforms of the circular components of the spin operators

$$s_{\mathbf{q}}^{+}=\frac{1}{\sqrt{N}}\sum_{\boldsymbol{\lambda}} s_{\boldsymbol{\lambda}}^{+}\exp(-i\mathbf{q}\cdot\boldsymbol{\lambda}),$$

$$s_{\mathbf{q}}^{-}=\frac{1}{\sqrt{N}}\sum_{\boldsymbol{\lambda}} s_{\boldsymbol{\lambda}}^{-}\exp(i\mathbf{q}\cdot\boldsymbol{\lambda}) \tag{10}$$

coincide with the operators $a_{\mathbf{q}}$ and $a_{\mathbf{q}}^{+}$ (6). Thus the latter are spin-deviation operators (in the site representation they are called Pauli oparators[14,16,18]), and in the low-temperature limit they are equivalent to the spin-wave annihilation and creation operators, a circumstance which provides a basis for the above interpretation of the relations (5) and (6).

It is assumed that the parameters of Hamiltonian (1) satisfy the inequalities

$$1/2S\ll 1,\ \ zT\ll 2JS,\ \ U/2JS\ll 1,$$
$$0<T\leqslant J,\ \ U>J,\ \ \xi\ll\nu_0,$$
$$\nu_0\ll zT/2S,\ \ \mu_B H<\nu_0, \tag{11}$$

where $z$ is the coordination number, and $n_0$ is the boundary energy of longitudinal vibrations of the lattice. In view of the relationship between the Curie temperature and the width of the magnon band,[18–21] which in this case should depend on the parameters of Hamiltonian (2), it is of interest to use its value for numerical estimates at both the intermediate and final stages of the calculations. In the model under consideration the magnetic ordering temperature depends on the electron hopping integral, the occupation of the band, and the structure of the crystal lattice.[1] In view of the existing ambiguity in the literature as to the form of this dependence (cf. Refs. 1 and 22, for example), in the present study we do a special analysis, obtain an analytical expression for the Curie temperature, and estimate its accuracy. Using the simplified expression $\theta_C\approx 0.1zTx$, where $x$ is the electron density per atom (the calculation will be given in Appendix B of Part II of this paper), the last three inequalities in (11) can be written in the form $\xi\ll\theta_D$, $\theta_D<\theta_C$, and $\mu_B H<\theta_D$, with the Debye temperature $\theta_D\approx\nu_0$ and the Curie temperature $\theta_C$ both given in energy units. Unless otherwise specified, we shall assume below that $x\approx 0.3$ (this value most closely corresponds to the ferromagnetic situation in a number of real systems[1,2,14,22]).

We note that the magnetic order and magnons in the system arise as a result of intersite hops of quasilocal electrons, the spin of which is polarized by a strong local $d-f$ exchange interaction (the main terms of the Hamiltonian (2)). This mechanism of ordering is close to that brought about by double exchange in magnetic $3d$ oxides,[1,2] which indicates the applicability of the model to an analysis of the properties of such objects. The ground state, thermodynamics, and conditions of ferromagnetic ordering for different choices of parameters of Hamiltonian (2) have been investigated by a number of authors (see, e.g., Refs. 14, 19, and 22). The initial assumptions of the present study are in agreement with the results of those studies.

Hamiltonian (5) is actually a rather complicated version of the electron–phonon interaction. In magnon variables, as follows from Fig. 3, it would correspond to the simplest scheme of taking the spin–lattice coupling into account in the investigated model of an isotropic ferromagnetic conductor. A detailed analysis of the conditions for this and other schemes for the coupling of the elementary excitations in the magnetic subsystem and crystal lattice (although they are intended mainly for magnetic insulators, in essence they also apply to metals) is contained in Ref. 20.

It should be noted that, besides the aforementioned differences of the operators $a_{\mathbf{q}}^{+}$ and $a_{\mathbf{q}}$ from magnon operators in the strict sense,[16,18] still another feature of Hamiltonian (5) is that the magnon–phonon coupling constant $\xi$ is of a different nature from the corresponding constant generated by a Heisenberg Hamiltonian with an exchange integral that depends on the interatomic distance.[16,18,20] The reason is that although Hamiltonian (2) (like the ''canonical'' double exchange[4]) also brings about ferromagnetic order and leads to the presence of magnons in the system, the intersite interaction of the magnetic moments does not reduce to Heisenberg form.[1,2]

## 4. DYNAMIC MAGNETIC SUSCEPTIBILITY

### 4.1. General scheme

Our object of study is the position and shape of the spectral bands of magnetic absorption (the imaginary part of the dynamic magnetic susceptibility) of a randomized ferromagnet under conditions of interaction with the elastic subsystem of the crystal. Following Ref. 8, we take the randomization into account only in the interaction Hamiltonian of the system with the external alternating magnetic field $\mathcal{H}_{\rm int}$ and let the $g$ factors in both magnetic subsystems be independent of the coordinates of the crystal lattice sites:

$$\mathcal{H}_{\rm int}=-\sum_{\boldsymbol{\lambda}}\mathbf{M}_{\boldsymbol{\lambda}}\cdot\tilde{\mathbf{H}}_{\boldsymbol{\lambda}}=-\frac{\tilde{H}_0}{2}\sum_{\boldsymbol{\lambda}}\{M_{\boldsymbol{\lambda}}^{+}\exp[-i(\mathbf{Q}\cdot\boldsymbol{\lambda}-\omega t)]+M_{\boldsymbol{\lambda}}^{-}\exp[i(\mathbf{Q}\cdot\boldsymbol{\lambda}-\omega t)]\}. \tag{12}$$

Here

$$\mathbf{M}_{\boldsymbol{\lambda}}=\mu_B(g_{f\boldsymbol{\lambda}}\mathbf{S}_{\boldsymbol{\lambda}}+g_{d\boldsymbol{\lambda}}\mathbf{s}_{\boldsymbol{\lambda}})$$

is the site magnetic moment of the crystal, $M_{\boldsymbol{\lambda}}^{\pm}=M_{\boldsymbol{\lambda}}^{x}\pm iM_{\boldsymbol{\lambda}}^{y}$ are its circular components,[17] and $\tilde{H}_0$ is the amplitude, $\mathbf{Q}$ the wave vector, and $\omega$ the angular frequency of the electromagnetic field.

We set $g_{j\boldsymbol{\lambda}}=g_j+\gamma_{j\boldsymbol{\lambda}}$, where $j$ is the index of the electron shell ($j=d,f$) and $\gamma_{j\boldsymbol{\lambda}}$ is a random function of the site index $\boldsymbol{\lambda}$ such that $\langle\gamma_{j\boldsymbol{\lambda}}\rangle_c=0$ (here the symbol $\langle\ldots\rangle_c$ stands for configurational averaging), and for the sake of definiteness we assume that $\gamma_{j\boldsymbol{\lambda}}/g_j<1$. Then we can write

$$\langle g_{j\boldsymbol{\lambda}}g_{j'\boldsymbol{\lambda}'}\rangle_c=g_jg_{j'}+\gamma_j^2\delta_{jj'}\delta_{\boldsymbol{\lambda}\boldsymbol{\lambda}'}, \tag{13}$$

where $\gamma_j^2=\langle\gamma_{j\boldsymbol{\lambda}}^2\rangle_c$ is the variance of the $g$ factor, and

$$\delta_{l,l'}=\begin{cases}1, & l=l'\\ 0, & l\neq l'\end{cases}$$

is the Kronecker delta ($l$ denotes the index of the electron shell ($l\in\{j\}$) or a translation vector of the crystal lattice ($l\in\{\boldsymbol{\lambda}\}$).

For a stationary inhomogeneous medium the transverse dynamic magnetic susceptibility characterizing the linear response of the system to a field $\tilde{H}_0\exp[-i(\mathbf{Q}\cdot\boldsymbol{\lambda}-\omega t)]$ has the form

$$\chi^{+-}(\mathbf{Q},\mathbf{Q}',\tilde{\varepsilon})=\frac{1}{N}\sum_{\boldsymbol{\lambda},\boldsymbol{\lambda}'}\langle\chi_{\boldsymbol{\lambda},\boldsymbol{\lambda}'}^{+-}(\tilde{\varepsilon})\rangle_c\exp[-i(\mathbf{Q}\cdot\boldsymbol{\lambda}+\mathbf{Q}'\cdot\boldsymbol{\lambda}')], \tag{14}$$

where the nonlocal susceptibility[23]

$$\chi_{\boldsymbol{\lambda},\boldsymbol{\lambda}'}^{+-}(\tilde{\varepsilon})=-\frac{1}{v_a}\langle\langle M_{\boldsymbol{\lambda}}^{+}|M_{\boldsymbol{\lambda}'}^{-}\rangle\rangle_{\tilde{\varepsilon}} \tag{15}$$

is expressed in terms of the retarded Green's function $\langle\langle\ldots\rangle\rangle_{\tilde{\varepsilon}}$ (Refs. 14–16 and 24) in the energy representation, $\tilde{\varepsilon}=\varepsilon+i\alpha$, $\alpha\to0$, $\varepsilon=\hbar\omega$, where $\hbar$ is Planck's constant and $v_a$ is the atomic volume.

As may be seen from Eqs. (12) and (15), the calculation of the susceptibility (14) involves the evaluation of four Green's functions:

$$\langle\langle S_{\boldsymbol{\lambda}}^{+}|S_{\boldsymbol{\lambda}'}^{-}\rangle\rangle_{\tilde{\varepsilon}},\ \langle\langle S_{\boldsymbol{\lambda}}^{+}|s_{\boldsymbol{\lambda}'}^{-}\rangle\rangle_{\tilde{\varepsilon}},\ \langle\langle s_{\boldsymbol{\lambda}}^{+}|S_{\boldsymbol{\lambda}'}^{-}\rangle\rangle_{\tilde{\varepsilon}}\ \text{and}\ \langle\langle s_{\boldsymbol{\lambda}}^{+}|s_{\boldsymbol{\lambda}'}^{-}\rangle\rangle_{\tilde{\varepsilon}}. \tag{16}$$

The evaluation of each of the Green's functions in (16) has much in common, and for illustration of the scheme of the calculations it is sufficient to calculate one of them. We note in this connection that in view of the presence of the interaction between the local and quasilocal spin subsystems, the system as a whole has a general energy spectrum determined by poles which are common to all of the Green's functions in (16).

### 4.2. Coherent and incoherent components

Randomization of the $g$ factors also leads to results that are common to all four contributions (16) to the total susceptibility (14), as can be illustrated for one of them as an example. We consider the "intrinsic" contribution of the quasilocal electrons to the transverse dynamic magnetic susceptibility

$$\chi_d^{+-}(\mathbf{Q},\mathbf{Q}',\tilde{\varepsilon})=-\frac{\mu_B^2}{Nv_a}\sum_{\boldsymbol{\lambda},\boldsymbol{\lambda}'}\langle g_{d\boldsymbol{\lambda}}g_{d\boldsymbol{\lambda}'}\rangle_c\langle\langle s_{\boldsymbol{\lambda}}^{+}|s_{\boldsymbol{\lambda}'}^{-}\rangle\rangle_{\tilde{\varepsilon}}\times\exp[-i(\mathbf{Q}\cdot\boldsymbol{\lambda}+\mathbf{Q}'\cdot\boldsymbol{\lambda}')], \tag{17}$$

where it has been taken into account that the configurational averaging affects only the $g$ factors of the electrons. Using relation (13) and transforming in the spin operators to the $\mathbf{k}$ representation (10), after performing the summation over $\boldsymbol{\lambda}$ and $\boldsymbol{\lambda}'$ we obtain two components of the susceptibility: a *coherent* component proportional to the square of the average electron $g$ factor $g_d^2$, and an *incoherent* component proportional to the mean square fluctuation $\gamma_d^2$ of the $g$ factor:[7,8,10]

$$\chi_d^{+-}(\mathbf{Q},\mathbf{Q}',\tilde{\varepsilon})=\chi_{d\rm coh}^{+-}(\mathbf{Q},\mathbf{Q}',\tilde{\varepsilon})+\chi_{d\rm incoh}^{+-}(\mathbf{Q},\mathbf{Q}',\tilde{\varepsilon}), \tag{18}$$

$$\chi_{d\rm coh}^{+-}(\mathbf{Q},\mathbf{Q}',\tilde{\varepsilon})=-\frac{\mu_B^2g_d^2}{v_a}\langle\langle s_{\mathbf{Q}}^{+}|s_{-\mathbf{Q}'}^{-}\rangle\rangle_{\tilde{\varepsilon}}, \tag{19}$$

$$\chi_{d\rm incoh}^{+-}(\mathbf{Q},\mathbf{Q}',\tilde{\varepsilon})=-\frac{\mu_B^2\gamma_d^2}{Nv_a}\sum_{\mathbf{q}}\langle\langle s_{\mathbf{q}+\mathbf{Q}}^{+}|s_{\mathbf{q}-\mathbf{Q}'}^{-}\rangle\rangle_{\tilde{\varepsilon}}. \tag{20}$$

As is seen from Eqs. (19) and (20), the formation of the incoherent component of the susceptibility, unlike that of the coherent component, involves the participation of all the quasimomenta of the spin excitations from the Brillouin zone. When relations (6) and (8)–(10) are taken into account, this means that, for example, in the homogeneous response to a uniform field ($\mathbf{Q}=\mathbf{Q}'=0$) the coherent component of the susceptibility (18) is formed by only "vertical" electronic transitions ($\mathbf{k}=\mathbf{k}'$), whereas the incoherent component is formed by electronic transitions with arbitrary quasimomenta ($\mathbf{k}\neq\mathbf{k}'$).

## 5. CALCULATIONS

### 5.1. Solution of the equations of motion

In the electron operator representation the Green's functions in (19) and (20) have the form

$$\langle\langle s_{\mathbf{q}}^{+}|s_{\mathbf{q}'}^{-}\rangle\rangle_{\tilde{\varepsilon}}=\frac{1}{N}\sum_{\mathbf{k},\mathbf{k}'}\langle\langle c_{\mathbf{k}\uparrow}^{+}c_{\mathbf{k}+\mathbf{q}\downarrow}|c_{\mathbf{k}'+\mathbf{q}'\downarrow}^{+}c_{\mathbf{k}',\uparrow}\rangle\rangle_{\tilde{\varepsilon}} \tag{21}$$

and the determination of the susceptibility (17) reduces to evaluation of the Green's function

$$G_d(\mathbf{k},\mathbf{q},\mathbf{k}',\mathbf{q}',\tilde{\varepsilon}) = \langle\langle c^+_{\mathbf{k}\uparrow} c_{\mathbf{k}+\mathbf{q}\downarrow} | c^+_{\mathbf{k}'+\mathbf{q}'\downarrow} c_{\mathbf{k}'\uparrow}\rangle\rangle_{\tilde{\varepsilon}}. \quad (22)$$

Considering only the case of rather low temperatures, we can write the equation of motion for the Green's function (22) in the form[16]

$$\tilde{\varepsilon}\langle\langle A|B\rangle\rangle_{\tilde{\varepsilon}} = \langle 0|[A,B]|0\rangle + \langle\langle [A,\mathcal{H}]|B\rangle\rangle_{\tilde{\varepsilon}}, \quad (23)$$

where $\mathcal{H}$ is the Hamiltonian (1), the square brackets [...,...] denote the commutator, and the averaging is done over the ferromagnetic ground state $|0\rangle$.

Equation (23) generates a chain of equations for the Green's functions of higher order. Using the inequality $1/2S \ll 1$, $U/2JS \ll 1$, and $\xi/2JS \ll 1$ (11), we break off this chain at the first step by decoupling the Green's functions of high order[15,18] (in this case, by linearization of the ternary electron operators by the Hartree–Fock scheme[14]). As a result, we obtain an equation relating the function (22) to three new Green's functions of minimal order with respect to the main operators:

$$G_{fd}(\boldsymbol{\lambda},\mathbf{k}',\mathbf{q}',\tilde{\varepsilon}) = \langle\langle S^+_{\boldsymbol{\lambda}} | c^+_{\mathbf{k}'+\mathbf{q}'\downarrow} c_{\mathbf{k}'\uparrow}\rangle\rangle_{\tilde{\varepsilon}}, \quad (24)$$

$$G_{d+}(\mathbf{k},\mathbf{q},\mathbf{k}',\mathbf{q}',\mathbf{p},\tilde{\varepsilon}) = \langle\langle c^+_{\mathbf{k}\uparrow} c_{\mathbf{k}+\mathbf{q}-\mathbf{p}\downarrow} b^+_{-\mathbf{p}} | c^+_{\mathbf{k}'+\mathbf{q}'\downarrow} c_{k'\uparrow}\rangle\rangle_{\tilde{\varepsilon}}, \quad (25)$$

$$G_{d-}(\mathbf{k},\mathbf{q},\mathbf{k}',\mathbf{q}',\mathbf{p},\tilde{\varepsilon}) = \langle\langle c^+_{\mathbf{k}\uparrow} c_{\mathbf{k}+\mathbf{q}-\mathbf{p}\downarrow} b_{\mathbf{p}} | c^+_{\mathbf{k}'+\mathbf{q}'\downarrow} c_{\mathbf{k}'\uparrow}\rangle\rangle_{\tilde{\varepsilon}}. \quad (26)$$

By composing the equations of motion (23) for the Green's functions (24)–(26) and performing their decoupling (in the present case, by averaging of the electron and phonon operators and also the operators of the $z$ projections of the local spins) at the first step with the use of the inequalities $1/2S \ll 1$, $U/2JS \ll 1$, and $\xi/2JS \ll 1$, we obtain two more Green's functions:

$$G_{fd+}(\boldsymbol{\lambda},\mathbf{k}',\mathbf{q}',\mathbf{p},\tilde{\varepsilon}) = \langle\langle S^+_{\boldsymbol{\lambda}} b^+_{-\mathbf{p}} | c^+_{\mathbf{k}'+\mathbf{q}'\downarrow} c_{\mathbf{k}'\uparrow}\rangle\rangle_{\tilde{\varepsilon}}, \quad (27)$$

$$G_{fd-}(\boldsymbol{\lambda},\mathbf{k}',\mathbf{q}',\mathbf{p},\tilde{\varepsilon}) = \langle\langle S^+_{\boldsymbol{\lambda}} b_{\mathbf{p}} | c^+_{\mathbf{k}'+\mathbf{q}'\downarrow} c_{k'\uparrow}\rangle\rangle_{\tilde{\varepsilon}}, \quad (28)$$

for which the equations of motion after the decoupling (in this case, by averaging of the electron operators and of the operators of the $z$ projection of the local spins) with the conditions $1/2S \ll 1$, $\xi/2JS \ll 1$ (11) and $\nu_{\mathbf{p}} = \nu_{-\mathbf{p}}$ (7) taken into account, no longer contain new Green's functions.

Thus we obtain a closed system of six integral equations for the Green's functions (22), (24)–(28), the solution of which can be written in the following, now integral form:

$$\sum_{\mathbf{k}} G_d(\mathbf{k},\mathbf{q},\mathbf{k}',\mathbf{q}',\tilde{\varepsilon}) = \frac{\dfrac{n_{k'\uparrow} - n_{\mathbf{k}'+\mathbf{q}\downarrow}}{\tilde{\varepsilon} - \Delta(\mathbf{k}',\mathbf{q})}\delta_{\mathbf{q},\mathbf{q}'}}{1 - \left(U - \dfrac{2J^2\langle S^z\rangle}{\tilde{\varepsilon} - 2J\langle s^z\rangle - \varepsilon_{0f}} - M(\mathbf{q},\tilde{\varepsilon})\right)\chi_0(\mathbf{q},\tilde{\varepsilon})}, \quad (29)$$

where

$$\Delta(\mathbf{k},\mathbf{q}) = 2J\langle S^z\rangle + 2U\langle s^z\rangle + \varepsilon_{0d} + E(\mathbf{k}+\mathbf{q}) - E(\mathbf{k}) \quad (30)$$

is the energy of the Stoner single-particle electronic excitations with a spin flip;[2)]

$$E(\mathbf{k}) = -T\sum_{\boldsymbol{\eta}} \exp(i\mathbf{k}\cdot\boldsymbol{\eta}) \quad (31)$$

is the one-electron energy ($E(0) = -zT$, $E(k_B) = zT$); $\langle S^z\rangle = 1/N\,\Sigma_{\boldsymbol{\lambda}}\langle 0|S^z_{\boldsymbol{\lambda}}|0\rangle$ and $\langle s^z\rangle = 1/2N\,\Sigma_{\mathbf{k}}(n_{\mathbf{k}\uparrow} - n_{\mathbf{k}\downarrow})$ are the average values of the local and quasilocal spins (since the averaging is done over the ground state, here we have merely reserved the possibility of considering an average number of spin carriers that is less than one per crystal lattice site, both for quasilocal and for local spins); $\varepsilon_{0d(f)} = \mu_B g_{d(f)} H$ is the Zeeman energy, the quantity

$$M(\mathbf{q},\tilde{\varepsilon}) = -\frac{1}{N}\sum_{\mathbf{p}} |\xi_{\mathbf{q},\mathbf{p}}|^2 \left\{ \frac{(1+n'_{\mathbf{p}})\chi_{-v}(\mathbf{q},\mathbf{p},\tilde{\varepsilon})}{1 - \zeta_-(\mathbf{p},\tilde{\varepsilon})\chi_{-v}(\mathbf{q},\mathbf{p},\tilde{\varepsilon})} + \frac{n'_{\mathbf{p}}\chi_{+v}(\mathbf{q},\mathbf{p},\tilde{\varepsilon})}{1 - \zeta_+(\mathbf{p},\tilde{\varepsilon})\chi_{+v}(\mathbf{q},\mathbf{p},\tilde{\varepsilon})} \right\} \quad (32)$$

is the magnon mass operator[16] (to within a factor that depends only weakly on $\mathbf{q}$ and $\varepsilon$ in the regions of the magnon branches; see Sec. 5.4);

$$\zeta_\pm(\mathbf{p},\tilde{\varepsilon}) = U - \frac{2J^2\langle S^z\rangle}{\tilde{\varepsilon} - 2J\langle s^z\rangle - \varepsilon_{0f} \pm v_{\mathbf{p}}} \quad (33)$$

is an energy-dependent effective "coupling constant;"[25] $n_{\mathbf{k}}$ is the electron distribution function; $n'_{\mathbf{p}}$ is the phonon distribution function; the quantity

$$\chi_{\pm\nu}(\mathbf{q},\mathbf{p},\tilde{\varepsilon}) = -\frac{1}{N}\sum_{\mathbf{k}} \frac{n_{\mathbf{k}\uparrow} - n_{\mathbf{k}+\mathbf{q}+\mathbf{p}\downarrow}}{\tilde{\varepsilon} - \Delta(\mathbf{k},\mathbf{q}+\mathbf{p}) \pm \nu_{\mathbf{p}}} \quad (34)$$

in the limit $\mathbf{p} = 0$ is known as the "polarization operator" of the conduction electrons in the random phase approximation and is the susceptibility of Hartree–Fock electrons:[14,24,26]

$$\chi_0(\mathbf{q},\tilde{\varepsilon}) \equiv \chi_{\pm\nu}(\mathbf{q},0,\tilde{\varepsilon}) = -\frac{1}{N}\sum_{\mathbf{k}} \frac{n_{\mathbf{k}\uparrow} - n_{\mathbf{k}+\mathbf{q}\downarrow}}{\tilde{\varepsilon} - \Delta(\mathbf{k},\mathbf{q})}. \quad (35)$$

The expressions obtained, Eqs. (21) and (26)–(35), completely determine the susceptibility that we seek (18). Using relations (18)–(22) and (29), we can write an expression for the coherent and incoherent components of the susceptibility of quasilocal electrons (18) in the form

$$\chi^{+-}_{d\mathrm{coh}}(\mathbf{Q},\mathbf{Q}',\tilde{\varepsilon}) = \chi^{+-}_{d\mathrm{coh}}(\mathbf{Q},\tilde{\varepsilon})\,\delta_{\mathbf{Q},-\mathbf{Q}'}, \quad (36)$$

$$\chi^{+-}_{d\mathrm{incoh}}(\mathbf{Q},\mathbf{Q}',\tilde{\varepsilon}) = \chi^{+-}_{d\mathrm{incoh}}(\tilde{\varepsilon})\,\delta_{\mathbf{Q},-\mathbf{Q}'}, \quad (37)$$

where

$$\chi^{+-}_{d\mathrm{coh}}(\mathbf{Q},\tilde{\varepsilon}) = \frac{\mu_B^2 g_d^2}{v_a} \frac{\chi_0(\mathbf{Q},\tilde{\varepsilon})}{1 - \left(U - \dfrac{2J^2\langle S^z\rangle}{\tilde{\varepsilon} - 2J\langle s^z\rangle - \varepsilon_{0f}} - M(\mathbf{Q},\tilde{\varepsilon})\right)\chi_0(\mathbf{Q},\tilde{\varepsilon})}, \quad (38)$$

$$\chi^{+-}_{d\text{incoh}}(\tilde{\varepsilon}) = \frac{\mu_B^2 \gamma_d^2}{N v_a} \sum_{\mathbf{q}} \times \frac{\chi_0(\mathbf{q},\tilde{\varepsilon})}{1-\left(U - \dfrac{2J^2\langle S^z\rangle}{\tilde{\varepsilon}-2J\langle s^z\rangle - \varepsilon_{0f}} - M(\mathbf{q},\tilde{\varepsilon})\right)\chi_0(\mathbf{q},\tilde{\varepsilon})}. \quad (39)$$

For a uniform external field ($Q=0$), i.e., for the case when the wavelength of the electromagnetic wave is much greater than the crystal lattice constant, the quantities of interest will then be functions of energy, $\chi^{+-}_{d\text{coh}}(0,\tilde{\varepsilon})$ and $\chi^{+-}_{d\text{incoh}}(\tilde{\varepsilon})$.

### 5.2. Spectrum of elementary excitations

The poles of the coherent component of the magnetic susceptibility (38) [or of the Green's function (29)] give the energy spectrum and damping of spin excitations of the system.[14,18,21] The Stoner continuum,[14,23–26] which is the spectrum of single-particle electron spin excitations [lying in a region of nonzero values of the imaginary part of $\chi_0(\mathbf{Q},\tilde{\varepsilon})$], is of only formal interest in the case of a randomized system such as we are considering here—the weak magnon–phonon interaction does not lead to any qualitatively new effects. This part of the spectrum will be studied in Part II of this paper. Here we consider the two additional (i.e., "split off" from the Stoner continuum) poles of the Green's function (29), which represent the energies of acoustic and optical magnon branches.[9,14] For $\mathbf{q}=0$ and $\xi=0$ the values of the energy for which in the denominator in (29) vanishes are the roots of the quadratic equation

$$\varepsilon^2 - \varepsilon(2J\langle S^z+s^z\rangle + \varepsilon_{0f}+\varepsilon_{0d}) + 2J\langle S^z\varepsilon_{0f} + s^z\varepsilon_{0d}\rangle + \varepsilon_{0f}\varepsilon_{0d} = 0. \quad (40)$$

In the approximation linear in $H$ the expressions for these roots have the form

$$\varepsilon_{\text{ac}0} = \mu_B H \frac{\langle g_f S^z + g_d s^z\rangle}{\langle S^z + s^z\rangle}, \quad (41)$$

$$\varepsilon_{\text{op}0} = 2J\langle S^z+s^z\rangle + \mu_B H \frac{\langle g_d S^z + g_f s^z\rangle}{\langle S^z+s^z\rangle}. \quad (42)$$

A power series expansion of the denominator in (29) about $\varepsilon_{\text{ac}0}$ and $\varepsilon_{\text{op}0}$ at $\xi=0$ shows that $\varepsilon(\mathbf{q})\propto\mathbf{q}^2$ for $\mathbf{q}\to 0$. In the case when the inequality $|\varepsilon-\Delta|\gg T$, where

$$\Delta\equiv\Delta(\mathbf{k},0) = 2J\langle S^z\rangle + 2U\langle s^z\rangle + \varepsilon_{0d}, \quad (43)$$

holds in the region of the magnon branches $\varepsilon\approx\varepsilon_{\text{ac(op)}}(\mathbf{q})$, the analysis of the situation simplifies substantially (as will be seen below, this is possible for $zT/\langle s^z\rangle(U-J)\ll 1$). Taking $(\varepsilon-\Delta)$ out from under the summation sign in the denominator of (29), linearizing the expression remaining in the sum with respect to $T/(\varepsilon-\Delta)$, and solving the cubic equation obtained in the case $\xi=0$ for the poles of the Green's function (29) with the use of relations (40)–(42), one can obtain, to leading order in $zT/J\langle S^z\rangle$, rather simple expressions for the dispersion laws $\varepsilon_{\text{ac}0}(\mathbf{q})$ and $\varepsilon_{\text{op}0}(\mathbf{q})$ of acoustic and optical magnons in the whole Brillouin zone (for the acoustic magnons this procedure remains valid under the weaker condition $zT/2J\langle S^z\rangle\ll 1$). In the one-dimensional case (a lattice with period $a$) the corresponding expressions are particularly transparent:

$$\varepsilon_{\text{ac}0}(q) = \varepsilon_{\text{ac}0} + T\frac{\sin(k_F a)}{\pi\langle S^z+s^z\rangle}[1-\cos(qa)], \quad (44)$$

$$\varepsilon_{\text{op}0}(q) = \varepsilon_{\text{op}0} + T\frac{\langle S^z\rangle}{\langle s^z\rangle}\frac{\sin(k_F a)}{\pi\langle S^z+s^z\rangle}[1-\cos(qa)]. \quad (45)$$

The energy gaps $\varepsilon_{\text{ac}0}$ and $\varepsilon_{\text{op}0}$ in the magnon spectra (44) and (45) are determined by expressions (41) and (42).

The third root of the cubic equation mentioned above corresponds to a fictitious mode that arises as a result of the technique used to find the poles of the function (29). This mode lies inside the Stoner continuum and should not be considered in view of the applicability condition of this technique [$\varepsilon\approx\varepsilon_{\text{ac(op)}}(\mathbf{q})$].

### 5.3. Mass operator

In an analogous way one can obtain expressions for the poles of the function (32). Taking (33) and (34) into account, we obtain

$$\varepsilon_{\text{ac}\pm}(\mathbf{q},\mathbf{p}) = \varepsilon_{\text{ac}0}(\mathbf{q}+\mathbf{p}) \pm \nu_{\mathbf{p}},$$
$$\varepsilon_{\text{op}\pm}(\mathbf{q},\mathbf{p}) = \varepsilon_{\text{op}0}(\mathbf{q}+\mathbf{p}) \pm \nu_{\mathbf{p}} \quad (46)$$

and below the Stoner continuum, to leading order in $1/2S$, Eq. (32) becomes

$$M(\mathbf{q},\tilde{\varepsilon}) = \frac{2\langle s^z\rangle}{N}\sum_{\mathbf{p}} |\xi_{\mathbf{q},\mathbf{p}}|^2[(1+n'_{\mathbf{p}})F_+(\mathbf{q},\mathbf{p},\tilde{\varepsilon}) + n'_{\mathbf{p}}F_-(\mathbf{q},\mathbf{p},\tilde{\varepsilon})],$$
$$F_\pm(\mathbf{q},\mathbf{p},\tilde{\varepsilon}) = \frac{(\tilde{\varepsilon}-2J\langle s^z\rangle - \varepsilon_{0f} \mp \nu_p)}{[\tilde{\varepsilon}-\varepsilon_{ac\pm}(\mathbf{q},\mathbf{p})][\tilde{\varepsilon}-\varepsilon_{\text{op}\pm}(\mathbf{q},\mathbf{p})]}. \quad (47)$$

Expanding (47) in partial fractions and using the identity $(x+i\alpha)^{-1} = \mathcal{P}(x^{-1}) - i\pi\delta(x)$, where the symbols $\mathcal{P}$ and $\delta$ stand for the principal value and the Dirac delta function, the real and imaginary components of the function $M(\mathbf{q},\tilde{\varepsilon}) = M'(\mathbf{q},\varepsilon) + iM''(\mathbf{q},\varepsilon)$ below the Stoner continuum can be written in the form

$$M'(\mathbf{q},\varepsilon) = \frac{2\langle s^z\rangle\xi^2}{N}\mathcal{P}\sum_{\mathbf{p}} |\Xi_{\mathbf{q},\mathbf{p}}|^2\{(1+n'_{\mathbf{p}})[F_{\text{op}+}(\mathbf{q},\mathbf{p},\varepsilon) - F_{\text{ac}+}(\mathbf{q},\mathbf{p},\varepsilon)] + n'_{\mathbf{p}}[F_{\text{op}-}(\mathbf{q},\mathbf{p},\varepsilon) - F_{ac-}(\mathbf{q},\mathbf{p},\varepsilon)]\},$$

$$F_{\text{ac(op)}\pm}(\mathbf{q},\mathbf{p},\varepsilon) = \frac{\varepsilon - 2J\langle s^z\rangle \mp \nu_{\mathbf{p}} - \varepsilon_{0f}}{[\varepsilon_{\text{op}0}(\mathbf{q}+\mathbf{p}) - \varepsilon_{\text{ac}0}(\mathbf{q}+\mathbf{p})][\varepsilon - \varepsilon_{\text{ac(op)}\pm}(\mathbf{q},\mathbf{p})]}, \quad (48)$$

$$M''(\mathbf{q},\varepsilon) = \frac{2\pi\langle s^z\rangle\xi^2}{N}\mathcal{P}\sum_{\mathbf{p}} |\Xi_{\mathbf{q},\mathbf{p}}|^2\{(1+n'_{\mathbf{p}})[\Phi_{\text{op}+}(\mathbf{q},\mathbf{p},\varepsilon) - \Phi_{\text{ac}+}(\mathbf{q},\mathbf{p},\varepsilon)] + n'_{\mathbf{p}}[\Phi_{\text{op}-}(\mathbf{q},\mathbf{p},\varepsilon) - \Phi_{ac-}(\mathbf{q},\mathbf{p},\varepsilon)]\},$$

$$\Phi_{\mathrm{ac(op)}\pm}(\mathbf{q},\mathbf{p},\varepsilon) = \frac{\varepsilon - 2J\langle s^z\rangle \mp \nu_{\mathbf{p}} - \varepsilon_{0f}}{\varepsilon_{\mathrm{op0}}(\mathbf{q}+\mathbf{p}) - \varepsilon_{\mathrm{ac0}}(\mathbf{q}+\mathbf{p})}\,\delta[\varepsilon - \varepsilon_{\mathrm{ac(op)}\pm}(\mathbf{q},\mathbf{p})]. \quad (49)$$

### 5.4. Resonance energies

In the energy regions below the poles of the mass operator, where the latter is a differentiable function of $\xi$ and $\varepsilon$, the contribution from the mass operator (32) to the roots of the equation $D(\varepsilon)=0$ for the poles of the function (29) [$D$ is the denominator in (29)] can be found to leading order in $\xi$ from the equation

$$\frac{\partial D(\mathbf{q},\varepsilon)}{\partial\varepsilon}[\varepsilon_{\mathrm{ac(op)}\xi}(\mathbf{q}) - \varepsilon_{\mathrm{ac(op)}0}(\mathbf{q})] - M(\mathbf{q},\varepsilon)\chi_0(\mathbf{q},\varepsilon) = 0. \quad (50)$$

The derivative of $D$ should be taken at $\xi=0$ and at the "unperturbed" values of the poles $\varepsilon=\varepsilon_{\mathrm{ac(op)}0}(\mathbf{q})$, which are also to be used in the same approximation for the argument of the functions in the product $M(\mathbf{q},\varepsilon)\chi_0(\mathbf{q},\varepsilon)$. Calculation of the derivative in (50) gives to leading order in $1/2S$

$$\varepsilon_{\mathrm{ac}\xi}(\mathbf{q}) = \varepsilon_{\mathrm{ac0}}(\mathbf{q}) + \frac{2\langle s^z\rangle^2}{\langle S^z + s^z\rangle} M(\mathbf{q},\varepsilon_{\mathrm{ac}\xi}(\mathbf{q})), \quad (51)$$

$$\varepsilon_{\mathrm{op}\xi}(\mathbf{q}) = \varepsilon_{\mathrm{op0}}(\mathbf{q}) + \frac{2\langle S^z\rangle\langle s^z\rangle}{\langle S^z + s^z\rangle} M(\mathbf{q},\varepsilon_{\mathrm{op}\xi}(\mathbf{q})). \quad (52)$$

It follows from (51) and (52) that the correction to the magnon energy due to the magnon–phonon interaction (i.e., the "mass operator"[3]) of the magnons) agrees with the function (32) up to a numerical factor that is individual for each magnon branch.

Expressions (51) and (52) are equations and thus still do not contain the magnon energies in explicit form. However, they do permit one to obtain an uncomplicated estimate for the energies in the region of small quasimomenta.

Let us estimate the value of the mass operator in (51) and (52) in the region of small values of the magnon quasimomenta, after representing the sum in expression (47) for $q \ll q_B$ in the form of a product of the value of the function in the summand at some point $\kappa$ of the region of summation times the number of terms of the sum. Then we obtain four important new parameters: $|\Xi_\kappa(\mathbf{q})|^2 \approx 0.25 q^2 a^2$, $\Delta\varepsilon_{\mathrm{ac}\kappa}$, $\Delta\varepsilon_{\mathrm{op}\kappa}$, and $\nu_\kappa$, which characterize the dimensionless normalized amplitude of the spin–lattice interaction (see Ref. 20) and the width of the magnon (acoustic and optical) and phonon bands, respectively. Being interested only in orders of magnitude, we replace the second of these parameters by the Curie temperature $\theta_C$, the fourth by the Debye temperature $\theta_D$, and we denote the third by $\theta'_C$. Considering the measure of the differences in the dispersion laws (44) and (45), we can assume that $\theta'_C$ is approximately $\langle S^z\rangle/\langle s^z\rangle$ times larger than $\theta_C$, but both these quantities are small compared to $J$. Substituting expression (47), thus simplified, into (51) and (52), we obtain quadratic equations for $\varepsilon_{\mathrm{ac(op)}\xi}(\mathbf{q})$; one of the roots of each of these equations lies in the region of the poles of the mass operator and must be rejected under the conditions of the approximation adopted here. The remaining roots of equations (51) and (52) give to leading order in $1/2s$, $T$ (i.e., $\theta_C$ and $\theta'_C$), $\theta_D$, $q$, $\xi$, and $H$:

$$\varepsilon_{\mathrm{ac}\xi}(\mathbf{q}) = \varepsilon_{\mathrm{ac0}}(\mathbf{q}) - \frac{\langle s^z\rangle^4}{\langle S^z + s^z\rangle^2}\,\frac{\xi^2}{\theta_C + \theta_D} q^2 a^2, \quad (53)$$

$$\varepsilon_{\mathrm{op}\xi}(\mathbf{q}) = \varepsilon_{\mathrm{op0}}(\mathbf{q}) - \frac{\langle S^z\rangle^2\langle s^z\rangle^2}{\langle S^z + s^z\rangle^2}\,\frac{\xi^2}{\theta'_C + \theta_D} q^2 a^2. \quad (54)$$

The "unperturbed" energies of the inhomogeneous ferromagnetic and exchange resonances $\varepsilon_{\mathrm{ac0}}(\mathbf{q})$ and $\varepsilon_{\mathrm{op0}}(\mathbf{q})$ in (53) and (54) in the one-dimensional case are determined by expressions (44) and (45). The effective masses of the acoustic and optical magnons, as follows from (44) and (45), are given by

$$m^*_{\mathrm{ac}} = \frac{\pi\langle S^z + s^z\rangle}{\sin(k_F a)}\,\frac{\hbar^2}{Ta^2}, \quad (55)$$

$$m^*_{\mathrm{op}} = \frac{\pi\langle s^z\rangle\langle S^z + s^z\rangle}{\langle S^z\rangle\sin(k_F a)}\,\frac{\hbar^2}{Ta^2}. \quad (56)$$

Thus expressions (53) and (54) determine the corresponding corrections to the effective masses (55) and (56):

$$\Delta m^*_{\mathrm{ac}} = \left[\frac{\pi\hbar\langle s^z\rangle^2\xi}{aT\sin(k_F a)}\right]^2 \frac{2}{\theta_C + \theta_D}, \quad (57)$$

$$\Delta m^*_{\mathrm{op}} = \left[\frac{\pi\hbar\langle s^z\rangle^2\xi}{aT\sin(k_F a)}\right]^2 \frac{2}{\theta'_C + \theta_D}. \quad (58)$$

## 6. MAIN EFFECTS IN THE MAGNON SPECTRUM

It follows from (18)–(20) that the spectrum of the susceptibility $\chi^{+-}(\varepsilon)$ decomposes into two components with different properties: a *coherent* component $\chi^{+-}_{\mathrm{coh}}$ and an *incoherent* component $\chi^{+-}_{\mathrm{incoh}}$. The first is formed by excitations of the spin subsystem with a quasi-wave vector that is coincident with the wave vector $\mathbf{Q}$ of the electromagnetic wave, while the second is formed by spin excitations with arbitrary wave vectors. The quantity $\chi^{+-}_{\mathrm{coh}}$ is determined by the average value of the $g$ factors of the magnetic moments of the $d$ and $f$ subsystems over the crystal, $g_{d(f)}$, while $\chi^{+-}_{\mathrm{incoh}}$ is determined by the fluctuations of these $g$ factors, $\gamma_{d(f)}$.

It follows from expressions (38), (39), (44), and (45) that the poles of $\chi^{+-}_{\mathrm{coh}}(\mathbf{q},\varepsilon)$ give a magnon spectrum $\varepsilon(\mathbf{q})$ consisting of an *acoustic* and an *optical* branch, while the residues of $\chi^{+-}_{\mathrm{incoh}}(\mathbf{q},\varepsilon)$ determine the total contribution to the susceptibility from all magnons with energy $\varepsilon$, i.e., they characterize the density of magnon states $N(\varepsilon)$ (see also Part II of this paper).

The interaction of the $d$ and $f$ electrons leads to an effective renormalization of the $g$ factors of both magnetic subsystems (41) and (42).

The main effects of a weak spin–lattice coupling in the magnon spectrum are determined by expressions (48), (49), and (51)–(54). The form of (51) and (52), as can be seen from a more detailed investigation of the poles of the function (29) in the approximation $|\varepsilon - \Delta| \gg T$ [$\Delta$ is given by expression (43)] by a method analogous to that used in Sec. 5.2, is also preserved in a region of the spectrum containing poles of the mass operator (46)–(49). Here the real part of (48) determines the renormalization of the magnon spectrum, while the imaginary part (49) determines the damping of the magnons. Both effects depend on temperature. The damping

of magnons at zero temperature is due to the spontaneous emission of phonons, and at finite temperature by their absorption as well. The effect at zero temperature, as follows from (49), (53), and (54), has a threshold character: only those magnons with a quasimomentum exceeding the value

$$q_{0\mathrm{ac}}=\frac{1}{a}\arcsin\frac{\pi\langle S^z+s^z\rangle\theta_D}{2T\sin(k_Fa)} \tag{59}$$

for the acoustic branch and the value

$$q_{0\mathrm{op}}=\frac{1}{a}\arcsin\frac{\pi\langle s^z\rangle\langle S^z+s^z\rangle\theta_D}{2T\langle S^z\rangle\sin(k_Fa)} \tag{60}$$

for the optical branch are damped [for simplicity we have given the expressions obtained for the one-dimensional case (44) and (45)].

It should be noted that the existence of threshold quasimomenta (59) and (60) has a direct relation to the Cherenkov effect:[27] the group velocity of magnons with a quasimomentum exceeding these values turns out to be greater than the speed of sound in the medium, and for this reason they spontaneously emit phonons. If the magnon velocity does not exceed the speed of sound, i.e., if the argument of the arcsine in (59) and (60) is greater than unity [in the three-dimensional case with allowance for the estimate of the Curie temperature (B.14) obtained in Appendix B of Part II of this paper, this should correspond to the inequality $\theta_D>\theta_C$], the interaction (5) at zero temperature does not lead to damping of the magnons.

The emission of phonons by magnons at zero temperature is made possible by the extraction of energy from the source of the external electromagnetic field by the magnetic subsystem. In the region of the poles of the mass operator the main effect of the spin–lattice coupling is damping of the magnons, which should be reflected mainly in the spectra of the magnetic susceptibility. The renormalization of the magnon energies in this spectral region has a less significant effect on the shape of the $\chi^{+-}(\mathbf{Q},\varepsilon)$ curve.

Thus the interaction (5) at zero temperature does not qualitatively alter the character of the spectrum of the magnetic susceptibility for $q<q_{0\mathrm{ac(op)}}$. It only changes the shape of the magnon bands [see (57) and (58)], resulting in a lowering of the frequencies of the inhomogeneous resonances. At a finite temperature all of the magnons will be damped as a result of the absorption of thermal phonons.

The authors thank V. V. Eremenko and N. F. Kharchenko for interest and support of this study and A. A. Loginov for helpful discussions and valuable comments.

*E-mail: beznosov@ilt.kharkov.ua

1) The form (5) used here allows one to rather quickly to pass to observable effects of the spin–lattice interaction in the system described by Hamiltonian (2). The function describing the interaction of the phonons with real collective spin excitations in such a system must differ from the amplitude $\xi_{\mathbf{q},\mathbf{p}}$ in (5) and is determined by the parameters of the magnetic subsystems of the quasilocal and local spins [see Eqs. (51)–(54)]. In this case it is sufficient to introduce an amplitude $\xi_{\mathbf{q},\mathbf{p}}$ in (5) formally, with an indication of the most general properties of such a function[16] without reference to the specifics of the magnetic system under study. More-detailed information about $\xi_{\mathbf{q},\mathbf{p}}$ is needed for a quantitative estimate of spin–lattice coupling effects [obtained in Part II of this paper, which will be published in the next issue of this journal, J. Low Temp. Phys. **30**, No. 10 (2004)].

2) There are two variant terminologies encountered in the literature: some authors call the Stoner excitations single-particle,[23,24] while others call them electron–hole pairs or individual Stoner excitations.[14] We shall stick with the first of these variants.

3) We use the terminology adopted in Ref. 16.

[1] V. M. Loktev and Yu. G. Pogorelov, Fiz. Nizk. Temp. **26**, 231 (2000) [Low Temp. Phys. **26**, 171 (2000)].
[2] E. Dagotto, T. Hotta, and A. Moreo, Phys. Rep. **344**, 1 (2001).
[3] J. M. De Teresa, M. R. Ibarra, P. A. Algarabel, C. Ritter, C. Marquina, J. Blasco, J. Garcia, A. del Moral, and Z. Arnold, Nature (London) **386**, 256 (1997).
[4] C. Zener, Phys. Rev. **82**, 440 (1951).
[5] A. B. Beznosov, B. I. Belevtsev, E. L. Fertman, V. A. Desnenko, D. G. Naugle, K. D. D. Rathnayaka, and A. Parasiris, Fiz. Nizk. Temp. **28**, 774 (2002) [Low Temp. Phys. **28**, 556 (2002)].
[6] A. B. Beznosov, V. A. Desnenko, E. L. Fertman, C. Ritter, and D. D. Khalyavin, Phys. Rev. B **68**, 054109 (2003).
[7] E. S. Orel and A. B. Beznosov, Ukr. Fiz. Zh. (Russ. Ed.) **40**, 579 (1995).
[8] A. B. Beznosov and E. S. Orel, Fiz. Nizk. Temp. **27**, 508 (2001) [Low Temp. Phys. **27**, 372 (2001)].
[9] E. S. Orel and A. B. Beznosov, in *Magnetic and Superconducting Materials*, Vol. B, M. Akhavan, J. Jensen, and K. Kitazawa, (eds.) Singapore, World Scientific (2000), p. 881.
[10] A. B. Beznosov, V. P. Gnezdilov, and V. V. Eremenko, JETP Lett. **38**, 587 (1983).
[11] B. N. Harmon and A. J. Freeman, Phys. Rev. B **10**, 1979 (1974) p. 881.
[12] T. A. Matveeva and D. F. Egorov, Fiz. Met. Metalloved. **51**, 717 (1981).
[13] B. N. Harmon, J. Physique **40**, Colloq. No 5, 65 (1979).
[14] E. V. Kuz'min, G. A. Petrakovskiĭ, and É. A. Zavadskiĭ, *Physics of Magnetically Ordered Substances* [in Russian], Nauka, Novosibirsk (1976).
[15] D. N. Zubarev, Usp. Fiz. Nauk **71**, 71 (1960).
[16] A. S. Davydov, *Solid State Theory* [in Russian], Nauka, Moscow (1976).
[17] S. V. Vonsovskiĭ, *Magnetism*, Vols. 1 and 2, Wiley, New York (1974), Nauka, Moscow (1971).
[18] S. V. Tyablikov, *Methods in the Quantum Theory of Magnetism* [in Russian], 2nd ed., Nauka, Moscow (1975) [transl. of 1st Russ. ed., Plenum Press, New York (1967)].
[19] É. L. Nagaev, *Physics of Magnetic Semiconductors*, Mir, Moscow (1983), Nauka, Moscow (1979).
[20] A. I. Akhiezer, V. G. Bar'yakhtar, and S. V. Peletminskiĭ, *Spin Waves*, North-Holland, Amsterdam (1968), Nauka, Moscow (1967).
[21] V. G. Bar'yakhtar, V. N. Krivoruchko, and D. A. Yablonskiĭ, *Green's Functions in the Theory of Magnetism* [in Russian], Naukova Dumka, Kiev (1984).
[22] M. Sh. Erukhimov and I. S. Sandalov, Fiz. Tverd. Tela (Leningrad) **19**, 2377 (1977) [Sov. Phys. Solid State **19**, 1391 (1977)].
[23] R. M. White, *Quantum Theory of Magnetism*, 2nd ed., Springer-Verlag, Berlin (1983), Mir, Moscow (1985).
[24] K. Elk, W. Gasser, *Die Methode der Greenschen Funktionen in der Festkorperphysik*, Akademie-Verlag, Berlin (1979).
[25] S. Doniach and E. P. Wohlfarth, Proc. R. Soc. London, Ser. A **296**, 442 (1967).
[26] A. A. Berdyshev, *Introduction to the Quantum Theory of Ferromagnetism* [in Russian], UGU, Sverdlovsk (1971).
[27] L. D. Landau and E. M. Lifshitz, *Electrodynamics of Continuous Media*, Pergamon Press, Oxford (1960), Gos. Izd-vo Fiz. Mat. Lit., Moscow (1959).

Translated by Steve Torstveit

## LOW-DIMENSIONAL AND DISORDERED SYSTEMS

# To the theory of spin–charge separation in one-dimensional correlated electron systems

A. A. Zvyagin*

*Max-Planck-Institut für Physik komplexer Systeme, Nöthnitzer Str., 38 D-01187, Dresden, Germany; B. Verkin Institute for Low Temperature Physics and Engineering of the National Academy of Sciences of Ukraine, 47 Lenin Ave., Kharkov 61103, Ukraine*

(Submitted February 2, 2004; revised March 16, 2004)
Fiz. Nizk. Temp. **30**, 969–973 (September 2004)

Spin–charge separation is considered to be one of the key properties that distinguish low-dimensional electron systems from others. Three-dimensional correlated electron systems are described by the Fermi liquid theory. There, low-energy excitations (quasiparticles) are reminiscent of noninteracting electrons: They carry charges $-e$ and spins 1/2. It is believed that for any one-dimensional correlated electron system, low-lying electron excitations carry either only spin and no charge, or only charge without spin. That is why recent experiments looked for such low-lying collective electron excitations, one of which carries only spin, and the other carries only charge. Here we show that despite the fact that for *exactly solvable* one-dimensional correlated electron models there exist excitations which carry only spin and only charge, in all these models with short-range interactions the low-energy physics is described by low-lying collective excitations, one of which carries *both spin and charge*. © *2004 American Institute of Physics.* [DOI: 10.1063/1.1802958]

The spin–charge separation phenomenon arising from interactions between electrons in low-dimensional condensed matter models has attracted considerable interest since the discovery of high-$T_c$ superconductivity in low-dimensional cuprates.[1,2] Other possible experimental realizations of spin–charge separation appear to exist in organic conductors[3,4] and in mesoscopic and nanoscale metallic systems,[5] e.g., quantum wires and carbon nanotubes. Physicists believe that the fundamental differences between low and higher dimensions can be traced back to the reduced phase space in the former, which results in the breakdown of the Fermi liquid description. Localization of the electrons in the presence of even a small amount of disorder, thermal fluctuations destroying long-range order at any nonzero temperature (if only short-range interactions are present), and quantum fluctuations tending to suppress a broken continuous symmetry are among the other features of low-dimensional correlated electron systems. For ''standard'' three-dimensional electron systems an interaction between electrons is described in the framework of Landau's Fermi liquid theory.[6]

A Fermi liquid consists of the Fermi sphere and a rarefied gas of weakly interacting ''quasiparticles'' defined via poles in the one-particle Green's functions.

Quasiparticles evolve continuously from free electrons when the interaction is adiabatically switched on and, hence, have the same quantum numbers and statistics as noninteracting electrons. In one space dimension the Fermi liquid quasiparticle pole disappears (its residue vanishes) and is replaced by incoherent structures, which follow from the global conformal invariance.[7,8] These structures involve nonuniversal power-law singularities. Although the Fermi surface is still properly defined, the discontinuity of the momentum distribution at the Fermi surface disappears as a consequence of the zero residue.[8,9] Systems displaying such breakdown of the Fermi liquid picture and exotic low-energy spectral properties are known as Luttinger liquids.[7,8] The theoretical understanding of two-dimensional electron systems is far from being complete. They frequently manifest the absence of ordering, and, hence, mean-field-like approximations fail. Many of the normal state properties of two-dimensional high-$T_c$ superconductors are very different from normal metals and cannot be reconciled with a standard Fermi liquid theory. A marginal Fermi or Luttinger liquid picture, similar to that for one-dimensional conductors, which uses a spin–charge separation, has been proposed to explain some of these features.[10]

An approximate description of one-dimensional correlated electron models in the framework of the bosonization approach[8] supports the Luttinger liquid picture. The latter is characterized, among other features, by a spin–charge separation: The charge and spin contents of wave functions move with different speeds and are related to different low-lying excitations of correlated electron systems. It is believed that for any one-dimensional correlated electron system the low-lying electron excitations carry either only spin and no charge, or only charge without spin.[8,9] However, the range of applicability of the Luttinger liquid bosonization theory is limited to the continuous models and weak enough interactions: The latter have to be smaller than the Fermi velocity (related to the bandwidth of electrons) by the consideration of only low-energy electrons close to Fermi points, for which one can linearize their dispersion law.[7,9] In recent experi-

 

ments that implied the observation of spin–charge separation these conditions were often not satisfied.[1–4] Nonetheless, for many one-dimensional correlated electron models with strong interaction between electrons the powerful Bethe ansatz method can be applied, in the framework of which collective electron excitations also have different velocities.[11] It is often stated that a spin–charge separation persists in that description also (see, e.g., Refs. 1, 8, and 9), justifying in that way the applicability of the Luttinger liquid picture to any one-dimensional correlated electron systems with metallic behavior. In our work we prove exactly that that conclusion is incorrect: We show that in none of the known Bethe ansatz solvable models do the correlated-electron Dirac seas, and, hence, low-energy excitations pertain to only spin-carrying and only charge-carrying quasiparticles: For those models one Dirac sea is necessarily formed by quasiparticles that carry *both spin and charge*. Unfortunately, this relatively simple statement has never been clearly stated in published papers devoted to the Bethe ansatz solvable correlated electron models, and this has led to many misunderstandings.

The exact solution by means of Bethe's ansatz of numerous models of one-dimensional correlated electron systems provides deep insight into the ground state of systems, complete classification of states, thermodynamic properties, etc. The best-known examples of strongly correlated electron models solved by the Bethe ansatz are the one-dimensional Hubbard model and supersymmetric $t-J$ model.[11] With this method the Hamiltonian is diagonalized in terms of a set of parameters (quantum numbers) known as rapidities. A system with internal degrees of freedom (such as spin) requires a sequence of nested generalized Bethe ansätze for wave functions. Each internal degree of freedom gives rise to one set of rapidities, i.e., in the case of electrons, which carry spin, one has two sets of rapidities. Rapidities parametrize the eigenfunctions and eigenvalues of a stationary Schrödinger equation. Independently of the symmetry of the wave function and spin, the energy eigenstates are occupied according to Fermi–Dirac statistics (hard-core particles). There are many other solutions of the Bethe ansatz equations for rapidities, which describe bound states of electrons with a complex structure.

In the Bethe ansatz description in the ground state (and at low temperatures) each internal degree of freedom contributes with one Fermi sea. The Fermi velocities of these Fermi seas are in general different, giving rise to what is often also called spin–charge separation. However, the question arises: Do these low-lying excitations really carry only charge or only spin, as in the Luttinger liquid picture? To answer this question, let us consider the Bethe ansatz equations for two sets of rapidities $u_{1,j}$, $(j=1,\ldots,M_1$, where $M_1$ is the total number of electrons) and $u_{2,j}$ $(j=1,\ldots,M_2$, where $M_2$ is the number of electrons with down spins). The Bethe ansatz equations for correlated electron chains with periodic boundary conditions can be written in the form:[11]

$$2\pi J_{i,j}=Lp_i^0(u_{i,j})-\sum_{m=1}^{2}\sum_{\substack{l=1,\\ l\neq j}}^{M_1}\varphi_{i,m}(u_{i,j},u_{l,m}),\quad i=1,2, \tag{1}$$

with $p_1^0(u_{1,j})=k_j$ (where $k_j$ are quasimomenta), $p_2^0(x)=\varphi_{1,1}(x,y)=0$, $\varphi_{i,j}(x,y)=-\varphi_{j,i}(y,x)$, where $L$ is the number of sites, $J_{i,j}$, are (half)integer numbers, different from each other for each set. This solution is valid in the domain of parameters $0\leqslant M_2\leqslant M_1$ and $0\leqslant M_1\leqslant L$. For the Hubbard model one has $u_{1,j}=\sin k_j$, $\varphi_{1,2}(x,y)=2\tan^{-1}[4(x-y)/U]$, $\varphi_{2,2}(x,y)=2\tan^{-1}[2(x-y)/U]$ ($U$ is the constant of the Hubbard local interaction between electrons situated at the same site of a ring but with different spin directions; the hopping integral between neighboring sites is equal to 1.) For the supersymmetric $t-J$ chain (for $J=2t=2$) these functions are

$$p_1^0(u_{1,j})=2\tan^{-1}2u_{1,j},$$

$$\varphi_{1,2}(x,y)=2\tan^{-1}[2(x-y)],$$

$$\varphi_{2,2}(x,y)=2\tan^{-1}(x-y)(k_j=2\tan^{-1}2p_j).$$

The energy of the state with $M_1$ electrons, $M_2$ of which have their spins down, is equal to

$$E=E_0+\sum_{i=1}^{2}\sum_{j=1}^{M_i}\varepsilon_i^0(u_{i,j}), \tag{2}$$

where $E_0$ is the energy for $M_i=0$, $\varepsilon_1^0=-\mu-H/2-2\cos k_j$, and for the repulsive Hubbard chain we have $\varepsilon_2^0(x)=H$, for the attractive Hubbard model

$$\varepsilon_2^0(x)=-2\mu-4\,\mathrm{Re}\sqrt{1-[x+i(U/4)]^2},$$

and for the supersymmetric $t-J$ model one uses

$$\varepsilon_2^0(x)=-2+2\pi a_2(x)-2\mu.$$

Here $a_n(x)=(n/2)/\pi[x^2+(n/2)^2]$, $\mu$ is the chemical potential, and $H$ is an external magnetic field. Solutions (each set of $u_{i,j}$ corresponds to only one eigenstate) of Eqs. (1) parametrize *all* eigenvalues and eigenfunctions in the domain[12,13] $0\leqslant M_2\leqslant M_1/2$, $0\leqslant M_1\leqslant L$. Actually, Eqs. (1) are quantization conditions for the rapidities. This can be recognized, e.g., for the $U=0$ case of the Hubbard chain, which pertains to the one-dimensional free lattice electron gas. "Separation" means that the Bethe ansatz eigenstate is determined by two sets of quantum numbers. However, Eqs. (1) imply that it is impossible to really separate their contributions: They are obviously coupled to each other.

Consider the case of the repulsive Hubbard chain. The ground state and low-energy excitations pertain to real rapidities $u_{i,j}$ (Ref. 11). What are the charges and spins related to those quantum numbers? Suppose one changes the number of rapidities $u_{2,j}$, keeping the number of $u_{1,j}$ fixed. Such a process yields a change of the total magnetic moment, while the total number of electrons is not changed. Hence, such excitations carry only spin, but not charge. [The redistribution of rapidities with their number fixed can produce only particle–hole excitations, which, by definition, carry no spin and charge (but can change the energy).] The simple way to see this without the involvement of other kinds of spin and/or charge-carrying excitations, related to the change of the number of $u_{1,j}$, is to consider the state with $M_1=L$ fixed (i.e., at half-filling, which belongs to the domain $0\leqslant M_2\leqslant M_1/2$, $0\leqslant M_1\leqslant L$), where the low-energy dynamics is known to be connected with only spin excitations.[11]

Let us now change the number of rapidities $u_{1,j}$, with the number of $u_{2,j}$ being fixed. Such a process produces a change of *both* the total charge *and* the total magnetic moment of the system. Thus, this kind of excitation carries both spin and charge. Again, to avoid connection to the other set of rapidities, one can consider the state with $M_2=0$, which also belongs to the domain $0\leqslant M_2\leqslant M_1/2,\ 0\leqslant M_1\leqslant L$. It is very difficult to believe that the fact that an excitation carries spin depends on the number of such excitations.

We emphasize that namely the above-mentioned two kinds of low-lying excitations are considered in the conformal limit of the Bethe ansatz solvable theories to compute correlation function exponents,[14] and namely those results of the Bethe ansatz considerations are used to compare with the Luttinger liquid (bosonization) approach.[8] This is why it is namely these two kinds of low-lying excitations that are the most important ones for the repulsive Hubbard chain.

Hence, low-lying excitations of the repulsive Hubbard chain are related to eigenstates, some of which carry only spin while others carry both charge and spin. These states are often called spinons and unbound electron excitations, respectively (sometimes, unbound electron excitations are called holons, which is, unfortunately, misleading). The SO(4) symmetry of the Hubbard Hamiltonian[15] implies the presence of excitations which carry only charge and no spin. They are spin-singlet bound states of electrons, e.g., local pairs. However, for the repulsive Hubbard chain these states have large energies and do not affect the low-energy thermodynamics.[11] These states (local spin-singlet pairs) are low-lying states for the attractive Hubbard chain, and together with unbound electron excitations determine low-energy properties of that model.[11] These low-energy excitations of the attractive Hubbard chain carry only charge and both spin and charge, respectively. Again, namely these two kinds of low-lying excitations for the attractive Hubbard chain are important, because they determine the correlation function exponents in the conformal limit.[16]

The fact that excitations involving a change of the number of rapidities $u_{1,j}$ for the Hubbard model carry both spin and charge does not depend on the value of $U\neq 0$. It is often misunderstood[8,9] that the eigenfunction of the repulsive Hubbard chain with $U\rightarrow\infty$ is reminiscent of the one of spinless fermions multiplied by the wave function of the Heisenberg spin-1/2 chain.[17] In fact, this limit $U\rightarrow\infty$ of the repulsive Hubbard chain has been the only argument used to prove the spin–charge separation for Bethe ansatz solvable models; cf. Ref. 8. However, a careful inspection of the expressions for the energies of charge-carrying excitations[11] in this limit shows that they carry also spin 1/2 (one can see this by taking the derivative of the energy with respect to $H$ and then putting $H\rightarrow 0$). It turns out that charge-carrying excitations (the wave function of which is reminiscent of spinless fermions) for the $U\rightarrow\infty$ repulsive Hubbard model pertain to the spin-polarized phase (the critical field of the quantum phase transition to the spin-polarized phase for the $0<U\rightarrow\infty$ case is zero[11]). But namely in the spin-polarized case the fact that charge-carrying excitations carry also spin is especially clear, see above. Hence, the claim that in the $U\rightarrow\infty$ repulsive Hubbard chain one has factorization of the wave function into only charge-carrying and only spin-carrying parts is incorrect.

The same conclusions follow from the study of low-energy properties of the supersymmetric $t-J$ chain. Here also one kind of low-energy excitations carries both spin and charge. Again, namely these excitations determine the correlation function exponents in the conformal limit.[18]

Hence, the statement that for any one-dimensional correlated electron system the low-energy excitations carry either only spin or only charge is invalid.

Why, then, does the Luttinger liquid description manifest a spin–charge separation? [Note that Luttinger liquid bosons formally do not carry either spin or charge, because they are particle–hole excitations of related correlated electron systems and, by definition, cannot carry spin and charge but can only change energies and momenta.] One can see that the Luttinger liquid approach and the Bethe ansatz approach use *different* sets of quantum numbers. As we have shown above, the Bethe ansatz eigenstates and eigenvalues are determined by two sets of quantum numbers, one of which is the total number of electrons and the other the total number of spins down. Contrarily, in the Luttinger liquid approach one classifies states with two sets of quantum numbers, one of which is again the total number of electrons but the other is the total magnetic moment of the electrons (not the number of spins down!).[7] Then, naturally, the Luttinger liquid approach manifests spin–charge separation, unlike the low-energy behavior of the Bethe ansatz solvable models of correlated electrons; see above.

Then one is faced with an obvious contradiction. The Bethe ansatz is the exact solution, and it does not manifest spin–charge separation, as we proved above. The Luttinger liquid approach (an approximate one) does manifest spin–charge separation for the same models of correlated electrons, e.g., for the Hubbard model. Where, then, can the Luttinger liquid approach be used? This can be seen, e.g., from the conformal limit of the Bethe ansatz solution of the Hubbard chain, where one linearizes the energy of low-lying excitations about Fermi points. In this limit for small $U$ it is possible to rewrite the Bethe ansatz result[14,19] in such a way that states will be classified not by the total number of electrons and number of spin-down electrons but by the former and the total magnetic moment. Such a result naturally coincides with the Luttinger liquid one.[8,9] However, this approach is only correct in the limit of weak electron–electron interactions and linearized dispersion laws of low-energy excitations. Simply by using the corrections of higher order in $U$, one can see that it is impossible to reformulate the Bethe ansatz conformal limit of the Hubbard chain in terms of *separated* contributions, which pertain to changes of the total number of electrons and the total magnetic moment. Hence, one can conclude that the approximate bosonization (Luttinger liquid) procedure can be correctly applied to exactly (Bethe ansatz) solvable correlated electron models only for *weak* electron–electron correlations; otherwise the results of the Luttinger liquid approach contradict known exact Bethe ansatz results.

Experiments[1–5] have actually observed low-lying excitations, characterized by two different energy scales. However, nothing permits one to conclude from those experiments that

one of these excitations carries only spin while the other carries only charge. Also, for the main issues of the Luttinger liquid-like theory for the two-dimensional correlated electron systems[10] it is not necessary that real spin–charge separation occurs. One needs only the presence of two low-lying excitations (with one of them carrying only spin) instead of Fermi liquid quasiparticles. It seems interesting to study the behavior of charge and spin persistent currents in correlated electron rings with a strong electron–electron interaction for nonzero $H$. In such a case different (but nonzero) spins (charges) of two kinds of low-energy excitations can yield an interference of oscillations of persistent currents with two different periods.[20]

Summarizing, in this work we have shown that for all known Bethe ansatz solvable one-dimensional models of correlated electrons with short-range interactions between electrons, one of the low-lying excitations carries *both spin and charge*. This is very different from what is often believed when considering the spin–charge separation in low-dimensional correlated electron models. This is why the applicability of the conclusions of the Luttinger liquid approach to the spin–charge separation for one-dimensional lattice models with short-range electron–electron interactions that are much stronger than the bandwidth of the electrons is under question.

I appreciate a discussion with P. W. Anderson on spin–charge separation theories for two-dimensional correlated electron models. I thank H. Johannesson for useful comments. This work was supported in part by the Swedish Foundation for International Cooperation in Research and Higher Education (STINT).

*E-mail: zvyagin@ilt.kharkov.ua

[1] S. Maekawa and T. Tohyama, Rep. Prog. Phys. **64**, 383 (2001).
[2] C. Kim, A. Y. Matsuura, Z.-X. Shen, N. Motoyama, H. Eisaki, S. Uchida, T. Tohyama, and S. Maekawa, Phys. Rev. Lett. **77**, 4054 (1996).
[3] R. Claesson, M. Sing, U. Schwingenschlögl, P. Blaha, M. Dressel, and S. C. Jacobsen, Phys. Rev. Lett. **88**, 096402 (2002).
[4] T. Lorenz, M. Hoffmann, M. Grüninger, A. Freimuth, G. S. Uhrig, M. Dumm, and M. Dressel, Nature (London) **418**, 614 (2002).
[5] P. Segovia, D. Purdie, M. Hengsberger, and Y. Baer, Nature (London) **402**, 504 (1999).
[6] D. Pines and P. Noziéres, *The Theory of Quantum Liquids*, Addison-Wesley, Redwood City (1989).
[7] F. D. M. Haldane, Phys. Rev. Lett. **47**, 1840 (1981).
[8] J. Voit, Rep. Prog. Phys. **58**, 977 (1995).
[9] H. J. Schulz, Int. J. Mod. Phys. **5**, 57 (1991); Phys. Rev. Lett. **64**, 2831 (1990).
[10] P. W. Anderson, Phys. Rev. Lett. **64**, 1839 (1990).
[11] P. Schlottmann, Int. J. Mod. Phys. **11**, 355 (1997).
[12] F. H. L. Essler, V. E. Korepin, and K. Schoutens, Nucl. Phys. B **384**, 431 (1992).
[13] A. Foerster and M. Karowski, Nucl. Phys. B **396**, 611 (1993).
[14] H. Frahm and V. E. Korepin, Phys. Rev. B **42**, 10533 (1990).
[15] C. N. Yang, Phys. Rev. Lett. **63**, 2144 (1989).
[16] N. M. Bogolyubov and V. E. Korepin, Teor. Mat. Fiz. **82**, 331 (1990) [Theor. Math. Phys. **82**, 231 (1990)].
[17] M. Ogata and H. Shiba, Phys. Rev. B **41**, 2326 (1990).
[18] N. Kawakami and S.-K. Yang, J. Phys.: Condens. Matter **3**, 5983 (1990).
[19] F. Woynarovich, J. Phys. A: Math. Gen. **22**, 4243 (1989).
[20] A. A. Zvyagin and I. V. Krive, Zh. Éksp. Teor. Fiz. **102**, 1376 (1992) [Sov. Phys. JETP **75**, 745 (1992)].

This article was published in English in the original Russian journal. Reproduced here with stylistic changes by AIP.

# Low-temperature features of thermodynamics of an open isotropic Heisenberg chain

A. A. Zvyagin*

*Max-Planck-Institut für Physik komplexer Systeme, Nöthnitser Str., 38 D-01187, Dresden, Germany;*
*B. Verkin Institute for Low Temperature Physics and Engineering of the National Academy of Sciences of Ukraine, 47 Lenin Ave., Kharkov 61103, Ukraine*

A. V. Makarova

*Kharkov State Economic University, 9a Lenin Ave., Kharkov 61001, Ukraine;*
*B. Verkin Institute for Low Temperature Physics and Engineering of the National Academy of Sciences of Ukraine, 47 Lenin Ave., Kharkov 61103, Ukraine*

(Submitted February 24, 2004)
Fiz. Nizk. Temp. **30**, 974–977 (September 2004)

Low-temperature magnetic susceptibility and specific heat of an antiferromagnetic Heisenberg chain with open boundary conditions are calculated with the help of the exact Bethe ansatz method. These characteristics behave with temperature in a different way from those of a periodic chain. © *2004 American Institute of Physics.* [DOI: 10.1063/1.1802971]

Low-dimensional quantum spin systems, as one of the most interesting phenomena in condensed matter physics, have attracted much interest of theorists and experimentalists during last years. For example, recent experiments on two-dimensional (2D) and 1D antiferromagnetic spin systems reveal very interesting behavior of nonmagnetic impurities.[1,2] In 2D Heisenberg antiferromagnets nonmagnetic impurities may give rise to divergent magnetic susceptibility.[3] In 1D spin chains nonmagnetic impurities cut chains.[4] The behavior of the latter is different from the behavior of bulk spins. The exact Bethe ansatz description of open quantum chains was initiated by Gaudin.[5] The thermodynamic characteristics of an essentially anisotropic XXZ spin-1/2 open chain were studied by the Bethe ansatz in Ref. 6. It was shown there that low-temperature characteristics of the XXZ chain may diverge at low temperatures. The ground state magnetic susceptibility of a Heisenberg chain with open boundary conditions was calculated in Ref. 7, where it was shown that edge contributions to the susceptibility diverge in the ground state as a function of a homogeneous magnetic field $H$. On the other hand, it is known that irrelevant boundary operators (in the renormalization group sense) usually give only subleading contributions to any physical quantities.

Very recently two groups studied the low-temperature behavior of characteristics of an open spin-1/2 chain with isotropic Heisenberg antiferromagnetic interactions between nearest spins perturbatively, using bosonization and renormalization group-like approaches.[8] However, there were no exact results for such characteristics. Motivated by these facts, in this work we study the low-temperature characteristics of a Heisenberg spin-1/2 chain.

Let us study the behavior of the Heisenberg antiferromagnetic spin-1/2 chain of length $L$ with open boundary conditions and with the Hamiltonian $\mathcal{H}=J\Sigma_{n=1}^{L-1}\mathbf{S}_n\cdot\mathbf{S}_{n+1}$, where $J$ is the exchange constant, using Bethe's ansatz. The principal difference between Bethe ansatz studies of periodic and open chains consists of reflections at the edges of the open chain, which not only produce permutations but also lead to negative values of the quantum numbers (rapidities) parametrizing the eigenfunctions and eigenvalues of the stationary Schrödinger equation.[5] The Bethe ansatz equations (BAE) for the set of rapidities $\{\lambda\}_{j=1}^{M}$, where $M$ is the number of down spins, is:[5,7]

$$\left(\frac{\lambda_j+(i/2)}{\lambda_j-(i/2)}\right)^{2L}\frac{\lambda_j+iS_1}{\lambda_j-iS_1}\frac{\lambda_j+iS_L}{\lambda_j-iS_L}=\prod_{\substack{l=1,\\ l\neq j}}^{M}\frac{\lambda_j-\lambda_l+i}{\lambda_j-\lambda_l-i}\frac{\lambda_j+\lambda_l+i}{\lambda_j+\lambda_l-i}, \tag{1}$$

$j=1,\ldots,M$. The energy is

$$E=\frac{1}{4}[-2H(L-2M)+2h_1+2h_2+(L-1)J]-2J\sum_{j=1}^{M}(4\lambda_j^2+1)^{-1}, \tag{2}$$

where $H$ is the value of the homogeneous magnetic field and $2S_{1,L}=(J/h_{1,L})-1$. Here $h_{1,L}$ are boundary magnetic fields, which act only on the spins at the sites 1 and $L$, respectively. The BAE for an open chain differ from those for a closed geometry[9] by the following: (i) there are not only differences but also sums of rapidities on the right-hand sides of the BAE for the open case; (ii) the effective length of a chain is doubled; (iii) on the left-hand sides of the BAE for the open case there are multipliers connected with nonzero boundary fields. $S_{1,L}$ play the role of effective ''boundary spins.'' These ''boundary spins'' depend on the values of the boundary fields $h_{1,L}$. For $h_{1,L}=0$ these boundary spins are infinite, leading to effective twists of $\pi$ at each edge. At $h_{1,L}=\pm J$ these effective ''boundary spins'' change their signs. This situation is related to the effective addition or removal of one site to or from the chain, respectively, with finite zero-field magnetic susceptibility. It leads to the onset of complex roots of the Bethe ansatz equations (1) in the ground state: For $-1/2<S_{1,L}<0$ there appear bound states parametrized by complex rapidities $\lambda_j=(i/2)[1-(J/h_{1,L})]$ localized at the

 

edges. Finally, for $h_{1,L}\to\pm\infty$ we have $S_{1,L}\to -1/2$, effectively removing one site, number 1 or $L$, respectively, from the system.

Consider how these differences affect the thermodynamic characteristics in the limit of large $L$ and $M$ (with $M/L$ fixed). In the framework of the string hypothesis[10] we look for the solution of Eqs. (1) in the form of strings $\lambda_j=\lambda_{j,m}+i[(m+1)/2-\nu]$ with $\nu=1,\ldots,m$, valid with the accuracy $O(\exp(-L))$; then taking the logarithm we get for the BAE:

$$0_{m,1}(\lambda_j^m)+\frac{1}{2L}[0_{m,2S_1}(\lambda_j^m)+0_{m,2S_2}(\lambda_j^m)]=\frac{\pi}{L}I_{j,m}+\frac{1}{2L}\sum_{\substack{n=1\\ n\neq m}}^{\infty}\sum_{l=1}^{M_n}[\Theta_{mn}(\lambda_j^m-\lambda_l^n)+\Theta_{mn}(\lambda_j^m+\lambda_l^n)], \tag{3}$$

where $\theta_n(x)=2\tan^{-1}(x/n)$,

$$\theta_{m,n}(x)=\sum_{l=1}^{\min([m],[n])}\theta_{m+1+n-2l}(x), \tag{4}$$

$[x]$ denotes the integer part of $x$,

$$\Theta_{mn}(x)=(1-\delta_{m,n})\theta_{|m-n|}(x)+2\theta_{|m-n|+2}(x)+\ldots+2\theta_{m+n-2}(x)+\theta_{m+n}(x), \tag{5}$$

and the integers

$$1\leqslant I_{j,m}\leqslant\left[L+M_m-2\sum_{n=1}^{\infty}\min(m,n)M_n\right]$$

appear because the logarithm is a multivalued function. We look for solutions to the thermodynamic BAE for large $L$, keeping corrections of order of $L^{-1}$, too. In this limit we introduce distribution functions (densities) for particles, $\rho_m(x)$, and holes, $\rho_{mh}(x)$, corresponding to strings of length $m$:

$$\rho_{mh}(\lambda)+\frac{1}{2}\sum_{n=1}^{\infty}[A_{m,n}(\lambda-\lambda')+A_{m,n}(\lambda+\lambda')]*[\rho_n(\lambda')-p(\lambda')\delta_{m,1}]=\frac{1}{2L}\sum_{n=1}^{\infty}[A_{m,n}(\lambda-\lambda')+A_{m,n}(\lambda+\lambda')]*p(\lambda')(\delta_{m,[2S_1]}+\delta_{m,[2S_2]}), \tag{6}$$

where $p(\lambda)=1/[4\cosh(\pi\lambda/2)]$, the asterisk $*$ denotes the convolution,

$$A_{m,n}(x)=a_{|m-n|}(x)+a_{m,n}(x)+2\sum_{l=1}^{\min(n,m)-1}a_{m+n-2l}(x), \tag{7}$$

and $a_m(x)=2m/[\pi(4x^2+m^2)]$. The internal energy $E$ and the total magnetic moment $M^z$ are given as

$$E=E_0-\frac{1}{2}\sum_{m=1}^{\infty}m\int_0^{\infty}d\lambda\,\theta'_{m,1}(\lambda)\rho_m(\lambda),$$

$$M^z=\frac{L}{2}-L\sum_{m=1}^{\infty}m\int_0^{\infty}d\lambda\rho_m(\lambda), \tag{8}$$

where $E_0=-[2(HL+h_1+h_2)-(L-1)J]/4$ is the energy of the ferromagnetic state. The (complementary) set of thermodynamic equations for the dressed energies $\varepsilon_n(\lambda)=T\ln[\rho_{nh}(\lambda)/\rho_n(\lambda)]=\eta_n(\lambda)$ is

$$Hm-J\theta'_{m,1}(\lambda)=T\ln[1+\eta_m(\lambda)]-\sum_n\frac{T}{2}[A_{n,m}(\lambda-\lambda')+A_{n,m}(\lambda+\lambda')]*\ln[1+\eta_n^{-1}(\lambda')]. \tag{9}$$

The thermodynamic BAE for densities are linear integral equations. There are two kinds of driving terms (not dependent on $\rho_m$ and $\rho_{mh}$: terms of order 1, and terms of order $L^{-1}$). Hence, we can divide the densities as $\rho_n(\lambda)=\rho_n^{(0)}(\lambda)+L^{-1}\rho_n^{(1)}(\lambda)$ (and the same for the densities of holes). Then one can separate the BAE for the densities into two sets: one of scale 1 for the main (of order $L$) contribution and the other of scale $L^{-1}$ for the finite contribution (of order 1). The former describes the thermodynamics of bulk spins, which is equivalent to those for the chain with periodic boundary conditions.[7] The latter reveals the contribution from the edges. In what follows we shall concentrate specifically on that contribution only. Since $\varepsilon_m(\lambda)$, $\rho_m(\lambda)$, and $\rho_{mh}(\lambda)$ are even functions, one can rewrite the thermodynamic BAE following Ref. 11 as [in what follows we drop the superscript (1)]

$$Hm-J\theta'_{m,1}(\lambda)=T\ln[1+\eta_m(\lambda)]-T\sum_n A_{n,m}(\lambda-\lambda')*\ln[1+\eta_n^{-1}(\lambda')], \tag{10}$$

and

$$\rho_{mh}(\lambda)=-\sum_{n=1}^{\infty}A_{mn}(\lambda-\lambda')*[\rho_n(\lambda')-p(\lambda')\times(\delta_{m,1}+\delta_{m,2}+\delta_{m,[2S_1]}+\delta_{m,[2S_2]})], \tag{11}$$

where we have introduced additional terms to avoid double counting due to the symmetrization of functions (with $\lambda=0$) and to take into account the term with $\lambda_\alpha=\lambda_\beta$ in the right-hand sides of Eqs. (1).

In what follows we shall concentrate on the low temperature, $T\ll J$, dependences of the magnetic susceptibility and specific heat caused by the free edges themselves (i.e., for $h_{1,L}=0$ and even $L$). Equations (10) and (11) are very similar in structure to those which describe the thermodynamics of a Kondo impurity in a metal.[12] The principal difference, however, is that the contributions of order 1 to the magnetization and the energy of the open spin-1/2 Heisenberg chain, see Eq. (8), have no terms that do not depend on the dressed densities, while such terms are present for the Bethe ansatz description of the Kondo problem.[12] Following known methods of consideration of the low-temperature corrections, we find the contribution to the free energy of the Heisenberg chain for $H\ll T$, caused by free edges:

$$F_{\text{edges}} = -\frac{H}{8}\tanh[H/2T]\left(\frac{1}{|\ln T_0/T|} - \frac{\ln|\ln T_0/T|}{2\ln^2 T_0/T}\right) - \frac{\pi^2 T}{32|\ln T_0/T|^3} + \dots , \quad (12)$$

where $T_0 = a\pi\sqrt{\pi/e}J$ ($a$ is a constant). This implies the expressions for the low-temperature magnetic susceptibility of an open Heisenberg chain, caused by free edges

$$\chi_{\text{edges}} = \frac{1}{8T|\ln T_0/T|}\left(1 - \frac{\ln|\ln T_0/T|}{2|\ln T_0/T|}\right) + \dots . \quad (13)$$

One can see that the magnetic susceptibility of open edges of the chain diverges as $T \to 0$. However, this divergency is different from the usually presumed Curie-like $1/T$ behavior. Logarithmic terms appear due to the interaction in the SU(2)-symmetric spin-1/2 system. This is different from the constant behavior of the magnetic susceptibility of bulk spins (and those of a periodic chain) at low temperatures.

The low-temperature entropy of the Heisenberg chain caused by free edges is calculated as

$$\mathcal{S}_{\text{edges}} = \frac{\pi^2}{32|\ln T_0/T|^3} + \dots , \quad (14)$$

which implies the low-temperature specific heat

$$c_{\text{edges}} = \frac{3\pi^2}{32\ln^4 T_0/T} + \dots . \quad (15)$$

The last equation implies that the low-temperature Sommerfeld coefficient is divergent as

$$\gamma_{\text{edges}} = \frac{3\pi^2}{32T\ln^4 T_0/T} + \dots . \quad (16)$$

This is again very different from the behavior of the specific heat of bulk spins (and those of a periodic chain) at low temperatures. While the Sommerfeld coefficient of free edges is divergent at low temperatures, the edges's entropy and specific heat are finite, as they must be. It turns out that the Wilson ratio of the contributions from free edges is divergent, in stark contrast with the finite value of that coefficient for bulk spins. It is important to emphasize that while Eq. (13) agrees with the expressions obtained in the approximate calculations,[8] the expressions for the low-temperature entropy and specific heat are different from those obtained using the approximate bosonization method. We point out that it is precisely terms cubic in $1/|\ln T_0/T|$ that appear for $H=0$ in the low-temperature corrections of the behavior of the free energy of the Kondo impurity[12] and the bulk free energy of a Heisenberg spin-1/2 chain,[13] while there are no linear terms in those dependences.

In conclusion, using the exact Bethe ansatz method we have calculated the low-temperature characteristics of free edges of an open Heisenberg antiferromagnetic spin-1/2 chain. We have shown that the magnetic susceptibility and low-temperature Sommerfeld coefficient of the specific heat of free edges of an open chain are divergent, unlike similar characteristics for bulk spins of the chain. Note that similar behavior of low-temperature magnetic susceptibility of quasi-one-dimensional compounds of Cu has been observed.[2]

*E-mail: zvyaginilt.kharkov.ua

[1] A. V. Mahajan, H. Alloul, G. Collin, and J. F. Marucco, Phys. Rev. Lett. **72**, 3100 (1994).
[2] G. Xu, G. Aeppli, M. E. Fisher, C. Broholm, J. F. DiTusa, C. D. Frost, T. Ito, K. Oka, R. L. Paul, H. Takagi, and M. M. J. Treacy, Science **289**, 419 (2000).
[3] K. H. Höglund and A. W. Sandvik, Phys. Rev. Lett. **91**, 077204 (2003); S. Sachdev, C. Buragohain, and M. Voita, Science **286**, 2479 (1999).
[4] S. Eggert, I. Affleck, and M. D. P. Horton, Phys. Rev. Lett. **89**, 047202 (2002); A. A. Zvyagin, *ibid.* **90**, 089701 (2003).
[5] M. Gaudin, Phys. Rev. A **4**, 386 (1971); *La Fonction d'Onde de Bethe*, Masson, Paris (1983).
[6] P. A. de Sa and A. M. Tsvelik, Phys. Rev. B **52**, 3067 (1995).
[7] H. Frahm and A. A. Zvyagin, J. Phys.: Condens. Matter **9**, 9939 (1997).
[8] S. Fujimoto and S. Eggert, preprint cond-mat/0310230; A. Furusaki and T. Hikihara, preprint cond-mat/0310517.
[9] H. Bethe, Z. Phys. **71**, 205 (1931).
[10] M. Takahashi, *Thermodynamics of One-Dimensional Solvable Models*, Cambridge University Press, Cambridge (1999).
[11] F. C. Alcaraz, M. N. Barber, M. T. Batchelor, R. J. Baxter, and G. R. W. Quispel, J. Phys. A: Math. Gen. **20**, 6397 (1987).
[12] A. M. Tsvelick and P. B. Wiegmann, Adv. Phys. **32**, 453 (1983).
[13] A. Klümper, Eur. Phys. J. B **5**, 677 (1998).

This article was published in English in the original Russian journal. Reproduced here with stylistic changes by AIP.

## SHORT NOTES

# Current oscillations and N-shaped current–voltage characteristic in the manganite $Sm_{1-x}Sr_xMnO_3$

I. K. Kamilov,* K. M. Aliev, Kh. O. Ibragimov, and N. S. Abakarova

*Institute of Physics of the Dagestan Science Center of the Russian Academy of Sciences, ul. M. Yaragskogo 94, Makhachkala 367003, Russia*

(Submitted September 4, 2003; revised February 18, 2004)
Fiz. Nizk. Temp. **30**, 978–980 (September 2004)

Samples of $Sm_{1-x}Sr_xMnO_3$ with $x=0.425$ and 0.450 are investigated experimentally at temperature of 77 K in pulsed and static electric $E$ and magnetic $H$ (up to 10 kOe) fields in the mutual orientations $\mathbf{H}\|\mathbf{E}$ and $\mathbf{H}\perp\mathbf{E}$. N-shaped current–voltage characteristics and high-frequency (up to 3 MHz) oscillations of the current are observed. © *2004 American Institute of Physics.* [DOI: 10.1063/1.1802972]

The discovery of colossal magnetoresistance (CMR) phenomena in manganites has stimulated research on charge transport processes in systems manifesting deeply interrelated magnetic, lattice, and electron subsystems.

The nonlinear current–voltage (I–V) characteristics of manganites and of heterostructures based on them and also the processes of current relaxation after application of a voltage to them have been studied in Refs. 1–10. Nonlinear I–V characteristics with sub- or superlinear behavior and S-shaped I–V characteristics have been observed.[1–4,6–10] It was shown in Ref. 5 that the establishment of a stable value of the electric current corresponding to an applied voltage is of a relaxational character with long characteristic times (up to 10 min). We note that the majority of the I–V characteristics studied display hysteresis, i.e., the ascending and descending branches of the I–V characteristic do not coincide. The physical mechanisms underlying the nonlinearities include the influence of the leakage current on the magnetic nonuniformity of the system,[1,2,4] inelastic scattering of charge carriers in macroscopically active layers at a contact junction,[3] and electric modulation of the double-exchange processes in ferromagnetic systems[6] with the formation and motion of charge density waves.[9,10]

The goal of the present study was to investigate the influence of electric field on the current transport in manganites for the particular example of $Sm_{1-x}Sr_xMnO_3$ with $x=0.425$ and 0.450 at 77 K in magnetic fields up to 10 kOe in the cases $\mathbf{H}\|\mathbf{E}$ and $\mathbf{H}\perp\mathbf{E}$.

According to x-ray data, the $Sm_{1-x}Sr_xMnO_3$ ceramics studied are orthorhombic perovskites with a uniform granulometric composition, having good cleavability and a porosity of around 20%. The results of a detailed experimental study of the heat capacity and electrical resistance of such samples (with $x=0.450$) over a wide temperature range were reported in Refs. 11 and 12. The dimensions of the samples with $x=0.425$ and 0.450 were $6\times1.7\times0.7$ and $2.5\times1.2\times0.7$ mm, respectively. Current contacts to the ends of the samples were made using silver paste. All of the measurements were made at a temperature of 77 K, which was monitored by a copper–Constantan thermocouple.

The current–voltage characteristics of the samples were measured both in the constant-current and pulsed modes of the voltage generator with $R_s \gg R^i$, where $R_s$ is the resistance of the sample and $R_i$ is the output resistance for current extraction, connected in series with the sample. The duration of the triangular pulse for which the I–V characteristic was measured did not exceed 120 $\mu$s, and the duration of the square pulses was not more than 80 $\mu$s, with a rise time of 0.1 $\mu$s or better.

Figure 1a shows the ascending and descending branches of the I–V characteristic for a sample with $x=0.425$, measured in the pulsed mode. These are curves with initial Ohmic regions that go over to superlinear, with a characteristic slope $I\sim U^n$, where $n=1.4–1.6$. Then at voltages $U\approx1.5$ V the I–V characteristic has an N-shaped part, which again goes over to a positive branch (where $dI/dU>0$) as the voltage is raised.

Depending on the maximum value of the applied voltage, the ascending and descending branches of the I–V characteristic do not coincide, i.e., they exhibit hysteresis in an amount that depends not only on the voltage but also on the value of the load resistance. For a suitable choice of load resistance the current pulse exhibits oscillations (Fig. 1b), the amplitude and frequency of which depend on the value of the applied voltage. These oscillations of the current in an electric field $E$ have the following characteristic features: 1) the frequency decreases and the amplitude increases with increasing field; 2) oscillations also appear on the second positive branch of the I–V characteristic out to high values of the voltage $U$ (20–30 V), and they demonstrate properties characteristic of chaotic systems (period doubling, quasiperiodicity, stochastic behavior or broadband noise, etc.). Figure 1b gives the frequency values corresponding to the maximum amplitudes, according to their Fourier analysis. The shape of the I–V characteristics is not affected by a change in the direction of the current in the sample—it is the same in both directions. The shape of the current oscillations does change

 

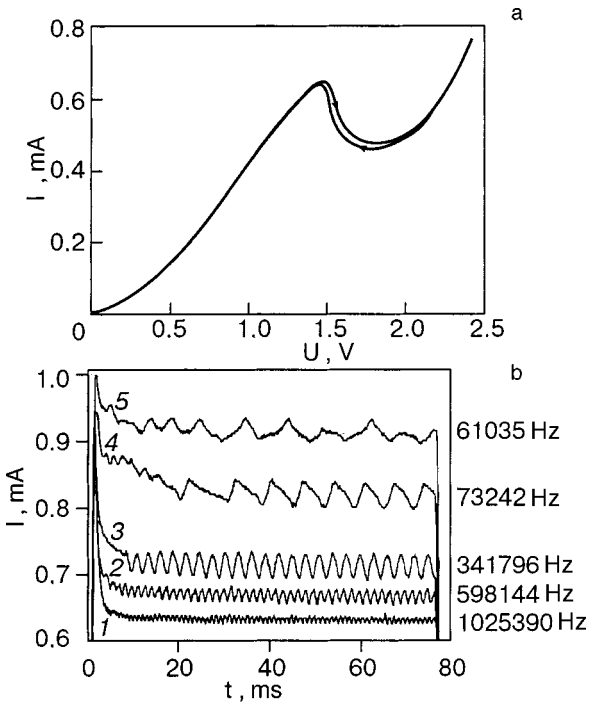


FIG. 1. Ascending and descending branches of the I–V characteristic (a) and oscillations on the current pulse for different values of the applied voltage $U$ [V]: 2.48 (*1*), 2.64 (*2*), 2.72 (*3*), 2.8 (*4*), 3.02 (*5*) (b) for a $Sm_{1-x}Sr_xMnO_3$ sample with $x=0.425$ at 77 K.

slightly, but the basic relationships are independent of the bias $U$. During N switching a drop in current occurs at the start of the current pulse, with characteristic times of the order of several microseconds.

For pulsed longitudinal ($\mathbf{H}\|\mathbf{E}$) and transverse ($\mathbf{H}\perp\mathbf{E}$) pulsed electric fields the CMR effect, calculated according to the formula $(\rho_H-\rho_0)/\rho_H$, reached 35%. It was noted that the magnetic field decreases the amplitude of the oscillations and shifts the threshold of the N switching to smaller electric fields.

Figure 2 shows the I–V characteristics for a sample with $x=0.450$ in longitudinal magnetic fields $\mathbf{H}\|\mathbf{E}$, measured in

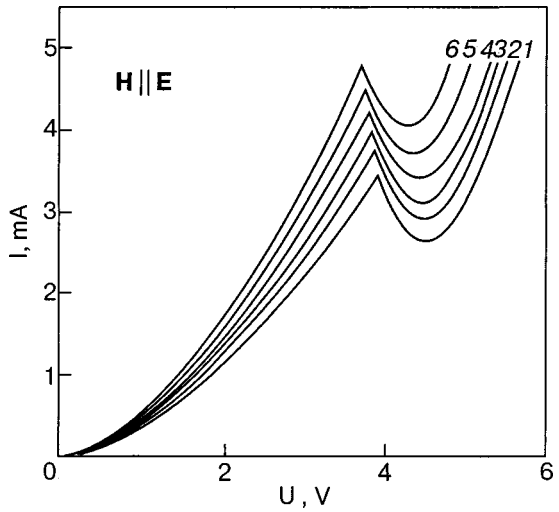


FIG. 2. I–V characteristics of a $Sm_{1-x}Sr_xMnO_3$ sample with $x=0.450$ at $T=77$ K and various values of the longitudinal magnetic field $H$ [kOe]: 0 (*1*), 1.38 (*2*), 2.25 (*3*), 4.5 (*4*), 6.7 (*5*), 8.5 (*6*).

dc electric fields. We emphasize that all of the measurements were made at a constant temperature $T=77$ K, which was monitored by a thermocouple, and the power dissipated in the sample did not cause Joule heating. In magnetic fields the I–V characteristics for the samples of this composition, like those for $x=0.425$, attest that the CMR reaches 35% and also demonstrate that the threshold for N switching decreases slightly with increasing magnetic field strength. As is seen in Fig. 2, the CMR decreases somewhat upon N switching, but at the minimum and on the second ascending branch of the I–V characteristic the CMR reaches the same or a noticeably higher value. In transverse magnetic fields $\mathbf{H}\perp\mathbf{E}$ the behavior of the I–V characteristic is completely identical to the case of longitudinal fields $\mathbf{H}\|\mathbf{E}$. We note that a slight anisotropy of the CMR is observed: the influence of a longitudinal magnetic field is stronger, and the CMR effect on all parts of the I–V characteristic is larger in longitudinal fields than in transverse fields. The value of the CMR on the parts of the I–V characteristics where the $I\sim U^{1.6}$ law holds is either constant or decreases slightly ($\sim 3\%$) as the voltage is increased to N switching.

Upon repeated thermocycling of the sample (more than 30 times) over the range 77–300 K we observed a qualitative change in the shape of the I–V characteristic and a sharp growth of the hysteresis on the ascending and descending branches of the I–V characteristic.

If there are no built-in hetero- or sandwich structures nor any point or other contacts with nonequilibrium properties, then for interpreting the results on the observation of the N-shaped I–V characteristic in manganites one can invoke the $\Delta m\tau$ model proposed in Ref. 13, in which the resistivity is calculated according to the Drude formula

$$\rho=\frac{m^*}{e^2 n\tau}, \tag{1}$$

where $e$ is the charge of the electron, $m^*$ is its effective mass, $n$ is the density of current carriers, and the relaxation time $\tau$ is represented in terms of the sum $\tau^{-1}=\tau_{\rm st}^{-1}+\tau_{\rm ph}^{-1}+\tau_m^{-1}$, where $\tau_{\rm st}$, $\tau_{\rm ph}$, and $\tau_m$ are the characteristic times for scattering on static disruptions of the translational symmetry of the system, phonons, and fluctuations of the local magnetic moments, respectively. The final expression with allowance for the activation energy $\Delta$ has the form

$$\rho=e^{2\Delta/3T}(\rho_{\rm st}+\rho_{\rm ph}+\rho_m). \tag{2}$$

Significant inelastic scattering of charge carriers at certain values of the threshold electric field can lead to sharp growth of the resistance owing to the change in relaxation time, especially when the second (polaron) and third (describing spin disorder) terms in parentheses in formula (2) are taken into account, which can lead to an N-shaped I–V characteristic.

Upon further increase of the voltage, which increases the energy of the charge carriers for overcoming the polaron and spin barriers, the I–V characteristic reaches a new current growth region. Here it cannot be ruled out that the magnetic uniformity of the systems is being influenced by the leakage current or by other mechanisms leading to a sharp change in

the density of current carriers owing to breakdown of the charge or orbital order and also because of the formation and motion of charge density waves.[1,2,5,9,10]

In closing, the authors express their gratitude to A. B. Batdalov and Sh. B. Abdulvagidov for a helpful discussion of the results of this study and to O. Yu. Gorbenko for providing the high-quality samples. This study was done with the financial support of RFBR Grant No. 02-02-17817 and Grant No. NSh-2253.03.2 through the Device Park of the Analytical Center of the Dagestan Science Center of the Russian Academy of Sciences.

*E-mail: kamilov@datacom.ru

[1] A. Guha, N. Khare, A. K. Raychaudhuri, and C. N. R. Rao, Phys. Rev. B **62**, R11941 (2000).
[2] A. Guha, A. K. Raychaudhuri, A. R. Raju, and C. N. R. Rao, Phys. Rev. B **62**, 5320 (2000).
[3] M. A. Belogolovskiĭ, Yu. F. Revenko, A. Yu. Gerasimenko, V. M. Svistunov, E. Hatta, G. Plituik, V. E. Shaternik, and E. M. Rudenko, Fiz. Nizk. Temp. **28**, 553 (2002) [Low Temp. Phys. **28**, 391 (2002)]; M. A. Belogolovskiĭ, Yu. F. Revenko, A. Yu. Gerasimenko, Yu. V. Medvedev, O. I. Chernyak, V. M. Svistunov, and G. Plitnik, Fiz. Nizk. Temp. **29**, 889 (2003) [Low Temp. Phys. **29**, 666 (2003)].
[4] S. Heim, T. Nachtrab, M. Mössle, R. Kleiner, R. Koch, S. Rother, O. Waldmann, P. Müller, T. Kimura, and Y. Tokura, Physica C **367**, 348 (2002).
[5] M. K. Gubkin, T. M. Perekalina, A. M. Balbashev, V. V. Kireev, and S. V. Pushko, Fiz. Tverd. Tela (St. Petersburg) **43**, 293 (2001) [Phys. Solid State **43**, 305 (2001)].
[6] M. Tanaka, J. Zhang, and T. Kawai, Phys. Rev. Lett. **88**, 027204–1 (2002).
[7] J. Z. Sun, J. Magn. Magn. Mater. **202**, 157 (1999).
[8] J. S. Moodera, J. Novak, and Rene J. M. van der Veerdonk, Phys. Rev. Lett. **80**, 2941 (1998).
[9] A. Wahl, V. Caignaert, and S. Mercone, arXiv: cond-mat/0306160 (2003).
[10] A. Wahl, S. Mercone, A. Pautrat *et al.*, arXiv: cond-mat/0306161 (2003).
[11] Sh. B. Abdulvagidov, I. K. Kamilov, A. M. Aliev, and A. B. Batdalov, Zh. Éksp. Teor. Fiz. **123**, 857 (2003) [JETP **96**, 757 (2003)].
[12] A. M. Aliev, Sh. B. Abdulvagidov, A. B. Batdalov, I. K. Kalimov, O. Yu. Gorbenko, V. A. Amelichev, A. R. Kaul', A. I. Kurbakov, and V. A. Trunov, Fiz. Tverd. Tela (St. Petersburg) **45**, 124 (2002) [Phys. Solid State **45**, 130 (2002)].
[13] A. B. Beznosov, B. I. Belevtsev, E. L. Fertman, V. A. Desnenko, D. G. Naugle, K. D. D. Rathnayka, and A. Parasiris, Fiz. Nizk. Temp. **28**, 774 (2002) [Low Temp. Phys. **28**, 556 (2002)]

Translated by Steve Torstveit

# Stochastic dynamics of nuclear magnetization in ferromagnets

L. L. Chotorlishvili* and V. M. Ckhvaradze

*Tbilisi State University, ul. Chavchavadze 3, Tbilisi 0128, Georgia*
(Submitted April 1, 2003; revised March 19, 2004)
Fiz. Nizk. Temp. **30**, 981–985 (September 2004)

The nonlinear dynamics of the nuclear magnetization in ferromagnets is studied with the use of numerical methods. An analytical solution for the nonlinear equations of momentum is obtained. It is shown that at a large value of the dynamic frequency shift an overlap of the nonlinear resonances and chaotization of the nuclear spin system can occur. © *2004 American Institute of Physics.* [DOI: 10.1063/1.1802991]

It is well known that the nuclear magnetic resonance (NMR) in ferromagnets is marked by large values of the dynamic shift of the NMR frequency, leading to nonlinearities in the equations describing the dynamics of the nuclear magnetization.[1,2] Because of this, a situation characteristic of nonlinear resonance can arise in the nuclear spin system,[3,4] wherein under conditions of continuous pumping a detuning of the resonance relation between the NMR frequency and the frequency of the external influence occurs as a result of the change of the $z$ projection of the nuclear magnetization $m_z$. On the other hand, this difficulty does not arise if a periodic series of pulses is used instead of a monochromatic pump. In that case the presence of a series of pulses with a large number of harmonics at frequencies that are multiples of the frequency $\Omega$ of the phase oscillations and the nonlinear character of the motion can bring about an overlap of resonances,[4] which is a criterion of the onset of dynamic stochasticity in classical Hamiltonian systems.[5,6] When this criterion holds, one can justify going over from a dynamical Hamiltonian description to a stochastic description and to the use of statistical averages for investigating the behavior of the system. This question was investigated in Refs. 7 and 8 in a treatment of the stochastic saturation of the nuclear spin system, and the following expression was obtained for the coefficient of stochasticity:

$$k=\omega_1\omega_p\tau T\sqrt{1-\frac{m_z^2}{m_0^2}}=\omega_1'\omega_p T^2\sqrt{1-\frac{m_z^2}{m_0^2}},$$

where $\omega_1=\eta\gamma_n h$, $\eta$ is the gain, $\gamma_n$ is the gyromagnetic ratio for the nuclear spins, $h$ is the amplitude of the alternating field, $\omega_p$ is the dynamic frequency shift (DFS), $m_0$ is the value of the nuclear magnetism, $m_z$ is the $z$ projection of the magnetization, $\tau$ is the pulse duration, and $T$ is the repetition period.[7,8] It is known that stochasticity arises in a system for $k\geqslant 1$.[4–6]

The goal of this study is to model numerically the equations describing the behavior of the nuclear magnetization in ferromagnets at large values of the DFS in the cases $k\geqslant 1$ and $k<1$.

Let us first consider the case of monochromatic pumping. The system of equations for the nuclear magnetization **m** for the time intervals $t\ll T_2<T_1$ (where $T_1$ and $T_2$ are the longitudinal and transverse relaxation times) has the form

$$\dot m_x=\left(\omega_n-\omega_p\frac{m_z}{m_0}-\omega\right)m_y, \tag{1}$$

$$\dot m_y=-\left(\omega_n-\omega_p\frac{m_z}{m_0}-\omega\right)m_x+\omega_1 m_z,$$

$$\dot m_z=-\omega_1 m_y,$$

where

$$H_{\text{eff}}^x=\frac{\omega_1}{\gamma_n}=\eta h,\quad H_{\text{eff}}^y=0,\quad H_{\text{eff}}^z=\frac{\Delta\omega_n(m_z)}{\gamma_n},$$

$$\Delta\omega_n(m_z)=\omega_n-\omega_p\frac{m_z}{m_0}-\omega,$$

$\omega_n$ is the NMR frequency, and $\omega$ is the frequency of the alternating field.[1]

We consider the following initial conditions:

$$m_z(0)=m_0,\quad m_x(0)=m_y(0)=0,\quad \omega_n=\omega_p+\omega,$$

$$\Delta\omega_n(m_0)=\omega_n-\omega_p.$$

Under these conditions system (1) becomes

$$\dot m_x=\omega_p\left(1-\frac{m_z}{m_0}\right)m_y,$$

$$\dot m_y=-\omega_p\left(1-\frac{m_z}{m_0}\right)m_x+\omega_1 m_z,\quad \dot m_z,\quad \dot m_z=-\omega_1 m_y. \tag{2}$$

Taking into account the presence of two integrals of the motion,

$$m_0^2=m_x^2(t)+m_y^2(t)+m_z^2(t),$$

$$E=\left[-(\omega_n-\omega)m_z(t)+\omega_p\frac{m_z^2(t)}{2m_0}-\omega_1 m_x(t)\right]\Big/\ \gamma_n,$$

where $E=m_0\omega_n/\gamma_n$, one can obtain from system (2) a closed equation for $m_z$:

$$\dot m_z=\omega_1\sqrt{m_0^2-m_z^2-\left(\frac{\omega_p}{2m_0\omega_1}\right)^2(m_z-m_0)^4}. \tag{3}$$

Equation (3) can be integrated analytically. For this we introduce the notation $a=m_0$, $x=m_z$, $b=(\omega_p/2m_0\omega_1)^2$ and rewrite Eq. (3) in the form

 

$$\int_a^{m_z(t)} \frac{dx}{\sqrt{a^2-x^2-b(x-a)^4}} = \omega_1 t. \tag{4}$$

In the integration (4) we obtain after some awkward manipulations

$$2\sqrt{\frac{(\beta-\delta)}{(\gamma-\beta)(\delta-\beta)(\alpha-\delta)}}F\left[\arcsin\left(\sqrt{\frac{(\beta-a)(\alpha-\delta)}{(\alpha-a)(\beta-\delta)}}\right);\ \frac{(\alpha-\gamma)(\beta-\delta)}{(\beta-\gamma)(\alpha-\delta)}\right]-2\sqrt{\frac{(\beta-\delta)}{(\gamma-\beta)(\delta-\beta)(\alpha-\delta)}}$$
$$\times F\left[\arcsin\left(\sqrt{\frac{(\beta-m_z(t))(\alpha-\delta)}{(\alpha-m_z(t))(\beta-\delta)}}\right);\ \frac{(\alpha-\gamma)(\beta-\delta)}{(\beta-\gamma)(\alpha-\delta)}\right]$$
$$=\omega_1 t. \tag{5}$$

Here $F(\ldots)$ is an elliptic integral of the first kind,[9–11] $\alpha$, $\beta$, $\gamma$, and $\delta$ are roots of the equation $a^2-x^2-b(x-a)^4=0$:

$$\alpha=a-\sqrt{\eta_1}-\sqrt{\eta_2}-\sqrt{\eta_3},$$
$$\beta=a-\sqrt{\eta_1}+\sqrt{\eta_2}-\sqrt{\eta_3},$$
$$\gamma=a+\sqrt{\eta_1}-\sqrt{\eta_2}-\sqrt{\eta_3},$$
$$\delta=a+\sqrt{\eta_3}-\sqrt{\eta_1}-\sqrt{\eta_2},$$

where

$$\eta_1=4a^2-2\beta_1+\beta_2+\beta_3,$$
$$\eta_2=8a^2-4\beta_1-\beta_2-1/\beta_3,$$
$$\eta_3=\frac{96a^3-48a\beta_1}{4\sqrt{4a^2-2\beta_1+\beta_2+1/\beta_3}},$$

with

$$\beta_1=\frac{1+6a^2b}{3b},$$
$$\beta_2=\frac{1+24a^2b}{3b(1-18a^2b+6\sqrt{3}\sqrt{a^2b+13a^4b^2-128a^6b^3})^{1/3}},$$
$$\beta_3=\frac{3b}{(1-18a^2b+6\sqrt{3}\sqrt{a^2b+13a^4b^2+128a^6b^3})^{1/3}}$$

Expression (5) contains the solution $m_z(t)$ of the differential equation (3) in the argument of the elliptic function of the first kind. To obtain a solution in explicit form it is necessary carry out transformation (5). After standard manipulations we obtain

$$m_z(t)=\frac{\dfrac{\delta\beta-\beta\alpha}{\beta-\delta}+\alpha\,\mathrm{sn}^2\left(\dfrac{A-t\omega_1}{B};\ \dfrac{(\alpha-\gamma)(\beta-\delta)}{(\beta-\gamma)(\alpha-\delta)}\right)}{\dfrac{\delta-\alpha}{\beta-\delta}+\mathrm{sn}^2\left(\dfrac{A-t\omega_1}{B};\ \dfrac{(\alpha-\gamma)(\beta-\delta)}{(\beta-\gamma)(\alpha-\delta)}\right)}, \tag{6}$$

where sn(...) is the Jacobi elliptic sine,[9–11] and

$$B=2\sqrt{\frac{(\beta-\delta)}{(\gamma-\beta)(\delta-\beta)(\alpha-\delta)}},$$

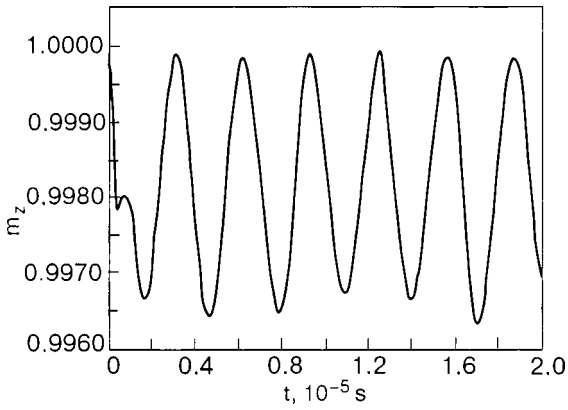


FIG. 1. Calculation of $m_z$ by numerical integration of equation (3) for the parameters values $\omega_1 \approx 10^6$ s$^{-1}$, $m_0 \approx 1$, $\omega_p \approx 10^8$ s$^{-1}$ in the case of a monochromatic influence.

$$A=BF\left(\arcsin\left(\sqrt{\frac{(\beta-a)(\alpha-\delta)}{(\alpha-a)(\beta-\delta)}}\right);\ \frac{(\alpha-\gamma)(\beta-\delta)}{(\beta-\gamma)(\alpha-\delta)}\right).$$

Expression (6) is the most general analytical solution, but in a numerical analysis it is easier to use numerical integration (3).

As we have said, as a consequence of the change of $m_z(t)$ a detuning of the resonance relation between $\omega_n - \omega_p m_z(t)/m_0$ and the frequency $\omega$ of the alternating field occurs, leading to a restriction on the deviation of **m** from the $z$ axis. The maximum angle of deviation determined from qualitative arguments has the form[1]

$$\theta_m = 2\arcsin\left(\frac{\omega_1}{2\omega_p}\right)^{1/3}. \tag{7}$$

Figure 1 shows the results of a numerical integration of equation (3) for the following parameter values: $m_0 \approx 1$, $\omega_p \approx 10^8$ s$^{-1}$, $\omega_1 \approx 10^6$ s$^{-1}$.

As is seen in Fig. 1, the component $m_z(t)$ executes oscillations about its equilibrium position, attesting to the smallness of the angle $\theta_m$. When the condition

$$\frac{\omega_p}{2\omega_1}\left(1-\frac{m_z}{m_0}\right)^2-\frac{m_z}{m_0}>0 \tag{8}$$

holds we can obtain the solution for (3) in a simpler form:

$$m_z(t)=m_0(1-\sqrt{2\omega_1/\omega_p}|\mathrm{sn}(\sqrt{\omega_1\omega_p/2}t;-1)|). \tag{9}$$

After using the expression for the Jacobi elliptic functions with a negative parameter we obtain

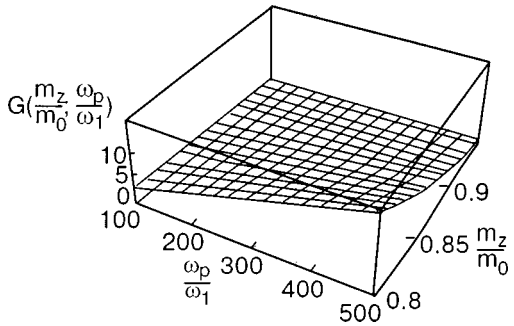


FIG. 2. Inequality (8) as a function of two variables, $G(m_z/m_0;\ \omega_p/\omega_1)$.

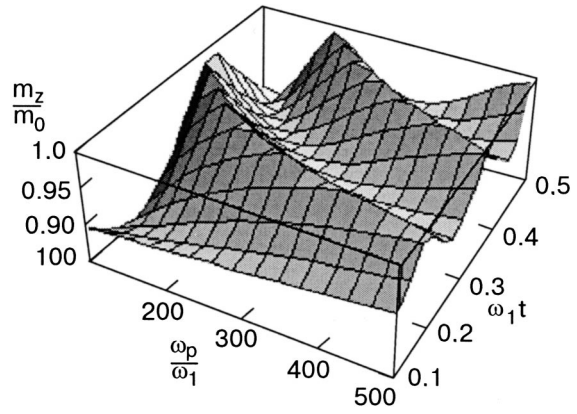


FIG. 3. Solution (10) as a function of the two variables $\omega_p/\omega_1$ and $\omega_1 t$.

$$m_z(t)=m_0\left(1-\sqrt{2\omega_1/\omega_p}\frac{|\mathrm{sn}(\sqrt{\omega_1\omega_p/2}t;1/2)|}{\mathrm{dn}(\sqrt{\omega_1\omega_p}t;1/2)}\right), \qquad (10)$$

where dn(...) are the Jacobi amplitudes.[10] It is seen from Eq. (10) that the amplitude of the deviation of **m** from the **z** axis is determined by the ratio $2\omega_1/\omega_p$. On the other hand, solution (10) is valid if condition (8) holds. It is easily seen from (8) that this condition depends on the ratios $m_z/m_0$ and $\omega_p/\omega_1$. Treating (8) as a function of two variables, $G(m_z/m_0;\omega_p/\omega_1)$, we can determine the domain of applicability of solution (10) (see Fig. 2):

$$0<\frac{m_z}{m_0}<0.95,\ \frac{\omega_p}{\omega_1}>300. \qquad (11)$$

Such initial values for $m_z(0)$, as will be shown below, can be obtained only after polychromatic pumping. In other words, solution (10) corresponds to the case when a monochromatic field acts on the system after a polychromatic pump has acted and sufficiently large deviations of **m** from the **z** axis have been attained.

Solution (10) is shown in Fig. 3 in the form of a function that depends on the parameter $\omega_p/\omega_1$ and the variable $\omega_1 t$.

Another situation arises in the case of polychromatic pumping, i.e., when a periodic train of pulses of duration $\tau$ and repetition period $T$ acts on the system. In this case the system of equations (2) takes the form[7,8]

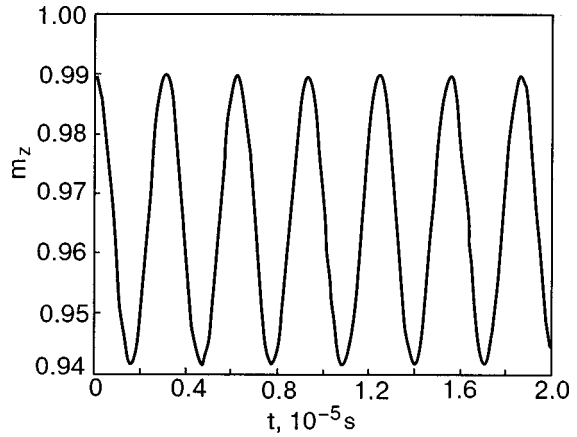


FIG. 4. Results of a numerical integration of equations (12) for the parameter values $\omega_1'\approx 5\times 10^4\ \mathrm{s}^{-1}$, $\omega_p\approx 2\times 10^7\ \mathrm{s}^{-1}$, $m_z(0)/m_0\approx 0.99$, $T\approx 10^{-6}$ s, and $k\approx 0.14$ in the case of a polychromatic influence.

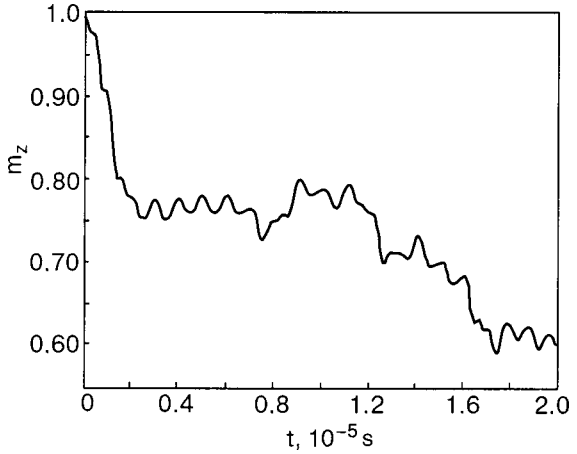


FIG. 5. Results of a numerical integration of equations (12) for the parameter values $\omega_1'\approx 2\times 10^5\ \mathrm{s}^{-1}$, $\omega_p\approx 10^8\ \mathrm{s}^{-1}$, $m_z(0)/m_0\approx 0.99$, $T\approx 10^{-6}$ s, and $k\approx 2.8$ in the case of a polychromatic influence.

$$\begin{aligned}
\dot m_x &= \omega_p\left(1-\frac{m_z}{m_0}\right)m_y,\\
\dot m_y &= -\omega_p\left(1-\frac{m_z}{m_0}\right)m_x+m_z\omega_1\sum_{n=-\infty}^{\infty}f\left(\frac{t}{T}-n\right), \qquad (12)\\
\dot m_z &= -m_y\omega_1\sum_{n=-\infty}^{\infty}f\left(\frac{t}{T}-n\right),
\end{aligned}$$

where

$$\sum_{n=-\infty}^{\infty}f\left(\frac{t}{T}-n\right)=\frac{\tau}{T}\sum_{n=-My}^{\infty}\cos(n\Omega t),\quad \Omega=\frac{2\pi}{T}.$$

Integration of the system of equations (12) can be done only by numerical methods. The results of a numerical integration for values of the stochasticity $k<1$ and $k>1$ are presented in Figs. 4 and 5, respectively.

Choosing typical parameter values for a ferromagnet, $\omega_1'\approx 2\times 10^5\ \mathrm{s}^{-1}$, $\omega_p\approx 10^8\ \mathrm{s}^{-1}$, $m_z(0)/m_0\approx 0.99$, and $T\approx 10^{-6}$ s, we obtain $k\approx 2.8$, and in the other limiting case $\omega_1'\approx 5\times 10^4\ \mathrm{s}^{-1}$, $\omega_p\approx 2\times 10^7\ \mathrm{s}^{-1}$, we obtain $k\approx 0.14$.

As is seen in Figs. 4 and 5, for $k<1$ a polychromatic influence is qualitatively no different from a monochromatic one, while for $k>1$ dynamic stochasticity arises in the system as a consequence of the overlapping of resonances.

*E-mail: lchotor@yahoo.com

[1] M. I. Kurkin and E. A. Turov, *NMR in Magnetically Ordered Substances and Its Application* [in Russian], Nauka, Moscow (1990).
[2] T. L. Buishvili, L. L. Chotorlishvili, and M. G. Tsanava, Fiz. Nizk. Temp. **26**, 733 (2000) [Low Temp. Phys. **26**, 537 (2000)].
[3] R. Z. Sagdeev and G. M. Zaslavskiĭ, *Nonlinear Physics*, Harwood Academic Publishers, New York (1988), Nauka, Moscow (1988).
[4] B. V. Chirkov, Phys. Rep. **52**, 263 (1979).
[5] G. M. Zaslavsky, Phys. Lett. A **69**, 145 (1978).
[6] M. C. Gutzwiller, *Chaos in Classical and Quantum Mechanics*, Springer, New York (1990).
[7] L. L. Buishvili and A. I. Ugulava, Fiz. Tverd. Tela (Leningrad) **25**, 2370 (1983) [Sov. Phys. Solid State **25**, 1361 (1983)].
[8] V. I. Kesaev and A. I. Ugulava, Fiz. Tverd. Tela (Leningrad) **27**, 1259 (1985) [Sov. Phys. Solid State **27**, 763 (1985)]; K. Nakamura, Y. Okazaki, and A. R. Bishop, Phys. Rev. Lett. **57**, 5 (1986).

[9] I. S. Gradshteyn and I. M. Ryzhik, *Tables of Integrals, Series, and Products*, Academic Press, New York (1980), Nauka, Moscow (1971).
[10] *Handbook of Mathematical Functions*, E. M. Abramovitz (ed.) National Bureau of Standards, Vol 55 of Appl. Math. Ser., Issued June (1964).
[11] E. Kamke, *Gewöhnliche Differentialgleichungen*, Akademie Verlag, Leipzig (1959), Nauka, Moscow (1976).

Translated by Steve Torstveit

## LETTERS TO THE EDITOR

# Size-induced structural transformations in argon clusters with a fivefold symmetry axis

O. G. Danylchenko,* S. I. Kovalenko, and V. N. Samovarov

*B. Verkin Institute for Low Temperature Physics and Engineering, National Academy of Sciences of Ukraine, pr. Lenina 47, Kharkov 61103, Ukraine*

(Submitted June 7, 2004)
Fiz. Nizk. Temp. **30**, 986–988 (September 2004)

An electron-diffraction study of the structure of free clusters of Ar is carried out in the interval of mean sizes $\bar{N}\approx 600-1500$ atoms/cluster. The existence of an amorphous (polyicosahedral) phase in large rare gas clusters with $\bar{N}\approx 600-800$ atoms/cluster is observed for the first time. It is shown that with increasing number of atoms in a cluster a transition to a multilayer icosahedral (ordered) phase occurs in a rather narrow size interval. © *2004 American Institute of Physics.* [DOI: 10.1063/1.1802992]

Nanoparticles can have a number of unusual properties due to their structural features. Clusters with a structure having fivefold symmetry are of significant interest. Such clusters, built up on the basis of icosahedral structures, were detected a comparatively long time ago in metals and solidified rare gases.[1,2]

In the case of aggregations containing several tens of atoms a molecular-dynamic modeling of a freezing drop of a Lennard-Jones liquid predicts that an amorphous (polyicosahedral) structure will be realized. Such a structure is formed by the conjoining of a number of elementary 13-atom icosahedra. The simplest way of conjoining involves the formation of twin icosahedra with arbitrarily oriented fivefold axes. The short-range order of the structure that forms is identical to polytetrahedral, which corresponds to an amorphous state of the substance.

According to thermodynamic calculations,[1] a polyicosahedral structure can persist in aggregations consisting of not more than 30–35 atoms, since at a larger number of atoms they become energetically unfavorable. As a result of a comparison of the electron-diffraction data with the calculated interference functions in Ref. 3 it was concluded that a polyicosahedral structure is realized in argon clusters with fewer than 50 atoms, corresponding to a linear size of the cluster $\approx 15$ Å.

As the number of atoms in the twin clusters increases, the stresses that arise due to the lowering of the density of surface atoms cause the polyicosahedral structure to become unstable. According to calculations, maximization of the surface density of atoms in clusters containing several hundred atoms is achieved in a multilayer icosahedron, where the fivefold axes penetrate the whole formation. One is actually talking about an ordered system of inter-embedded icosahedra, where the total number of atoms can reach a thousand.

Up till now it has been assumed that the transition from the amorphous to the multilayer icosahedral structure is realized in the early stages of cluster growth, when the size of the cluster is only a few tens of atoms. The size interval of the transition has not been investigated in detail because of the methodological complexities of determining the cluster sizes.

In this report we present the results of a study of the structure of free clusters of argon in the homogeneous nucleation regime. The experiments were performed on an apparatus consisting of an electron diffraction unit, a supersonic cluster beam generator, and a liquid hydrogen cooled condensation pump for removing the jet gas. A detailed description of the whole apparatus is presented in Ref. 4. The average cluster size $\bar{N}$ was varied by varying the gas pressure $P_0$ and gas temperature $T_0$ at the entrance to the supersonic nozzle. The lowest value of $T_0$ used was 100 K. It should be noted that such a low nozzle temperature has not been used in electron-diffraction studies of cluster beams. The value of $\bar{N}$ in the case $T_0=\text{const}$ was set by the value of $P_0$, which was varied up to 0.2 MPa. To eliminate heterogeneous nucleation a high initial vacuum ($\sim 10^{-7}$ torr) was produced in the apparatus. The method of determining the average cluster size is described in detail in our previous paper.[5] The diffraction region was set off to a distance of around 100 mm from the exit section of the nozzle, to a place where the tempera-

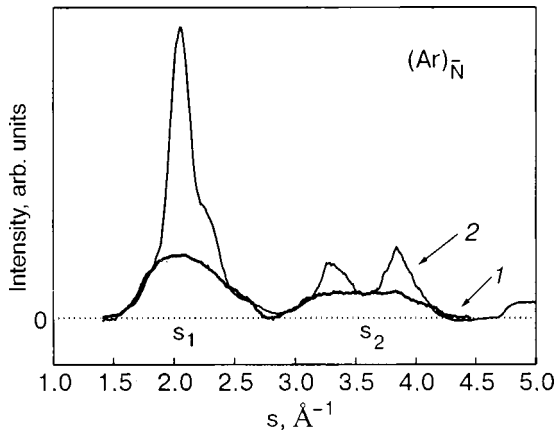


FIG. 1. Densitometer traces of free Ar clusters with different $\bar{N}$ [atoms/cluster]: 800 (*1*), 1350 (*2*).

 

ture of the clusters had reached a constant value $T=(38\pm5)$ K.

To enlarge the data set obtained during a single experiment the diffraction patterns were registered photographically out to values of the diffraction vector $s=5$ Å$^{-1}$. The background component of the electrode diffraction patterns was removed by the method described in Ref. 5.

The results of studies done for $\overline{N}<1500$ atoms/cluster are illustrated in Fig. 1. Curve *1* is a densitometer trace of clusters whose average size is approximately 800 atoms/cluster. Even in the case of the maximum possible error in the estimate of $\overline{N}$ the observed diffraction pattern pertains to aggregations containing at least 500–600 atoms/cluster. A characteristic feature in this case is the presence of two pronounced ''halos'' on the densitometer trace rather than individual diffraction peaks. The intensity distribution shown in the figure (curve *1*) is typical for a liquid or amorphous state of a monatomic substance, in particular, of a metal with the fcc lattice.[6] For example, the ratio of the position of the second ''halo'' $s_2$ to the position of the first halo $s_1$ is equal to 1.7, which agrees with the value of this quantity for fcc metals in the amorphous state, while the height $H_1$ of the first halo is approximately twice as high as the height $H_2$ of the second, as is also characteristic of an amorphous state.

Thus there is no doubt that the observed diffraction pattern is due to an amorphous structure of the clusters.

Also shown in the figure is the intensity distribution of the electrons diffracted on cluster beams with $\overline{N}\approx1350$ atoms/cluster (curve *2*). In this case the curve of the intensity is typical for a multilayer icosahedral structure.[5] This is attested to by the anomalously large height of the first peak, the presence of an inflection point on it in the region $s=2.25$ Å$^{-1}$, and the fact that the heights of the peaks lying in the region of the fcc peaks (220) and (311) are uncharacteristically low for the a cubic phase. In addition, the shape of the peaks is well approximated by a Lorentzian, and that, as we showed previously in Ref. 5, is characteristic for an icosahedral structure.

Thus we have observed experimentally for the first time the existence of an amorphous (polyicosahedral) phase in large clusters with 600–800 atoms/cluster, which for Ar corresponds to a linear size of the aggregations of 30–35 Å, and the transition of the polyicosahedral (amorphous) phase to a multilayer icosahedral (ordered) phase is realized in large clusters in a rather narrow interval of cluster sizes.

The results obtained might serve as the subject of a theoretical treatment of the mechanisms of formation and stability of large polyicosahedral aggregations. Such aggregations might be a set of small twin icosahedral complexes. In addition, it is of interest to elucidate the factors that stimulate the rather sharp disorder–order phase transition in systems with a fivefold symmetry axis.

*E-mail: danylchenko@ilt.kharkov.ua

[1] I. Farges, M. F. de Feraudy, B. Raoult, and G. Torchet, Adv. Chem. Phys. **70**, 45 (1988).
[2] Yu. I. Petrov, *Clusters and Small Particles* [in Russian], Nauka, Moscow (1986).
[3] I. Farges, M. F. de Feraudy, B. Raoult, and G. Torchet, J. Chem. Phys. **78**, 5067 (1983).
[4] S. I. Kovalenko, D. D. Solnyshkin, É. T. Verkhovtseva, and V. V. Eremenko, Fiz. Nizk. Temp. **20**, 961 (1994) [Low Temp. Phys. **20**, 758 (1994)].
[5] O. G. Danylchenko, S. I. Kovalenko, and V. N. Samovarov, Fiz. Nizk. Temp. **30**, 226 (2004) [Low Temp. Phys. **30**, 166 (2004)].
[6] L. I. Tatarinova, *Structure of Solid Amorphous and Liquid Substances* [in Russian], Nauka, Moscow (1983).

Translated by Steve Torstveit